Modelling the Energy Consumption and associated Carbon Emissions of Machine Tools for Machining Cylindrical Parts

THESIS

Submitted in partial fulfilment of the requirements for the degree of

DOCTOR OF PHILOSOPHY

by

SHAILENDRA PAWANR

2017PHXF0402P

Under the supervision of
Dr. Girish Kant Garg

and co-supervision of
Prof. Srikanta Routroy

BITS Pilani
Pilani | Dubai | Goa | Hyderabad

BIRLA INSTITUTE OF TECHNOLOGY & SCIENCE, PILANI – 333031 (RAJASTHAN), INDIA
2023

Birla Institute of Technology & Science, Pilani
Pilani Campus

CERTIFICATE

This is to certify that the thesis entitled "**Modelling the Energy Consumption and associated Carbon Emissions of Machine Tools for Machining Cylindrical Parts**" submitted by Shailendra Pawanr, ID. No. 2017PHXF0402P for award of PhD degree of the Institute embodies original work done by him under our supervision.

Signature (Co-Supervisor)

PROF. SRIKANTA ROUTROY

Professor,

Department of Mechanical Engineering,

BITS Pilani, Pilani campus

Date:

Signature (Supervisor)

DR. GIRISH KANT GARG

Assistant Professor,

Department of Mechanical Engineering,

BITS Pilani, Pilani campus

Date:

Acknowledgment

First and foremost, I would like to express my deep gratitude and sincere thanks to my PhD supervisors **Dr. Girish Kant Garg** and **Prof. Srikanta Routroy,** for their stimulating guidance and unwavering support throughout my research work. This thesis could not have attained its present form in content and presentation without their active interest, direction and help. I am extremely grateful to both guides, who have been tremendous mentors for me, for their consistent support to overcome the difficulties so that I could confidently march towards completion of the research work.

I am immensely thankful to **Prof. V. Ramgopal Rao (**Vice-Chancellor, BITS Pilani)**, Prof. Souvik Bhattacharyya** (Ex Vice-Chancellor, BITS Pilani), and **Prof. Sudhirkumar Barai**, Director, BITS Pilani, Pilani Campus, for their support and blessings. I express my gratitude to **Prof. S.K. Verma** (Dean, Administration, BITS Pilani, Pilani Campus) and **Prof. Raj Kumar Gupta** (Associate Dean, Sponsored Research Consultancy Division, SRCD) and **Prof. Navneet Gupta** (Ex Associate Dean, SRCD) for providing the necessary facilities and support to carry out the current research work. I also express my sincere thanks to **Prof. M.B. Srinivas**, Dean, Academic-Graduate Studies & Research Division (AGSRD), **Prof. Shamik Chakraborty**, Associate Dean, Academic-Graduate Studies & Research Division (AGSRD) and **Prof. Jitendra Panwar**, Ex Associate Dean, AGSRD for their motivation, constant support and encouragement. I thank the Head of the Department of Mechanical Engineering for his valuable support and guidance. I am highly indebted to the Associate Dean, Student Welfare Division (SWD), for his encouragement and suggestions.

I would also like to thank the doctoral advisory committee (DAC) members **Prof. Rajesh Prasad Mishra**, Department of Mechanical Engineering and **Dr. Prateek Kala**,

Department of Mechanical Engineering, for sparing their valuable time in reviewing my thesis draft. I must acknowledge that their constructive criticisms and valuable suggestions have immensely helped in improving the quality of my PhD thesis report. I would like to thank **Prof. Arun Kumar Jalan**, Convener, DRC, Department of Mechanical Engineering. They provided me with all the possible support during my research work.

I also like to express my gratitude to **Prof. Kuldeep Singh Sangwan**, Unit Chief Workshop, for providing workshop resources without any time restrictions.

My thanks are extended to, my colleagues and co-researchers **Mr. Ashish Kumar Srivastava**, **Dr. Santosh Kumar Saraswat**, **Mr. Amresh Kumar** and **Mr. Rahul Ukey** for providing moral support whenever I needed. I believe that all those who have helped me ever, directly or indirectly, will forgive me for my inability to name them here; however, I express my gratitude and indebtedness to them.

I also express my gratitude to all staff members of BITS Pilani Workshop, especially **Mr. Ashok Kumar Lagri**, **Mr. Rakesh Kumar**, **Mr. Vinod Naruka, Mr. Madan lal Saini** and **Mr. Rajkumar Saini,** for their efforts in assisting me in the experimental work.

Lastly, I owe my deep thanks to my mother **Shreemati Kamla Panwar,** and my wife **Mrs. Nitu Panwar** for their encouragement and unlimited support, which cannot be expressed in words. Without their countless sacrifices, I could not have completed my research work. My heartfelt appreciation goes to my small and loving daughter **Rudrakshi Panwar** and my son **Gourang Singh Panwar**. Last but not least, I pray and thank the Almighty for showering HIS divine blessings and giving me inner strength and patience.

Shailendra Pawanr

Abstract

Stringent regulations imposed throughout the globe due to growing environmental issues, reducing energy consumption and associated carbon emissions (CEM*)* have become one of the essential requirements of manufacturing industries. Machine tools plays a significant role in manufacturing industries, are unfortunately responsible for huge energy consumption, and associated CEM. Establishing an accurate energy consumption and CEM model for machine tools is a prerequisite for realising the implementation of energy-efficient and low CEM approaches such as energy-efficient process planning and scheduling. The power characteristics of a machine tool is complex and vary continuously, making it challenging to develop a single energy consumption model for the entire process. The energy consumption of the machine tool can be divided into different energy modules; startup, standby, spindle acceleration, idle, tool change, air-cutting, coolant pump, cutting tool rapid positioning and cutting. The cutting energy consumption module can be further subdivided into the Constant Power Consumption (CPC) machining process e.g. turning and Variable Power Consumption (VPC) machining process e.g. end facing and grooving. Predicting the energy consumption and associated CEM of a machine tool for machining cylindrical parts remains challenging for industrial applications because the previous energy prediction models are typically developed with the CPC machining processes only. In industry, the length and diameter are reduced to obtain the final dimensions of a cylindrical part. Typically, external turning operation is used to reduce the diameter of the part i.e. CPC machining process and facing is conducted to reduce the length of the part i.e. VPC machining process. The cutting power characteristics of the VPC machining processes are more complex and dynamic due to change in one of the process parameters (e.g. cutting speed during end facing) than the CPC machining (e.g. turning).

Furthermore, majority of studies considered the energy consumed for a particular period of a machining process. However, machining of a cylindrical part includes spindle acceleration periods, standby periods, idle periods, air-cut periods, tool changing periods, and cutting periods, due to which existing models are incapable to assess energy consumption and corresponding CEM accurately in industries for machining of cylindrical parts. This study modelled the energy consumption and associated CEM of machine tools for machining cylindrical parts.

An empirical model is developed to predict the energy consumption of the VPC machining process i.e. end facing. The experiments were performed on a LMW-Smarturn CNC lathe machine tool in the dry and wet environment to obtain the fitting coefficients of the developed model. The validation experiments confirm the accuracy of the developed model is more than 96%.

The developed model is further used as an input for the formulation of a multi-objective optimization model to select the optimal parameters leading towards minimum energy consumption and maximum material removal rate (productivity). The optimization results shows that the productivity improves to 99.97% with only a 10.08% increase in the energy consumption on common optimal parameters compared to optimal parameters with mono optimization of energy consumption.

The energy consumption models of the previously mentioned different energy modules were established, and the developed model of the VPC machining process was integrated to evaluate the energy consumption of machine tools for machining cylindrical parts. Experiments are conducted in the dry and wet environment to obtain the fitting coefficients of the developed models for different energy modules. The validation test results show that the developed model's accuracy is more than 97%.

The developed energy consumption model of the machine tool is used to establish an empirical model to quantify their carbon emissions for the machining of cylindrical parts.

The CEM of a machine tool for machining a cylindrical part were segregated into CEM from electrical energy consumption, material consumption, cutting tool wear, coolant consumption and from the disposal of machining waste materials (i.e. chips). In which the CEM due to machine tool electrical energy consumption was calculated using the previously developed machine tool energy consumption model for machining cylindrical parts. CEM models for the remaining factors (material consumption, cutting tool wear, coolant consumption and chip disposal) were developed and integrated to quantify the total CEM of the machine tool for machining cylindrical parts. The developed model was applied to a cylindrical part with three different process plans to investigate the effect of process parameters on CEM.

Soft computing techniques have become increasingly popular for modelling in various engineering applications due to their ability to make accurate predictions, work with inherent complexity, and capture non-linear behaviour between input and output parameters. Three soft computing techniques, multi-gene genetic programming (MGGP), least square-support vector machine (LS-SVM) and fuzzy logic, are applied to model a machine tool's energy efficiency, power factor and associated CEM. The experiments were performed to obtain the data required for development of models. The coefficients of determination (R^2) and five error indices were used to evaluate and compare the accuracy of the developed models. The models' comparative performance evaluation reveals that the LS-SVM consistently outperforms the other models i.e. MGGP and fuzzy logic. Further, A multi-objective optimization model has been developed to determine the optimal process parameters for power factor, product quality, productivity and CEM of machine tools using GRA coupled with Taguchi technique, considering the impact of weight assigning methods. The optimization results obtained with different weight assigning methods have been compared with the equal weight's results and verified using the confirmation experimental tests.

Table of Content

Abbreviation/Symbol	Description
AHP	Analytical Hierarchy Process
ANOVA	Analysis of variance
CEM	Carbon emission
CEM_{elec}	CEM due to electrical energy consumption
CEM_{cool}	CEM due to the coolant consumption
CEM_{oil}	CEM due to the manufacture of pure mineral oil
CEM_{wc}	CEM due to the disposal of cutting fluid waste
CEM_{tool}	CEM due to the tool wear
CEM_{m}	CEM due to the material consumption
CEM_{chip}	CEM due to the post-processing of chips
CEF_{elec}	CEM factor for electrical energy consumption
CEF_{oil}	CEM factor for the manufacturing of coolant
CEF_{wc}	CEM factor for the disposal of the used coolant
CEF_{tool}	CEM factor for the cutting tool wear
CEF_{m}	CEM factor for the material consumption
CEF_{chip}	CEM factor for the chips post-processing
CO_2	Carbon dioxide
CPC	Constant-power consumption
CPI	Cumulative Performance Index
CR	Consistency ratio
CI	Consistency index
$Cov\ (g_i(j), g_i(l))$	Covariance of sequence $g_i(j), g_i(l)$
$DC_{q\times p}$	Decision matrix
d_{ij}	Elements of the decision matrix
EI_j	Entropy index
DIV_j	Degree of divergence
D	Part diameter

D_v	Targeted value of the response
d_c	Depth of cut
EE	Energy efficiency
Ew_j	Entropy weights
E_{total}	Total energy consumption
$E_{startup}$	Startup energy consumption
$E_{s\tan dby}$	Standby energy consumption
E_{acc}	Spindle acceleration energy consumption
E_{rapid}	Rapid positioning energy consumption
E_{idle}	Idle energy consumption
E_{tc}	Tool change energy consumption
E_{air}	Air cut energy consumption
E_{cool}	Coolant pump energy consumption
E_{cut}	Cutting energy consumption
E_{cut_CPC}	CPC machining process energy consumption
E_{cut_VPC}	VPC machining process energy consumption
f_r	Feed speed
GHG	Greenhouse gas
GRA	Grey Relational Analysis
GRC	Grey Relational Coefficients
GRG	Grey Relational Grades
GM	Geometric mean
$G_{\mathrm{q\times p}}$	Multiple-quality characteristics matrix
$g_i(j)$	Elements of $G_{\mathrm{q\times p}}$
$K_{i,J,k}$	Average-GRC at each level of each response
LS-SVM	Least square-SVM
MAE	Mean absolute error
MSE	Mean square error
MGGP	Multi-gene genetic programming
MRR	Material Removal Rate

$\overline{MRR}$	Average- MRR
MOCI	Multi-objective combined Index
Max $x_p(q)$	Maximum value in the sequence
Min $x_p(q)$	Minimum value in the sequence
NM_{ij}	Normalize matrix
$Max(d_{ij})_j$	Maximum values of the j^{th} response
$Mini(d_{ij})_j$	Minimum values of the j^{th} response
n	Spindle angular velocity
N	Quantity of sub-intervals
p	Number of performance characteristics
PCA	Principal Component Analysis
PF	Power Factor
PO_{ij}	Probability of occurrence
P_{total}	Total power consumption
$P_{startup}$	Startup power consumption
$P_{standby}$	Standby power consumption
$P_{acc}(t)$	Spindle acceleration power consumption at an instant t
$P_{rapid}(t)$	Rapid positioning power consumption at an instant t
P_{idle}	Idle power consumption
P_{tc}	Tool change power consumption
P_{air}	Air cut power consumption
P_{cool}	Coolant pump power consumption
P_{cut}	Cutting power consumption
P_m	Material removal power consumption
P_{m_CPC}	P_m for the CPC machining process
P_{m_VPC}	P_m for the VPC machining process
P_{cut_CPC}	P_{cut} in the CPC machining process
$P_{cut\_VPC}(t)$	P_{cut} at an instant t in the VPC machining process
P_f	Feed axes power consumption

P_{fx}	x -axis feed power consumption
P_{fz}	z -axis feed power consumption
q	Number of experimental runs
Q_m	Mass of material
r	Tool nose radius
R_a	Surface roughness
R^2	Coefficient of determination
RMSE	Root mean square error
RPE	Relative percentage error
$R_{p\times p}$	Pairwise matrix
RI	Random Index
R_{jl}	Correlation coefficient matrix
R_{ij}	Range of the average-GRC
s	Number of cutting parameters
SSE	Sum of squared error
SVM	Support vector machine
SN ratio	Signal to noise ratio
T_{life}	Tool life in seconds
T_{cut}	Total cutting time
t_{stp}	Startup time
t_{std}	Standby time
t_{acc}	Spindle acceleration time
t_{idle}	Idle time
t_{tc}	Tool change time
t_{rpd}	Rapid positioning time
t_{air}	Air cut time
t_{cool}	Coolant flow time
t_{cut}	Cutting time
t_{CPC}	CPC machining process time
t_{VPC}	VPC machining process time

VPC	Variable-power consumption
V_{in}	Initial volume of the coolant in liter
V_{ad}	Additional volume of coolant in liter
v_c	Cutting velocity
$v_{\max}$	Maximum cutting velocity
WGRA	Weighted Grey Relational Analysis
w_j	Weight of j^{th} response
w_{tool}	Weight of the cutting tool/inserts
$x_p^*(q)$	Normalized sequence
$x_p(q)$	Actual (experimental) sequence
y	Experimental outcome
$\bar{y}$	Average value of y
δ	Coolant concentration
λ_{max}	Maximum Eigenvalue
λ_k	Eigenvalues
V_{lk}	Eigenvectors
ρ	Density of the material
σ_y^2	Variance of y
$\sigma g_i(j)$	Standard deviation of sequence $g_i(j)$
$\sigma g_i(j)$	Standard deviation of sequence $g_i(l)$
$\Delta_{op}(q)$	Deviational sequence
K, n, p and q	Tool life constants
x_i, $i=1,2,3$	Fitting coefficient of spindle acceleration energy model
y_i, $i=1,2,3$	Fitting coefficient of idle power consumption model
C_{CP}, α_c, β_c, λ_c, δ_c	Fitting coefficients of P_{m_CPC} model
C_{VP}, α_v, β_v, λ_v, δ_v	Fitting coefficients of P_{m_VPC} model
M_i	M_i is the model predicted value
A_i	A_i is the experimental values
i	$i = 1,2,3,\dots,q$
j	$j = 1,2,3,\dots.\mathrm{p}$
J	$J = 1,2,3,\dots.s$

k	$k = 1,2,3, \dots, p$
l	$l = 1,2,3, \dots .\mathrm{p}$

Chapter 1:

Introduction

1.1. Introduction

The impact of global warming is growing severely due to significant increase in greenhouse gas (GHG) emissions and reflected in intensifying heatwaves, threats to biodiversity, melting glaciers and rising sea levels, raising concerns about life's sustainability and future existence. The focus of reducing GHG emissions is receiving widespread attention from climate change experts to combat global warming and its adverse effects on the ecosystem, which has been periodically alerted by the Intergovernmental Panel on Climate Change (IPCC, 2014, 2007, 2001; Pye et al., 2021). Energy consumption accounts for more than 70% of global GHG emissions (Panagiotopoulou et al., 2022). The industrial sector is one of the major drivers of economic development (U.S. EIA, 2016) and the primary contributor to the global energy demand i.e. nearly half of global energy demand (U.S. EIA, 2019, 2017), resulting in one of the main causes of GHG emissions (Brillinger et al., 2021). Manufacturing is an imperative part of the industrial sector (Zhao et al., 2017), and developing countries have made substantial efforts and initiatives to expand the manufacturing industries to achieve higher economic growth (Garg et al., 2016). Manufacturing in the industrial sector accounts for 37% of the world's energy consumption (Diaz-Elsayed et al., 2015) and 38% of the direct and indirect GHGs emissions (Sealy et al., 2016). Machining is a vital process for transforming raw materials into finished products in manufacturing industries. Computer Numerical Control (CNC) machine tools play an imperative role in the manufacturing industry and consumes a significant amount of energy in machining processes e.g. turning, milling and drilling (Kant and Sangwan, 2014; Lv et al., 2016; Tuo et al., 2018). The energy efficiency of machine tools is low i.e. around 30% (He et al., 2012), and the electrical energy spent by the machine tools during

their deployment in machining processes is accountable for more than 99% of their environmental impacts (Li et al., 2011). For instance, in one year, a machine tool emits carbon dioxide (CO_2), one of the prominent GHGs, equivalent to 61 sports utility vehicles (Liu et al., 2015). Machine tools are enlisted as one of the critical products in the European Union's Eco-design directive 2009/125/EC to meet the carbon emission standard (Tuo et al., 2018). The use of electrical energy by a machine tool in a machining process generates a significant quantity of CEM (Panagiotopoulou et al., 2022). Hence, machine tools have a high potential to save energy consumption and to reduce associated CEM. Therefore, reducing the energy consumption of the machine tools is one of the major challenges for the industries to meet sustainable manufacturing (Diaz-Elsayed et al., 2015; Hu et al., 2017; Xiao et al., 2019).

Process parameter optimization of machine tools in existing production lines is one of the most effective strategies to reduce energy consumption and associated carbon emissions (Bagaber and Yusoff, 2019; Campatelli et al., 2014; Duflou et al., 2012; Hu et al., 2020; Jiang et al., 2022; Warsi et al., 2018). This strategy can be broadly classified into two categories: modelling of machine tool’s energy consumption (Edem et al., 2017; Jia et al., 2016; Liu et al., 2015, 2020; Zhou et al., 2017), and optimization of machining process parameters (Alswat and Mativenga, 2020; Bilga et al., 2016; Kumar et al., 2017). The first approach focuses on establishing accurate models to describe a machine tool's energy consumption and associated CEM process, whereas the second is involved in determining the optimal process parameters that minimise energy consumption and associated CEM. Establishing an accurate energy consumption model for machine tools is a necessary prerequisite for realising energy-efficient cutting parameter optimization (Hu et al., 2020; Jia et al., 2016). The lack of an accurate and realistic energy consumption model has

hindered the implementation of energy-efficient approaches such as energy-efficient process planning and scheduling (Lv et al., 2018; Wang et al., 2015).

The power characteristics of a machine tool are complex and dynamic and developing a single energy consumption model for the entire process is challenging. The power profile of a machine tool during machining of a cylindrical part is shown in Figure 1.1 and is considered a basis to describe their energy consumption. The energy consumption (E_{total}) can be decomposed into different modules: startup energy ($E_{startup}$), standby energy ($E_{standby}$), spindle acceleration energy (E_{acc}), idle energy (E_{idle}), tool change energy (E_{tc}), air-cutting energy (E_{air}), coolant pump energy (E_{cool}), cutting tool rapid positioning energy (E_{rapid}) and cutting energy (E_{cut}).

$$E_{total} = E_{startup} + E_{standby} + E_{acc} + E_{rapid} + E_{idle} + E_{tc} + E_{air} + E_{cool} + E_{cut} \quad (1)$$

In Eq. (1), E_{cut} is the cutting module energy consumption i.e. during which material is removed from the cylindrical part. The cutting energy for machining a cylindrical part can be further divided into cutting energy of the Constant Power Consumption (CPC) machining process (E_{cut_CPC}) e.g. turning and cutting energy of the Variable Power Consumption (VPC) machining process (E_{cut_VPC}) e.g. end facing, and can be expressed as:

$$E_{cut} = E_{cut\_CPC} + E_{cut\_VPC} \quad (2)$$

By substituting Eq. (2) in Eq. (1), the total energy consumption of a machine tool for machining of a cylindrical part can be expressed as:

$$E_{total} = E_{startup} + E_{standby} + E_{acc} + E_{rapid} + E_{idle} + E_{tc} + E_{air} + E_{cool} + E_{cut\_CPC} + E_{cut\_VPC} \quad (3)$$

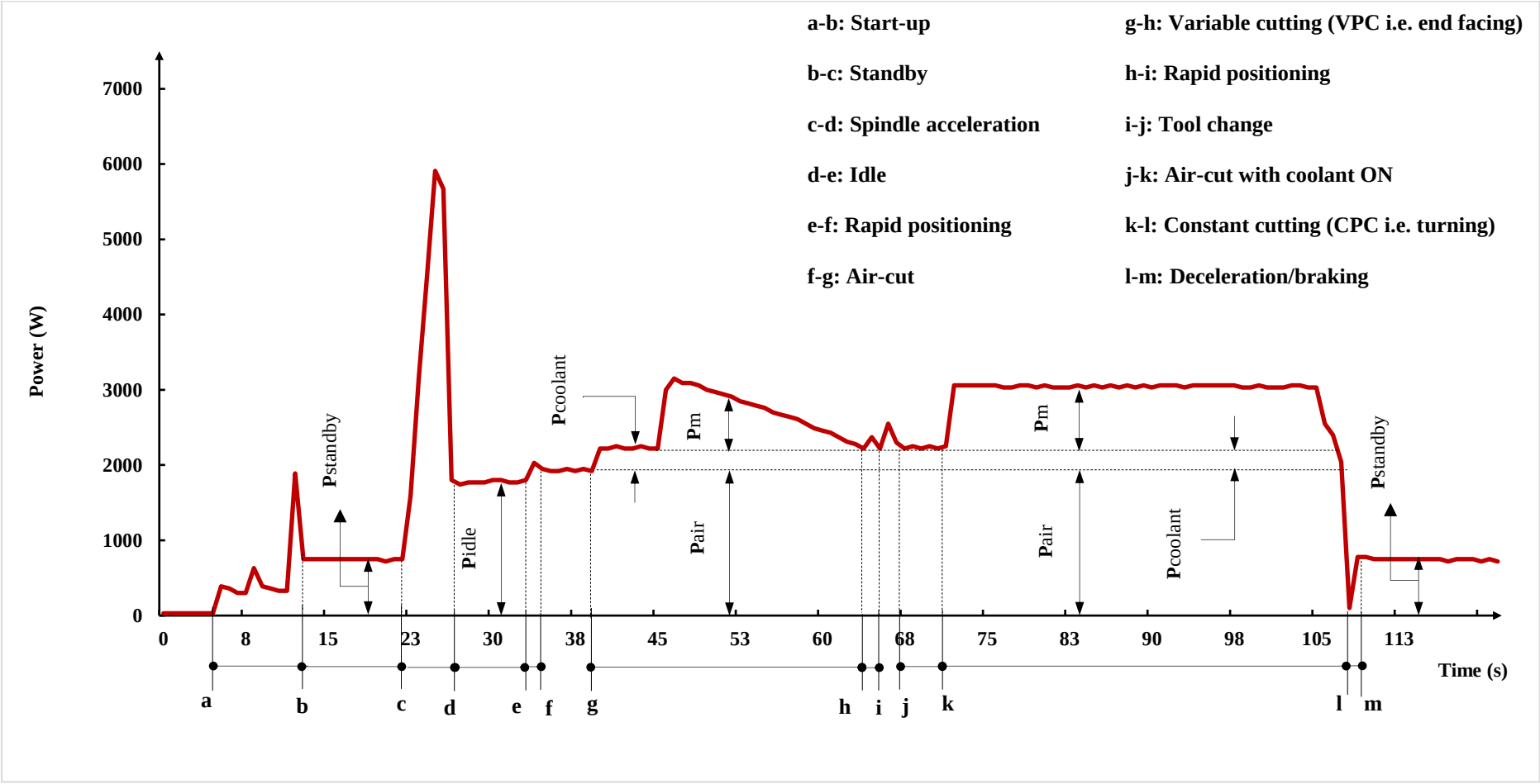

Figure 1.1. A typical power profile of a machine tool during machining of a cylindrical part.

The previously reported energy consumption models are significant but still lack to evaluate a machine tool's energy consumption for machining a cylindrical part in industrial applications. In industry, the length and diameter of a cylindrical part are reduced to obtain the final dimensions of a product. Typically, external turning operation is used to reduce the diameter of the part i.e. CPC machining process and end facing operation is conducted to reduce the length of the part i.e. VPC machining process. The energy evaluation models reported in the literature for machine tools were developed based on CPC machining processes only, while the machining of a cylindrical part includes the CPC and VPC both machining processes to manufacture the final product, which result in inaccurate estimation of the machine tool's energy consumption and associated CEM. Furthermore, majority of studies considered the energy consumed for a particular period of a machining process. However, machining of a cylindrical part includes spindle acceleration periods, standby periods, idle periods, air-cut periods, tool changing periods, and cutting periods, due to which existing models are incapable to assess energy consumption and associated CEM accurately in industries for machining of cylindrical parts.

Significant studies reported in the literature for the modelling of energy consumption of machine tools focus only on CPC machining processes e.g. turning, drilling and milling. The energy modelling for the VPC machining processes (e.g. end facing, grooving and chamfering) is very limited. In the CPC machining process, the process parameters i.e. cutting speed, feed rate and cutting depth remain constant. Consequently, the machining power also remains constant for the given process time. Whereas in the VPC machining process, at least one of the process parameters (for example cutting speed in end facing) changes over time. Hence, the cutting power is dynamically changing, and its characteristics become more complex than the CPC machining process. Jia et al. (2016) study is the only significant work reported in the literature for the VPC machining process.

Furthermore, in the literature, little attention received by the spindle acceleration energy consumption modelling because the regularity of the spindle acceleration power is complicated, its computing model parameters are difficult to acquire, and its time duration is generally considered to be very short. Therefore, limited existing research (Huang et al., 2016; Lv et al., 2017; Zhang et al., 2022) about the spindle acceleration, and limited researcher (Liu et al., 2015; Zhong et al., 2016) considered it for modelling the energy consumption of machine tools or even neglects the spindle acceleration process entirely. These approaches can lead to considerable errors of up to 78% with regard to machine tools that frequently activate their main spindle system in a running state (Huang et al., 2016).

Further, process parameters such as spindle speed, cutting depth, and feed rate have a significant impact on carbon emissions in machining processes (Li et al., 2015). The changes in process parameters have a significant impact on the energy consumption of a machining process (Newman et al., 2012). Previous research has shown that appropriate selection of the process parameters can result in carbon emission reduction up to 40% (Zhao et al., 2021). Therefore, with the increasing global adoption of carbon neutralization policies (carbon tax and carbon labelling) and increased manufacturer competitiveness, the machining process and machine tools should be optimized to minimize carbon emissions and maximize efficient energy utilization, productivity and product quality.

Altogether, modelling and optimization approaches are pre-requisite for the selection of optimum process parameters leading to minimum energy consumption and associated carbon emissions of machine tools. An accurate energy consumption model is beneficial to predict the energy requirement of a particular product in its initial development stage and to identify the most energy-efficient and low carbon emission process parameters using optimization techniques (Bhushan, 2013; Li et al., 2013; Sato et al., 2018).

1.2. Research Motivation

India is the world's third-largest producer and consumer of electricity followed by China and USA (U.S. EIA, 2017), with a national electric grid installed capacity of 382.73 GW (Shameem P et al., 2022). Indian industrial sector accounted for more than half of the total national energy demand followed by transport, domestic (National Statistics Office, 2022, 2020). The industrial sector accounts for about 56% of total energy consumption (Bal et al., 2022; National Statistics Office, 2020), where more than 60% of industrial energy consumption is contributed by the manufacturing industries (Soni et al., 2017). India has the third-highest CO_2 emissions in the world, one of the most prominent GHG (Li et al., 2015). It is ranked at fifth place in list of CO_2 emitting countries since 2000, with CO_2 emissions rising from 866 million metric tonnes (Mmt) to 2315 Mmt between 2000 and 2019 (U.S. Energy Information Adm, 2022). As part of the Paris Agreement, India committed to reducing its GHG emissions intensity by 33-35% by 2030 compared to 2005 levels (IEA, 2021). The Government of India have established national goal for a 45% reduction in carbon intensity of gross domestic product by 2030 and a Net Zero target by 2070 (Pradhan and Ghosh, 2022).

India has emerged as the sixth largest manufacturing economy in the world, and it is expected that manufacturing will further boost in India due to government thrust on “Make in India” plan. India is the 13th largest manufacturer of machine tools in the world as per the Indian Machine Tool Manufacturer’s Association (IMTMA). The Indian market for machine tools reached 120.36 billion in 2020-21, with domestic production of machine tools worth 66.02 billion (IMTMA, 2022). An accurate and realistic energy consumption model can facilitate the implementation of energy-efficient approaches such as energy-efficient process planning in manufacturing industries

1.3. Objective of the Study

The objective of the present study is to model the energy consumption and associated CEM of machine tools for machining cylindrical parts, and to optimize the process parameters for machine tools to minimize carbon emissions and maximize efficient energy utilization, productivity, and product quality. The detailed objectives are as follows:

- Development of a model for Variable Power Consumption (VPC) machining processes - A case of end facing
- Selection of process parameters for the VPC machining process – A case of end facing
- Development of a model to predict the energy consumption of machine tools for machining cylindrical parts.
- Development of a model to quantify the carbon emission of machine tools for machining cylindrical parts.
- Prediction of energy efficiency, power factor and associated carbon emission of machine tools using soft computing techniques
- Multi-objective optimization of machining process performance indicators considering the impact of weight assignment methods

1.4. Methodology

The different phases of the adopted methodology to achieve the objectives are as follows:

Phase-I: An empirical model has been developed to determine the energy consumption of the VPC machining process (i.e. end facing) of the machine tool. The fitting coefficients of the model have been determined by conducting experiments on a LMW-CNC lathe machine tool under dry and wet environments. Validation experiments have been performed to confirm the prediction accuracy of the developed model.

Phase-II: The model in phase-I is further used as an input for the formulation of a multi-objective optimization model to select the optimal parameters leading towards minimum energy consumption and maximum material removal rate (productivity). The Grey Relational Analysis coupled with Taguchi technique have been used to determine the common optimal level of process parameters on which energy consumption and material removal rate are optimized simultaneously.

Phase-III: An empirical model has been developed to predict the energy consumption of machine tools for machining cylindrical parts by dividing the energy consumption of machine tool into different energy modules: start-up, standby, spindle acceleration, idle, rapid positioning, air-cutting, and cutting. The cutting energy consumption module is further separated in the VPC and CPC machining process. The energy consumption models of the different energy modules were established, and the developed model of the VPC in phase-I was integrated to evaluate the energy consumption of machine tools for machining cylindrical parts. The fitting coefficients of each energy module have been determined by conducting experiments in dry and wet environment. Validation experiments have been carried out to ensure the proposed model's prediction accuracy.

Phase-IV: An empirical model has been developed to quantify the CEM of machine tools for machining cylindrical parts. The CEM of a machine tool for machining a cylindrical part have been decomposed into CEM due to electrical energy consumption, material consumption, cutting tool wear, coolant consumption and the disposal of machining waste materials (i.e. chips). The CEM due to machine tool electrical energy consumption has been calculated using the previously developed model in phase -III. The developed model has been applied on a cylindrical part with three different process plans to validate the developed model for practical implementation in industry.

Phase-V: Soft computing-based models have been developed to predict the energy efficiency, power factor and associated CEM of machine tools. Three soft computing techniques; multi-gene genetic programming (MGGP), least square-support vector machine (LS-SVM) and fuzzy logic have been used to develop the predictive models. The experiments were performed to obtain the data required for development of models. The performance of the developed models have been evaluated based on coefficient of determination and five error indices. The models have been validated using the hypothesis testing i.e. mean paired t-test and variance of F-test.

Phase-VI: A multi-objective optimization model has been developed to determine the optimal parameters for power factor, carbon-emission, productivity, and product quality using GRA coupled with Taguchi technique, considering the impact of weight assigning methods. The optimization results obtained with different weight assigning methods have been compared with the equal weight's results and verified using the confirmation experimental tests.

1.5. Significance of the Study

An accurate energy consumption and associated CEM model can facilitate the implementation of energy-efficient approaches such as energy-efficient process planning in manufacturing industries. This study developed accurate and industry applicable models which can be utilized by the process planners to identify the most energy-efficient based process plan before actual machining of a cylindrical part on a machine tool. Evaluating each option to ascertain the energy consumption is not practicable and necessitates a large number of lengthy trials, which increases costs and time. Further, provides optimal process parameters to minimize carbon emissions and maximize efficient energy utilization, productivity and product quality. The developed energy consumption model is capable to

predict the energy consumption of machine tool and associated CEM accurately for industrial applications. The developed model can assist in mitigating machine tool environmental impacts and facilitates the exploration of low energy efficiency and high CEM machining process.

Further, this study could be beneficial for mass production, where the different factors, such as machine tools, workpiece materials, and cutting tools, remain constant. Machine tools have a complex and dynamic structure due to the diverse and complex interaction of various materials, process parameters, and cutting tools, which directly impact their behaviour analysis. However, in mass production systems, the factor of diversification could be reduced, and the presented approach may be practically possible.

1.6. Organization of the Thesis

The thesis is organized in nine chapters. **Chapter 1** provided the introduction of the present thesis. A review of literature related to energy consumption modelling and optimization process parameters of machine tools is presented in **Chapter 2**. The available models and optimization methods are analysed to identify research gaps, and the study's objectives is identified based on the existing knowledge and research gaps. In **Chapter 3**, an empirical modelling to predict the energy consumption of the variable-power consumption machining process i.e. end facing is presented. In **Chapter 4**, the empirical model developed in previous chapter 3 is used as an input for the formulation of a multi-objective optimization model to select the optimal parameters leading towards minimum energy consumption and maximum material removal rate (productivity). In **Chapter 5**, the modelling of energy consumption of machine tools for machining cylindrical parts is presented. The energy consumption of a machine tool is divided into different energy modules and their models are established. The energy consumption models of the different energy modules and the developed model of the VPC machining process in Chapter 3 is integrated to evaluate the

energy consumption of machine tools for machining cylindrical parts. In **Chapter 6**, the modelling to quantify carbon emissions of machine tools for machining cylindrical parts is presented. The causes of carbon emissions from machine tools for machining cylindrical parts are classified into various factors, and corresponding models are developed, and integrated to quantify the carbon emissions of machine tools for machining cylindrical parts. In **Chapter 7**, the application of soft computing techniques for the modelling of machine tool's performance indicators is presented. Three soft computing techniques are used to develop models and their performances are evaluated on five error indices. In **Chapter 8**, the multi-objective optimization for low carbon emission and high efficiency in terms of carbon emission and power factor, surface roughness, and material removal rate is developed. This chapter also investigates the impact of the response weighting methods on the optimization results. Finally, **Chapter 9** summarises the modelling and optimization efforts, the limitations of the present work, and the direction of future research.

2.1. Introduction

The Intergovernmental Panel on Climate Change (IPCC) has repeatedly cautioned about the severe effect of rising temperature on ecosystem (IPCC, 2014, 2007, 2001; Pye et al., 2021). Therefore, the notion of net-zero greenhouse gas (GHG) emissions is attracting a lot of interest from climate change researchers in order to prevent global warming and its negative consequences on ecosystems. The use of fossil fuels (coal, oil, and natural gas) to meet global energy demand is the leading source the GHGs. Fossil fuels are expected to rise to 35.4 Gigatons in 2035 (Campatelli et al., 2015), and despite increased usage of renewable energy, fossil fuels will remain the largest source of primary energy in 2050 (U.S. EIA, 2021). Figure 2.1 illustrates a historical perspective of global and Indian carbon dioxide (one of the primary GHGs) emissions.

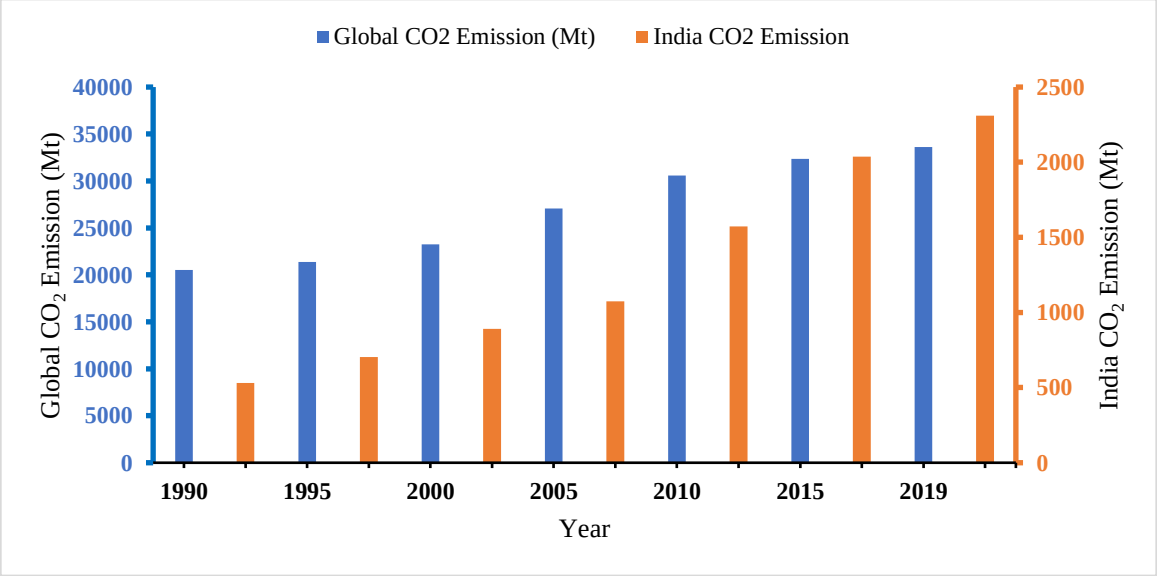

Figure 2.1 Illustrates a historical perspective of global and Indian carbon dioxide emissions.

According to the US Energy Information Administration, global energy demand will double by 2050 compared to 2020 (U.S. EIA, 2021), with the industrial sector serving as the primary energy user in several countries worldwide (U.S. EIA, 2017, 2016). Figure 2.2 illustrates the total and industrial energy consumption historical trends (a) Global scenario (b) Indian scenario.

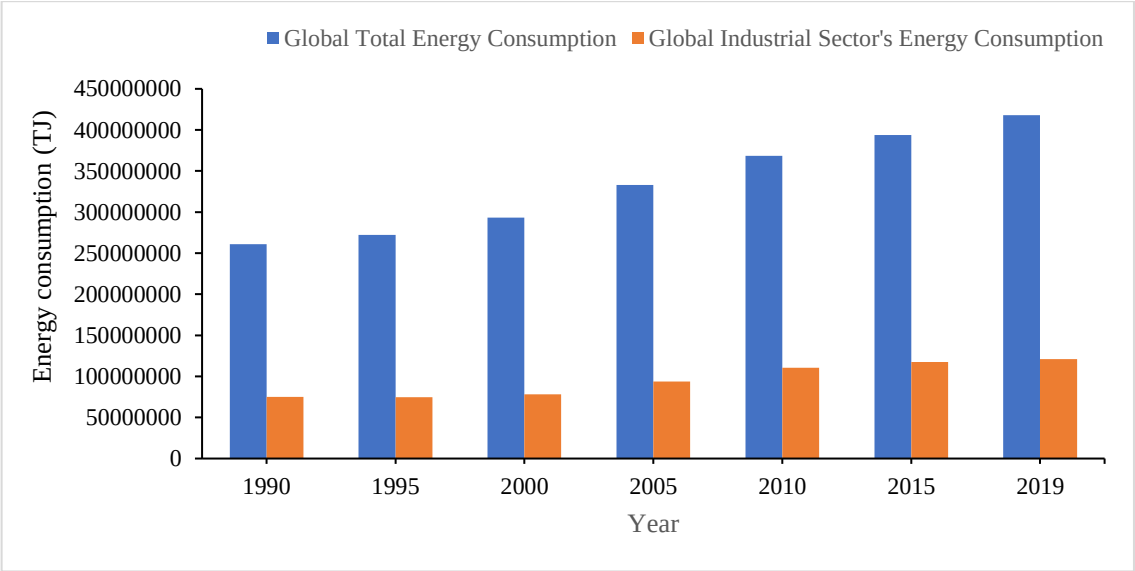

(a) Global total and industrial energy consumption

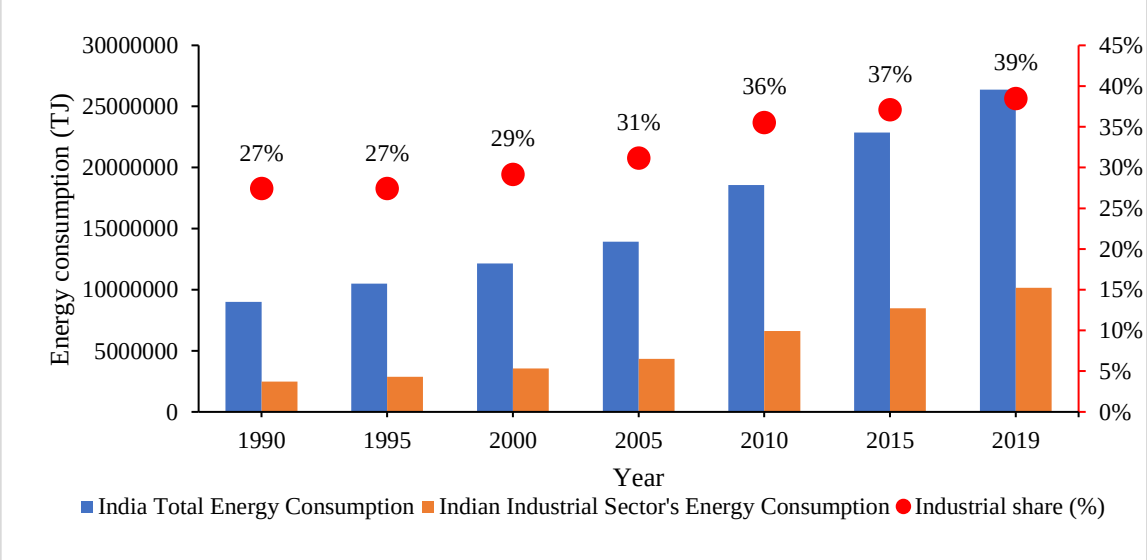

(b) India's total and industrial energy consumption

Figure 2.2 Historical trends of total vs industrial sector energy consumption (a) Global scenario and (b) Indian scenario.

Manufacturing is a vital part of the industrial sector and among the most important activities for the growth of the economy, but it also accounts for more than 30% of global total energy consumption (Diaz-Elsayed et al., 2015; Xie et al., 2021) and 36% of GHG emissions (Sealy et al., 2016; Sihag and Sangwan, 2020). Machining is vital for transforming raw materials into finished products in manufacturing industries. Machine tools are one of the most common equipment and machinery used to manufacture components, with sales of $144.6 billion in 2018 and an expected $174 billion in 2023 (Triebe et al., 2021). The machine tools e.g. lathe, milling and drilling, are commonly used in discreet part manufacturing and consume a significant amount of the total energy demand of the manufacturing industry i.e. 90% (Liu et al., 2020; Lv et al., 2016; Triebe et al., 2021; Tuo et al., 2018) with low energy efficiency (Ji et al., 2020; Xie et al., 2021). For instance, in one year, a machine tool emits CO_2 equivalent to 61 sports utility vehicles (Liu et al., 2015). The machine tools' average energy efficiency was approximately 30% (Liu et al., 2015; Xie et al., 2021), and in one of the investigations, Gutowski et al. (2006) reported the machine tool's energy efficiency less than 15%. Several prior studies have found that the energy utilisation phase of machine tools is responsible for almost 99% of their environmental impacts (Xie et al., 2016). The low energy efficiency and high energy consumption of machine tools signify a lot of scope for energy savings and reduced environmental effect. As a result, the administrative authorities, academician and industry professionals are becoming increasingly interested in promoting the energy efficiency of machine tools. For example, in Eco-design directive 2009/125/EC, the European Commission listed machine tools as one of the key products in its 2020 vision, a 37% reduction in United Kingdom’s carbon emissions by 2020 compared to 1990 (Schudeleit et al., 2016; Xie et al., 2021). Hence, Machine tools have a high potential to save energy consumption and reduce GHG emissions. Therefore, reducing the energy consumption of

the machine tool is one of the major challenges for the industries to meet sustainable manufacturing (Diaz-Elsayed et al., 2015; Hu et al., 2017; Xiao et al., 2019).

As previously stated that the potential strategies for reducing energy consumption and carbon emissions in the manufacturing sector can be achieved either by development of energy-efficient machine tools or by optimizing existing machine tools and machining processes (Jiang et al., 2022; Warsi et al., 2018). Given the large amount of existing machine tools in use, the first strategies require solid economic provisions for technological development and can only be implemented by replacing existing production lines. The second approach can be implemented with relative ease and lesser resources. Parameter optimization of existing machining processes and machine tools can be applied to existing production lines with relative ease and with minimal resources (Bagaber and Yusoff, 2019; Hu et al., 2020). Previous research has shown that by selecting the optimal process parameters, energy consumption and associated CEM can be reduced by up to 40% (Chen et al., 2021; H. Zhang et al., 2017). As a result, process parameters play a crucial role in machining, and selecting the correct parameters is critical for energy-efficient machining (Zhou et al., 2019). A survey of the available literature reveals several advances in this area. First group of researchers attempts to address this issue by modelling and assessing the energy consumption of CNC machine tools, processes, and systems. Second group of rising number of authors are focusing on evaluating the CEM of machining operations. The third group is involved with process optimization. The current literature review is divided into two sections. The modelling of energy consumption and CEM for the machining process and machine tools is presented in the first section: Section 2.2. The second section: Section 2.3, focuses on the advancement of optimization in the literature.

2.2. Modelling of Energy Consumption and Carbon Emissions of Machine Tools

Modelling and optimization approaches are prerequisites for selecting optimum process parameters, leading to minimum energy consumption in a machining process. The energy consumption model is beneficial for predicting the energy requirement of a particular product in its initial development stage and identifying the most energy-efficient process parameters (Bhushan, 2013; Li et al., 2013; Sato et al., 2018).

Change in Process parameters have a significant impact on energy consumption and the associated CEM of machine tools (Newman et al., 2012). Unreasonable cutting parameters can result in increased energy consumption and associated carbon emissions. Previous research has shown that the appropriate selection of process parameters can reduce energy consumption and associated carbon emissions by up to 40% (Zhao et al., 2021).

2.2.1. Energy consumption modelling

Various empirical models are proposed by authors in the literature as a function of process parameters to assess the energy consumption of the machining process. The significant studies are discussed in the following paragraphs:

Early studies on machining process energy consumption attempted to develop models for predicting the tool tip-work interface energy consumption, i.e. the energy required to remove material from the workpiece in the form of chips. Researchers (Bayoumi et al., 1994; Chetan et al., 2018; Dautzenberg et al., 1981; HA et al., 2004; Munoz and Sheng, 1995; Pawade et al., 2009; Shao et al., 2004; Wang et al., 2016) established theoretical energy consumption model based on metal plastic deformation analysis. Dautzenberg et al. (1981) model is one of the primary models for estimating the energy consumption for the material removal in a machining process. He divided the cutting zone into primary and secondary shear zones and developed the following model:

$$E_{cut} = E_P + E_S = \frac{\tau}{n+1}(cot\phi + \frac{\tan(\phi+\gamma_0)^{n+1} a_e \times f \times V_c}{\sqrt{3}}) + F_f \times V_{ch} \quad (1)$$

Where E_{cut}, E_p and E_S represents the cutting energy, cutting energy of primary shear zone and cutting energy of secondary shear zone. $\tau, \phi, \gamma_0, n, a_e, f, V_c$ and F_f represents the shear stress, shear angle, strain hardening exponent, width of cut, feed rate, cutting velocity and friction force respectively. Bayoumi et al. (1994) developed a model for specific cutting energy (SCE) consumption as a function of process parameters as shown in Eq. (2). He reported that the chip's friction, flank wear, and thickness have a significant impact on cutting power consumption.

$$SCE_{eff} = \frac{K_{neff}\left(F + GK_{feff}\right)}{\sin\theta_h} + \frac{k_{nfeff} \times k_{ffeff} \times cos\theta_h \times l_f}{f_t\left(1 - cos\alpha_{en}\right)} \quad (2)$$

Where SCE_{eff} represents the effective SCE. $K_{neff}, K_{feff}, K_{nfeff}, K_{ffeff}, F, f, \theta_h, l_f, \alpha_{en}$ represents the effective average pressure, effective average friction, effective flank pressure, effective flank friction, cutting force, feed rate, cutting helix angle, width of the flank wear land and radial engagement angle respectively. Munoz and Sheng (1995) developed a cutting energy consumption model as shown in Eq. (3). The model incorporates the effect of lubrication and tool wear and is applicable for both orthogonal and oblique machining.

$$E_{cutting} = \left(\frac{\cos(\beta-\gamma) \times cos\eta_s \times cos\lambda + \cos(\varphi+\beta-\gamma)}{\cos(\varphi+\beta-\gamma)}\right) \times \left(\frac{\tau \times MRV}{sin\varphi \times cos\lambda}\right) \quad (3)$$

Where, β, γ, η_s, λ, φ represents the normal friction angle, normal rake angle, shear flow angle, oblique angle and shear plane angles in radian respectively. τ represents the workpiece flow stress in N/mm^2. Shao et al. (2004) quantifies cutting power while taking

tool wear and the influence of the cutting environment into account during the face milling process and proposed the following model:

$$\bar{P} = Z \times n \times D \times a_p \times \frac{\left[K \times \bar{h}^{-c} \times f_z \times \left(\cos(\varphi_{in}) - \cos(\varphi_{in} + \psi) \right) + \mu \times H \times \overline{VB} \times \psi \right]}{2} \quad (4)$$

Where $\bar{P}$ is the average power consumption in Watt; a_p, c, f_z, h, H, K, $\overline{VB}$, Z, μ, φ_{in} and ψ represents the axial depth of cut in mm, chip thickness constants in mm, feed rate in mm/*tooth*, chip thickness in mm, Brinell hardness in N/mm^2, cutting force constants in *MN*/*m*, average flank wear in mm, number of teeth, coefficient of friction, angle of approach in rad and immersion angle in *rad*. HA et al. (2004) developed a SCE model for the orthogonal cutting of a metal matrix composite material as stated in Eq. (5). He divided the cutting energy into primary and secondary shear zone energy and the energy required to debond the particle from the matrix.

$$SEC = E_p + E_s + E_D \quad (5)$$

E_p, E_s and E_D represent the specific energies for plastic deformation in the primary zone, secondary shear zone and specific energy for debonding the particle from the matrix respectively. Pawade et al. (2009) divided the specific shearing energy (E_{ST}) consumption at tool-work interface into specific cutting energy of primary shear zone (E_{psz}) and specific cutting energy for ploughing (E_{splo}) and established the following model:

$$E_{ST} = E_{psz} + E_{splo} = \frac{\bar{\sigma}\bar{\varepsilon}}{n+1} + \frac{F_{Sp} \cos\zeta_s V_s}{a_e f V_c} \quad (6)$$

Where $\bar{\sigma}$, $\bar{\varepsilon}$, n, F_{SP}, a_e, f, V_c and V_s are flow stress, shearing strain, strain hardening exponent, ploughing force component, width of cut, feed, cutting velocity and shear

velocity respectively. Wang et al. (2016) divided the cutting energy of the tooltip into three parts: the energy of the primary shear zone (E_p), the energy required to overcome frictional forces (E_f), and the kinetic energy of the flowing chip (E_k) and proposed the following model:

$$E = E_p + E_f + E_k = \int_0^{\gamma} \tau \times (\gamma, \dot{\gamma}, T) d\gamma + \frac{\overline{\tau_s} \times A_s \times V_c \times \sin\beta}{a_C \times a_w \times \cos(\varphi + \beta - \gamma_0)} + \frac{\rho \times V^2 \times \sin^2 \varphi}{2 \times \cos^2(\varphi - \gamma_0)} \quad (7)$$

V is the cutting speed, V_c is the chip sliding speed along the tool rake face, V_s is the chip shearing speed along the primary deformation zone, a_c is the undeformed chip thickness, a_w is the cutting width parallel to cutting edge, $\overline{\tau_s}$ average shear stress , S is the width of the adiabatic shear band, L is the upper boundary displacement of the adiabatic shear band, α is the tool rake angle, φ is the shear angle between shear plane and shear strain and β is the friction angle.

The models mentioned so far were significant, but they only account for the tooltip energy consumption of the machine tool. Filippi and Ippolito (1981) investigated the energy consumption of ten different machine tools. They found that although the energy needed for material removal was significant in each machine tool, the total energy demand of a machine tool was predominant. Gutowski et al. (2006) model is one of the primary studies addressing the total power consumption of a machine tool, as shown in Eq. (8). He proposed an empirical model as a functional relationship between power consumption and material removal rate (MRR).

$$P_{total} = P_o + k \times MRR \quad (8)$$

Where P_{total} and P_o are the total power and idle power in kW respectively. *k* represents the constant in kJ/cm^3. Li and Kara (2011) modified the Gutowski et al. (2006) equation and proposed a specific energy consumption (specific energy is the energy consumed in removing per unit volume of material) model as written in Eq. (9).

$$SEC = C_o + \frac{C_1}{MRR} \tag{9}$$

Where SEC represents the specific energy consumption. C_0 and C_1 are machine tool-specific coefficients. Li et al. (2013) segregated the idle power into standby power and spindle rotation power and proposed a modified power consumption and SEC model, as shown below.

$$P_{total} = P_{standby} + k_1 \times n + b + k_o \times MRR$$

$$SEC = \frac{P_{total}}{MRR} = k_o + \frac{k_1.n}{MRR} + \frac{k_2}{MRR} \tag{10}$$

Where n is spindle rotation per minute, k_o is machining process-specific constant, $k_2 = P_{standby} + b$, k_1 and b are specific coefficients of the spindle motor. However, the models (Gutowski et al., 2006; Li et al., 2013; Li and Kara, 2011) could not include the effect of the input parameters on power consumption. Zhou et al. (2017) proposed a modified model that includes MRR, spindle rotation and the machining parameters, as shown in Eq. (11).

$$P_{total} = C_1^{'} + C_2^{'} \times n + C_3^{'} \times n^{C_4^{'}} \times v_f^{C_5^{'}} \times d_c^{C_6^{'}} \times a_e^{C_7^{'}}$$

$$SEC = \frac{P_{total}}{MRR} = \frac{C_1^{'}}{MRR} + \frac{C_2^{'} \times n}{MRR} + \frac{C_3^{'} \times n^{C_4^{'}} \times v_f^{C_5^{'}} \times d_c^{C_6^{'}} \times a_e^{C_7^{'}}}{MRR} \tag{11}$$

Where $c_1^{'} \sim c_7^{'}$ are fitting constants, v_f is feed rate in mm/min, d_c is cutting depth in mm and a_e is the width of cut in mm. Guo et al. (2012) revealed that the workpiece's diameter also significantly influences the energy consumption of the turning process. He pointed out that to maintain a particular cutting speed during the turning process, the diameter of the workpiece affects the spindle speed. Therefore, Guo et al. (2012) incorporated workpiece diameter into the SEC model, as shown in Eq. (12).

$$SEC = \frac{C_1}{v_c \times f_r \times d_c} + c_2 \times v_c^{c_3} \times f_r^{c_4} \times d_c^{c_5} \times D_o^{c_6} \tag{12}$$

Where $c_1 \sim c_6$ are fitting coefficients and D_o is workpiece diameter in *mm*, f_r is feed rate in *mm/rev* and v_c is cutting speed in *m/min*.

Balogun et al. (2015) investigated the influence of the chip thickness, tool wear, cutter nose radius and cutting environment on the specific cutting energy (SCE) consumption and developed an energy consumption model for the machining process by dividing the entire energy requirement into basic energy, ready energy, and cutting energy as shown in Eq. (13). He reported that the machining parameters significantly influence the SCE and indeed the total energy consumption of machine tools.

$$E_{total} = \left(P_{basic} \times t_{basic}\right) + \left(P_{ready} \times t_{ready}\right) + \left(k \times Q \times t_{cutting}\right) \tag{13}$$

Where E_{total} is total energy consumption; P_{basic} and P_{ready} are the power consumption in the basic and ready state respectively; t_{ready} and $t_{cutting}$ are the time of ready and cutting state; k is the specific cutting energy coefficient (J/mm^3) and Q is the MRR (mm^3/s). Edem and Balogun (2018) investigated the effect of cutting edge radius on the SCE and surface roughness and stated that energy efficiency can be enhanced by machining parts with

smaller cutting-edge radius inserts. Warsi et al. (2018) studied the SCE and SEC for high-speed machining and developed energy consumption maps indicating high and low specific energy consumption zones.

Other strategies for modelling the energy consumption of machine tools include disaggregating the machine tool's energy consumption into energy-consuming elements such as the spindle, feed axis, coolant pump, tool change system, and components that use constant energy. He et al. (2012) evaluated the total energy consumption of a machine tool by dividing it into fixed energy, coolant energy, feed energy, spindle energy and cutting energy and proposed the following model:

$$E_{total} = E_{spindle} + E_{feed} + E_{tool} + E_{cool} + E_{fix} \tag{14}$$

Where E_{total} is the total energy consumption; $E_{spindle}$, E_{feed}, E_{tool}, E_{cool} and E_{fix} are the energy consumption of spindle, feed table, tool indexing, coolant spray, and the basic energy consumption respectively. Yoon et al. (2014) proposed a model of total energy consumption by dividing it into basic energy, spindle rotational energy, worktable feed energy and cutting energy. He stated that tool wears significantly impacts cutting power consumption, which he incorporated into the energy consumption model shown in Eq. (15).

$$E_{total} = \int \left\{ f_1\left(n, f, a_p\right) + \left(f_2, n, f, a_p\right) \times \overline{VB}\left(t\right) \right\} dt \tag{15}$$

Where $f_1\left(n, f, a_p\right)$ is a second order function of process parameters: spindle speed (n), feed rate (f) and depth of cut (a_p) and $\overline{VB}\left(t\right)$ is the function of tool flank wear.

Balogun and Mativenga (2013) introduced a new state called ‘Ready state’ between the ‘Basic (idle) state’ and ‘Cutting state’ of a machine tool and evaluated the energy

consumption as shown in Eq. (16). In the ready state, the spindle reaches the target speed for the required cutting speed, and the feed drives bring the tool and workpiece to the cutting position.

$$E_{total} = E_b + E_r + P_{tc}t_{tc}\left[INT\left(\frac{t_c}{T}\right)+1\right] + P_{air}t_{air} + \left(mN + C + P_{cool} + k\dot{v}\right)t_c \quad (16)$$

Where E_b and E_r represents the basic state and ready state energy consumption respectively. P_{air} and P_{cool} represents the air cut and coolant pump power consumption in *Watt* respectively. t_c t_b, t_r and t_{air} represents the cutting, basic, ready and air cut state time in *s* respectively. k is the SCE in *kJ/cm*^{3}, m is the coefficient, N is the spindle speed in *rev/min* and $\dot{v}$ is the MRR in cm^3/s. Edem and Mativenga (2017) predicted total energy consumption by modelling the energy demand of different CNC machine tool numerical codes, as shown in below Eq. (17).

$$E_{total} = E_b + P_{tc}t_{tc}\left[INT\left(\frac{t_c}{T}\right)+1\right] + P_{spindle\_run}t_{spindle\_run} + P_c t_c + P_{feed}t_{feed} + P_{cool}t_{cool} \quad (17)$$

Where $P_{feed} = P_{G01/G02/G03\_feed} + P_{G00\_feed(approach)} + P_{G00\_feed(retract)}$. Edem and Mativenga (2016) incorporated the weight of the feed drive and workpiece into the energy consumption model and improved the practical applicability of the energy model in actual machining. The proposed model is shown in Eq. (18).

$$E_f = P_0 \times t_{cy}\left(a \times W_{v_f} + b \times W\right)t_{cy} + F_f \times v_c \times t_c \quad (18)$$

Where, P_0 is idle power consumption in *Watt*, W is total weight including weight of the feed axis, vice and workpiece, P_{f_x} and P_{v_y} are power consumption of x and y feed axis

respectively in *Watt*, F_f and v_f is feed force and feed axes velocity respectively, t_{cy} and t_c are the total cycle time and actual cutting time respectively. Kim et al. (2015) studied and analysed machine tool energy consumption by monitoring six machine tools and observed that cutting energy can be separated from total energy consumption. He divided the total power consumption into idle (P_{Idle}), coolant (P_{Cool}), spindle ($P_{Spindle}$), feed (P_{Feed}) and cutting (P_{cut}) energy consumption and proposed the following model:

$$P_{total} = P_{Idle} + P_{Cool} + P_{Spindle} + P_{Feed} + P_{cut}; \begin{cases} P_{idle} = C_{1i} \\ P_{Cool} = C_{1c} \\ P_{Spindle} = C_{0_s}.RPM + C_{1_s} \\ P_{Feed} = C_{0_f}.Feedrate + C_{1_f} \\ P_{cut} = C_{0_m}.MRR + C_{1_m} \end{cases} \quad (19)$$

Where C_{0_s}, C_{1_f}, C_{0_m} C_{1_i} and C_{1_c} are the coefficients. Lv et al. (2016) investigated the energy consumption of seven machine tools including CNC lathes and milling. He developed parametric models for the non-cutting status: standby, coolant spraying, spindle rotation and feed axes and cutting status, as shown in Eq. (20). He reported that the cutting power is almost independent of the machine tool.

$$\text{Power models} = \begin{cases} P_s = C_{s1}n + C_{s0} \\ P_f = C_{f1}f_r + C_{f2}f_r^2 \\ P_{C\_turn} = C_T a_p^{x_T} f^{y_T} v^{n_T} \\ P_{C\_mill} = C_M a_p^{x_M} f_Z^{y_M} v^{n_M} a_e^{u_M} \end{cases} \quad (20)$$

Where P_s and P_f represent the spindle and feed power consumption respectively in Watt. C_{s1}, C_{s0}, C_{f1} and C_{f2} are the coefficients. P_{C_turn} and P_{c_mill} are the turning and milling power consumption respectively in Watt. a_p is the depth of cut in mm, f_r is feed rate in

mm/rev., v is the cutting speed m/min and n is the spindle speed in rev/min. C_T, x_T, y_T and n_T are coefficients of the turning power model and , C_M, x_M, y_M, n_M and u_M are coefficients of the milling power model.

Some researchers (Diaz et al., 2010; Huang et al., 2016; Liu et al., 2015; Mori et al., 2011) (Lv et al., 2017) investigated machine tools' transient states to enhance the energy consumption models' accuracy. The transient state is the process of transitioning between two steady states (Jia et al., 2017). Diaz et al. (2010) was one of the earliest studies to look into the transient state of machine tools (acceleration of the spindle and feed axis) and proposed a total energy consumption (E_{total}) model for machining tools, as shown in Eq. (21). He includes the fixed energy consumption (E_{const}), transient state energy consumption (E_{trant}) and steady-state energy consumption (E_{steady}).

$$E_{total} = E_{const} + +E_{trant} + E_{steady} + E_{cut} \tag{21}$$

Where $E_{cut} = k.d_c.a_p.z^b.f_r^{1-b}.n^b$, in which a_p is the width of cut, z is the number of flutes, b and k are fitting coefficients. Avram and Xirouchakis (2011) incorporated the spindle and feed axis acceleration and proposed the equation below for the one pass of the milling process. He estimated energy consumption using torque and angular velocity.

$$E_{per-pass} = \int_{t_0'}^{t_1'} P_{aY}\,dt + \int_{t_1'}^{t_2'} P_{SY}\,dt + \int_{t_2'}^{t_3'} P_{dY}\,dt + \int_{t_0'}^{t_3'} P_{run}\,dt + \int_{t_1'}^{t_3'} P_c\,dt \tag{22}$$

P_{aY} is Y axes feed acceleration power in *Watt*, P_{SY} is Y axes feed study state power in *Watt*, P_{dY} is Y axes power during deceleration in *Watt*, P_c is spindle power to cut material in Watt, P_{run} is spindle idle steady-state power in *Watt*. Mori et al. (2011) proposed a total

power consumption model that quantified different power consumption related to basic operations, material-cutting and spindle's steady and transient rotation shown as:

$$P_{total} = P_1 \times (T_1 + T_2) + P_2 \times T_2 + P_3 \times T_3 \quad (23)$$

Where P_1, P_2 and P_3 are the constant, cutting and feeding power consumption in *Watt* respectively; T_1, T_2 and T_3 are the cycle time of the non-cutting state, cutting state, position the work and accelerate the spindle respectively. Liu et al. (2015) investigated the energy consumption of the main driving system of a machine tool and developed the energy consumption model as shown in Eq. (24). He segregated the machining process into three periods: startup, idle and cutting. He developed empirical models for the energy consumption of the startup and idle periods as a function of spindle speed and used a cutting parameter-based exponential model for the cutting power.

$$E_{total} = \sum_{j=1}^{Q_s} \left(\chi_1 \times n_j^2 + \chi_2 \times n_j + \chi_3 \right) + \sum_{j=1}^{Q_u} \left(P_{uj} \times t_{uj} \right) + \sum_{j=1}^{Q_c} \left[\int_0^{t_{cj}} \begin{pmatrix} \left(\propto_{2j} \times P_c^2 \right) + \\ \left(\left(1 + \propto_{1j} \right) \times P_c \right) + P_{uj} \end{pmatrix} dt \right] \quad (24)$$

Where n is the spindle speed in rpm; P and t power consumption and time; subscript s, u and c denote startup, unload (idle) and cutting, respectively; Q_s Q_u and Q_c represents the number of startup periods, idle periods, and cutting periods respectively; α_1 and α_2 are the constants.

Researchers (Huang et al., 2016; Lv et al., 2017) highlight that spindle acceleration is one of machine tools' major energy-intensive transient states. Huang et al. (2016) analyzed the power characteristics of one primary energy-intensive machine tool module, spindle acceleration, and developed an energy consumption model as shown in Eq. (25). He

categorized the spindle acceleration power profile into three curves: linear, thermite and cubical.

$$E_{spindle_{st}} = \int P_{st1_{n_s}}\, dt + \int P_{st2_{n_s}}\, dt + \int P_{st3_{n_s}}\, dt \tag{25}$$

Where $P_{st1_{n_s}}$, $P_{st2_{n_s}}$ and $P_{st3_{n_s}}$ are the power corresponding to the linear curve, thermite curve and cubic curve function respectively. Lv et al. (2017) investigated the spindle acceleration power characteristics and proposed an inertial-based energy prediction model for the spindle acceleration energy consumption (E_{SA}), as shown below.

$$E_{SA} = \int_0^{t_{SA}} P_{SA}\, dt \tag{26}$$

Where $P_{SA} = P_{SR} \times (n) + T_{SA} \times w_M$. P_{SA} and P_{SR} represents the spindle acceleration and spindle rotation power in *Watt*. t_{SA} represent the time period of spindle acceleration in *s*. T_{SA} is the acceleration torque in *N-m*, w_M is the angular speed of the spindle motor in *rad/s*.

Energy efficiency research on machining systems has received attention to minimise energy consumption and increase energy efficiency. Liu et al. (2017) established an energy efficiency (η_{EE}) evaluation model for the machine tool using the machine tool's primary data, spindle speed, and input power data, as presented in Eq (27).

$$\eta_{EE} = \frac{\sqrt{c_t^2 s_t^2 \left(c_i s_i + 1\right)^2 + 4 c_m s_m c_t^2 \left(c_i s_i + 1\right)\left(P_{cnc,i} - P_{cnc,u}\right)} - c_t s_t \left(c_i s_i + 1\right)}{2 c_m s_m c_t^2 \left(c_i s_i + 1\right)} \tag{27}$$

Where $P_{cnc,u}$ and $P_{cnc,i}$ are the idle power consumption and input power consumption in *Watt* respectively, c_m and s_m are the basic coefficient of the motor, c_i and s_i are the basic coefficient of frequency inverter; c_t and s_t are the basic coefficient of the machine tool.

Xie et al. (2021) proposed a torque and angular velocity-based energy efficiency monitoring methodology for machine tools, as shown in Eq. (28). He split the energy consumption of machine tools into idle and cutting modules to develop the energy efficiency model.

$$\eta_{EE} = \frac{-g^{'}(w_s) \times w_s + \sqrt{g^{'2}(w_s) + 4 f^{'}(w_s)(I_s - I_{s0}(w_s)) \times w_s}}{2P_{in} \times f^{'}(w_s)} \tag{28}$$

Where P_{in} is the input power of the machine tool. w_s is the angular velocity of the spindle. $I_{s0}(w_s)$ is the idle current of spindle motor at the given angular velocity. I_s is the equivalent current of the spindle system. $g^{'}(w_s)$ and $f^{'}(w_s)$ represent the coefficients of the current increment model of the machine tool in the cutting state. Da Costa et al. (2022) highlighted the significance of the conventional lathe machine tools in the micro-scale manufacturing industries and proposed an energy efficiency model:

$$\eta_{EE} = \frac{P_E - L_{Gz}}{P_E} \tag{29}$$

Where P_E and L_{Gz} are the input electric power and idle loss power respectively.

Some researchers adopted specific approaches to model the energy consumption of machine tools, such as treating machine tools as thermodynamic systems (Imani Asrai et al., 2018) and Therblig-based modelling (Lv et al., 2014). Imani Asrai et al. (2018) evaluated the energy consumption of a milling process by considering the machine tool as a thermodynamic system and developed the energy consumption model as:

$$P_{total} = \begin{bmatrix} C + \left(A_f \times f + B_f \times f^2 + D_f \times f^3\right) + \left(A_s \times s + B_s \times s^2 + C_s \times s^3 + D_s \times s^4\right) + \\ \left(\left(E + F_f \times f + F_s \times s + G_s \times s^2 + G_f \times f^2\right) \times \left(MRR\right)\right) + \left(K \times \left(MRR^2\right)\right) \end{bmatrix} \tag{30}$$

Where f and s are feed rate and spindle speed respectively; $A_f \sim D_f$, $A_s \sim D_s$ E, F_f, F_s, G_s and G_f are the constants. Lv et al. (2014) developed a Therblig-based energy model to evaluate the total power demand of a machine tool, as shown in Eq. (31). He used parametric-base empirical models to estimate the power consumption related to different Therbligs.

$$P_{total} = P_{so} + P_L + P_{CPM} + P_{SR} + P_{FD} + P_{TC} + P_{cut} \quad (31)$$

Where P_{SO}, P_L, P_{CPM}, P_{SR}, P_{FD}, P_{TC} and P_C are the power of therblig of standby operation, lightening, coolant spraying, spindle rotation, feed, tool selection, and cutting. He et al. (2016) established parametric process models for the machine tool's different movements (spindle rotation, feed drive motions and material cutting) and then integrated them with standby and coolant power consumption to evaluate the total energy consumption of the machine tool. Afterwards, the developed model was coupled with CAM file software to predict energy consumption for machining a part. Rief et al. (2017) classified machining energy consumption into four categories: basic energy demand of the machine tool, energy required in material removal (cutting energy), energy consumption in coolant systems, and energy required in tool manufacturing and proposed total energy consumption model.

In recent years, studies (Luan et al., 2019; Zhou et al., 2022) have focused on machine tools' non-cutting status energy consumption. Luan et al. (2019) focused on the non-cutting status energy consumption of machine tools, including spindle power consumption and feed power (x,y,z-up and z-down) and proposed the following parametric models:

$$P_{non-cutting}=\begin{cases} P_{SR}=\begin{cases} C_1n+C_2n^2+C_0 & (0<n\le n_1) \\ C_1n+C_2n^2+C_0 & (n_1<n\le n_2) \\ \cdots & \cdots \\ C_1n+C_2n^2+C_0 & (n_{n-1}<n\le n_{max}) \end{cases} \\ P_{xf}=C_xv_f+b_{1x}v_f^2-b_{2x}v_f^3+\ldots...+b_{nx}v_f^n \\ P_{xf}=C_xv_f+b_{1x}v_f^2-b_{2x}v_f^3+\ldots...+b_{nx}v_f^n \\ P_{yf}=C_yv_f+b_{1y}v_f^2-b_{2y}v_f^3+\ldots...+b_{ny}v_f^n \\ P_{z-up}=\begin{pmatrix} C_{z-up}v_{fz-up}+b_{1z-up}v_{fz-up}^2-b_{2z-up}v_{fz-up}^3+ \\ \ldots...+b_{nz-up}v_{fz-up}^n \end{pmatrix} \\ P_{z-down}=\begin{pmatrix} C_{z-down}v_{fz-down}+b_{1z-down}v_{fz-down}^2-b_{2z-down}v_{fz-down}^3+ \\ \ldots...+b_{nz-down}v_{fz-down}^n \end{pmatrix} \end{cases} \tag{32}$$

Where n is the spindle speed, v_f is the feed rate and $C_{x/y/z-upand/z-down}$ represents the corresponding fitting coefficient. Zhou et al. (2022) investigated machine tool non-cutting power consumption: standby and auxiliary power. He presented empirical models for machine tools' weak and strong current demands. The models for the standby power consumption ($P_{s\tan dby}$) are shown in Eq. (33).

$$P_{s\tan dby}=\begin{cases} P_{control}+P_{screen}+P_{fan} & \text{(weak current loop)} \\ P_{control}+P_{screen}+P_{fan}+P_{\text{lub}}+\text{P}_{spcool} & \text{(strong current loop)} \end{cases} \tag{33}$$

Where $P_{control}$, P_{screen}, P_{fan}, P_{lub} and P_{spcool} represents the power consumed by the control system, display system, fan device, basic lubrication device and the spindle forced cooling device respectively. For auxiliary power (P_{aux}):

$$P_{aux}=P_{light}i_1+P_{spray\_cool}i_2+P_{tool\_change}i_3+P_{chip\_remove}i_4+P_{spray\_air}i_5 \tag{34}$$

Where P_{light}, P_{spray_cool}, P_{tool_change}, P_{chip_remove} and P_{spray_air} represents the power of lighting device, the cutting fluid injection device, the tool changing device, the chip removal device, and the blowing cleaning or blowing cooling device respectively; $i_1 \sim i_5 = 0$ or 1 (0 represents turn off status of the device; 1 represent turn on status of the device)

Furthermore, several researchers (Bhinge et al., 2017; Brillinger et al., 2021; Garg et al., 2016, 2015; Pan et al., 2021) used artificial intelligence-based algorithms to assess the energy consumption of machine tools. Garg et al. (2016) applied soft computing approaches such as genetic programming (GP), support vector regression (SVR), and Multi-adaptive regression splines (MARS) to develop tool life and power consumption models. He evaluated the model's performance using various statistical indicators and found that the GP outperformed SVR and MARS. In another study. In another work, Garg et al. (2015) used complexity-based multi-gene GP to model the energy consumption of the milling process. Garg and Lam (2015) proposed an ensemble-based-Multi Gene GP (EN-MGGP) to model the surface roughness, tool life and power consumption. Literature shows that an increasing number of authors employed soft computing for modelling in different engineering applications (Abd and Abd, 2017; Garg et al., 2016, 2014; Gupta, 2010; Iqbal and Dar, 2011; Liman et al., 2021; Naseri et al., 2017; Shafiullah et al., 2019; Su et al., 2021; Tseng et al., 2016; Vukman et al., 2020; Zhang and Zhang, 2016).

Pan et al. (2021) used a generative adversarial imputation networks-based data-driven approach to model the energy consumption of the machine tool as:

$$E_{total} = \int \left(P_{st} + P_u + P_{cut} + P_a \right) dt \tag{35}$$

Where P_{st}, P_u, P_{cut} and P_a is the power of standby power, unload power, cutting power, and additional loss; t is the cutting time. Bhinge et al. (2017) developed a generalized energy prediction model for a machine tool based on Gaussian process regression, as shown in Eq. (36).

$$E_q = \sum_{\left\{ \left(x^i, y^i \right) \in D_q \right\}} \mu_q \left(x^i \intercal D_q \right) \times l^i \tag{36}$$

Where E_q is the total energy consumption, x^i and y^i are the input and output features respectively, l^i is the length of the cut, q is the type of machining process and $\mu_q\left(x^i \intercal D_q\right)$ is the mean energy density function. Brillinger et al. (2021) developed a machine learning-based energy prediction model for a CNC machining process as follows:

$$E_{total} = \sum_{i=1}^{n}\sum_{j=1}^{m} P_{ij}\Delta t \tag{37}$$

Where E_{total} is the total energy consumption, P_{ij} is the power consumption, n and m are the numerical control instruction and consecutive measurements results respectively. Liu et al. (2020) developed a dynamic energy consumption model for the feed axes of machine tools using the bond graph approach, as shown in Eq. (38).

$$E(t) = \int \frac{Se_1 \times p_{16}}{m_x \times I_{16}}.dt \tag{38}$$

Zhang et al. (2022) employed a similar approach to model spindle energy consumption, as shown below.

$$E(t) = \int_0^t \frac{Se_1 \times p_8}{I_8}.dt \tag{39}$$

where $E(t)$ is the system (i.e. feed axis and spindle) energy consumption in *J*. Se_1 represent the effort source. p_{16} and p_8 represents the generalized momentum of the feed axis and spindle respectively, m_x is the conversion constant of the ball screw nut pair. I_{16} and I_8 represents the inertial elements of the feed axis and spindle respectively.

A summary of energy consumption evaluation models of machine tools, along with their strengths and limitations, are presented in Table 2.1.

Table 2.1 A summary of machine tool energy consumption evaluation models

Author (s)	Model	Strength (s)	Limitation (s)
Dautzenberg et al. (1981)	$E_{cut} = E_P + E_S = \frac{\tau}{n+1}(cot\phi + \frac{\tan(\phi+\gamma_0)^{n+1} a_e \times f \times V_c}{\sqrt{3}}) + F_f \times V_{ch}$ Where E_{cut}, E_p and E_S represents the cutting energy, cutting energy of primary shear zone and cutting energy of secondary shear zone. $\tau, \phi, \gamma_0, n, a_e, f, V_c$ and F_f represents the shear stress, shear angle, strain hardening exponent, width of cut, feed rate, cutting velocity and friction force respectively	One of the primary models to evaluate the material removal energy consumption	Only evaluates the energy consumption of material removal (tooltip).
Bayoumi et al. (1994)	$SCE_{eff} = \frac{K_{neff}\left(F + GK_{feff}\right)}{\sin\theta_h} + \frac{k_{nfeff} \times k_{ffeff} \times cos\theta_h \times l_f}{f_t\left(1 - cos\alpha_{en}\right)}$ Where SCE_{eff} represents the effective SCE. $K_{neff}, K_{feff}, K_{nfeff}, K_{ffeff}, F, f, \theta_h, l_f, \alpha_{en}$ represents the effective average pressure, effective average friction, effective flank pressure, effective flank friction, cutting force, feed rate, cutting helix angle, width of the flank wear land and radial engagement angle respectively	Investigated the influence of cutting speed, feed rate and flank wear land width on SCE.	Only evaluates the specific cutting energy of material removal (tooltip).

Munoz and Sheng (1995)	$E_{cutting} = \left[\left(\frac{\cos(\beta-\gamma)\times cos\eta_s \times}{\cos(\varphi+\beta-\gamma)} \right) \times \left(\frac{\tau \times MRV}{sin\varphi \times cos\lambda} \right) \right]$ Where, β, γ, η_s, λ, φ represents the normal friction angle, normal rake angle, shear flow angle, oblique angle and shear plane angles in radian respectively. τ represent the workpiece flow stress in *N/mm²*	Incorporates lubrication and tool wear effects and the model applicable to both orthogonal and oblique machining	Only evaluates the energy consumption of material removal (tooltip).
Shao et al. (2004)	$\bar{P} = Z \times n \times D \times a_p \times \left[\frac{\left[K \times \bar{h}^{-c} \times f_z \times \left(\cos(\varphi_{in}) - \cos(\varphi_{in}+\psi) \right) + \mu \times H \times \overline{VB} \times \psi \right]}{2} \right]$ Where $\bar{P}$ is the average power consumption in *Watt*; a_p, c, f_z, h, H, K, $\overline{VB}$, Z, μ, φ_{in} and ψ represents the axial depth of cut in *mm*, chip thickness constants in mm, feed rate in *mm*/*tooth*, chip thickness in mm,	Considered the effects of tool wear and cutting environment on the tooltip power consumption	Only evaluates the tooltip power consumption

	Brinell hardness in N/mm^2, cutting force constants in MN/m, average flank wear in mm, number of teeth, coefficient of friction, angle of approach in rad and immersion angle in rad		
HA et al. (2004)	$SEC = E_p + E_s + E_D$ E_p, E_s and E_D are specific energy for plastic deformation in primary zone, in the secondary shear zone and specific energy for debonding the particle from the matrix	Evaluates the tooltip power consumption of orthogonal cutting of a metal matrix composite material	Only evaluates the power consumption of material removal (tooltip).
Pawade et al. (2009)	$E_{ST} = E_{psz} + E_{splo} = \frac{\overline{\sigma\varepsilon}}{n+1} + \frac{F_{Sp} cos\zeta_s V_s}{a_e f V_c}$ Where $\bar{\sigma}$, $\bar{\varepsilon}$, n, F_{SP}, a_e, f, V_c and V_s are flow stress, shearing strain, strain hardening exponent, ploughing force component, width of cut, feed, cutting velocity and shear velocity respectively	Evaluates the specific shearing energy consumption of material removal	Only evaluates the specific shearing energy consumption of the tooltip interface
Wang et al. (2016)	$E = E_p + E_f + E_k$ $= \left[\int_0^{\gamma} \tau \times (\gamma, \dot{\gamma}, T) d\gamma + \frac{\overline{\tau_s} \times A_s \times V_c \times \sin\beta}{a_C \times a_w \times \cos(\varphi + \beta - \gamma_0)} + \frac{\rho \times V^2 \times \sin^2 \varphi}{2 \times \cos^2(\varphi - \gamma_0)} \right]$ V is the cutting speed, V_c is the chip sliding speed along the tool rake face, V_s is the chip shearing speed along the primary deformation zone,		Tooltip material removal energy consumption modelled only

	a_c is the undeformed chip thickness, a_w is the cutting width parallel to the cutting edge, $\overline{\tau_s}$ average shear stress , S is the width of the adiabatic shear band, L is the upper boundary displacement of the adiabatic shear band, α is the tool rake angle, φ is the shear angle between the shear plane and shear strain β is the friction angle		
Gutowski et al. (2006)	$P = P_o + k \times MRR$ Where P and P_o are the total power and idle power in kW respectively, and k is a constant in kJ/cm^3	An exergy-based empirical model between energy consumption and MRR; one of the primary models to evaluate the total energy consumption of the machine tool	Different combinations can yield similar MRR; thus, the model cannot incorporate the effect of changes in the combination of parameters on power consumption. Spindle acceleration power, feed axis power, and VPC were not considered
Kara and Li (2011)	$SEC = C_o + \frac{C_1}{MRR}$	An empirical model to evaluate the energy	Because different combinations of

	Where SEC is specific energy consumption, C_0 and C_1 are machine tool-specific coefficients.	consumption to take away a unit volume of part material; provides a combined indicator of energy consumption and productivity i.e. SEC	parameters can produce equivalent MRR, the model is unable to account for the influence of changing the combination of parameters on power. The spindle acceleration power, feed axis power, and VPC machining are not considered.
Diaz et al. (2010)	$E_t = E_{const} + +E_{trant} + E_{steady} + E_{cut}$ Where $E_{cut} = k.d_c.a_p.z^b.f_r^{1-b}.n^b$, in which a_p is the width of cut, z is the number of flutes, b and k are fitting coefficients.	One of the earliest studies to look into the transient state of machine tools (acceleration of the spindle and feed axis)	
Avram and Xirouchakis (2011)	$E_{per-pass} = \int_{t_0}^{t_1'} P_{aY}dt + \int_{t_1}^{t_2'} P_{SY}dt + \int_{t_2}^{t_3'} P_{dY}dt + \int_{t_0}^{t_3'} P_{run}dt + \int_{t_1}^{t_3'} P_c dt$	Investigated and considered transient state energy consumption	

	P_{aY} is Y axes feed acceleration power in *Watt*, P_{SY} is Y axes feed study state power in Watt, P_{dY} is Y axes power during deceleration in *Watt*, P_c is spindle power to cut material in *Watt*, P_{run} is spindle idle steady-state power in *Watt*		
Mori et al. (2011)	$P_{total} = P_1 \times (T_1 + T_2) + P_2 \times T_2 + P_3 \times T_3$ Where P_{total} is the total power consumption in *Watt*, P_1, P_2 and P_3 are the constant, cutting and feeding power consumption respectively; T_1, T_2 and T_3 are the cycle time of the non-cutting state, cutting state, position the work and accelerate the spindle respectively	Evaluate total energy consumption of the machine tool; synchronized spindle acceleration/deceleration with the feed system during rapid traverse to reduce power consumption	VPC machining not considered
Guo et al. (2012)	$SEC = \frac{C_1}{(v_c \times f_r \times d)_c} + \left(c_2 \times v_c^{c_3} \times_r^{c_4} \times d_c^{c_5} \times D_o^{c_6}\right)$ Where $c_1 \sim c_6$, D_o, f_r and v_c are fitting coefficients, part diameter in mm, feed rate in mm/rev, and cutting velocity in m/min respectively	A model capable of incorporating the effect of spindle speed, cutting parameters, and part diameter on power consumption	Spindle acceleration, feed axis power, and VPC machining not considered
He et al. (2012)	$E_{total} = E_{spindle} + E_{feed} + E_{tool} + E_{cool} + E_{fix}$	Evaluate total energy consumption based upon	Spindle acceleration and VPC machining not

	Where E_{total} is the total energy consumption; $E_{spindle}$, E_{feed}, E_{tool}, E_{cool} and E_{fix} are the energy consumption of spindle, feed table, tool indexing, coolant spray, and the basic energy consumption respectively.	the energy demand of respective Numeric Control execution of machine tool	considered
Li et al. (2013)	$SEC = k_o + \frac{k_1 \times n}{MRR} + \frac{k_2}{MRR}$ Where n is spindle rotation per minute, k_o is machining process-specific constant, $k_2 = P_{standby} + b$, k_1 and b are specific coefficients of the spindle motor; $P_{standby}$ is standby power consumption	The idle power was divided into standby power and spindle rotation power and provided insight into the effect of n on the SEC	Different combinations can yield similar MRR; thus, the model cannot incorporate the effect of changes in the combination of parameters on power consumption. Spindle acceleration power, feed axis power, and VPC machining not considered
Balogun and Mativenga (2013)	$E_{total} = E_b + E_r + P_{tc}t_{tc}\left[INT\left(\frac{t_c}{T}\right)+1\right] + P_{air}t_{air} + \left(mN + C + P_{cool} + k\dot{v}\right)t_c$ Where E_b and E_r represents the basic state and ready state energy consumption respectively. P_{air} and P_{cool} represents the air cut and	(Balogun and Mativenga, 2013)Introduced a new state called 'Ready state' between the 'Basic (idle)	Spindle acceleration energy consumption not considered

	coolant pump power consumption in *Watt* respectively. t_c t_b, t_r and t_{air} represents the cutting, basic, ready and air cut state time in *s* respectively. k is the SCE in kJ/cm^3, m is the coefficient, N is the spindle speed in *rev/min* and $\dot{v}$ is the MRR in cm^3/s	state' and 'Cutting state' of a machine tool.	
Lv et al. (2014)	$P_{total} = P_{so} + P_L + P_{CPM} + P_{SR} + P_{FD} + P_{TC} + P_{cut}$ Where P_{total} is total power consumption; P_{SO}, P_L, P_{CPM}, P_{SR}, P_{FD}, P_{TC} and P_{cut} are the power of therblig of standby operation, lightening, coolant spraying, spindle rotation, feed, tool selection, and cutting	Therblig-based total power evaluation of machine tool; provided insights of energy consumption of different operations during machining	Spindle acceleration, feed axis power, and VPC machining are not considered
Yoon et al. (2014)	$E_{total} = \int \left\{ f_1\left(n, f, a_p\right) + (f_2, n, f, a_p) \times \overline{VB}\left(t\right) \right\} dt$ Where $f_1\left(n, f, a_p\right)$ is a second order function of process parameters: spindle speed (n), feed rate (f) and depth of cut (a_p) and $\overline{VB}\left(t\right)$ is the function of tool flank wear	Capable to encompasses the influence of process parameters and tool wear influence on the machine tool's energy consumption	The spindle acceleration and VPC machining are not taken into account
Balogun et al. (2015)	$E_{total} = \left(P_{basic} \times t_{basic}\right) + \left(P_{ready} \times t_{ready}\right) + \left(k \times Q \times t_{cutting}\right)$ Where E_{total} is total energy consumption; P_{basic} and P_{ready} are the power	Evaluate total energy consumption of the machine tool; Provided	The spindle acceleration, feed axis power, and VPC

	consumption in the basic and ready state respectively; t_{ready} and $t_{cutting}$ are the time of ready and cutting state; k is the specific cutting energy coefficient (J/mm^3) and Q is the MRR (mm^3/s)	insight into the energy consumption of machine tools by introducing an intermediate 'ready state' between the basic and cutting states of the machine tool	machining not taken into account.
Liu et al. (2015)	$E_{total} = \left[\begin{array}{l} \sum_{j=1}^{Q_s} \left(\chi_1 \times n_j^2 + \chi_2 \times n_j + \chi_3 \right) + \sum_{j=1}^{Q_u} \left(P_{uj} \times t_{uj} \right) + \\ \sum_{j=1}^{Q_c} \left[\int_0^{t_{cj}} \left(\left(\propto_{2j} \times P_c^2 \right) + \left(\left(1 + \propto_{1j} \right) \times P_c \right) + P_{uj} \right) dt \right] \end{array} \right]$ E_{total} is the total energy; n is the spindle speed in rpm; P and t power consumption and time; subscript s, u and c denote startup, unload (idle) and cutting, respectively; Q_s, Q_u and Q_c denotes the number of startup periods, idle periods, and cutting periods respectively; α_1 and α_2 are the constants	Modelled the energy consumption for the main drive system (spindle system) of the machine tool; incorporated spindle startup in the model	Modelled only the energy consumption of the spindle system and unable to account the VPC machining process energy consumption

Kim et al. (2015)	$P_{Total} = P_{Idle} + P_{Cool} + P_{Spindle} + P_{Feed} + P_{cut}$; $\begin{cases} P_{idle} = C_{1i} \\ P_{Cool} = C_{1c} \\ P_{Spindle} = C_{0_s}.RPM + C_{1_s} \\ P_{Feed} = C_{0_f}.Feedrate + C_{1_f} \\ P_{cut} = C_{0_m}.MRR + C_{1_m} \end{cases}$ Where C_{0_s}, C_{1_f}, C_{0_m} C_{1_i} and C_{1_c} are the coefficients	Monitored six different machine tools energy consumption in different states and observed that cutting energy can be separated from total energy consumption	Does not consider spindle acceleration and VPC machining energy consumption
Lv et al. (2016)	$P_{total} = P_s + P_f + P_{cut}$ Where P_{total} is the total power consumption, P_s, P_f and P_{cut} are the power consumption of spindle rotation, feed axis, and cutting respectively	Evaluate total power consumption of machine tool and provide insights into the energy consumption in different motions of the machine tool	Spindle acceleration and VPC machining not considered
Edem and Mativenga (2016)	$E_f = P_0 \times t_{cy}\left(a \times W_{v_f} + b \times W\right)t_{cy} + F_f \times v_c \times t_c$ Where, P_0 is idle power consumption in *Watt*, W is total weight including weight of the feed axis, vice and workpiece, P_{f_x} and P_{v_y} are power consumption of x and y feed axis respectively, F_f and v_f is	Incorporated the weight of the feed drive and workpiece into the energy consumption model	Spindle acceleration energy consumption not considered

	feed force and feed axes velocity respectively, t_{cy} and t_c are the total cycle time and actual cutting time respectively		
Huang et al. (2016)	$E_{spindle_{st}} = \int P_{st1_{n_s}} dt + \int P_{st2_{n_s}} dt + \int P_{st3_{n_s}} dt$ Where $P_{st1_{n_s}}$, $P_{st2_{n_s}}$ and $P_{st3_{n_s}}$ are the power corresponding to the linear curve, thermite curve, and cubic curve function respectively.	Modelled spindle acceleration energy consumption and provided insights on its power characteristics	Modelled the energy consumption of only one component (spindle) of the machine tool.
Lv et al. (2017)	$E_{SA} = \int_0^{t_{SA}} P_{SA} dt$ where $P_{SA} = P_{SR} \bullet (n) + T_{SA} \bullet w_M$ P_{SA} and P_{SR} represents the spindle acceleration and spindle rotation power in *Watt*. t_{SA} represent the time period of spindle acceleration in *s*. T_{SA} is the acceleration torque in *N-m* w_M is the angular speed of the spindle motor in *rad/s*.	Investigated the spindle acceleration power characteristics and proposed an inertial-based energy consumption model	Only one component (the spindle) of the machine tool's energy consumption was modelled.
Liu et al. (2017)	$\eta_{EE} = \frac{\sqrt{c_t^2 s_t^2 (c_i s_i + 1)^2 + 4 c_m s_m c_t^2 (c_i s_i + 1)(P_{cnc,i} - P_{cnc,u})} - c_t s_t (c_i s_i + 1)}{2 c_m s_m c_t^2 (c_i s_i + 1)}$ Where $P_{cnc,u}$ and $P_{cnc,i}$ is the idle power consumption and input power cosnumption in *Watt* respectively, c_m and s_m are basic coefficient of	Established an energy efficiency model for the machine tool using the machine tool's primary data, spindle speed, and input power data	Spindle acceleration and VPC energy consumption are not considered

	the motor, c_i and s_i are the basic coefficient of frequency inverter; c_t and s_t are the basic coefficient of the machine tool.		
Zhou et al. (2017)	$P_T = \frac{C_1^{'}}{MRR} + \frac{C_2^{'} \times n}{MRR} + \frac{C_3^{'} \times n^{C_4^{'}} \times v_f^{C_5^{'}} \times d_c^{C_6^{'}} \times a_e^{C_7^{'}}}{MRR}$ Where $c_1^{'} \sim c_7^{'}$, v_f, d_c and a_e are the fitting coefficients, feed rate in mm/min, cutting depth in mm, and the width of cut in mm respectively	A model capable of incorporating the effect of cutting parameters and spindle speed on power consumption	Spindle acceleration, feed axis power, and VPC machining are not considered
Edem and Mativenga (2017)	$E_{total} = \begin{pmatrix} E_b + P_{tc} t_{tc} \left[INT\left(\frac{t_c}{T}\right) + 1 \right] + P_{spindle\_run} t_{spindle\_run} + \\ P_c t_c + P_{feed} t_{feed} + P_{cool} t_{cool} \end{pmatrix}$ Where $P_{feed} = P_{G01/G02/G03\_feed} + P_{G00\_feed(approach)} + P_{G00\_feed(retract)}$	Numerical Code based modelling of CNC machine tools	Spindle acceleration energy consumption is not considered
Bhinge et al. (2017)	$E_q = \sum_{\{(x^i, y^i) \in D_q\}} \mu_q \left(x^i \intercal D_q \right) \times l^i$ Where E_q is the total energy consumption, x^i and y^i are the input and output features respectively, l^i is the length of the cut, q is the type of machining process and $\mu_q \left(x^i \intercal D_q \right)$ is the mean energy density function	An energy prediction model based on machine learning.	Model development requires high-speed power meters and complex computational calculations.

Imani Asrai et al. (2018)	$P_{total} = \begin{bmatrix} C + \left(A_f \times f + B_f \times f^2 + D_f \times f^3\right) + \\ \left(A_s \times s + B_s \times s^2 + C_s \times s^3 + D_s \times s^4\right) + \\ \left(\left(E + F_f \times f + F_s \times s + G_s \times s^2 + G_f \times f^2\right) \times \left(MRR\right)\right) + \\ \left(K \times \left(MRR^2\right)\right) \end{bmatrix}$ Where f and s are feed rate and spindle speed respectively; $A_f \sim D_f$, $A_s \sim D_s$ E, F_f, F_s, G_s and G_f are the constants	A mechanistic model by considering machine tools as a thermodynamic system. Incorporated the impact of the machining parameters on the power consumption	Spindle acceleration and VPC machining not considered
Luan et al. (2019)	$P_{SR} = \begin{cases} C_1 n + C_2 n^2 + C_0 & (0 < n \le n_1) \\ C_1 n + C_2 n^2 + C_0 & (n_1 < n \le n_2) \\ \cdots & \cdots \\ C_1 n + C_2 n^2 + C_0 & (n_{n-1} < n \le n_{max}) \end{cases}$ $P_{xf} = C_x v_f + b_{1x} v_f^2 - b_{2x} v_f^3 + \ldots\ldots + b_{nx} v_f^n$ $P_{yf} = C_y v_f + b_{1y} v_f^2 - b_{2y} v_f^3 + \ldots\ldots + b_{ny} v_f^n$ $P_{z-up} = C_{z-up} v_{fz-up} + b_{1z-up} v_{fz-up}^2 - b_{2z-up} v_{fz-up}^3 + \ldots\ldots + b_{nz-up} v_{fz-up}^n$ $P_{z-down} = \begin{pmatrix} C_{z-down} v_{fz-down} + b_{1z-down} v_{fz-down}^2 - b_{2z-down} v_{fz-down}^3 + \ldots\ldots \\ + b_{nz-down} v_{fz-down}^n \end{pmatrix}$ Where n is the spindle speed, v_f is the feed rate and $C_{x/y/z-upand/z-down}$ represents the corresponding fitting coefficient	Focused on the non-cutting status energy consumption of machine tools	Non-cutting condition energy consumption was only investigated; The spindle acceleration energy consumption was not considered. Unable to evaluate energy consumption for a part machining

Liu et al. (2020)	$E(t)=\int \frac{Se_1 \times p_{16}}{m_x \times I_{16}} dt$ where $E(t)$ is the system energy consumption in W. Se_1 and p_{16} are the effort source and comprehensive momentum of the bond diagram model, m_x is the conversion constant of ball screw nut pair and I_{16} is Bond graph element of worktable mass	A bond graph-based energy consumption evaluation of machine tool dynamic features is proposed.	Modelled the energy consumption of only one component (feed axis) of the machine tool.
Pan et al. (2021)	$E_{total} = \int \left(P_{st} + P_u + P_{cut} + P_a\right) dt$ Where E_{total} is the total energy consumption; P_{st}, P_u, P_{cut} and P_a is the power of standby power, unload power, cutting power, and additional loss; t is the cutting time.	A data-driven artificial intelligence model that can compensate for missing data and estimate machine tool energy consumption.	A complex and time-consuming method
Xie et al. (2021)	$\eta_{EE} = \frac{-g'(w_s) \times w_s + \sqrt{g'^2(w_s) + 4f'(w_s) \times (I_s - I_{s0}(w_s)) \times w_s}}{2P_{in} \times f'(w_s)}$ Where I_s is equivalent current of the spindle system, I_{s0} is equivalent idle current of the spindle motor, ω_s is the angular velocity of the spindle motor, P_{in} is the input power of machine tool, $f'(\omega_s)$ and $g'(\omega_s)$ are representing the coefficients	Torque and angular velocity-based energy efficiency monitoring methodology for machine tools	Only idle state and cutting state are considered for evaluating the energy consumption
Brillinger et al. (2021)	$E_{total} = \sum_{i=1}^{n}\sum_{j=1}^{m} P_{ij} \Delta t$	An energy prediction model based on machine	High-sampling data and complicated

	Where E_{total} is the total energy consumption, P_{ij} is the power consumption, n and m are the numerical control instruction and consecutive measurements results respectively	learning techniques	computational calculations are required to develop the model. Unable to incorporate the power characteristics of spindle acceleration, and VPC machining
Da Costa et al. (2022)	$\eta_{EE} = \frac{P_E - L_{Gz}}{P_E}$, Where P_E and L_{Gz} are the input electric power and idle loss power respectively	Developed energy efficiency model for conventional lathe and highlighted their significance in the micro-scale manufacturing industries	Power characteristics curves for each gear combination of the headstock are required to calculate the *EE*. Spindle acceleration and the VPC machining process are not considered
Zhou et al. (2022)	$P_{s\tan dby} = \begin{cases} P_{control} + P_{screen} + P_{fan} & \text{(weak current loop)} \\ P_{control} + P_{screen} + P_{fan} + P_{\text{lub}} + P_{spcool} & \text{(strong current loop)} \end{cases}$ $P_{aux} = P_{light} i_1 + P_{spray\_cool} i_2 + P_{tool\_change} i_3 + P_{chip\_remove} i_4 + P_{spray\_air} i_5$	The non-cutting status energy consumption of machine tools was studied	Unable to predict the energy consumption for part machining

	$P_{s\tan dby}, P_{control}$, P_{screen}, P_{fan}, P_{lub} and P_{spcool} represents the power consumed by the standby, control system, display system, fan device, basic lubrication device and the spindle forced cooling device respectively. P_{aux}, P_{light}, P_{spray_cool}, P_{tool_change}, P_{chip_remove} and P_{spray_air} represents the power consumption of auxiliary, lighting device, the cutting fluid injection device, the tool changing device, the chip removal device, and the blowing cleaning or blowing cooling device respectively in Watt.	in detail	
Alswat and Mativenga (2022)	$E_{total} = \begin{pmatrix} E_{Basic} + E_{Ready\_state} + E_{Cutting} + E_{Compressor} + \\ E_{Tooling} + E_{Chips} + E_{Cutting\_Fluid} + E_{Lubrication\_Oil} \end{pmatrix}$ Where E_{Basic}, E_{Ready_state}, $E_{Compressor}$ and $E_{Cutting}$ are the direct energy consumptions and represents the basic, ready state, compressor and cutting energy consumption respectively. $E_{Tooling}$, E_{Chips}, $E_{Cutting\_Fluid}$ and $E_{Lubrication\_Oil}$ are the embodied energy consumptions and represents the energy consumed in the cutting tools, chips recycling, cutting fluid and lubricant oil production respectively.	The model encompasses the machining process's direct and indirect (embodied) energy consumption.	VPC machining not considered

2.2.2. Carbon emissions modelling

Due to growing environmental issues and stringent carbon emission regulations imposed throughout the globe, low carbon emission has become one of the essential requirements of manufacturing industries. Literature reveals that a growing number of other authors are focusing on assessing the CEM of machining processes. Li et al. (2015) presented an analytical approach for calculating the CEM produced by a CNC-based machining process. This study investigated the contribution of the electrical energy, cutting fluid, cutting tool wear, material utilization and chip disposal to the overall CEM of the machining process. Zhou et al. (2018a) developed a cutting power model considering the tool wear to calculate the carbon emission of a machining process, and the scope of this research is confined to assessing carbon emissions from electrical energy use only. Zhou et al. (2018b) developed a carbon emission-Process Bill of Material based approach to quantify CEM for a part machining process. They found that process parameters such as cutting speed, feed rate, and depth of cut significantly impact the CEM of a machining process. Deng et al. (2020) established a carbon efficiency index to evaluate the CEM of machining processes. The carbon efficiency index was determined as the ratio of CEM from material removal to CEM from the entire machining process. Sihag and Sangwan (2019) presented a Therblig-based method for reducing CEM during machining. They developed a value stream map for evaluating the machining process energy and CEM.

Although the existing energy consumption and carbon emission models reported in Section 2.1.1 and 2.1.2 are significant but still lack to accurately evaluate the energy consumption and associated CEM of a CNC-based machining process for industrial applications.

2.3. Optimization of Process Parameters for Various Responses

Optimization is one of the practical approaches to obtaining the optimum process parameters for the targeted response. Numerous studies have identified process parameter optimization as

a realistic approach for significantly improving machining performance (Sihag and Sangwan, 2020). Previous research has shown that an appropriate selection of the process parameters can result in energy consumption and associated carbon emission reduction of up to 40% (Zhao et al., 2021). Multi-objective optimization emerged as a practical approach for setting optimal cutting parameters where multiple responses need to be optimized simultaneously (Bagaber and Yusoff, 2017). Previously, process parameters were optimised for cost, productivity, and product quality. However, in recent years, due to increasing GHG emissions, energy-related performance responses such as power consumption, energy consumption, and associated CEM responses have been optimised for the machining process (Camposeco-Negrete, 2015) (Nguyen et al., 2020), and the significant studies are discussed below.

Hanafi et al. (2012) optimized the cutting parameters to minimize surface roughness and cutting power for turning a composite material using carbide inserts. He achieved multi-objective optimization by Grey relational analysis (GRA) coupled with the Taguchi technique. He assigned equal weights to the responses: surface roughness and cutting power. Lu et al. (2009) optimized the cutting parameters to minimize tool wear and maximize the material removal rate (MRR) for end milling. He applied GRA for multi-objective optimization and assigned the weights of the responses based on the Principal Component Analysis (PCA). Bhushan (2013) developed the Response Surface Methodology (RSM) based models and optimized the cutting parameters to minimize power consumption and maximize tool life for turning an aluminium-based composite material using carbide inserts. He assigned random weights to responses in the multi-objective optimization. Yan and Li (2013) optimized the surface roughness, MRR, and cutting energy consumption using GRA coupled with RSM. He proposed a new method based on grey relational coefficients to decide the weights of the responses. Wang et al. (2014) developed a multi-objective optimization model for process cost, energy consumption and surface roughness for a turning process using a non-segregated genetic

algorithm and reported that the cutting parameters significantly influenced the energy consumption of the turning process. He did not report the response weight assigning criteria. Kant and Sangwan (2014) developed a multi-objective optimization model for power consumption and surface roughness using GRA coupled with RSM. He used PCA to decide the weight of the responses and found that feed rate was the most influencing cutting parameter. Gok (2015) compared the results of two multi-objective optimization techniques: Fuzzy-Technique for Order of Preference by Similarity to Ideal Solution (TOPSIS) and GRA, for optimizing surface roughness and cutting forces during the turning process. He applied equal weights to both responses, and both techniques produced similar results. Mia and Dhar (2017) used the Taguchi technique to optimize surface roughness and cutting temperature while considering hardness as an input parameter. The optimization results revealed that hardness was both responses' most influential input parameter. Deng et al. (2017) optimized cutting-specific energy consumption and processing time to reduce the energy consumption of the milling process. He developed a multi-objective optimization model using a quantum genetic algorithm and assigned equal weights to the responses. Bagaber and Yusoff (2017) developed an RSM-based multi-objective optimization model for responses: power consumption, surface roughness and tool wear during turning stainless steel in a dry environment using uncoated carbide inserts, while assigning equal weights to each response. In another study, Bagaber and Yusoff (2018) studied the turning of Stainless Steel grade 316 using carbon boron nitride cutting edges under a dry cutting environment. He optimized the cutting parameters for power consumption and surface quality via multi-objective optimization using RSM, in which equal weights were assigned to each response. Mia (2018) developed a RSM-based model of surface roughness and specific cutting energy during machining AISI 4140 steel and then used the Taguchi approach to optimize the process parameters. Bagaber and Yusoff (2019) developed a RSM and non-segregated genetic algorithm based on a multi-objective optimization model to

optimize machining cost and total energy consumption during the turning of stainless steel AISI 316 using uncoated carbide inserts under the dry and wet cutting environment. Sivaiah and Chakradhar (2019) used GRA and TOPSIS coupled with Taguchi technique to optimize the process parameters for product quality, tool life, and productivity for turning of 17-4 PH stainless steel. Meral et al. (2019) optimized surface roughness, thrust force, and drilling torque for a proposed drill design. The optimal levels of the process parameters were obtained using GRA coupled with Taguchi method. Li et al. (2022) modelled the energy consumption of machine tools considering tool wear. He developed a multi-objective model using a Teaching learning-based technique for energy consumption, productivity and surface quality. Feng et al. (2022) optimized the cutting parameters for energy consumption, machining time and surface roughness to improve energy efficiency using a genetic algorithm.

With growing environmental issues and stringent carbon emission regulations, low carbon emission has become one of the essential requirements of manufacturing industries. Due to this growing number of authors are considering CEM as machining performance in multi-objective optimization. C. Zhang et al. (2017) developed regression-based models for surface roughness, MRR and carbon emissions and performed multi-objective optimization using a genetic algorithm. H. Zhang et al. (2017) developed cutting parameter-based empirical models and performed multi-objective optimization to improve energy efficiency and reduce energy consumption and carbon emission. They adopted equal weights for the processing time and energy consumption and the weight of carbon emissions equivalent to the total weight of the processing time and energy consumption. Zhou et al. (2019) developed a multi-objective optimization model for the carbon emissions, processing time and machining cost, considering their equal relative importance using the Game theory coupled with a genetic algorithm. Li et al. (2018) optimized the toolpath to improve energy efficiency, reducing energy consumption and carbon emission considering the cutter-workpiece interaction. They used the linear

weighted summation method for transforming multiple responses into a single objective. Khan et al. (2021) modelled product quality, energy consumption, cost and CEM for a turning process and optimized via multi-objective optimization using the particle swarm optimization technique. Jiang et al. (2022) developed a genetic algorithm coupled with a TOPSIS-based multi-objective optimization model to minimize processing cost and carbon emissions for a turning process. The optimization results revealed that a monotonous cost reduction and a decline in carbon emissions can be achieved by increasing cutting depth and feed rate. Iç et al. (2022) developed goal programming coupled with the TOPSIS model to optimise carbon emission and processing time for a turning process. The optimization results show that the cutting speed was the most influencing parameter for carbon emission.

Table 2.2 Summarises the literature survey on various responses and weight assigning methods considered in multi-objective optimization.

Table 2.2. Summary of the literature survey

Author (s)	Response (s)	Weight assigning method (s)
Singh and Kumar (2006)	R_a, T_{life}, F_c and P_c	Equal weight
Aggarwal et al. (2008)	P_c	Mono-optimization
Hanafi et al. (2012)	R_a and P_c	Equal weights
Bhushan (2013)	P_c and T_{life}	Arbitrarily assigned
Kuram et al. (2013)	SEC, T_{life} and R_a	Not available
Camposeco-Negrete (2013)	P, E and R_a	Mono-optimization
Yan and Li (2013)	R_a, MRR and E	WGRA

Kant and Sangwan (2014)	P and R_a	PCA
Wang et al. (2014)	R_a, E_c and Cost	Not available
Gok (2015)	F_c and R_a	Equal weight
Camposeco-Negrete (2015)	STEC and R_a	Equal weights
Pusavec et al. (2015)	R_a, P_c, T_{life} and chip breakability index	Mono-optimization
Bilga et al. (2016)	E_c, EE and PF	Mono-optimization
Park et al. (2016)	SCE, EE	Entropy method
Mia and Dhar (2017)	R_a and T_{temp}	Mono-optimization
Kumar et al. (2017)	E, EE, PF, P_c, MRR and R_a	Equal weight, AHP and Entropy method
Deng et al. (2017)	SCE and T_{proc}	Equal weight
Bagaber and Yusoff (2017)	P, R_a and T_{wear}	Equal weight
H. Zhang et al. (2017)	CEM, E and T_{proc}	Equal weight
Bagaber and Yusoff (2018)	P and R_a	Equal weight
Mia (2018)	SCE and R_a	Equal weight
Li et al. (2018)	CEM, EE and E	Equal weight
Bagaber and Yusoff (2019)	E, R_a and Cost	Equal weight
Mia et al. (2019)	F_c, T_{temp}, R_a, SCE and MRR	Equal weight
Sivaiah and Chakradhar (2019)	R_a, T_{wear} and MRR	Equal weight
Zhou et al. (2019)	CEM, T_{proc} and Cost	Equal weight

Nguyen et al. (2020)	PF, E and R_a	PCA
Hu et al. (2020)	E	Mono-optimization
Wang et al. (2021)	R_a, T_{proc} and P	Not available
Khan et al. (2021)	R_a, E, Cost and CEM	Entropy method
Jiang et al. (2022)	CEM and Cost	Not available
Feng et al. (2022)	E, T_{proc} and R_a	Not available
Li et al. (2022)	SEC and R_a	Equal weight

F_c: Cutting force, P: power consumption, R_a: Surface roughness E: energy consumption, SCE: specific cutting energy, SEC: Specific energy consumption, MRR: material removal rate, CEM: carbon emission, T_{life}: tool life, T_{wear}: tool wear, T_{temp}: cutting temperature, T_{proc}: processing time

Although, as shown in Table 2.1, the summarized studies reported in the literature survey are significant, but limited authors optimized the cutting parameters for low carbon emission Only two studies (Kumar et al., 2017; Nguyen et al., 2020) considered PF as a performance indicator (response) for machine tools during multi-objective optimization. In addition, most authors assigned equal weights to responses in multi-objective optimization.

2.4. Gaps in Existing Literature

The reviewed literature included energy consumption and associated CEM modelling of machine tools and optimization of process parameters for various responses. The literature reveals that a huge amount of energy is consumed by machine tools in the manufacturing sector, and researchers have reported different techniques and results to reduce the energy consumption of machine tools. The following research gaps have been identified in the reviewed literature:

(1) The reported energy consumption models and modelling approaches are significant but focus only on constant-power consumption machining processes e.g. turning, drilling and milling. The energy modelling for variable-power consumption (VPC) machining processes (e.g. end facing, grooving and chamfering) is very limited. Only a single significant study (Jia et al., 2016) reported in the literature on the VPC machining processes, and the modelling of the VPC machining process remains relatively unexplored.

Significant studies on the machining process optimisation reported in the literature focused only on CPC machining process optimisation, and multi-objective optimization for the VPC machining process is rarely reported. The only available study in the literature for the VPC machining process optimization is Hu et al. (2020), which only optimizes energy consumption and has limited scope for establishing optimal process parameters when productivity needs to be simultaneously maximized.

Further, it has been well established in the literature that not only process parameters, but tool geometry also influences the energy consumption of machine tools. Several researchers investigated (Garg et al., 2016; Kumar et al., 2017; Kuram, 2017; Ma et al., 2014; Parida and Maity, 2017) the influence of tool nose radius on the power consumption and found that the tool nose radius has a significant influence on the power consumption of the machine tool. The studies reported in the literature are significant, but they focused only on CPC machining process and the literature shows that no work have been reported related to the VPC machining process considering the cutting tool nose radius.

(2) Modelling of energy consumption for machine tools is the foundation and prerequisite for optimising the machining process for selecting optimum process parameters leading to minimum energy consumption and associated CEM. Although the existing carbon

emission models are significant, still lack to evaluate the total energy consumption of a machine tool and associated CEM during the machining of a cylindrical part for industrial applications. The existing energy consumption evaluation models only consider CPC machining processes, whereas cylindrical part machining includes both CPC and VPC machining processes to manufacture the final product, which result in inaccurate quantification of the energy consumption and associated CEM for machining a cylindrical part. Furthermore, most studies considered the energy consumed for a particular period of a machining process. Therefore, it is vital to develop an industrially applicable model and fill this knowledge gap in order to accurately evaluate machine tools' total energy consumption and associated CEM for machining cylindrical parts and to develop energy-efficient and low-emission machining strategies.

(3) Soft computing techniques have been increasingly popular in recent years for modelling in a variety of engineering applications due to their reliable predictability, ability to work with the inherent complexity and to capture non-linear behaviour between input and output parameters. Literature shows that an increasing number of authors applied soft computing for modelling in different engineering applications. The literature survey indicates that soft computing techniques such as GP, SVM, and fuzzy logic are widely used for modelling in a variety of engineering applications and manufacturing processes. However, there appears to be an abundance of literature on the modelling of various process responses such as energy consumption, productivity and surface quality (Bhinge et al., 2017; Garg et al., 2016, 2015; Gupta, 2010; Pan et al., 2021), but to the best of the author's knowledge, none of the literature reported modelling of energy efficiency, power factor and carbon emissions using soft computing techniques for machine tools.

(4) The *PF* is an important indicator of efficient electrical energy utilization of the machine tool's electrical system. There are no studies reported on parametric modelling of *PF* for machine tools in the reviewed literature, and few researchers (Kumar et al., 2017; Nguyen et al., 2020) optimised the cutting parameters while considering the *PF* as one of the machining process responses during multi-objective optimization. The multi-objective optimization of *PF* with CEM as a machining process response is not explicitly investigated. In addition, most authors assigned equal weights to responses in multi-objective optimization in the reviewed literature. The selection of the weight of responses could provide a better solution to determine the optimal cutting parameter for a machining process. Therefore, weights of the responses can be decided based on qualitative and quantitative techniques. Therefore, the impact of weighting methods on multi-objective optimization results should be explored. Kumar et al. (2017) is the only significant work reported so far that used two alternative weight assigning methods in addition to equal weigh methods for multi-objective optimization of the machining process.

Chapter 3:

Modelling of Variable Power Consumption Machining Processes – A Case of End Facing

In this chapter, an empirical model is developed to predict the cutting energy consumption of the variable-power consumption machining process i.e. end facing. The fitting coefficients of the model are determined by conducting experiments on a LMW-CNC lathe machine tool under dry and wet environments. The validation experiments confirm that the accuracy of the developed model is more than 96%. Further, the predicted power profiles were in good agreement with the measured power profiles, which shows that the developed model satisfactorily encompasses the influences of the process parameters on the cutting power consumption.

3.1. Introduction

A review of the existing literature presented in **Chapter 2** reveals that the reported energy consumption modelling approaches are significant but focus only on constant-power consumption (CPC) machining processes e.g. turning, drilling and milling. The energy modelling for variable-power consumption (VPC) machining processes (e.g. end facing, grooving and chamfering) is very limited. Figure 3.1 shows the power profile for the CPC machining process and VPC machining process. In the CPC machining process, the process parameters i.e. cutting speed (v_c), feed rate (f_r) and cutting depth (d_c) remain constant. Consequently, the machining power also remains constant for the given process time. Whereas in the VPC machining process, at least one of the process parameters (for example v_c in end facing) changes over time. Hence, the cutting power is dynamically changing, and its characteristics become more complex. Jia et al. (2016) study is the only significant work reported in the literature for the VPC machining process. He investigated the power

characteristics for the end facing of ASTM 1045 steel workpiece using carbide inserts and proposed an energy consumption model without considering cutting tool nose radius. Over the years, several studies have analyzed the influence of cutting tool geometry and process parameters on the cutting power, surface roughness, and tool life during CPC machining processes.

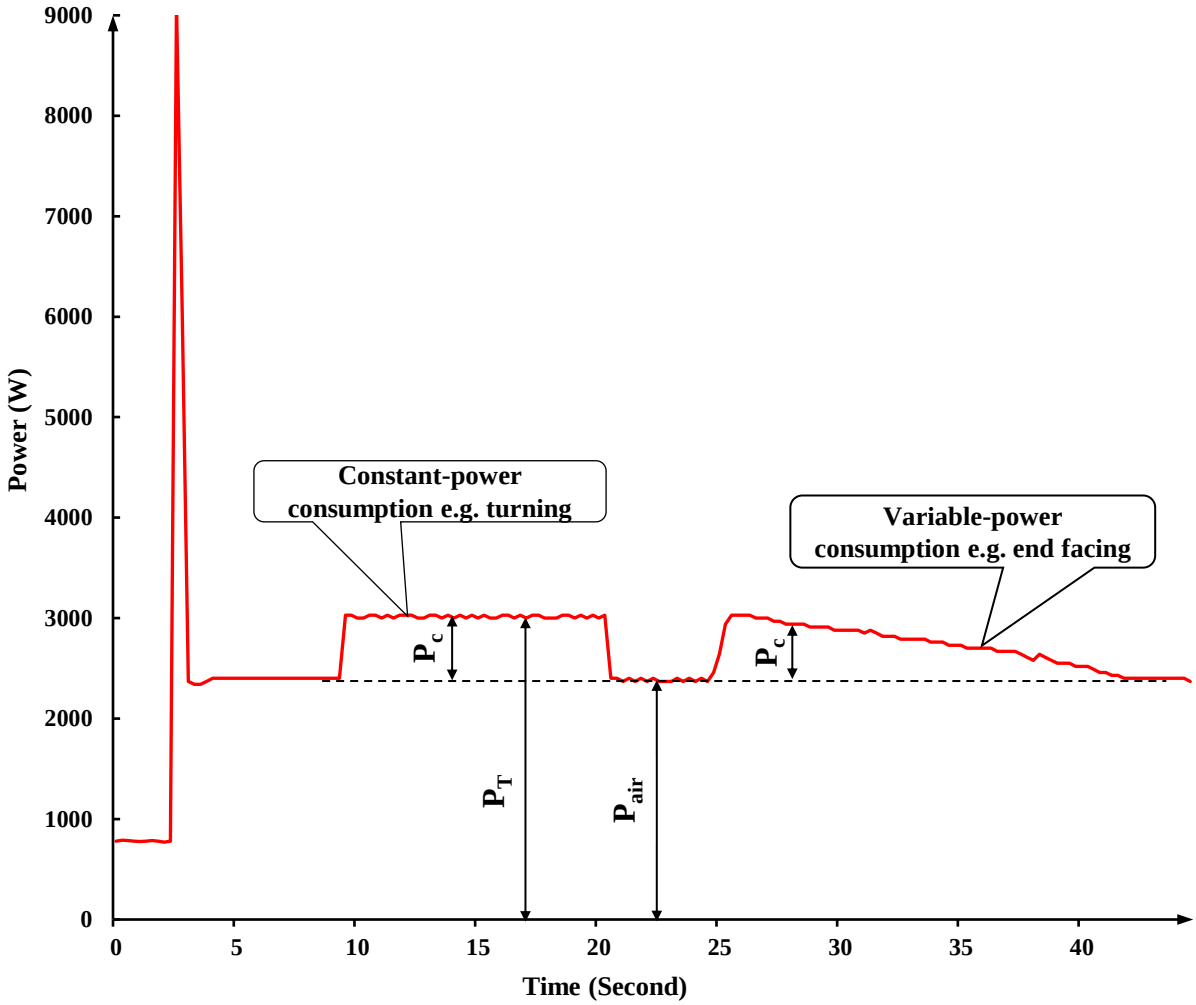

Figure 3.1 Power profile of constant-power consumption and variable-power consumption machining process

It has been well established that not only process parameters but tool geometry also influence the cutting energy (Kuram, 2017). Ma et al. (2014) had investigated the influence of nose radius and process parameters on cutting energy consumption and energy efficiency

during machining of AISI 4140. He reported that the nose radius is one of the significant parameters for cutting energy consumption. Kuram (2017) investigated the effect of nose radius during milling of AISI 304 for surface roughness and cutting force. He reported that the cutting force decreases with an increase in the nose radius significantly. Kumar et al. (2017) found that tool nose radius is the most significant factor during the turning of EN 353 alloy. Similarly, Garg et al. (2016) and Parida and Maity (2017) had found the nose radius to be one of the significant parameters during their work. The above discussion (Garg et al., 2016; Kumar et al., 2017; Kuram, 2017; Ma et al., 2014; Parida and Maity, 2017) concludes that the nose radius has a significant influence on the power consumption of a machining process. The above literature shows that no work has been reported for the development of an empirical model for the VPC machining process considering the cutting tool nose radius as a process parameter during the end facing of Al 6061. In the present work, an empirical model is developed to predict the cutting energy consumption for the VPC machining process considering the cutting parameters and tool geometry. The fitting coefficients of the developed model are obtained by conducting end facing experiments on an Aluminum Al 6061 workpiece in a dry and wet environment. The cutting speed, feed rate, cutting depth and tool nose radius are chosen as the process parameters. Establishing an accurate and practical energy prediction model for machining a workpiece is the foundation for reduction of energy consumption of machine tools. The proposed model can be used to select the cutting parameters for a VPC machining process and to develop an energy consumption model of machine tools for machining cylindrical parts.

3.2. Modelling Methodology

The total power consumed by a machine tool during the machining process can be segregated into two categories: air-cut power (P_{air}) and cutting power (P_c) as shown in Figure 3.1. The air cutting power is the power consumed without machining and keeping

all the other process parameters constant. The balance between the total power and the air-cutting power is the power required to cut the material from a workpiece as chips and is generally known as cutting power. The contribution of air-cut power is equal in the CPC machining process and the VPC machining process. The main difference between the constant-power machining process and the variable-power machining process is due to the cutting power only. The cutting power for CPC machining can be expressed as the exponential function of process parameters (Lv et al., 2019, 2016; Xie et al., 2016).

$$P_c = C_p v_c^{\alpha} f_r^{\beta} d_c^{\gamma} \quad (1)$$

Where C_p is a constant and α, β and γ are coefficients of cutting speed, feed rate and cutting depth respectively. In the CPC machining process, the process parameters i.e. $v_c,\ f_r$ and d_c remain constant and consequently, the machining power also remains constant for the given process time. Whereas in the VPC machining process, at least one of the process parameters (for example v_c in end facing) changes with time and the cutting power change dynamically. Thus, to obtain the cutting power, the VPC machining process can be divided into N sub-intervals for the given machining time as shown in Figure 3.2.

In Figure 3.2, the more the value of N, each sub-interval will be very small and can be considered as equivalent to the CPC machining process. Based on Eq. (1), the cutting power for i^{th} subinterval can be expressed as:

$$P_{c_i} = C_p . v_{c_i}^{\alpha} f_{r_i}^{\beta} d_{c_i}^{\gamma} \quad (2)$$

Where v_{c_i} is the average cutting speed in m/min of i^{th} sub-interval; f_{r_i}, average feed rate in mm/rev of i^{th} sub-interval; d_{c_i} is average cutting depth in mm of i^{th} sub-interval.

Subsequently, the P_c for the whole process of VPC can be expressed as:

$$P_c = \sum_{i=1}^{N} C_p \, v_{c_i}^{\alpha} f_{r_i}^{\beta} d_{c_i}^{\gamma} \tag{3}$$

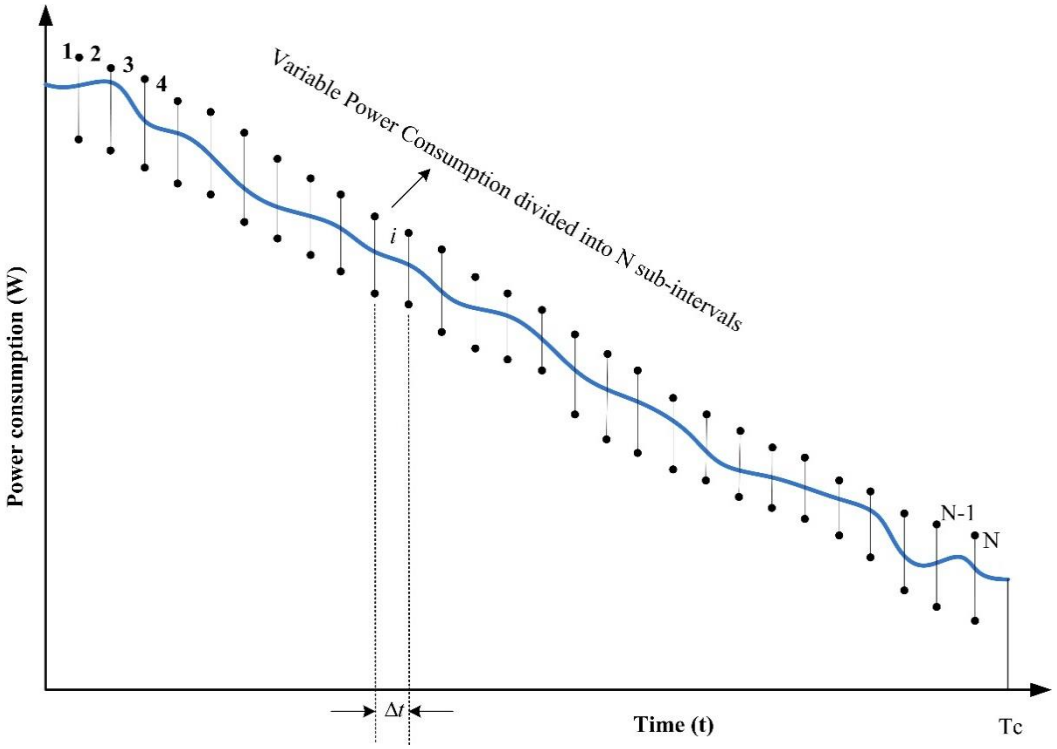

Figure 3.2 Schematic profile of variable power consumption divided into N sub-interval- A case of end facing.

Where N is the number of sub-intervals. Δt is the duration of each subinterval in second and can be written as $\Delta t = T_c/N$, T_c is the total machining time in second. Eq. (3) as a function of time can be expressed as follows:

$$P_c = C_p v_c(t)^{\alpha} f_r(t)^{\beta} d_c(t)^{\gamma} \tag{4}$$

However, the cutting power model as shown in Eq. (4) incorporated the influence of process parameters on the cutting power but unable to include the influences of nose radius (r). Several researchers (Garg et al., 2016; Kumar et al., 2017; Kuram, 2017; Ma et al., 2014; Parida and Maity, 2017) have reported that the cutting tool nose radius is one of the

important tool geometry that significantly influences the cutting power. This indicates that the nose radius should be included in the cutting power model. The cutter nose radius does not change during the machining process and the cutting power model stated in Eq. (4) can be expressed as:

$$P_c = C_p v_c(t)^{\alpha} f_r(t)^{\beta} d_c(t)^{\gamma} r^{\delta} \quad (5)$$

The cutting power model as stated in Eq. (5) incorporated different cutting parameters as a function of time and can be adopted for different VPC processes viz. end facing, chamfering, taper turning and grooving etc. Since, depending on the type of VPC machining process, a mathematical formula for the changing parameters can be obtained as a function of time using which the related power consumption model can be derived. In the present study, end facing is considered and the corresponding model is developed.

The end facing machining process encompasses three stages: cutting tool entering, fully cutting and cutting tool exit. In the cutting tool entering-stage, the feed rate remains constant while cutting speed and depth of cut changes and satisfied the following relations (Jia et al., 2016):

$$d_c(t) = d_c.\, t/t_{en} \quad (6)$$

$$v_c(t) = \frac{\pi n}{1000}\left(D_o - \left(\frac{2 f_r n}{60} t\right)\right) = v_{max} - \frac{2 f_r \pi n^2}{60000} t \quad (7)$$

Where $v_{max} = \frac{\pi n D_o}{1000}$ is the maximum initial cutting speed in m/min and n is spindle speed in rev/min and t is time in seconds. t_{en} is the cutting tool entering time in seconds and can be calculated using Eq. (8).

$$t_{en} = \frac{d_c.cot\kappa_r}{\frac{nfr}{60}} \quad (8)$$

Where κ_r is the main cutting-edge angle of the cutting tool in degree. Based on Eqs. (5), (6) and (7), the cutting power for the tool entering-stage can be expressed as:

$$P_{c\_en} = C_p \left(v_{max} - \frac{2f_r \pi n^2}{60000} t\right)^{\alpha} f_r^{\beta} \left(d_c \frac{t}{t_{en}}\right)^{\gamma} r^{\delta} \quad (9)$$

In the fully cutting stage, the cutter is completely engaged in the workpiece and the depth of cut does not change with further advancement of the tool. The cutting tool continuously moves in the direction of the center of the workpiece and results in a gradual reduction in cutting speed as stated in Eq. (7), while the depth of cut and feed rate are constant. Based on Eqs. (5) and (7), the cutting power during the fully cutting-stage can be expressed as:

$$P_{c\_cut} = C_p (v_{max} - \frac{2f\pi n^2}{60000} t)^{\alpha} f_r^{\beta} d_c^{\gamma} r^{\delta} \quad (10)$$

In the cutting tool exit-stage, the feed rate remains constant while the cutting speed and depth of cut change. Cutting speed satisfied the relation stated in Eq. (7) and the cutting depth satisfied the following relations:

$$d_c(t) = d_c - (d_c . \frac{t}{t_{ex}}) \quad (11)$$

Where t_{ex} is the cutting tool exit time in seconds. Based on equations (5), (7) and (11), the cutting power for the cutting tool exit-stage can be expressed as:

$$P_{c\_ex} = C_p \left(v_{max} - \frac{2f_r \pi n^2}{60000} t\right)^{\alpha} f_r^{\beta} \left(d_c - (d_c \frac{t}{t_{ex}})\right)^{\gamma} r^{\delta} \quad (12)$$

According to Eq. (9), (10) and (12), the cutting power during end facing can be calculated as:

$$P_C = \begin{cases} C_p\left(v_{max} - \frac{2f_r\pi n^2}{60000}t\right)^{\alpha} f_r^{\beta}\left(d_c\frac{t}{t_{en}}\right)^{\gamma} r^{\delta}, & 0 \le t < t_{en} \\ C_p(v_{max} - \frac{2f_r\pi n^2}{60000}t)^{\alpha} f_r^{\beta} d_c^{\gamma} r^{\delta}, & t_{en} \le t < t_{en} + t_{cut} \\ C_p\left(v_{max} - \frac{2f_r\pi n^2}{60000}t\right)^{\alpha} f_r^{\beta}\left(d_c - (d_c\frac{t}{t_{ex}})\right)^{\gamma} r^{\delta}, & t_{en} \le t < t_{en} + t_{cut} + t_{ex} \end{cases} \quad (13)$$

Where t_{cut} is the fully cutting-stage time in seconds. The cutting energy consumption corresponding to the different stages (i.e. entering, fully cutting and exit) can be calculated using Eq. (14), (15) and (16) respectively.

$$E_{en} = \int_0^{t_{en}} C_p\left(v_{max} - \frac{2f_r\pi n^2}{60000}t\right)^{\alpha} f_r^{\beta}\left(d_c\frac{t}{t_{en}}\right)^{\gamma} r^{\delta} dt \quad (14)$$

$$E_{cut} = \int_{t_{en}}^{t_{en}+t_{cut}} C_p\left(v_{max} - \frac{2f_r\pi n^2}{60000}t\right)^{\alpha} f_r^{\beta} d_c^{\gamma} r^{\delta} dt \quad (15)$$

$$E_{ex} = \int_{t_{en}+t_{cut}}^{t_{en}+t_{cut}+t_{ex}} C_p\left(v_{max} - \frac{2f_r\pi n^2}{60000}t\right)^{\alpha} f_r^{\beta}\left(d_c - (d_c\frac{t}{t_{ex}})\right)^{\gamma} r^{\delta} dt \quad (16)$$

Hence, the total cutting energy during end facing can be expressed as:

$$\mathrm{E_c} = E_{en} + E_{cut} + E_{ex}$$

$$E_c = \int_0^{t_{en}} P_{c\_en}\, dt + \int_{t_{en}}^{t_{en}+t_{cut}} P_{cut}\, dt + \int_{t_{en}+t_{cut}}^{t_{en}+t_{cut}+t_{ex}} P_{c\_ex}\, dt$$

$$E_c = \int_0^{t_{en}} C_p\left(v_{max} - \frac{2f_r\pi n^2}{60000}t\right)^{\alpha} f_r^{\beta}\left(d_c\frac{t}{t_{en}}\right)^{\gamma} r^{\delta} dt + \int_{t_{en}}^{t_{en}+t_{cut}} C_p\left(v_{max} - \frac{2f_r\pi n^2}{60000}t\right)^{\alpha} f_r^{\beta} d_c^{\gamma} r^{\delta} dt + \int_{t_{en}+t_{cut}}^{t_{en}+t_{cut}+t_{ex}} C_p\left(v_{max} - \frac{2f_r\pi n^2}{60000}t\right)^{\alpha} f_r^{\beta}\left(d_c - (d_c\frac{t}{t_{ex}})\right)^{\gamma} r^{\delta} dt \quad (17)$$

In end facing machining process, the cutting tool entering and exit period are generally of short duration. Even in the exit stage, the cutting speed is nearly zero. Further, as can be seen in Eq. (8) that the cutter entering time is highly dependent on the tool geometry. According to our pilot experiments, it was found that the cutter entering time was less than 1% of total end facing time and corresponding energy consumption was less than <10J. The inclusion of energy consumption related to the cutter's entering phase and exit phase unnecessarily complicates the calculations and can be ignored without compromising model accuracy. Thus, the end facing cutting power Eq. (13) and corresponding energy consumption Eq. (17) can be reduced as:

$$P_c = C_p \left(v_{max} - \frac{2f_r \pi n^2}{60000} t\right)^{\alpha} f_r^{\beta} d_c^{\gamma} r^{\delta} \tag{18}$$

$$E_c = \int_0^{T_c} C_p \left(v_{max} - \frac{2f_r \pi n^2}{60000} t\right)^{\alpha} f_r^{\beta} d_c^{\gamma} r^{\delta} dt \tag{19}$$

Where $T_c = t_{en} + t_{cut} + t_{ex}$.

3.3. Experimental Planning

The experimental setup and the methodology followed in this study are shown in Figure 3.3. A LMW-Smarturn CNC Lathe in a dry and wet environment was used to perform the end facing experiments. Aluminium of grade Al 6061 was taken as workpiece material. Aluminium has wide utilization in the manufacturing industry due to its good mechanical and corrosive resistance properties. Further, aluminium has good sustainable assessment due to its abundant availability, ease of reuse and recycling with less adverse environmental impacts (Camposeco-Negrete and de Dios Calderón-Nájera, 2019; Warsi et al., 2018). Sandvik carbide inserts of different nose radius of ISO designation: CNMG 120404, CNMG 120408 and CNMG 120412 were selected as cutting tools with tool holder PCLNR 2020 K 12. The technical details of the machine tool are provided in Table 3.1.

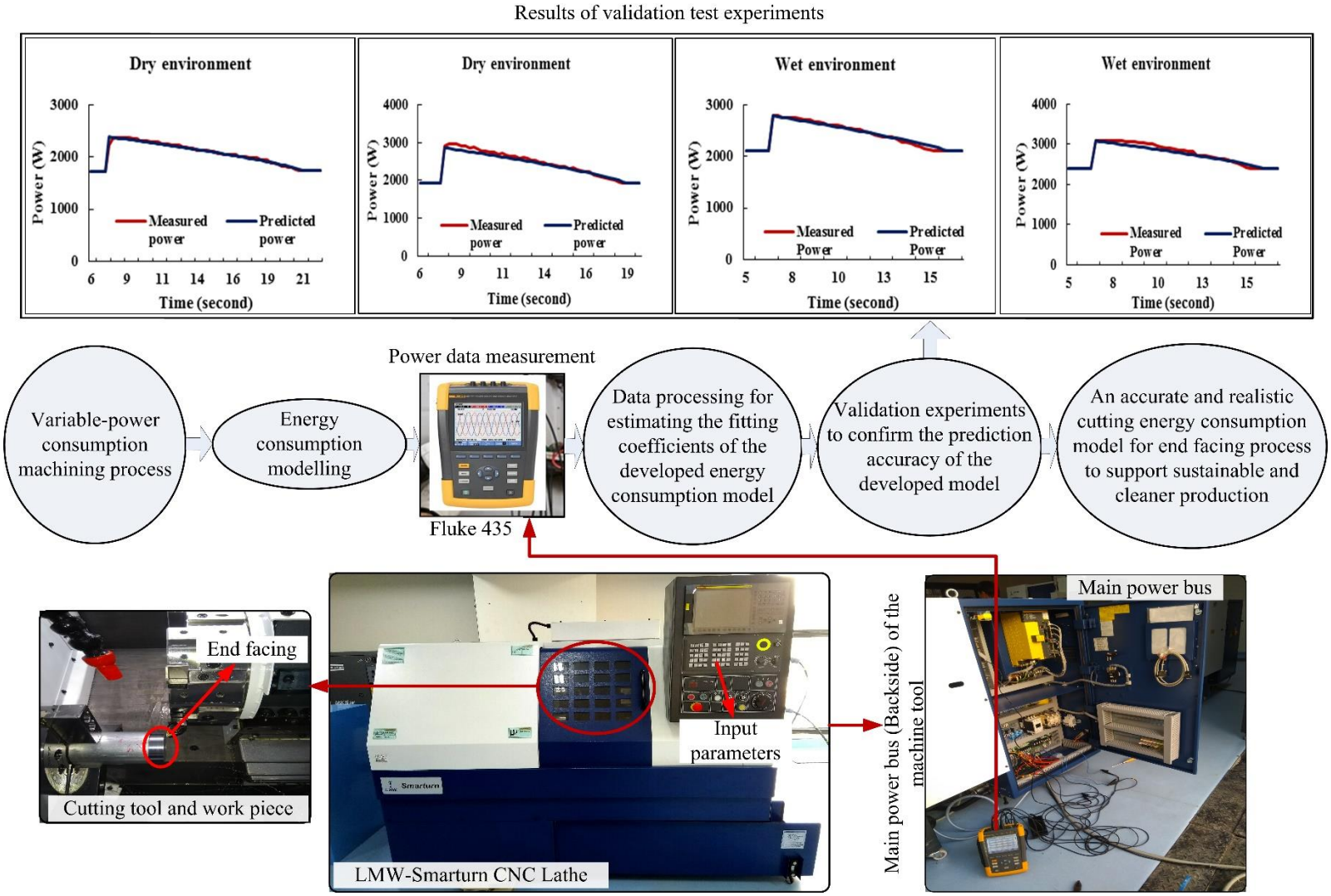

Figure 3.3 Experimental setup and adopted methodology.

Table 3.1 Specifications of the machine tool

Specification	Data
Manufacturer/model	LMW Ltd./ Smarturn CNC lathe
Machine dimensions (L×B×H)	2275 mm× 1640 mm× 1620 mm
Spindle motor power rating	5.5 kW (Fanuc β6i)
Max. spindle speed	4500 revolution/min
Controller type	Fanuc oi-TF
Maximum turning diameter	200 mm
Swing over bed/carriage	480 mm/260 mm
Maximum turning length	262 mm
Turret (No. of tool station)	8

In end facing, cutting speed is varying continuously during machining and depends upon workpiece diameter (D_o) and spindle speed (n). Therefore, n, f_r, d_c and r were selected as machining process parameters and the diameter of the workpiece was kept constant. The considered parameters are tabulated with their levels in Table 3.2. The levels of the process parameters were customized based on machine tool considerations, cutting tool supplier's recommendations and data available in the literature (Bharathi Raja and Baskar, 2011; Camposeco-Negrete, 2015; Lv et al., 2018). Taguchi's L_9 orthogonal array was used to design the experimental plan. L_9 is the most recommended orthogonal array for a combination of four process parameters at three levels to reduce the experimental cost and time (Sadat-Shojai et al., 2012). The power drawn by the CNC machine tool was directly measured from the main power bus using the Fluke 435 series II Power Analyzer as shown in Figure 3.3. The power analyzer was connected to the 3-phase main power bus supply using three current probes and three voltage probes embedded with alligator clips.

The power analyzer was set to record the power readings at the interval of every 0.25 seconds.

Table 3.2 Machining process parameters and their considered levels

Variables		n (rev/min)	f_r (mm/rev)	d_c (mm)	r (mm)
Level	I	1600	0.08	1.0	0.4
	II	2000	0.12	1.4	0.8
	III	2400	0.16	1.8	1.2

The measured total power (P_T), air cut power (P_{air}) and corresponding calculated cutting power (Total cutting power−Air cutting power) for experiment number seven under dry environment is summarized in Table 3.3.

Table 3.3 Power consumption experimental data for experiment number seven under dry environment

S. No	t (second)	v_c (m/min)	P_T (W)	P_{air} (W)	P_c (W)
7-1	0.25	447.64	3330	2070	1260
7-2	0.50	435.58	3320	2070	1250
7-3	0.75	423.52	3300	2070	1230
7-4	1.00	411.47	3300	2070	1230
7-5	1.25	399.41	3270	2070	1200
7-6	1.50	387.35	3240	2070	1170
7-7	1.75	375.29	3210	2070	1140
7-8	2.00	363.24	3180	2070	1110

7-9	2.25	351.18	3150	2070	1080
7-10	2.50	339.12	3120	2070	1050
7-11	2.75	327.06	3090	2070	1020
7-12	3.00	315.00	3060	2070	990
7-13	3.25	302.95	3000	2070	930
7-14	3.50	290.89	2970	2070	900
7-15	3.75	278.83	2940	2070	870
….	….	….	….	….	….
….	….	….	….	….	….
7-34	8.50	49.74	2280	2070	210
7-35	8.75	37.68	2220	2070	150
7-36	9.00	25.62	2190	2070	120
7-37	9.25	13.56	2160	2070	90
7-38	9.50	1.51	2070	2070	0

$D_o = 61$ mm, $n = 2400$ rev/min, $f_r = 0.08$ mm/rev, $d_c = 1.8$ mm and $r = 1.2$ mm

Similarly, the data of the remaining eight experiments were compiled for further calculations. Further, the regression analysis was performed for all nine experimental data sets to determine the fitting coefficients of the model developed in Eq. (19). The values of fitting coefficients obtained after performing regression analysis are provided in Table 3.4. The p-values for the fitting coefficients of process parameters are less than 0.05, which reveals that all the process parameters are statistically significant. The R^2 and Adjusted (Adj.) R^2 values shown in Table 3.4 are more than 91% which shows that the cutting power model has an adequate prediction accuracy for P_c under various combinations of v_c, f_r, d_c and r.

Table 3.4 Regression analysis results for the developed model

Cutting environment	Fitting coefficients	Values	Std. Error	t-value	p-value	Regression Statistics	
Dry	C_p	99.5115	0.0603	33.1466	0.0000	R^2	0.9167
	α	0.7641	0.0159	47.9120	0.0000	Adj. R^2	0.9155
	β	1.1385	0.0514	22.1449	0.0000	Std. Error	0.1046
	γ	1.1145	0.0618	18.0454	0.0000	Observations	281
	δ	-0.2331	0.0324	-7.1939	0.0000		
Wet	C_p	34.5943	0.0521	29.5625	0.0000	R^2	0.9448
	α	0.8232	0.0136	60.7491	0.0000	Adj. R^2	0.9440
	β	0.8387	0.0433	19.3655	0.0000	Std. Error	0.0886
	γ	1.3399	0.0522	25.6470	0.0000	Observations	283
	δ	-0.2516	0.0276	-9.1238	0.0000		

By substituting the values of coefficients listed in Table 3.4 into Eq. (18), the cutting power consumption for end facing under dry environment can be calculated as:

$$P_{C_{dry}} = 99.51\left(v_{max} - \frac{2f_r\pi n^2}{60000}t\right)^{0.7641} f_r^{1.1385}\, d_c^{1.1145} r^{-0.2331} \quad (20)$$

Further, Analysis of variance (ANOVA) was used to analyze the statistical significance of the developed model. The ANOVA results for the cutting power model based on Eq. (18) under a dry environment are summarized in Table 3.5.

Table 3.5 ANOVA for the developed model

Cutting environment		DF	SS	MS	F	Significance P
Dry	Regression	4	33.2375	8.3094	759.7037	0.0000
	Residual	276	3.0188	0.0109		
	Total	280	36.2563			
Wet	Regression	4	37.3921	9.3480	1189.6267	0.0000
	Residual	278	2.1845	0.0079		
	Total	282	39.5766			

DF: Degree of freedom, SS: Sum of squares, MS: Mean of square

The p-value for regression in Table 3.5 is less than 0.05 at a 95% confidence interval, which shows that the cutting power model is statistically significant. Similarly, the large F value 759.7037 of regression in Table 3.5 reveals a strong relationship between the process parameters and cutting power. Hence, based on Eq. (19), the cutting energy consumption of the end facing process under a dry environment ($E_{C_{dry}}$) can be calculated as follows:

$$E_{C_{dry}} = \int_0^{T_c} 99.51 \left(v_{max} - \frac{2f_r \pi n^2}{60000} t\right)^{0.7641} f_r^{1.1385}\, d_c^{1.1145} r^{-0.2331} dt \quad (21)$$

Similarly, fitting coefficients of the cutting power model under a wet cutting environment were determined. By substituting the values of coefficients listed in Table 3.4 into Eq. (18), the cutting power consumption for end facing under a wet environment can be calculated as:

$$P_{C_{wet}} = 34.59\left(v_{max} - \frac{2f_r\pi n^2}{60000}t\right)^{0.8232} f_r^{0.8387}\, d_c^{1.3399} r^{-0.2516} \quad (22)$$

The regression analysis and ANOVA result for cutting power model under wet environment based on Eq. (18) are also summarized in Table 3.4 and Table 3.5 respectively and it is found that the developed model is statistically significant in the wet environment also. Hence, based on Eq. (19), the cutting energy consumption of the end facing in a wet environment can be calculated as follows:

$$E_{C_{wet}} = \int_0^{T_c} 34.59\left(v_{max} - \frac{2f_r\pi n^2}{60000}t\right)^{0.8232} f_r^{0.8387}\, d_c^{1.3399} r^{-0.2516} dt \quad (23)$$

The developed model for cutting energy consumption of end facing process under dry and wet environment are summarized in Table 3.6. Once the fitting coefficients are obtained, the cutting power profile of end facing operation could be predicted using Eq. (20) and Eq. (22) under dry and wet environments respectively for the different combinations of the process parameters. The predicted power profiles using the developed model and the corresponding measured power profile are shown in Figure 3.4.

Table 3.6 Cutting energy consumption model for end facing process under dry and wet environment

Cutting energy consumption model
For a dry environment
$\int_0^{T_c} 99.51\left(v_{max} - \frac{2f_r\pi n^2}{60000}t\right)^{0.7641} f_r^{1.1385}\, d_c^{1.1145} r^{-0.2331} dt$
For a wet environment
$\int_0^{T_c} 34.59\left(v_{max} - \frac{2f_r\pi n^2}{60000}t\right)^{0.8232} f_r^{0.8387}\, d_c^{1.3399} r^{-0.2516} dt$

Further, the corresponding cutting energy consumption can be calculated using Eq. (21) and Eq. (23) under dry and wet environments respectively.

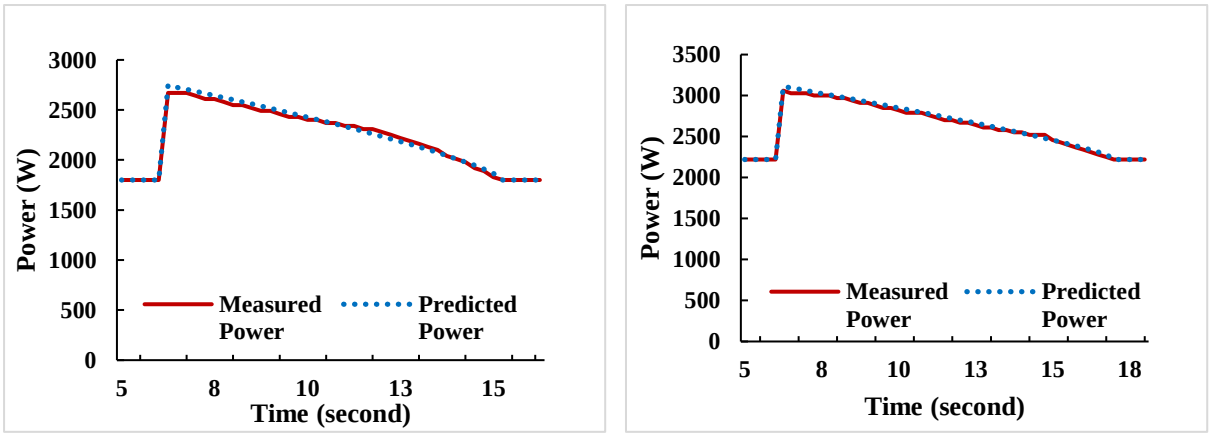

(a) Dry environment **(b) Wet environment**

Figure 3.4 Predicted power profile using developed model vs measured power profile: (a) Dry cutting environment, $n = 1600$ rev/min, $D_o = 61$ mm, f_r =0.12 mm/rev, d_c =1.4 mm and $r = 1.2$ (b) Wet cutting environment, $n = 2000$ rev/min, $D_o = 61$ mm, $f_r = 0.08$ mm/rev, d_c =1.4 mm and $r = 0.8$ mm.

3.4. Validation of the Model

Four experiments were conducted to validate the energy consumption prediction capability of the developed model. The combination of process parameters used for validation are shown in Table 3.7 and were kept different from the combination at which the fitting coefficients of the model were obtained.

The cutting energy consumption for each validation experiment was predicted using the developed model as listed in Table 3.6 for a dry and wet environment and the results are summarized in Table 3.8.

Table 3.7 Process parameters of validation experiments

Cutting environment	Test No.	D_o (mm)	Process parameters n (rev/min)	f_r (mm/rev)	d_c (mm)	r (mm)
Dry	I	61	1600	0.08	1.4	0.8
	II	61	2000	0.08	1.8	1.2
Wet	III	61	1600	0.12	1	0.8
	IV	61	2400	0.08	1	0.4

Table 3.8 Prediction accuracy of the cutting energy consumption for validation experiments

Cutting environment	Test No.	Cutting energy consumption (J) Predicted (E_{c_Pred})	Measured (E_{c_Meas})	Accuracy (%)
Dry	I	5542.50	5482.50	99.91
	II	6324.98	6563.80	96.36
Wet	III	3599.19	3720.00	96.75
	IV	4258.07	4166.30	97.80

Accuracy (%) = $(1 - \left|\frac{E_{c\_Pred} - E_{c\_Meas}}{E_{c\_Meas}}\right|) \times 100$

As shown in Table 3.8, the prediction accuracy of the developed model is more than 96% for each validation test and hence it can be effectively utilized for predicting the cutting energy consumption of end facing process. Further, the power profiles of the predicted power consumption based on the developed cutting power models (Eq. (20) for dry environment and Eq. (22) for wet environment) for each validation test are plotted in Figure 3.5 against the corresponding actual measured power profile. As shown in Figure

3.5, the predicted power profiles of the validation experiments are in good agreement with the measured power profiles in both dry and wet environments. It shows that the developed model adequately encompasses the effects of the process parameters on the power profile.

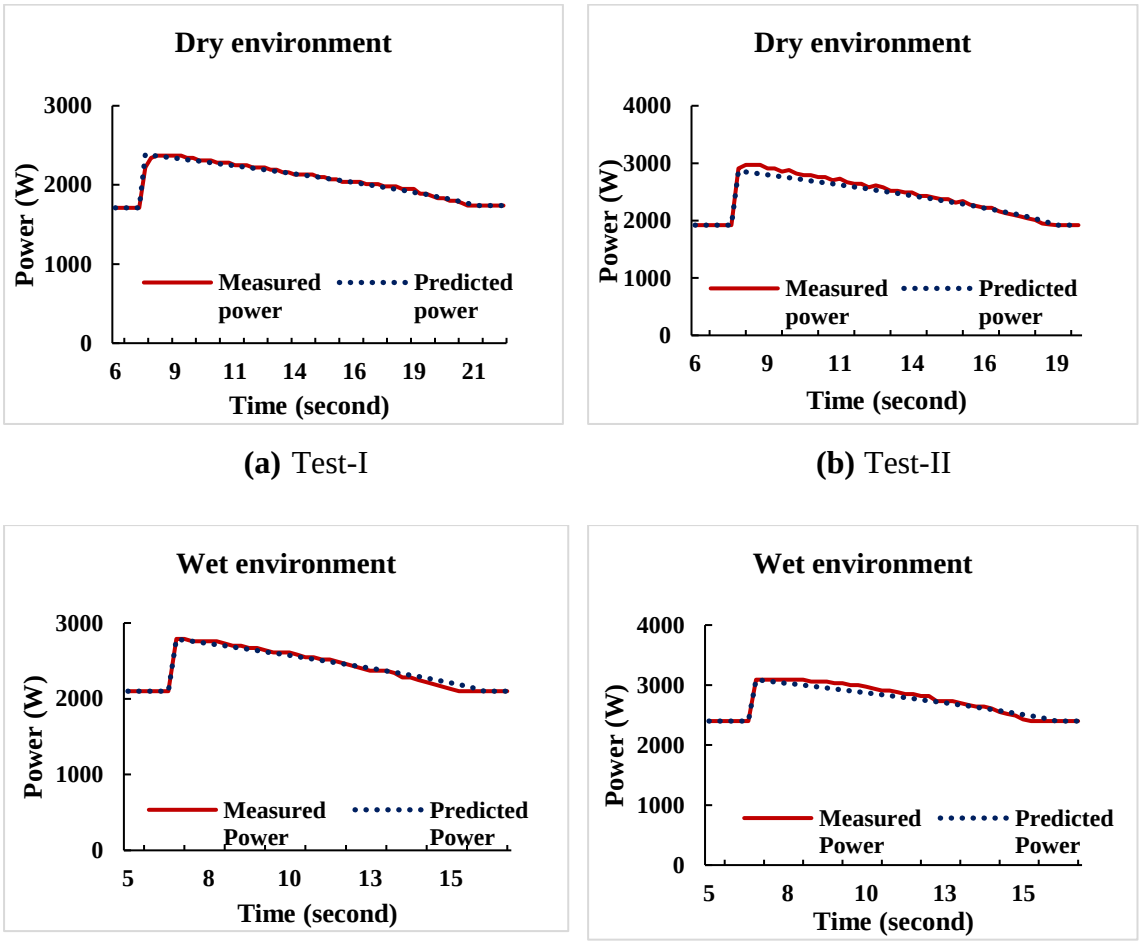

(a) Test-I **(b)** Test-II

(c) Test-III **(d)** Test-IV

Figure 3.5 Predicted power profile using developed model vs measured power profile of the validation tests: (a) Test-I: Dry cutting environment, $\boldsymbol{n = 16}00$ rev/min, $\boldsymbol{D_o}$ = 61 mm, $\boldsymbol{f_r}$ = 0.08 mm/rev, $\boldsymbol{d_c}$ =1.4 mm and $\boldsymbol{r}$ = 0.8 mm; (b) Test-II: Dry cutting environment, $\boldsymbol{n = 20}00$ rev/min, $\boldsymbol{D_o}$ = 61 mm, $\boldsymbol{f_r}$ = 0.08 mm/rev, $\boldsymbol{d_c}$ =1.8 mm and $\boldsymbol{r}$ = 1.2 mm; (c) Test-III: Wet cutting environment $\boldsymbol{D_o}$ = 61 mm, $\boldsymbol{n = 16}00$ rev/min, $\boldsymbol{f_r}$ = 0.12 mm/rev, $\boldsymbol{d_c}$ =1.0 mm and $\boldsymbol{r}$ = 0.8 mm; (d) Test-IV: Wet cutting environment, $\boldsymbol{D_o}$ = 61 mm, $\boldsymbol{n = 24}00$ rev/min, $\boldsymbol{f_r}$ =0.08 mm/rev, $\boldsymbol{d_c}$ = 1.0 mm and $\boldsymbol{r}$ = 0.4 mm.

The proposed model can be applied to optimize cutting parameters for a VPC machining process and to develop energy consumption model of machine tools for

machining cylindrical parts. Predicting the energy consumption of machine tools for machining cylindrical parts remains challenging because the previous energy prediction models are typically developed with CPC machining processes. The machining of a workpiece includes the non-cutting process and cutting process (CPC and VPC machining process). By integrating the proposed model with the energy models of the non-cutting process and CPC machining process, an energy consumption model of machine tools for machining cylindrical parts can be established.

In industries, an accurate and practical energy consumption prediction model can be used during the initial design phase of a workpiece to estimate the energy consumption in their machining which can provide an opportunity to identify the most sustainable cutting parameters. In the process planning phase, there are several possibilities of different combinations of the process parameters by which a component can be machined. However, it is not reasonable to experiment with each alternative to evaluate their energy performance. Under such circumstances, the proposed model can be useful to identify the most sustainable and clean process plans.

3.5. Summary

An accurate and realistic energy consumption model is essential to estimate the energy needed for the machining of a product beforehand in its initial development stage and can provide an opportunity to identify the most sustainable and cleaner process parameters. In this chapter, a cutting energy consumption model for the VPC machining process i.e., end facing is developed. The cutting speed, feed rate, cutting depth and cutting tool nose radius were chosen as process parameters. The fitting coefficients of the model were determined by conducting experiments on Al 6061 workpiece using carbide inserts under dry and wet environments. The p-values for the fitting coefficients of process parameters were found

less than 0.05 and hence all the considered process parameters are statistically significant. The R^2 values for dry and wet environments were found more than 91% and 94% respectively, which shows that the developed model has acceptable accuracy for predicting the cutting power under various combinations of process parameters. Four validation experiments confirm the prediction capability of the developed model. The validation experiments confirm that the accuracy of the developed model is more than 96%. Further, the predicted power profiles of the end facing were in good agreement with the measured power profiles, which shows that the developed model satisfactorily encompasses the influences of the process parameters on the cutting power consumption.

Chapter 4:

Optimization of Variable Power Consumption Machining Processes – A Case of End Facing

In this chapter, the empirical model developed in **Chapter 3** is used as an input for the formulation of a multi-objective optimization model of cutting energy consumption and average-material removal rate. First, the optimal parameters are determined by mono-objective optimization using the Taguchi technique. Second, Grey relational analysis (GRA) coupled with Taguchi method is used to determine the optimal parameters to minimize the power consumption and maximize the average-material removal rate simultaneously.

4.1. Introduction

According to the previous studies reported in the literature, machine tools have an average energy efficiency of less than 30% (Liu et al., 2017). Energy-efficient machine tools can be developed, or existing machining processes can be optimized, to reduce the amount of electrical energy consumed by machining processes (Warsi et al., 2018). The development of energy-efficient machine tools requires solid economic provisions for technology development and can be implemented only by replacing the existing machine tools (Warsi et al., 2018). Optimizing existing machining processes is one of the most effective strategies to increase energy efficiency, and it can be applied on existing production lines with relative ease and with minimal resources (Bagaber and Yusoff, 2019; Hu et al., 2020). Cutting parameters are critical variables in the machining process, and manufacturers have a range of options for selecting them based on the workpiece's cutting requirements and the machining conditions (Chen et al., 2021). Earlier studies have shown that by selecting the appropriate process parameters, tools, and tool paths, energy savings of up to 40% can be achieved (Chen et al., 2021; Zhang et al., 2017). This shows that the change in the process

parameters significantly influences the energy consumption of a machining process (Newman et al., 2012). As a result, process parameters play a key role in metal cutting, and selecting the correct parameters is critical for energy-efficient machining (Zhou et al., 2019).

However, one group of researchers appears to be completely focused on modelling (Aramcharoen and Mativenga, 2014; Edem et al., 2017; Jia et al., 2016; Liu et al., 2015, 2020; Zhou et al., 2017), while the other appears to be solely focused on optimization (Alswat and Mativenga, 2020; Bilga et al., 2016; Kumar et al., 2017), as a result, industry deployment of energy-saving solutions is impeded. Further, the use of experimental design approaches to determine optimum process parameters necessitates a large number of lengthy trials, which increases costs and time (Zerti et al., 2019). During the process planning, many alternative combinations of process parameters can be used to manufacture a workpiece by machining process. Evaluating each option to ascertain the machining energy consumption is not practicable. In these scenarios, an existing predictive model can be utilized to compute energy consumption based on process plans (Jia et al., 2016; Liu et al., 2015). As a result, there is a need to focus on the optimization of process parameters using pre-developed energy models (Chen et al., 2021). To bridge this gap, in the present chapter empirical model developed in **Chapter 3** is integrated to the optimization approach to select the process parameters to tradeoff between the cutting energy consumption and average-MRR ($\overline{MRR}$) for the variable power consumption machining process. The integrated approach will reduce the cost required for the time-consuming measurement procedures and advanced laboratory setup.

4.2. Research Gap

The work presented in the literature shows that many notable research on machining process optimization has been published, however, they primarily focus on constant-power consumption (CPC) machining processes like turning, drilling and milling, and optimization for the variable-power consumption (VPC) machining process is limited. As already discussed in **Chapter 3** that, the machining process parameters: cutting velocity (v_c), feed (f_r) and depth of cut (d_c) remain constant in the CPC machining process, and as a result, the cutting power remains unchanged. Whereas at least one of the machining parameters in the VPC machining process changes with time. As a result, the cutting power varies and its characteristics become more complicated.

To the best of the authors' knowledge, Hu et al. (2020) is the only work reported on VPC machining process optimization in which process parameters: spindle speed, feed rate and cutting depth were optimized for energy consumption during the end facing of ASTM 1045 steel workpiece using carbide inserts. The cutting energy is affected by a number of factors, including cutting parameters as well as cutter nose radius (Kumar et al., 2017; Kuram, 2017; Ma et al., 2014; Parida and Maity, 2017). Hu et al. (2020) study optimized only energy consumption without taking into account the cutter nose radius and has limited scope for establishing optimal process parameters, when there is a need to simultaneously maximize productivity. To bridge this gap, in this chapter, the cutting energy consumption model for the VPC machining process (i.e. end facing) developed in previous **Chapter 3** as a function of cutting parameters and nose radius is used as an input to optimize the cutting energy consumption and productivity (material removal rate) simultaneously. The common optimal parameters were determined by analyzing mono-objective optimization and multi-objective optimization. Firstly, the optimal parameters for the individual performance characteristics were determined by mono-objective optimization based on the

Taguchi technique. Then, GRA coupled with Taguchi is used for multi-objective optimization to determine the common optimal parameters for cutting energy consumption and average-material removal rate. The adopted methodology of the present study is shown in Figure 4.1.

4.3. Optimization for VPC Machining Process- A Case of End Facing

Manufacturing industries are under intense pressure to lower the energy usage of the metal cutting processes without sacrificing productivity, owing to the fast-rising worldwide market and environmental issues. Therefore, two performance characteristics: cutting energy consumption and average-material removal rate as an indicator of productivity, are simultaneously optimized for the selection of optimal process parameters during the end facing of an aluminium workpiece using carbide inserts. The optimization is performed in two stages: mono-objective optimization and multi-objective optimization. Spindle speed (n), feed per revolution (f_r), cutting depth (d_c) and cutter nose radius (r) are considered as the process parameters.

The various combinations of the considered process parameters were obtained according to Taguchi's L_{27} orthogonal array and are shown in Table 4.1. Furthermore, in this chapter, instead of performing the experiments on these combinations of process parameters, the cutting energy consumption in this chapter is determined using empirical model developed in **Chapter 3** to follow the integrated modelling and optimization approach for the VPC machining process. It will reduce the cost required for the time-consuming measurement procedures and advanced laboratory setup. The cutting energy consumption in a dry cutting environment ($E_{C_{dry}}$) for the various combinations of the process parameters based on L_{27} orthogonal array was computed using Eq. (1).

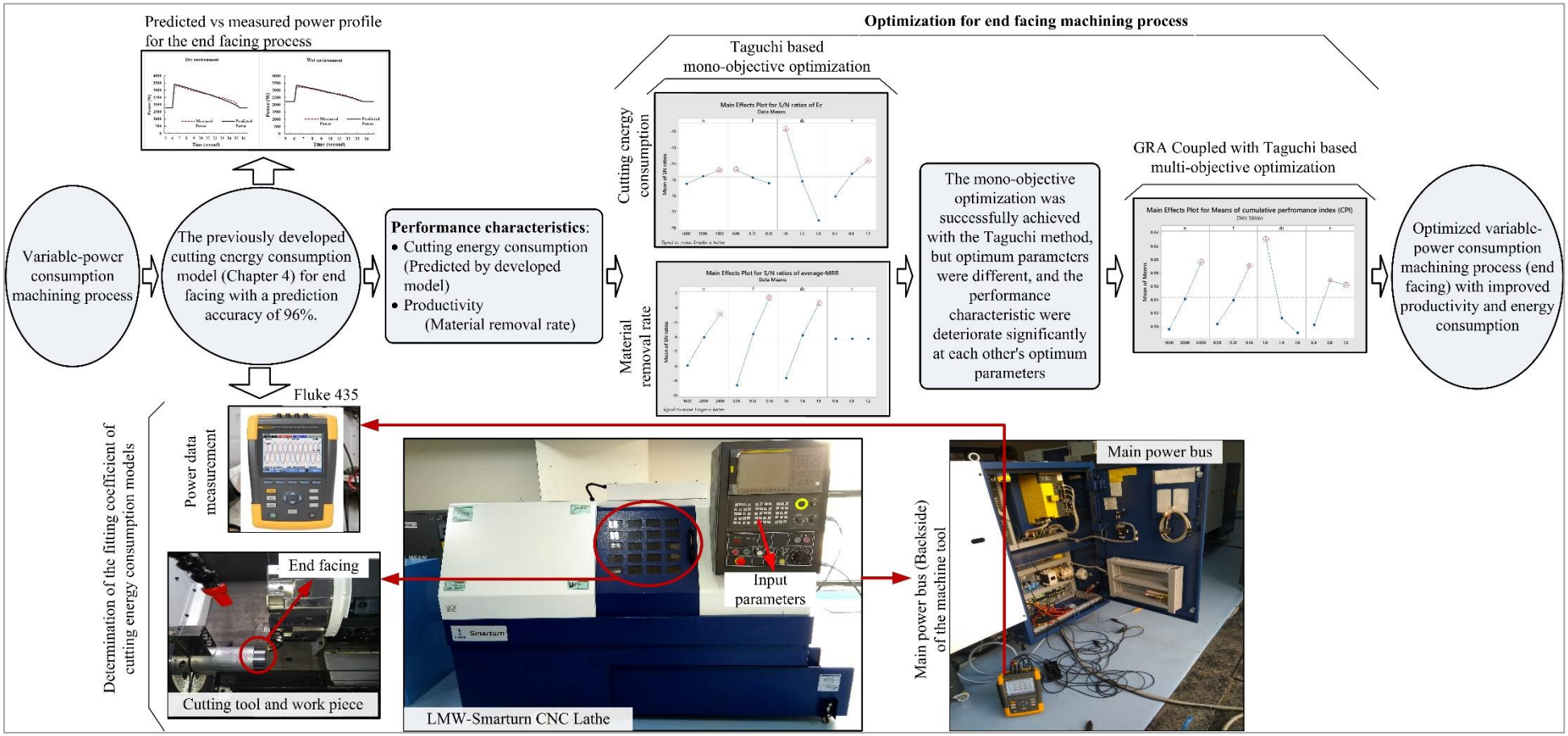

Figure 4. 1 Experimental setup and adopted methodology.

$$E_{C_{dry}} = \int_0^{T_c} 99.5115\left(v_{max} - \frac{2 f_r \pi n^2}{60000} t\right)^{\alpha} f_r^{\beta} d_c^{\gamma} r^{\delta} dt \quad (1)$$

Where α, β, γ and δ are 0.7641, 1.1385, 1.1145 and -0.2331 for dry cutting environment and 0.08382, 0.8387, 1.3399 and -0.2516 for wet cutting environment respectively. The cutting energy consumption in a dry cutting environment ($E_{C_{dry}}$) for the various combinations of the process parameters based on L_{27} orthogonal array was computed using Eq. (1). The calculated values are listed in Table 4.1. Due to variable cutting speed, the material removal rate is changing continuously during the end facing machining process, and therefore the $\overline{MRR}$ is adopted as productivity and calculated using Eq. (2).

$$\overline{MRR}\ \left(\frac{mm^3}{sec}\right) = \frac{\pi D^2 d_c}{4000.T_c} \times 1000 \quad (2)$$

Where D is the diameter of the workpiece in mm and T_c is the end facing time in seconds. The calculated $\overline{MRR}$ for different combinations of process parameters according to the L_{27} orthogonal array are listed in Table 4.1. The Taguchi method was used for mono optimization of the performance characteristics: $E_{C_{dry}}$ and $\overline{MRR}$, and the GRA coupled with Taguchi technique is used for multi-objective optimization. The mono and multi-objective optimizations are discussed in the subsequent sections.

Table 4.1 L_{27} orthogonal array and corresponding values of the performance characteristics

Exp. No.	Process parameters				Performance characteristics	
	n (rev/min)	f_r (mm/rev)	d_c (mm)	r (mm)	$E_{C_{dry}}$ (J)	$\overline{MRR}$ (mm^3/sec)
1	1600	0.08	1.0	0.4	4471.75	204.31
2	1600	0.08	1.4	0.8	5535.63	286.03

3	1600	0.08	1.8	1.2	6664.41	367.76
4	1600	0.12	1.0	0.8	4023.28	306.46
5	1600	0.12	1.4	1.2	5325.90	429.05
6	1600	0.12	1.8	0.4	9104.40	551.64
7	1600	0.16	1.0	1.2	3810.25	408.62
8	1600	0.16	1.4	0.4	7161.93	572.07
9	1600	0.16	1.8	0.8	8063.09	735.51
10	2000	0.08	1.0	0.4	4241.32	255.39
11	2000	0.08	1.4	0.8	5250.38	357.54
12	2000	0.08	1.8	1.2	6320.99	459.70
13	2000	0.12	1.0	0.8	3816.97	383.08
14	2000	0.12	1.4	1.2	5052.80	536.31
15	2000	0.12	1.8	0.4	8637.54	689.54
16	2000	0.16	1.0	1.2	3613.94	510.77
17	2000	0.16	1.4	0.4	6792.93	715.08
18	2000	0.16	1.8	0.8	7647.66	919.39
19	2400	0.08	1.0	0.4	4062.80	306.46
20	2400	0.08	1.4	0.8	5029.38	429.05
21	2400	0.08	1.8	1.2	6054.93	551.64
22	2400	0.12	1.0	0.8	3656.28	459.70
23	2400	0.12	1.4	1.2	4840.07	643.57
24	2400	0.12	1.8	0.4	8273.90	827.45
25	2400	0.16	1.0	1.2	3461.76	612.93
26	2400	0.16	1.4	0.4	6506.90	858.10
27	2400	0.16	1.8	0.8	7325.64	1103.27

4.3.1. Mono-objective optimization using Taguchi method

The Taguchi method was introduced by Genichi Taguchi uses the signal-to-noise ratio (SN) principle that ensures minimization in variation and improvement of the mean for the given set of data (Öztürk et al., 2019). The SN ratio is the ratio of predictable signal values with unpredicted noise values (Meral et al., 2019). Therefore, the process parameter level corresponding to the highest S/N ratio is considered as the optimal level for the observed performance characteristics (Sivaiah and Chakradhar, 2019). Primarily, three types of principles as stated in Eqs. (3), (4), and (5) are applied in the Taguchi technique to compute the SN ratio and a particular principle is applied to calculate the SN ratio depending on the nature of the performance characteristics or aim of the study (Meral et al., 2019).

Larger is the better principle:

$$\frac{S}{N} = -\log\frac{1}{q}\left(\sum\frac{1}{y^2}\right) \tag{3}$$

Smaller is the better principle:

$$\frac{S}{N} = -10\log\frac{1}{q}\left(\sum y^2\right) \tag{4}$$

Nominal is the better principle:

$$\frac{S}{N} = 10\log\frac{1}{q}\left(\frac{\bar{y}}{\sigma_y^2}\right) \tag{5}$$

Where y is the outcome of the dependent variable ($\overline{MRR}$ or $E_{C_{dry}}$); $\bar{y}$ is the average of y; σ_y^2 is the variance of y; and q is the total number of experimental runs (i.e. 27).

In this chapter, the objective is to maximizing the $\overline{MRR}$ and minimising the cutting energy consumption, Eqs. (3) and (4) are used to determine the corresponding SN ratios respectively. The calculated values are listed in Table 4.2.

Table 4.2. The calculated values of the SN ratios

Exp. no.	Process parameters				SN ratios	
	n (rev/min)	f_r (mm/rev)	d_c (mm)	r (mm)	$E_{C_{dry}}$	$\overline{MRR}$
1	1600	0.08	1.0	0.4	-73.0096	-13.7942
2	1600	0.08	1.4	0.8	-74.8633	-10.8717
3	1600	0.08	1.8	1.2	-76.4752	-8.6888
4	1600	0.12	1.0	0.8	-72.0916	-10.2724
5	1600	0.12	1.4	1.2	-74.5279	-7.3498
6	1600	0.12	1.8	0.4	-79.1850	-5.1670
7	1600	0.16	1.0	1.2	-71.6191	-7.7736
8	1600	0.16	1.4	0.4	-77.1006	-4.8511
9	1600	0.16	1.8	0.8	-78.1300	-2.6682
10	2000	0.08	1.0	0.4	-72.5500	-11.8560
11	2000	0.08	1.4	0.8	-74.4038	-8.9335
12	2000	0.08	1.8	1.2	-76.0157	-6.7506
13	2000	0.12	1.0	0.8	-71.6344	-8.3342
14	2000	0.12	1.4	1.2	-74.0706	-5.4116
15	2000	0.12	1.8	0.4	-78.7278	-3.2288
16	2000	0.16	1.0	1.2	-71.1596	-5.8354
17	2000	0.16	1.4	0.4	-76.6411	-2.9129

18	2000	0.16	1.8	0.8	-77.6706	-0.7300
19	2400	0.08	1.0	0.4	-72.1765	-10.2724
20	2400	0.08	1.4	0.8	-74.0303	-7.3498
21	2400	0.08	1.8	1.2	-75.6422	-5.1670
22	2400	0.12	1.0	0.8	-71.2608	-6.7506
23	2400	0.12	1.4	1.2	-73.6970	-3.8280
24	2400	0.12	1.8	0.4	-78.3542	-1.6451
25	2400	0.16	1.0	1.2	-70.7859	-4.2518
26	2400	0.16	1.4	0.4	-76.2675	-1.3293
27	2400	0.16	1.8	0.8	-77.2969	0.8536

Further, the main effect plot of SN ratios are used to analyze the influence of the process parameters on the performance characteristics and are shown in Figure 4.2 and Figure 4.3 for $E_{C_{dry}}$ and $\overline{MRR}$ respectively.

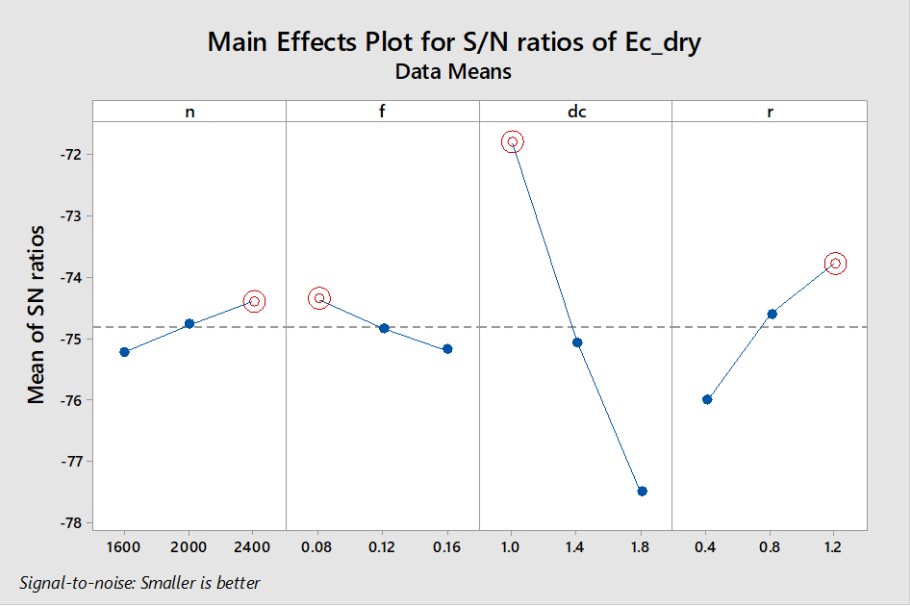

Figure 4.2 Main effect plot of SN ratios for cutting energy consumption.

The level of the process parameter with the highest *SN* ratio indicates its optimal level. Accordingly, as shown in Figure 4.2, the highest value of spindle speed and nose radius i.e. $n_3 = 2400$ rev/min and $r_3 = 1.2$ mm, and the lowest value of the feed rate and cutting depth i.e. $f_{r_1} = 0.08$ mm/rev and $d_{c_1} = 1.0$ mm are the optimum combination to achieve minimum cutting energy consumption.

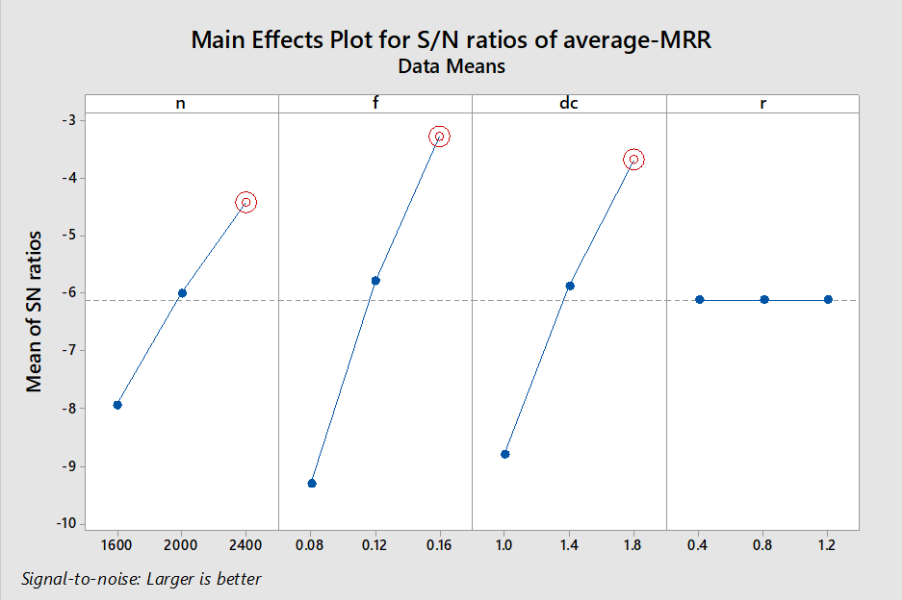

Figure 4.3 Main effect plot of *SN* ratios for average-material removal rate.

The energy consumption reduces as the angular speed of the spindle increases, because the machining time is decreased. Increases in feed rate and cutting depth results in a larger undeformed chip region, requiring more force and power to remove the material, resulting in increased energy consumption. A similar trend for the feed rate and cutting depth was reported by Kant and Sangwan (2014). Furthermore, increasing the nose radius results in smoother cutting, which minimizes vibrations and improves the *SN* ratios. These findings are consistent with previously published research Bilga et al. (2016) and Kuram (2017).

For maximum material removal rate ($\overline{MRR}$), as shown in Figure 4.3, the highest values of the spindle speed, feed rate, cutting depth and nose radius i.e. $n_3 = 2400$ rev/min of,

f_{r_3} = 0.16 mm/rev, d_{c_3} = 1.8 mm and r_3 = 1.2 mm with the maximum values of corresponding *SN* ratio are the optimal combination of the cutting parameters. Higher cutting depths and feed rates produce a larger undeformed chip zone, resulting in more material removal. The high angular speed accelerates the material removal. The nose radius for the $\overline{MRR}'s$ *SN* ratio is theoretically insignificant and therefore changes in the nose radius do not affect it. However, the nose radius of the cutter, which produces the desired result, should be used.

The combinations of the optimal levels of the process parameter for cutting energy consumption i.e. $n_3, f_{r_1}, d_{c_1}, r_3$ and for average-material removal rate i.e. $n_3, f_{r_3}, d_{c_3}, r_3$ achieved after Taguchi analysis are different from the L_{27} orthogonal array i.e. Table 4.1. Hence, $\overline{MRR}$ at their optimum cutting parameters is calculated using Eq. (2) and found to be 1119.20 mm^3/sec. Eq. (1) is used to compute the cutting energy consumption at their optimum process parameters and the validation experiment was conducted on the optimal process parameters to obtain the cutting energy consumption. The experiment was repeated three times, and the average value of the three measurements was adopted. The results are shown in Table 4.3.

Table 4.3 Optimal parameters by mono-objective optimization

Performance Characteristics	Optimal parameters	Comparison		
	$n_3, f_{r_1}, d_{c_1}, r_3$	Measured	Predicted	Error (%)
$E_{C_{dry}}$	2400, 0.08, 1.0, 1.2	3062.5 J	3144.88 J	2.7

Nevertheless, the Taguchi method has shown effective in achieving mono-objective optimization, but the optimal level of cutting parameters differs based on the performance characteristic e.g. the higher level of cutting parameters is desirable for material removal rate while in the case of cutting energy consumption, the lower values of feed rate and

cutting depth are desirable. Thus, energy consumption increases when the $\overline{MRR}$'s optimal parameters are satisfied, while the $\overline{MRR}$ decreases when the energy consumption's optimal parameters are fulfilled. For example, the $\overline{MRR}$ value decreases by 72.61% (from 1119.20 mm^3/sec to 306.46 mm^3/sec) at the optimum parameters of energy consumption. Thus, to obtain the common optimal levels of the cutting parameters, the GRA coupled with the Taguchi method was adopted and the details are discussed in **Section** 4.3.2.

4.3.2. Multi-objective optimization using GRA based Taguchi method

The major limitation of mono optimization is that it improves a particular performance characteristic while ignoring the other necessary contradictory performance characteristics and determining local optimal parameters (Bagaber and Yusoff, 2018). Although the Taguchi method is one of the popular methods for mono optimization, it is inefficient for a system where multiple performance characteristics have to be optimized simultaneously. Therefore, Grey Relational Analysis (GRA) was used to obtain the cumulative performance index (CPI) of the performance characteristics: cutting energy consumption and $\overline{MRR}$. Further, Taguchi method was used to optimize the CPI.

The following steps are commonly used to calculate the CPI for multi-objective optimization using GRA (Kant and Sangwan, 2014; Meral et al., 2019):

Step 1: Normalization

The performance characteristics are normalized to bring them on a common comparable scale because the range and units of the performance characteristics may differ from each other. Depending on the nature of the performance characteristics, one of the criteria: "Larger is the better"; "Smaller is the better" and "Nominal is the better" may be used for their normalization. The present study aims to minimize cutting energy consumption and

maximize $\overline{MRR}$, and therefore, "smaller is the better" and "larger is the better" criteria respectively as stated in Eqs. (6) and (7) were used for their normalization.

Smaller the better criteria:

$$x_p^*(q) = \frac{Max\ x_p(q) - x_p(q)}{Max\ x_p(q) - Min\ x_p(q)} \tag{6}$$

Larger is the better criteria:

$$x_p^*(q) = \frac{x_p(q) - Min\ x_p(q)}{Max\ x_p(q) - Min\ x_p(q)} \tag{7}$$

Where, $x_p^*(q)$ is the normalized value/sequence of the performance characteristics, $x_p(q)$ is the actual (predicted/calculated) value of the performance characteristics, Max $x_p(q)$ and Min $x_p(q)$ are the maximum and minimum values of the actual data. The calculated normalized values of cutting energy consumption and $\overline{MRR}$ based on Eqs. (6) and (7) respectively are summarized in Table 4.4.

Step 2: Grey Relational Coefficient

Grey Relational Coefficient (GRC) reveals the relationship between ideal and normalized performance characteristics values and can be calculated as follows:

$$GRC(q) = \frac{\Delta_{\min} + \zeta\Delta_{max}}{\Delta_{op}(q) + \zeta\Delta_{max}} \tag{8}$$

Where ζ is the distinguish coefficient and its value is found in the range of 0 to 1. In the present study, it is taken 0.5 as recommended in the literature by Hanafi et al. (2012) and Kant and Sangwan (2014). $\Delta_{op}(q)$ represents the deviation from the target value and can be calculated as follows:

$$\Delta_{op}(q) = \left| x_o^{\circ}(q) - x_p^{*}(q) \right|$$

Where $x_o^{\circ}(q)$ is the ideal sequence and $x_p^{\circ}(q)$ is the current sequence. The calculated GRCs using Eq. (8) are listed in Table 4.4.

Step 3: Grey Relational Grades

GRG is the weighted sum of each GRC and can be calculated by multiplying each GRC and its assigned weight. The CPI is essentially the GRG for each experimental run, and it will be used in place of the GRG in the rest of the paper. The equal weights were assigned to both the performance characteristics and Eq. (9) is used to calculate the CPI.

$$CPI_i = \sum_{j=0}^{p} \left[w_j * \mathrm{GRC}_i \right] \tag{9}$$

Where p is the total number of performance characteristics. w_j is the assigned weight to the performance characteristic such that $\sum_{j=1}^{p} w_j = 1$. Table 4.4 shows the calculated CPIs for each of the experimental runs.

Table 4.4 The computed values of normalized sequence, deviational sequence, Grey Relational Coefficient, and Cumulative Performance Index

Exp. No.	Normalized sequences		Deviational sequences		Grey Relational Coefficient		Cumulative Performance Index	
	E_{Cdry}	$\overline{MRR}$	E_{Cdry}	$\overline{MRR}$	E_{Cdry}	$\overline{MRR}$	Size	Ranking
1	0.8210	0.0000	0.1790	1.0000	0.7364	0.3333	0.5349	14
2	0.6325	0.0909	0.3675	0.9091	0.5763	0.3548	0.4656	21
3	0.4324	0.1818	0.5676	0.8182	0.4683	0.3793	0.4238	26
4	0.9005	0.1136	0.0995	0.8864	0.8340	0.3607	0.5973	7

5	0.6696	0.2500	0.3304	0.7500	0.6021	0.4000	0.5011	16
6	0.0000	0.3864	1.0000	0.6136	0.3333	0.4490	0.3912	27
7	0.9382	0.2273	0.0618	0.7727	0.8901	0.3929	0.6415	5
8	0.3442	0.4091	0.6558	0.5909	0.4326	0.4583	0.4455	24
9	0.1845	0.5909	0.8155	0.4091	0.3801	0.5500	0.4650	22
10	0.8618	0.0568	0.1382	0.9432	0.7835	0.3465	0.5650	10
11	0.6830	0.1705	0.3170	0.8295	0.6120	0.3761	0.4940	19
12	0.4933	0.2841	0.5067	0.7159	0.4967	0.4112	0.4539	23
13	0.9370	0.1989	0.0630	0.8011	0.8882	0.3843	0.6362	6
14	0.7180	0.3693	0.2820	0.6307	0.6394	0.4422	0.5408	13
15	0.0827	0.5398	0.9173	0.4602	0.3528	0.5207	0.4368	25
16	0.9730	0.3409	0.0270	0.6591	0.9488	0.4314	0.6901	3
17	0.4096	0.5682	0.5904	0.4318	0.4586	0.5366	0.4976	17
18	0.2582	0.7955	0.7418	0.2045	0.4026	0.7097	0.5562	12
19	0.8935	0.1136	0.1065	0.8864	0.8244	0.3607	0.5925	8
20	0.7222	0.2500	0.2778	0.7500	0.6428	0.4000	0.5214	15
21	0.5404	0.3864	0.4596	0.6136	0.5211	0.4490	0.4850	20
22	0.9655	0.2841	0.0345	0.7159	0.9355	0.4112	0.6734	4
23	0.7557	0.4886	0.2443	0.5114	0.6718	0.4944	0.5831	9
24	0.1472	0.6932	0.8528	0.3068	0.3696	0.6197	0.4947	18
25*	1.0000	0.4545	0.0000	0.5455	1.0000	0.4783	0.7391	1
26	0.4603	0.7273	0.5397	0.2727	0.4809	0.6471	0.5640	11
27	0.3152	1.0000	0.6848	0.0000	0.4220	1.0000	0.7110	2

***** Represents the optimum level of the process parameters

Step 4: Cumulative Performance Index ranking

The high CPI value indicates that the selected performance characteristics are improved simultaneously and that their performance is better when they act together (Mia et al., 2019). Hence, a rank of 1 represents the optimal combination of process parameters. Experiment number 25 is ranked first in Table 4.4, and the corresponding values of the process parameters are: 2400 rev/min of spindle angular speed, 0.16 mm/rev of feed rate, 1.0 mm of cutting depth, and 1.2 mm nose radius are found to be optimal parameters for simultaneous better performance of E_{Cdry} and $\overline{MRR}$.

The main effect plot of CPI is plotted using the Taguchi technique to analyze the influence of each level of the process parameter, and the results are shown in Figure 4.4 and Table 4.5.

Table 4.5 Responses table for means of the CPI

Process parameters		n	f_r	d_c	r
Level	I	0.4962	0.5040	0.6300*	0.5024
	II	0.5412	0.5394	0.5126	0.5689
	III	0.5960*	0.5900*	0.4908	0.5621*
Delta		0.0998	0.0860	0.1392	0.0665
Rank		2	3	1	4

***** Represents the optimum level of the process parameters

The larger the CPI, the better is the corresponding performance characteristics (Kant and Sangwan, 2014). Hence, the level of the process parameter corresponding to the highest mean is adopted as their optimal level for the CPI. Thus, as shown in Figure 4.4 and Table 4.5, level 3 of spindle speed (i.e. 2400 rev/min), level 3 of feed rate (0.16 mm/rev), and

level 1 of cutting depth (1.0 mm) are adopted as optimal parameters for CPI. It can be seen in Table 4.5 and Figure 4.4, that the difference in the mean of level 2 and level 3 for the nose radius is insignificant. However, the cutter nose radius that provides the intended outcome can be used. As shown in Eq. (1), keeping other parameters constant, a higher nose radius reduces cutting energy consumption and does not affect the $\overline{MRR}$. Therefore, level 3 i.e. 1.2 mm was adopted as the optimal level of nose radius for the CPI.

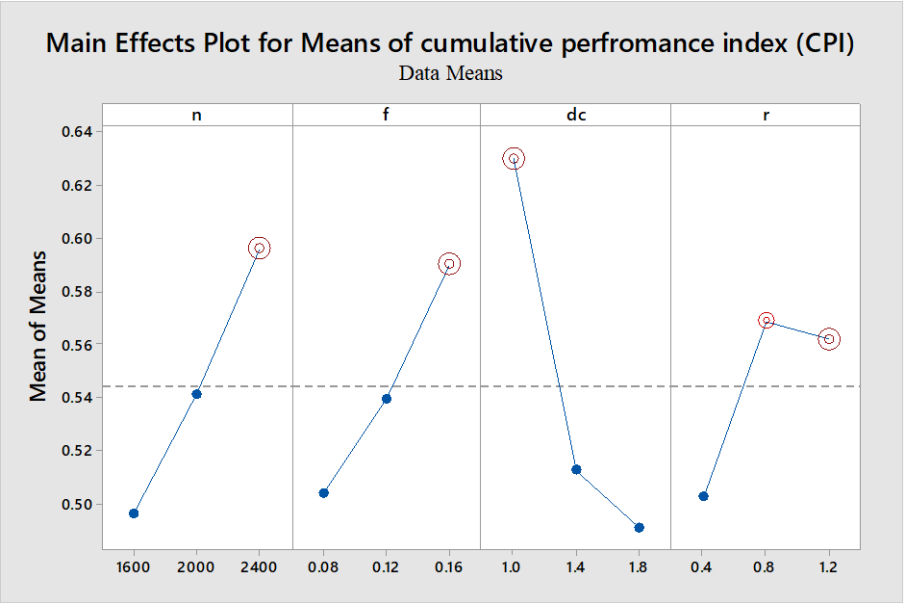

Figure 4.4. Main effect plot for means of Cumulative Performance Index (CPI)

For each process parameter, delta is calculated which is the difference between the highest and lowest average CPI values. The delta value indicates the relative effect of each factor on the CPI, the higher the value, the greater the effect. As shown in Table 4.5, the d_c was found to be the most influential parameter on the CPI followed by n, f_r and r. Further, analysis of variance (ANOVA) was used to test the statistical significance of the process parameters on the CPI at a 95% confidence level, as shown in Table 4.6.

As shown in Table 4.6, the p-values for each parameter (v_c, f_r, d_c and r) is less than 0.05 which shows that each process parameter is statistically significant for the CPI. The

large F-values ($F > 4$) indicates the strong relationship between the process parameters and the CPI. The percentage contribution of ANOVA analysis validated the effect of the process parameters on the CPI found with the Taguchi technique as shown in Table 4.5.

Table 4.6 ANOVA for Cumulative Performance Index.

Parameters	DF	SS	MS	F-Value	p-Value	PC
Model	4	0.181	0.045	24.280	0.000	81.53
n	1	0.181	0.045	24.280	0.000*	20.17
f_r	1	0.045	0.045	24.030	0.000*	14.96
d_c	1	0.033	0.033	17.830	0.000*	39.20
r	1	0.087	0.087	46.700	0.000*	7.19
Error	22	0.016	0.016	8.570	0.008	18.47
Total	26	0.041	0.002			100.00

* Represent the significant process parameters; DF: degree of freedom; SS: sum of squares; MS: mean of squares; PC: percentage contribution

The cutting depth was found to be the highest contributor for CPI with a value of 39.20%, and the percentage contribution of spindle speed, feed rate, and nose radius was found to be 20.17%, 14.96%, and 7.19% respectively. The validation experiments were conducted on the optimal level of the process parameters i.e. $n_3, f_{r_3}, d_{c_1}, r_3$ predicted using the integrated modelling and optimization approach i.e. GRA coupled with Taguchi, and the corresponding measured and predicted values of the cutting energy consumption are shown in Table 4.7.

The experiments on optimal process parameters were repeated three times, and the mean value was adopted. Table 4.7 shows that energy consumption values predicted by the integrated modelling and optimization approach are close to the experimental values.

Table 4.7 Optimized process parameters with multi-objective optimization based on GRA coupled with Taguchi method.

Optimized process parameters	Performance Characteristics			
	$\overline{MRR}$ (mm^3/sec)	$E_{C_{dry}}$ (J)		
n_3, f_{r_3}, d_{c_1}, r_3		Measured	Predicted	Error (%)
2400, 0.16, 1.0, 1.2	612.93	3349.2	3461.76	3.36

4.4. Discussion

The results of mono-objective and multi-objective optimization are summarized in Table 4.8. It is evident that in multi-objective optimization studies, improvements in a performance characteristic may cause the deterioration of other performance characteristics (Camposeco-Negrete, 2015; Kumar et al., 2017; Yan and Li, 2013).

Table 4.8 Summary of optimizations results and their comparison

Optimization approach	*MRR* (mm^3/sec)	E_{Cdry} (J)
Mono-objective optimization of E_{Cdry}	306.46	3144.88
Mono-objective optimization of $\overline{MRR}$	1119.20	6664.71
multi-objective optimization	612.93	3461.76
Change as compared to mono-objective optimization of E_{Cdry}	99.97% (improved)	10.08% (deteriorate)
Change as compared to mono-objective optimization of $\overline{MRR}$	-45.24% (deteriorate)	-48.06% (improved)

$+$ve change represents an improvement in $\overline{MRR}$ and $-$ve change represents an improvement in E_{cdry}

In Table 4.8, a deterioration in both $E_{c_{dry}}$ and $\overline{MRR}$ was observed at the common optimum parameters compared to their corresponding mono-objective optimization. However, multi-objective optimization, on the other hand, provides a common optimal level of process parameters, at which $E_{c_{dry}}$ and $\overline{MRR}$ are optimized simultaneously, providing better-compromised decisions. For example, When the $\overline{MRR}$ and $E_{c_{dry}}$ values on common optimal parameters are compared to their values at optimal parameters with mono optimization of $E_{c_{dry}}$, the $\overline{MRR}$ improves to 99.97%, while cutting energy consumption only increases by 10.08%. When the $\overline{MRR}$ and $E_{c_{dry}}$ values on common optimal parameters are compared to their values on optimal parameters with mono optimization of $\overline{MRR}$, the $E_{c_{dry}}$ improves to 45.24% while the $\overline{MRR}$ decreases to 48.06%.

4.5. Summary

In this chapter, an integrated modelling and optimization approach was used to select the optimal process parameters for a VPC machining process to trade-off between productivity and cutting energy consumption. The empirical model was used to determine the values of cutting energy consumption without conducting actual experiments and is integrated to the optimization model. The integrated approach reduced the cost required for the time-consuming measurement procedures and advanced laboratory setup. Multi-objective optimization i.e. GRA coupled with Taguchi was used to determine the common optimal level of process parameters on which cutting energy consumption and average-material removal rate are optimized simultaneously, resulting in better-compromised decisions. On the common optimal process parameters i.e. $n_3, f_{r_3}, d_{c_1}, r_3$ the values of the cutting energy consumption and average- material removal rate are found to be 3461.76 *J* and 612.93 mm^3/sec respectively. The validation experiments were performed on the optimal level of process parameters obtained through mono and multi-objective optimization, and the error

in each case was limited to 4% only. Further, ANOVA revealed that all process parameters have statistical significance where the cutting depth was found to be most influencing process parameter followed by spindle speed, feed rate, and cutter nose radius respectively. The results obtained by ANOVA analysis validated the effect of process parameters found with the integrated modelling and optimization approach.

Further, the proposed approach could be beneficial for mass production, where the different factors, such as machine tools, workpiece materials, and cutting tools, remain constant. Machine tools have a complex and dynamic structure due to the diverse and complex interaction of various materials, process parameters, and cutting tools. However, in mass production systems, factor of diversification could reduce, and the projected approach may be practically possible. This approach can be used in other machining and industrial processes for energy-efficient process planning and can assist industries in achieving high-level sustainable performance.

Chapter 5:

Modelling the Energy Consumption of Machine Tools

In this chapter, energy consumption of a machine tool is divided into different energy modules: start-up, standby, spindle acceleration, idle, rapid positioning, air-cutting, Constant Power Consumption (CPC) machining process and Variable Power Consumption (VPC) machining process. Energy consumption models for each module were developed and integrated to establish the energy consumption for a machine tool. The fitting coefficients of the model are determined by conducting experiments under dry and wet environments. The validation experiments confirm that the accuracy of the developed model is 97%.

5.1. Introduction

Computer Numerical Control (CNC) machine tools play an imperative role in the manufacturing industry and consumes a significant amount of energy in machining processes e.g. turning, milling and drilling (Kant and Sangwan, 2014; Lv et al., 2016; Tuo et al., 2018). As previously mentioned that the machine tools have an average energy efficiency of less than 30% (Yan He et al., 2012). The European Commission has enlisted machine tools as one of the vital products to reduce electric energy consumption in the manufacturing processes (Schudeleit et al., 2016). Therefore, reducing the energy consumption of the machine tools is one of the major challenges for the industries to meet sustainable manufacturing (Diaz-Elsayed et al., 2015; Hu et al., 2017; Xiao et al., 2019). Establishing an accurate energy consumption model for machine tools is the basis for reducing energy consumption. The lack of an accurate and realistic energy consumption model has hindered the implementation of energy-efficient approaches such as energy-efficient process planning and scheduling (Lv et al., 2018; Wang et al., 2015).

A review of the existing literature presented in **Chapter 2** reveals several advancements in this direction. Several models have been proposed in the literature to assess the energy consumption of machine tools in machining processes. The reported studies are significant but still lack to evaluate the energy consumption of machine tools for machining cylindrical part in industrial applications. In industry, the length and diameter are reduced to obtain the final dimensions of a cylindrical part. Typically, external turning operation is used to reduce the diameter of the part i.e. Constant-Power Consumption (CPC) machining process and end facing operation is conducted to reduce the length of the part i.e. Variable-Power Consumption (VPC) machining process. As previously discussed in **Chapter 3**, the cutting power characteristic of the VPC machining process (e.g. end facing) is complicated and dynamic due to one of the changing input process parameters (e.g. cutting velocity in end facing) during machining than the CPC machining process (e.g. turning). The existing energy consumption models only consider CPC machining processes, whereas cylindrical part machining includes both CPC and VPC machining processes to manufacture the final product, which result in inaccurate quantification of the energy consumption. To overcome the above-mentioned research gaps, in this chapter, an energy consumption prediction model of machine tools for machining cylindrical parts is established. The energy consumption of a machine tool is separated into different energy modules: start-up, standby, spindle acceleration, idle, rapid positioning, air-cutting, and cutting. The cutting energy consumption module is further subdivided into the CPC machining process and VPC machining process. Energy consumption models are developed for each module and are integrated to establish the energy consumption model of the machine tool. Experiments under no-load i.e. non-cutting and cutting were conducted on a LMW-Smarturn CNC lathe machine tool to acquire the fitting coefficients of the developed models for different

modules. Four experiments were performed to validate the prediction accuracy of the developed model.

5.2. Energy Consumption Modelling Methodology

The power profile of a machine tool during machining of a cylindrical part is shown in Figure 5.1 and is considered a basis to describe their energy consumption. As shown in Figure 5.1, the power varies continuously, and it is challenging to develop a single energy consumption model for the entire process. The total energy consumption (E_{total}) can be decomposed into different modules: startup energy ($E_{startup}$), standby energy ($E_{standby}$), spindle acceleration energy (E_{acc}), idle energy (E_{idle}), tool change energy (E_{tc}), air-cutting energy (E_{air}), coolant pump energy (E_{cool}), cutting tool rapid positioning energy (E_{rapid}) and cutting energy (E_{cut}).

$$E_{total} = E_{startup} + E_{standby} + E_{acc} + E_{rapid} + E_{idle} + E_{tc} + E_{air} + E_{cool} + E_{cut} \quad (1)$$

Specific models can be obtained for each module based on the power characteristics, and their definite integration can evaluate the respective energy consumption. Thus, Eq. (1) can be expressed as:

$$E_{total} = \begin{bmatrix} \int_0^{t_{stp}} P_{startup}(t)\,dt + \int_0^{t_{std}} P_{standby}\,dt + \int_0^{t_{acc}} P_{acc}(t)\,dt + \int_0^{t_{rpd}} P_{rapid}(t)\,dt + \\ \int_0^{t_{idle}} P_{idle}\,dt + \int_0^{t_{tc}} P_{tc}\,dt + \int_0^{t_{air}} P_{air}\,dt + \int_0^{t_{cool}} P_{cool}\,dt + \int_0^{t_{cut}} P_{cut}\,dt \end{bmatrix} \quad (2)$$

Where $P_{startup}(t)$, $P_{standby}$, $P_{acc}(t)$, $P_{rapid}(t)$, P_{idle}, P_{tc}, P_{air}, P_{cool} and P_{cut} are the startup power at an instant *t*, standby power, spindle acceleration power at an instant *t*, rapid power at an instant *t*, idle power, tool change power, air-cut power, coolant pump power, and cutting power respectively. t_{stp}, t_{std}, t_{acc}, t_{rpd}, t_{idle}, t_{tc}, t_{air}, t_{cool} and t_{cut} are the periods of different modules: startup, standby, spindle acceleration, rapid positioning, idle, tool change, air-cut, coolant, and cutting respectively.

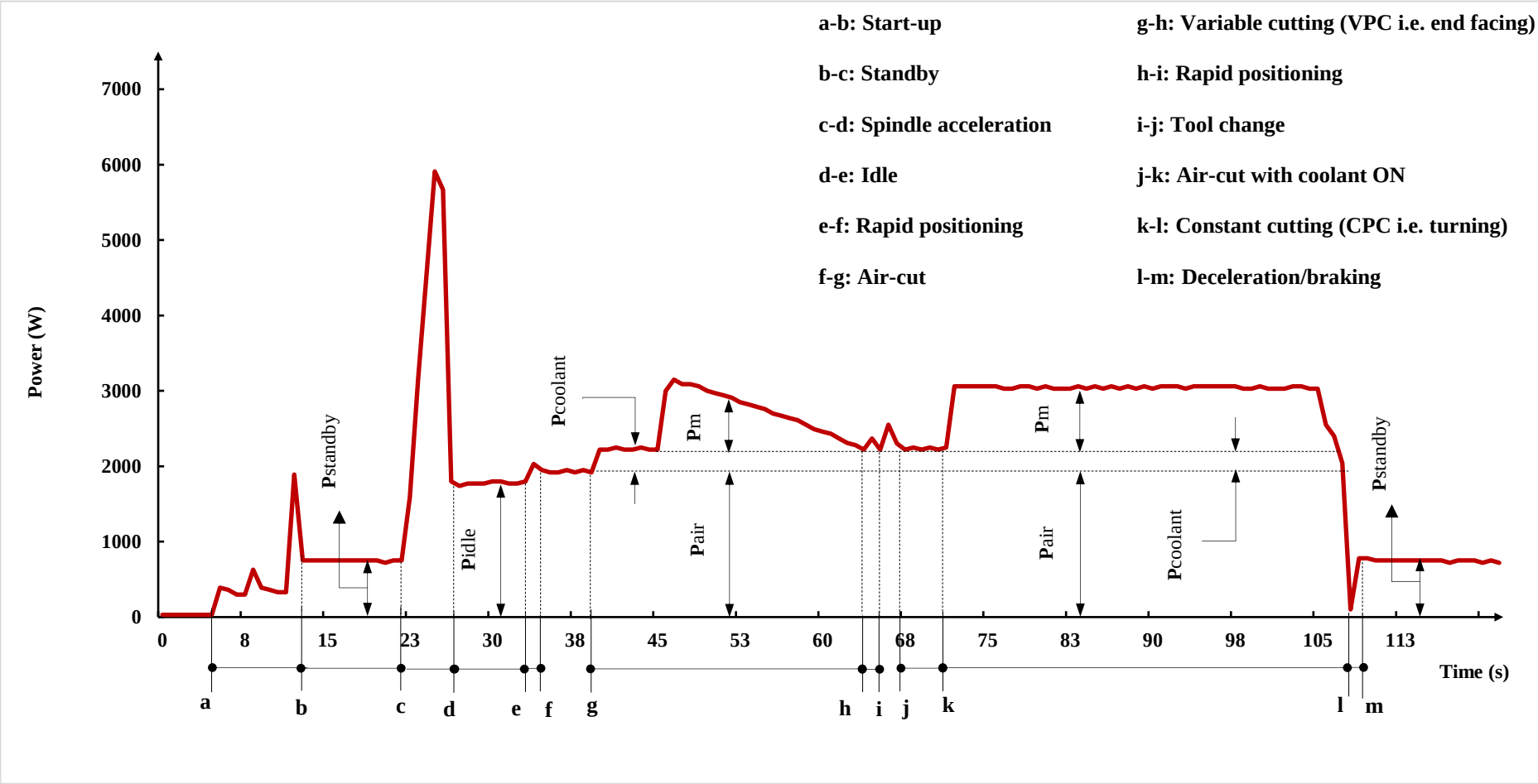

Figure 5.1. A typical power profile of a machine tool during machining of a cylindrical part.

In Eq. (1), E_{cut} is the cutting module energy consumption i.e. during which material is removed from the cylindrical part. However, as previously mentioned, the cutting energy for machining a cylindrical part can be further divided into cutting energy of the CPC machining process (E_{cut_CPC}) and cutting energy of the VPC machining process (E_{cut_VPC}) and can be expressed as:

$$E_{cut} = E_{cut\_CPC} + E_{cut\_VPC}$$

$$E_{cut} = \int_0^{t_{cut}} P_{cut} dt = \int_0^{t_{CPC}} P_{cut\_CPC} dt + \int_0^{t_{VPC}} P_{cut\_VPC}(t)\, dt \tag{3}$$

Where P_{cut_CPC} is the power consumption in the CPC machining process and $P_{cut\_VPC}(t)$ is the power consumption at an instant t in the VPC machining process. $t_{cut} = t_{CPC} + t_{VPC}$, where t_{CPC} and t_{VPC} are the time of the CPC machining and VPC machining process respectively. By substituting Eq. (3) in Eq. (2), the total energy consumption of a machine tool for machining of a cylindrical part can be expressed as:

$$E_{total} = \left[\begin{array}{l} \int_0^{t_{stp}} P_{startup}(t)\, dt + \int_0^{t_{std}} P_{standby} dt + \int_0^{t_{acc}} P_{acc}(t)\, dt + \int_0^{t_{rpd}} P_{rapid}(t)\, dt + \int_0^{t_{idle}} P_{idle}(t)\, dt + \\ \int_0^{t_{tc}} P_{tc} dt + \int_0^{t_{air}} P_{air} dt + \int_0^{t_{cool}} P_{cool} dt + \int_0^{t_{CPC}} P_{cut\_CPC} dt + \int_0^{t_{VPC}} P_{cut\_VPC}(t)\, dt \end{array} \right] \tag{4}$$

The energy demand estimation for the aforementioned different energy modules is presented in the following subsections.

5.2.1 Start-up energy consumption

Start-up energy provides power to cooling systems, hydraulic systems, control panels, and display devices for a short duration. It is constant for a machine tool and does not depends on the process parameters as shown in Figure 5.1. It can be calculated by the definite integral of power with respect to time. Hence, the start-up energy can be calculated as:

$$E_{startup} = \int_0^{t_{stp}} P_{startup}(t)\,dt \tag{5}$$

5.2.2 Standby energy consumption

Standby power is a fixed power required by a machine tool once the start-up power spike stabilizes. In the standby state, the various systems such as the cooling systems, hydraulic systems, control panel and visualizing components are in an active state and confirm the normal operative condition of the machine tool (Y He et al., 2012). This power is steady and does not depend on the process parameters, although standby time depends on the type of machine tool, part/tool holding device, and proficiency of the operator. The standby power can be experimentally measured, and the standby energy consumption can be computed as:

$$E_{standby} = \int_0^{t_{std}} P_{standby}\,dt = P_{standby} \times t_{std} \tag{6}$$

5.2.3 Spindle acceleration energy consumption

The spindle system typically includes a spindle motor, frequency converter, speed sensor, and mechanical transmission gear/pulley arrangements. A significant power spike occurs during spindle acceleration because the spindle system needs the power to endure the substantial standing inertia of the spindle motor and transmission system in order to run the spindle at the desired speed. The energy spent during spindle acceleration is a function of power, as illustrated in Figure 5.1, and can be estimated using the definite integral of power with the function of time. So, the spindle acceleration energy can be computed as:

$$E_{acc} = \int_0^{t_{acc}} P_{acc}(t)\,dt \tag{7}$$

The laws governing the power characteristics of spindle acceleration are complex and difficult to determine. However, for a given spindle speed acceleration, energy

consumption is constant, this indicates that there is a functional relationship between spindle acceleration energy and spindle speed (Liu et al., 2015). Hence, the spindle acceleration energy consumption for several selected angular speeds can be recorded, and based on these data its regression model in terms of angular speed can be developed as shown in Eq. (8).

$$E_{acc} = x_1 \times n^2 + x_2 \times n + x_3 \tag{8}$$

Where x_1, x_2 and x_3 are fitting coefficients, n is spindle angular velocity in rev/min.

5.2.4 Coolant pump energy consumption

Coolant pump power is a fixed power required by a machine tool once the coolant pump motor is turned on for the wet cutting environment. This power is steady and does not depend on the process parameters and is generally mentioned in the technical specifications of the machine tools or can be experimentally measured and the corresponding energy consumption can be calculated as:

$$E_{cool} = \int_0^{t_{cool}} P_{cool} \times dt = P_{cool} \times t_{cool} \tag{9}$$

5.2.5 Tool change energy consumption

CNC lathe machine tools are equipped with an automatic tool changing rotary tool post which is mainly driven by an electric motor. The tool change procedure is regulated by the electromagnetic reversing valve and sequencing valve, which comprises indexing, raising, and locking the tool post (Zhou et al., 2022). Although the procedure of automatically changing tools is complex, the time required is very short. The tool changing power can be measured experimentally, and the energy demand is calculated as follows:

$$E_{tc} = \int_0^{t_{tc}} P_{tc}\, dt = P_{tc} \times t_{tc} \tag{10}$$

5.2.6 Idle, air-cut, and rapid positioning energy consumption

In the idle module the spindle runs at a specific speed and the machine is in functioning readiness as shown in Figure 5.1. The idle power contains the standby power and spindle power; and for a given spindle angular speed, the value P_{idle} is constant (Liu et al., 2015). Therefore, the idle power can be logged for several selected spindle angular speeds, and based on this data its regression model as a function of spindle angular speed can be developed as stated in Eq. (11).

$$P_{idle} = y_1 \times n^2 + y_2 \times n + y_3 \tag{11}$$

Where y_1, y_2 and y_3 are fitting coefficients.

For a given idle period (t_{idl}), the idle energy can be calculated as:

$$E_{idle} = \int_0^{t_{idle}} P_{idle} dt = P_{idle} \times t_{idle} \tag{12}$$

Air-cutting power (P_{air}) includes idle power and feeding power when the cutting tool is not engaged in cutting the part. The air cutting module is intended for the safe entry of the cutter for the cutting operation i.e. approach length for the cutter. Air cutting power is the power consumption in the absence of actual machining, in which process parameters such as feed rate and tool path are kept the same as those followed during the actual machining and can be expressed as:

$$P_{air} = P_{idle} + P_f \tag{13}$$

Where P_f is feed power. For the given air-cut period (t_{air}), the air-cut energy can be calculated as:

$$E_{air} = \int_0^{t_{air}} P_{air}\ dt = P_{air} \times t_{air} \tag{14}$$

In Eq. (14), P_f can be the z-axis feed power (P_{fz}) or x-axis feed power (P_{fx}) depending on the machining process e.g. P_{fz} in the turning process and P_{fx} in end facing. For each feed axes, the feed power can be recorded for several selected feed rates and a linear regression model in terms of a feed rate can be developed (Lee et al., 2016). The feed axis power consumption can be expressed as:

$$P_f = c_o \times f_r + c_1 \tag{15}$$

Where c_o and c_1 are fitting constants.

Rapid positioning involves the cutting tool moving quickly along a single axis or multiple axes to take the position needed for the subsequent cutting operation. Rapid positioning is a non-productive activity accomplished with the maximum possible feed rate of the machine tool. CNC machine axis generally has a very high rapid positioning acceleration, which makes the duration very short (Jia et al., 2017). Although it can result in high power peaks (corresponding to the maximum feed rate), the feeding axis decelerates for precise positioning before reaching the maximum feed rate, resulting in lower energy demand. Therefore, short-time power peaks are produced during the rapid positioning, which does not significantly affect the machine tool's total power consumption. Thus, in the present study, the power consumption during rapid positioning was adopted as equivalent to idle power.

5.2.7 Cutting energy consumption

The power required to remove the material from the part in the form of chips is called the material-removal power (P_m). The power demand of a machine tool during the cutting module is the sum of P_{idle}, P_f, and P_m and can be expressed as:

$$P_{cut} = P_{idle} + P_f + P_m \tag{16}$$

In Eq. (16), the material-removal power can be calculated as (Deng et al., 2017):

$$P_m = \left(1 + L_c\right) \times P_{cut} \tag{17}$$

Where P_{cut} is the theoretical cutting power and L_c is the power loss constant.

$$P_{cut} = F_c \times \frac{v_c}{60} \tag{18}$$

Where, F_c is the main cutting force in N. Empirically F_c can be represented as (Jia et al., 2016):

$$F_c = k_{F_c} \times C_{F_c} \times v_c^{n_{Fc}} \times f_r^{y_{F_c}} \times d_c^{x_{F_c}} \tag{19}$$

Based on Eqs. (17) ~ (19), the P_m can be expressed as:

$$P_m = \left(1 + L_c\right) \times k_{F_c} \times C_{F_c} \times \left(\frac{v_c^{n_{Fc}+1}}{60} \right) \times f_r^{y_{F_c}} \times d_c^{x_{F_c}} \tag{20}$$

The above empirical formula shown in Eq. (20) can be expressed as:

$$P_m = C \times v_c^{\alpha} \times f_r^{\beta} \times d_c^{\gamma} \tag{21}$$

Where $C = \left(1 + L_c\right) \times k_{F_c} \times \frac{C_{F_c}}{60}$, $\alpha = n_{Fc} + 1$, $\beta = y_{F_c}$ and $\gamma = x_{F_c}$.

In a CPC machining process, the process parameters (v_c, f_r and d_c) remain unchanged and thus, the material removal power should be constant for the given process time, and hence, based on Eq. (21), the P_m for CPC machining process (P_{m_CPC}) can be expressed as:

$$P_{m\_CPC} = C_{CP} \times v_c^{\alpha_c} \times f_r^{\beta_c} \times d_c^{\gamma_c} \tag{22}$$

Where C_{CP} is a constant and α_c, β_c, and γ_c are exponents (i.e. coefficients) of cutting velocity, feed rate and cutting depth respectively in P_{m_CPC} model. Several authors (Ma et al., 2014; Parida and Maity, 2017) have reported that the cutting tool nose radius is one of the vital tool geometry that significantly influences the cutting power. This signifies that the cutting power model should incorporate the nose radius, and the cutting power model in Eq. (22) can be written as

$$P_{m\_CPC} = C_{CP} \times v_c^{\alpha_c} \times f_r^{\beta_c} \times d_c^{\gamma_c} \times r^{\delta_c} \tag{23}$$

Where δ_c is the exponent for tool nose radius. The material-removal power can be measured for several combinations of the process parameters in the cutting experiments and can be used to determine the fitting coefficients of Eq. (23). The corresponding energy consumption can be expressed as:

$$E_{m\_CPC} = \int_0^{t_{CPC}} P_{cut\_CPC}\, dt = C_{CP} \times v_c^{\alpha_c} \times f_r^{\beta_c} \times d_c^{\gamma_c} \times r^{\delta_c} \times t_{CPC} \tag{24}$$

In the present study, turning is considered as a CPC machining process and based on Eq. (16), the total cutting energy can be evaluated as:

$$E_{cut\_CPC} = \int_0^{t_{CPC}} P_{idle}\, dt + \int_0^{t_{CPC}} P_{fz}\, dt + \int_0^{t_{CPC}} P_{cut\_CPC}\, dt$$

$$E_{cut\_CPC} = (P_{idle} \times t_{CPC}) + \left(P_{fz} \times t_{CPC}\right) + (C_{CP} \times v_c^{\alpha_c} \times f_r^{\beta_c} \times d_c^{\gamma_c} \times r^{\delta_c} \times t_{CPC}) \tag{25}$$

Whereas, as previously mentioned in **Chapter 3,** at least one of the machining parameters in the VPC machining process changes with time. As a result, the cutting power varies, and its characteristics become more complicated. The power consumption of the VPC machining process can be broken down into S sub-intervals. Each sub-interval will become a CPC machining process as the number of sub-intervals increases (**Chapter 3**). The material-removal power model of the VPC machining process can incorporates various time-dependent cutting parameters and can be used for a variety of VPC machining processes such as end facing, chamfering and grooving. Based on the kind of VPC machining process, a mathematical formula for time-dependent changing process parameters can be established and utilized to develop the VPC machining process model. In this study, the VPC machining process i.e. end facing is considered and the model was developed in previous **Chapter 3: Eq. (18)** as stated in the following equation:

$$P_{m\_VPC} = C_{VP} \times \left(v_{max} - \left(\frac{2 \times f_r \times \pi \times n^2}{60000} \right) \times t \right)^{\alpha_v} \times f_r^{\beta_v} \times d_c^{\gamma_v} \times r^{\delta_v} \quad (26)$$

Where C_{VP} is a constant and α_c, β_c, γ_c and δ_v are exponents of cutting velocity, feed rate, cutting depth and tool nose radius respectively in P_{m_VPC} model. The material-removal energy ($E_{,\_VPC}$) can be calculated as:

$$E_{m\_VPC} = \int_0^{t_{VPC}} P_{m\_VPC} \, dt \quad (27)$$

Based on Eq. (16), the total cutting energy during the end facing VPC machining process can be evaluated as:

$$E_{cut\_VPC} = \int_0^{t_{VPC}} P_{idle} dt + \int_0^{t_{VPC}} P_{fx} dt + \int_0^{t_{VPC}} P_{cut\_VPC} dt$$

$$E_{cut\_VPC} = \left[\begin{array}{l} P_{idle} \times t_{VPC} + P_{fx} \times t_{VPC} + \\ \int_0^{t_{VPC}} \left(C_{VP} \times \left(v_{max} - \left(\frac{2 \times f_r \times \pi \times n^2}{60000} \right) \times t \right)^{\alpha_v} \times f_r^{\beta_v} \times d_c^{\gamma_v} \times r^{\delta_v} \right) dt \end{array} \right] \quad (28)$$

5.2.8 Energy consumption of machine tool for machining a cylindrical part

The summation of the energy consumption of each module contributes to the total energy consumption of a machine tool for machining a cylindrical part. Hence, based on Eq. (4) and Eqs (5), (6), (8), (9), (10), (12), (14), (25) and (28), the energy consumption of a machine tool for machining a cylindrical part can be written as:

$$E_{total} = \left\{ \begin{array}{l} \sum_{j=1}^{Q_{stp}} E_{startup} + \sum_{j=1}^{Q_{std}} \left(P_{standby} \times t_{std} \right) + \\ \sum_{j=1}^{Q_{acc}} \left(x_1 \times n^2 + x_2 \times n + x_3 \right) + \sum_{j=1}^{Q_{idle}} \left(P_{idle} \times t_{idle} \right) + \sum_{j=1}^{Q_{tc}} \left(P_{tc} \times t_{tc} \right) + \sum_{j=1}^{Q_{air}} \left(P_{air} \times t_{air} \right) + \\ \sum_{J=1}^{Q_{cool}} (P_{cool} \times t_{cool}) + \sum_{j=1}^{Q_{CPC}} (P_{idle} \times t_{CPC} + P_{fz} \times t_{CPC} + C_{CM} \times v_c^{\alpha_c} \times f_r^{\beta_c} \times d_c^{\gamma_c} \times r^{\delta_c} \times t_{CPC}) \\ + \sum_{j=1}^{Q_{VPC}} \left(\begin{array}{l} P_{idle} \times t_{VPC} + P_{fx} \times t_{VPC} + \\ \int_0^{t_{VPC}} \left(C_{VP} \times \left(v_{max} - \left(\frac{2 \times f_r \times \pi \times n^2}{60000} \right) \times t \right)^{\alpha_v} \times f_r^{\beta_v} \times d_c^{\gamma_v} \times r^{\delta_v} \right) dt \end{array} \right) \end{array} \right\} \quad (29)$$

Where $Q_{stp,}$ Q_{std}, Q_{acc}, Q_{idle}, Q_{tc}, Q_{air}, Q_{cool}, Q_{CPC} and Q_{VPC} represents the quantity of: standby, spindle acceleration, idle, tool change, air-cut, coolant ON, CPC cutting, and VPC cutting modules respectively.

5.3. Experimental Scheme

Experiments were conducted on an LMW-Smarturn CNC lathe machine tool in the dry and wet environment to obtain the fitting constants of the different modules of the energy consumption model as stated in Eq. (29). The machine tool's technical specifications are listed in Table 5.1. The cutting inserts manufactured by the Sandvik of ISO designation

CNMG 120408 were used for performing the cutting operations and were mounted on a tool holder of ISO designation PCLNR 2020 K 12. Aluminum of grade Al 6061 was chosen as the part material due to its wide range of applications in the manufacturing industries. The Fluke 435 series II Power Analyzer was used to measure the power consumed by the CNC machine tool straight from the main supply bus. Three current sensors and three voltage sensors integrated with alligator clamps were used to link the power analyzer to the CNC machine tool's 3-phase main power bus supply.

Table 5.1 The machine tool's technical specifications.

Specification	Data
Manufacturer/type	LMW Ltd./ Smarturn CNC lathe
Machine sizes (L×B×H)	2275 mm× 1640 mm× 1620 mm
Power rating of the spindle motor	5.5 kW (Fanuc β6i)
x/z axes motor power rating	1.2 kW (Fanuc βiSc8)
Coolant pump motor power rating	0.3 kW
Max. spindle angular velocity	4500 rev/min
Type of Controller	Fanuc oi-TF
Maximum diameter to be turned	200 mm
Swing over bed/carriage	480 mm/260 mm
Maximum length to be turned	262 mm
Maximum travel range:	
x-axis	105 mm
z-axis	320 mm
Rapid traverse (x/z axes)	10000 mm/min
Turret/tool indexing head (No. of tool station)	8
Tool shank size	20 × 20

Figure 5.2 depicts the experimental setup and approach used in this investigation. The cutting parameters: speed (v_c), feed rate (f_r), cutting depth (d_c) and tool nose radius (r) were selected as process parameters for the CPC machining process of cutting energy module i.e. turning process, and are provided in Table 5.2.

Table 5.2 Process parameters and their related levels for the turning process

Process parameters		v_c (m/min)	f_r (mm/rev)	d_c (mm)	r (mm)
Level	I	144	0.10	0.5	0.4
	II	184	0.15	1.0	0.8
	III	224	0.20	1.5	1.2

In the VPC machining process of cutting energy module i.e. end facing, the v_c change continuously until the tool reaches to the center of the part and therefore instead of v_c, spindle angular speed (n) was selected with feed rate (f_r) and cutting depth (d_c) as process parameters. The detailed information on the design of experiments, experimental setup, power consumption measurement and related peripheral conditions for obtaining the fitting coefficients of VPC machining process i.e. end facing model shown in Eq. (28) have been discussed in Chapter 3. Machine tool constraints and cutting tool supplier guidelines were used to adopt the values of the process parameters. The design of experiments was prepared based on Taguchi's L_9 orthogonal array and shown in Table 5.3. To reduce the experimental cost and time, the L_9 orthogonal array is mainly chosen for a combination of four process parameters at three levels.

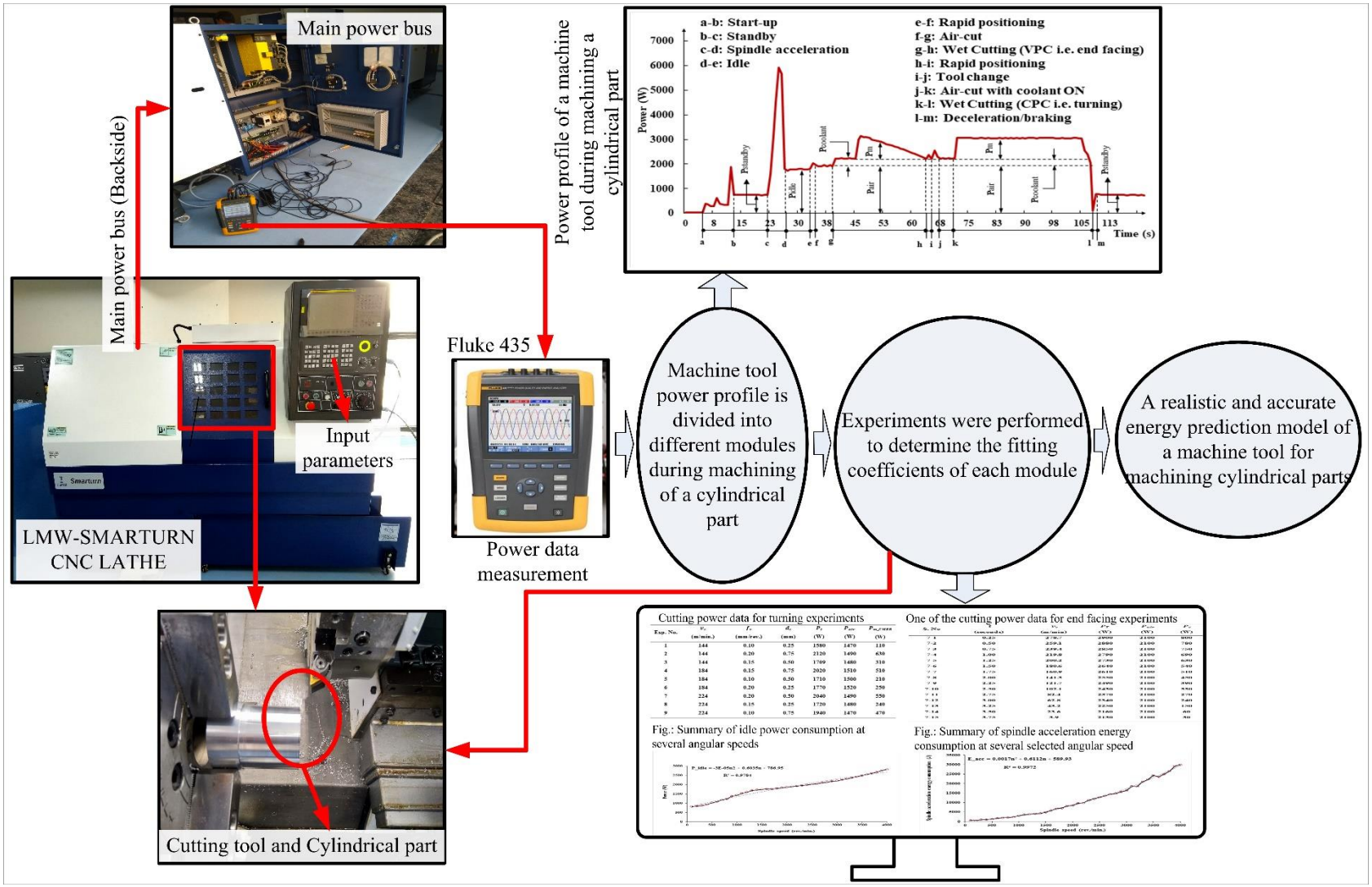

Figure 5.2. Experimental setup and adopted methodology.

Table 5.3 Taguchi's L_9 orthogonal array for the turning process experiments

Experiment No.	Process parameters			
	v_c (m/min)	f_r (mm/rev)	d_c (mm)	r (mm)
1	144	0.10	0.5	0.4
2	144	0.15	1.0	1.2
3	144	0.20	1.5	0.8
4	184	0.10	1.0	0.8
5	184	0.15	1.5	0.4
6	184	0.20	0.5	1.2
7	224	0.10	1.5	1.2
8	224	0.15	0.5	0.8
9	224	0.20	1.0	0.4

5.4. Determining the Fitting Coefficients of Different Energy Modules

The fitting coefficients of different energy modules were determined by applying regression analysis to the experimental data. The corresponding computations of energy consumption for each module are discussed below.

The start-up energy and standby power of the LMW-Smarturn were measured three times and found to be 21.12 kJ and 0.75 *kW* respectively. According to the machine tool technical specification in Table 5.1, the coolant pump power consumption is 0.3 *kW*, which was confirmed by measurement. Further, experiments were performed at intervals of 100 rpm for several spindle speeds to measure spindle acceleration and idle energy consumption. This database was used to determine the fitting coefficients of the spindle acceleration energy consumption module and idle power module. The experimental results

of spindle acceleration energy consumption and idle power consumption are summarized in Figure 5.3 and Figure 5.4 respectively.

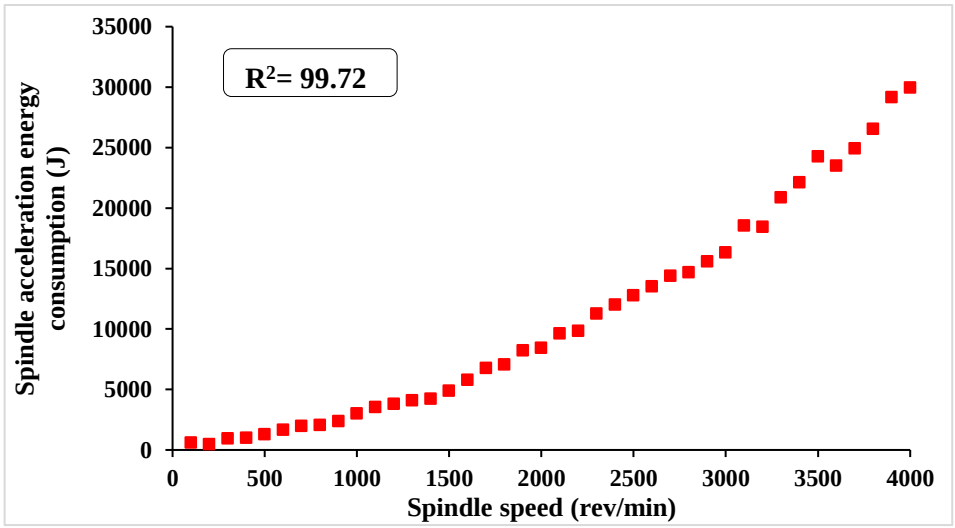

Figure 5.3. Spindle acceleration energy consumption at intervals of 100 rpm.

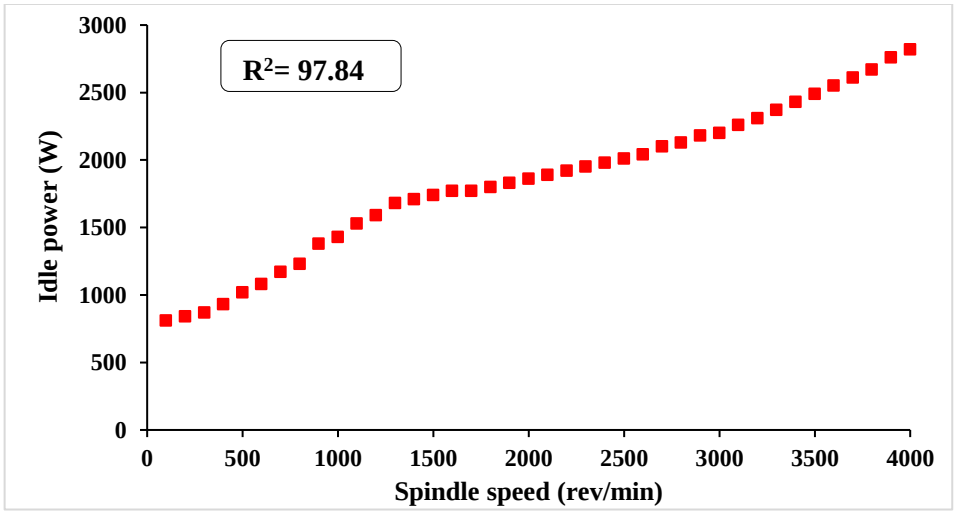

Figure 5.4. Idle power consumption at intervals of 100 rpm.

According to Section 5.2.3, measured spindle acceleration energy data was used to determine the fitting coefficient of Eq. (8), and corresponding spindle acceleration energy consumption can be computed using the following equation.

$$E_{acc}(J) = \left(0.0017 \times n^2\right) + \left(0.6112 \times n\right) + 589.93 \quad (30)$$

According to Section 5.2.6, measured idle power data was used to determine the fitting coefficient of Eq. (11), and corresponding idle power can be estimated using the following equation.

$$P_{idle}(W) = \left(-3.3\times10^{-5}\times n^2\right) + \left(0.6035\times n\right) + 786.95 \quad (31)$$

Further, to determine the fitting coefficients of the feed axes power models: z-axis and x-axis; x-axis up and x-axis down, the feed power under no-load condition for each feed axis is measured at an interval of 500 mm/min for the range of 500-5000 mm/min. The experimental results are provided in Table 5.4. In the LMW-Smarturn machine tool, the x-axis feed drive is at an inclination, and therefore the feed power is measured for both directions: up (considered as $+ve$) and down (considered as $-ve$) separately.

Table 5.4 Experimental results of feed axes power under no-load condition.

Feed (mm/min) ($\times100$)	5	10	15	20	25	30	35	40	45	50
P_f (W)										
z-axis	40	40	40	40	40	70	70	70	100	100
x-axis (down)	20	20	20	20	20	20	50	50	50	50
x-axis (up)	40	40	70	70	100	100	130	130	160	190

The measured feed power data of Table 5.4 was further used to determine the fitting coefficients of Eq. (15) and the corresponding feed power can be calculated using the following equations:

For *Z*-axis feed drive:

$$P_{fz}(W) = \left(0.0149\times f_r\right) + 20.00 \quad (32)$$

For *x*-axis (up) feed drive:

$$P_{fx+}(W) = (0.0324 \times f_r) + 14.00 \tag{33}$$

For *x*-axis (down) feed drive:

$$P_{fx-}(W) = (0.0087 \times f_r) + 8.00 \tag{34}$$

According to Section 5.2.6, based on Eq. (13) and Eq. (32), the air-cut power can be calculated as:

$$P_{air} = \left(\left(-3.3 \times 10^{-5} \times n^2\right) + (0.6035 \times n) + 786.95\right) + P_f \tag{35}$$

The cutting experiments of the turning process for different combinations of process parameters were performed according to Table 5.3 to acquire the fitting coefficients of the material removal power model of the turning process. The measured total power (P_{total}), air cut power (P_{air}) and corresponding calculated material removal power ($P_{total} - P_{air}$) under a dry cutting environment are listed in Table 5.5.

According to Section 5.2.7, based on experimental data shown in Table 5.5, the fitting coefficients of the material-removal power model for turning, as stated in Eq. (23), were determined. The values of the fitting coefficients were: $C_{CM} = 0.3071$, $\alpha_c = 0.3844$, $\beta_c = 0.6520$, $\gamma_c = 0.9268$ and $\delta_c = -0.2184$. By substituting the values of the coefficients into Eq. (23), the material-removal power can be calculated using Eq. (36).

$$P_{m\_CPC}(kW) = 0.3071 \times v_c^{0.3844} \times f_r^{0.6520} \times d_c^{0.9268} \times r^{-0.2184} \tag{36}$$

As stated in Eq. (25) and based on Eqs. (31), (32) and (36), the total cutting energy consumption during the turning process can be evaluated as:

$$E_{cut\_CPC}\left(kJ\right)=\left[\begin{array}{l}\left(\dfrac{\left(-3.3\times10^{-5}\times n^{2}+0.6035\times n+786.95\right)}{1000}\right)\times t_{CPC}+\\ \left(\dfrac{\left(0.0149\times f_{r}+20.00\right)}{1000}\right)\times t_{CPC}+\\ \left(0.3071\times\ v_{c}^{0.3844}\times f_{r}^{0.6520}\times d_{c}^{0.9268}\times r^{-0.2184}\right)\times t_{CPC}\end{array}\right] \quad (37)$$

Similarly, fitting coefficients for the material removal power during the turning processes in a wet environment can be obtained, and the corresponding total cutting energy can be calculated.

Table 5.5 Cutting power data for turning experiments.

Exp. No.	v_c (m/min)	f_r (mm/rev)	d_c (mm)	r (mm)	P_{total} (kW)	P_{air} (kW)	P_{m_CPC} (kW)
1	144	0.10	0.5	0.4	1.800	1.490	0.310
2	144	0.15	1.0	1.2	2.100	1.500	0.600
3	144	0.20	1.5	0.8	2.640	1.510	1.130
4	184	0.10	1.0	0.8	1.950	1.490	0.460
5	184	0.15	1.5	0.4	2.670	1.500	1.170
6	184	0.20	0.5	1.2	1.890	1.510	0.380
7	224	0.10	1.5	1.2	2.310	1.490	0.820
8	224	0.15	0.5	0.8	1.920	1.500	0.420
9	224	0.20	1.0	0.4	2.550	1.510	1.040

P_{total}: Total power consumption, P_{air}: air cut power consumption

The fitting coefficients of the VPC machining process (end facing) model shown in Eq. (26) were determined in a previous **Chapter 3** for the same workpiece and cutting tool

combination (i.e. aluminium Al 6061 and carbide inserts). The VPC machining process model for end facing can be expressed as:

$$P_{m\_VPC}\left(kW\right)=99.51\times10^{-3}\times\left(v_{max}-\frac{2\times f_r\times\pi\times n^2}{60000}\times t\right)^{0.7641}\times f_r^{1.1385}\times d_c^{1.1145}\times r^{-0.2331} \quad (38)$$

As stated in Eq. (28) and based on Eqs. (31), (34) and (38), the total cutting energy during the end facing can be evaluated as:

$$E_{cut\_\mathrm{VPC}}\left(kJ\right)=$$

$$\left[\begin{array}{l}\left(\frac{\left(-3.3\times10^{-5}\times n^2+0.6035\times n+786.95\right)}{1000}\right)\times t_{VPC}+\\ \left(\frac{\left(0.0087\times f_r+8.00\right)}{1000}\right)\times t_{VPC}+\\ \int_0^{t_{VPC}}\left(99.51\times10^{-3}\left(v_{max}-\frac{2\times f_r\times\pi\times n^2}{60000}\times t\right)^{0.7641}\times f_r^{1.1385}\times d_c^{1.1145}\times r^{-0.2331}\right)dt\end{array}\right] \quad (39)$$

Since, in this study, the turning and end facing experiments were performed with the same cutting tool and no tool change occurred, hence the tool change energy consumption was not considered. In total, based on Eq. (29) and Eqs. (30), (31), (35), (37) and (39), the total energy consumption prediction model of a machine tool for the machining of a cylindrical part can be expressed as:

$$
\begin{aligned}
E_{total}(kJ) = \Bigg[& \underbrace{\sum_{j=1}^{Q_{stp}} 21.125}_{E_{star-up}} + \underbrace{\sum_{j=1}^{Q_{std}} \left(0.75 \times t_{std}\right)}_{E_{standby}} + \underbrace{\sum_{j=1}^{Q_{acc}} \left(\frac{\left(\left(0.0017 \times n^2\right) + \left(0.6112 \times n\right) + 589.93\right)}{1000} \right)}_{E_{acc}} + \\
& \underbrace{\sum_{j=1}^{Q_{idle}} \left(\left(\frac{\left(\left(-3.3 \times 10^{-5} \times n^2\right) + \left(0.6035 \times n\right) + 786.95\right)}{1000} \right) \times t_{idle} \right)}_{E_{idle}} + \underbrace{\sum_{J=1}^{Q_{tc}} (P_{tc} \times t_{tc})}_{E_{tc}} + \\
& \underbrace{\sum_{j=1}^{Q_{air}} \left(\left(\frac{\left(\left(\left(-3.3 \times 10^{-5} \times n^2\right) + \left(0.6035 \times n\right) + 786.95\right) + P_f\right)}{1000} \right) \times t_{air} \right)}_{E_{air}} + \underbrace{\sum_{J=1}^{Q_{cool}} (P_{cool} \times t_{cool})}_{E_{cool}} + \\
& \underbrace{\sum_{j=1}^{Q_{CPC}} \left(\begin{array}{l} \left(\frac{\left(-3.3 \times 10^{-5} \times n^2 + 0.6035 \times n + 786.95\right)}{1000} \right) \times t_{CPC} + \left(\frac{\left(0.0149 \times f_r + 20.00\right)}{1000} \right) \times t_{CPC} \\ + \left(0.3071 \times v_c^{\alpha_{CM}} \times f_r^{\beta_C} \times d_c^{\gamma_C} \times r^{\delta_C}\right) \times t_{CPC} \end{array} \right)}_{E_{CPC}} + \\
& \underbrace{\sum_{j=1}^{Q_{VPC}} \left(\begin{array}{l} \left(\frac{\left(-3.3 \times 10^{-5} \times n^2 + 0.6035 \times n + 786.95\right)}{1000} \right) \times t_{VPC} + \left(\frac{\left(0.0087 \times f_r + 8.00\right)}{1000} \right) \times t_{VPC} + \\ \int_0^{t_{VPC}} \left(99.51 \times 10^{-3} \left(v_{max} - \frac{2 \times f_r \times \pi \times n^2}{60000} \times t \right)^{\alpha_{VM}} \times f_r^{\beta_V} \times d_c^{\gamma_V} \times r^{\delta_V} \right) dt \end{array} \right)}_{E_{VPC}} \Bigg]
\end{aligned}
$$

(40)

Whereas the values of the fitting coefficients corresponding to the cutting environment are summarized in Table 5.6.

Table 5.6 Fitting coefficients of total energy consumption model.

Cutting environment	Fitting coefficients
Dry	$C_{CM} = 0.3071$, $\alpha_c = 0.3844$, $\beta_c = 0.6520$, $\gamma_c = 0.9268$, δ_c = -0.2184
	$C_{CV} = 99.5115$, $\alpha_v = 0.7641$, $\beta_v = 1.1385$, $\gamma_v = 1.1145$, δ_v = -0.2331
Wet	$C_{CM} = 0.1479$, $\alpha_c = 0.5676$, $\beta_c = 0.7407$, $\gamma_c = 1.0308$, δ_c = -0.0208
	$C_{CV} = 34.5943$, $\alpha_v = 0.8232$, $\beta_v = 0.8387$, $\gamma_v = 1.3399$, δ_v = -0.2516

5.5. Validation of the Proposed Model

In order to verify the proposed model's prediction accuracy, four validation experiments were performed; two in the dry environment and two in the wet environment. The initial blank size of the cylindrical part to perform validation experiments is shown in Figure 5.5. To prove the practical applicability of the developed model, a cylindrical part was chosen which incorporates both turning i.e. CPC machining and end facing VPC machining processes. Furthermore, the levels of the process parameters used for validation experiments were kept different from the levels used to acquire the fitting coefficients of the models and are listed in Table 5.7.

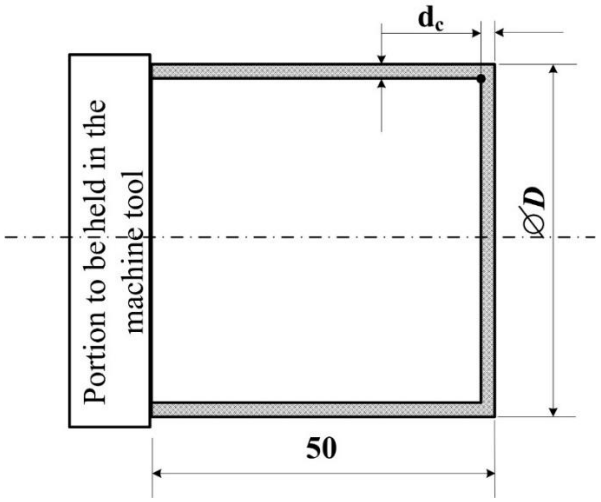

**All dimensions are in mm*

Figure 5.5. The orthographic drawing of the cylindrical part.

The operational details of each module, process parameters, process time, and corresponding energy consumption for validation Test-I are shown in Table 5.8. The machine tool is in standby mode (sequence number 2 of Table 5.8) during the setup of the cylindrical part in the chuck, and the energy consumption for a setup time of 5 seconds can be calculated using Eq. (6) as follows.

$$E_{standby} = \sum_{j=1}^{Q_{std}=1} P_{standby} \times t_{std} = 750 \times 5 = 3750\,J \tag{41}$$

Table 5.7 Process parameters for the validation experiments.

Test No.	Cutting environment	D (mm)	n (rev/min)	v_c (m/min)	f_r (mm/rev)	d_c (mm)	r (mm)	Length (mm)
I	Dry	50.0	800	125.60	0.05	0.6	0.8	50
II		49.0	1200	184.63	0.10	1.8	0.8	50
III	Wet	47.0	800	118.06	0.05	0.6	0.8	50
IV		47.5	1200	178.98	0.10	1.8	0.8	50

The spindle acceleration energy consumption (E_{acc}) for angular speed of 800 rev/min (sequence number 3 of Table 5.8) can be calculated using Eq. (30).

$$E_{acc} = \sum_{j=1}^{Q_{acc}=1} E_{acc} = \left(0.0017 \times 800^2\right) + \left(0.6112 \times 800\right) + 589.93 = 2166.89\,J \tag{42}$$

The idle power (P_{idle}) at a spindle speed of 800 rev/min can be calculated using the Eq. (31):

$$P_{idle} = \left(-3.3 \times 10^{-5} \times 800^2\right) + \left(0.6035 \times 800\right) + 786.95 = 1248.63\ \text{W}$$

Table 5.8 Summary of the validation process for Test-I on LMW-Smarturn CNC lathe

Seq. No.	Description	Module	Parameters				Time (s)	Energy
			L* (mm)	n (rev/ min)	f_r (mm /rev)	d_c (mm)		
1	Start-up	Start-up	-	-	-	-	-	$E_{startup}$
2	Setup of the part in the chuck	Standby	-	-	-	-	5	$E_{standby}$
3	Spindle powered	Spindle acceleration	-	800	-	-	-	E_{acc}
4	Idle	Idle	-	800	-	-	1	E_{idle1}
5	Rapid Positioning of cutting tool	Idle	250	800	-	-	1.5	E_{idle2}
6	Cutter approach for end facing	Air-cut	2	800	0.05	-	3	E_{air1}
7	End facing	VPC cutting	25	800	0.05	0.6	37.5	E_{cut_VPC}
8	Rapid Positioning of cutting tool	Idle	27	800	-	-	0.2	E_{idle3}
9	Cutter approach for end facing	Air-cut	2	800	0.05	-	3	E_{air2}
10	Turning	CPC cutting	50	800	0.05	0.6	75	E_{cut_CPC}

*L is the distance travelled in the respective operation.

As shown in Table 5.8, there are three idle modules (sequence numbers 4, 5, and 8 of Table 5.8) and the corresponding energy consumptions can be calculated using Eq. (12) as follows:

$$E_{idle} = \sum_{j=1}^{Q_{idle}=3} P_{idle} t_{idle} = (1248.63 \times 1) + (1248.63 \times 1.5) + (1248.63 \times 0.2) = 3371.30\, J \qquad (43)$$

As shown in Table 5.8, there are two air-cut modules (sequence numbers 6 and 9 of Table 5.8) i.e. end facing (E_{air1}) and turning (E_{air2}). The corresponding energy consumption can be calculated using Eq. (14) and Eq. (35) as follows:

$$E_{air} = \sum_{j=1}^{Q_{air}=2} P_{air} t_{air} = E_{air1} + E_{air2}$$

$$E_{air} = \begin{bmatrix} \left(\left(\left(-3.3\times10^{-5}\times800^2 + 0.6035\times800 + 786.95\right) + \left(0.0087\times40 + 8.00\right)\right)\times3\right) + \\ \left(\left(\left(-3.3\times10^{-5}\times800^2 + 0.6035\times800 + 786.95\right) + \left(0.0149\times40 + 20.00\right)\right)\times3\right) \end{bmatrix}$$

$$E_{air} = 3770.93 + 3807.67 = 7578.61J \qquad (44)$$

The cutting energy consumption of the end-facing operation (sequence number 7 of Table 5.8) can be computed using Eq. (39).

$$E_{cut\_VPC} = \sum_{j=1}^{Q_{VPC}=1} \left[\begin{array}{l} \left(1248.63 \times 37.50\right) + \left(\left(0.0087\times40 + 8.00\times37.50\right)\right) + \\ \int_0^{37.50} \left(99.51 \times \left(125.60 - \left(\frac{2\times0.05\times\pi\times800^2}{60000} \right)\times t \right)^{0.7641} \times 0.05^{1.1385} \right. \\ \left. \times 0.6^{1.1145} \times 0.8^{-0.2331} \right) dt \end{array} \right]$$

$$E_{cut\_VPC} = 48808.18\ J \qquad (45)$$

The cutting energy consumption of the turning operation (sequence number 10 of Table 5.8) can be computed using Eq. (37).

$$E_{cut\_CPC} = \sum_{j=1}^{Q_{CPC}=1} \left[\begin{array}{l} \left(1248.63 \times 75\right) + \left(\left(0.0149 \times 40 + 20.00\right) \times 75\right) + \\ \left(\left(307.12 \times 125.60^{0.3844} \times 0.05^{0.6520} \times 0.6^{0.9268} \times 0.8^{-0.2184}\right) \times 75\right) \end{array} \right]$$

$$E_{cut\_CMRR} = 108884.3J \tag{46}$$

Finally, as shown in Eq. (40), the total energy consumption (E_{total}) for machining a cylindrical part can be determined by aggregating the energy consumption of the different modules i.e. Eq. (41), (42), (43), (44), (45), and (46).

$$E_{total} = \sum E_{start-up} + \sum E_{standby} + \sum E_{acc} + \sum E_{idle} + \sum E_{air} + \sum E_{cut\_CMRR} + \sum E_{cut\_VMRR}$$

$$E_{total} = 195684.24\ J$$

The same methodology was followed to determine the total energy consumption of the remaining validation experiments. The total computed energy consumption and corresponding measured total energy consumption of each validation test are summarized in Table 5.9. The prediction accuracy of each validation experiment is calculated using the following Eq. (47).

$$\text{Accuracy (\%)} = \left(1 - \left|\frac{E_{total_{pred}} - E_{total_{meas}}}{E_{total_{meas}}}\right|\right) \times 100 \tag{47}$$

Where $E_{total_{pred}}$ represents the total computed energy consumption of the machine tool of each validation test and $E_{total_{meas}}$ represents the corresponding actual measured total energy consumption.

Table 5.9 shows that the proposed model's prediction accuracy is more than 97% in each test process, hence the model can be effectively applied to predict the energy consumption of a machine tool beforehand. Accurate prediction of the energy consumption of a machine tool before actual machining is important information for a process planner. Based on this data, the process planner can evaluate several processes plans and identify the most energy-efficient ones.

Table 5.9 Summary of validation test results.

Test No.	Cutting environment	Total energy consumption (J)		Accuracy (%)
		$E_{total_{pred}}$	$E_{total_{meas}}$	
I	Dry	195684.24	193220	98.72
II		119243.21	116204	97.38
III	Wet	223671.88	222780	99.60
IV		130474.22	126480	96.84

5.6. Summary

This chapter presents a novel approach to model the energy consumption of a machine tool for the machining of cylindrical parts in dry and wet environment. The energy consumption is divided into different energy modules: start-up, standby, spindle acceleration, idle, rapid positioning, air-cutting, and cutting. The developed model overcomes the limitations of existing energy consumption models for accurate estimation of cutting energy consumption by incorporating separate energy modules for the VPC machining process and CPC machining process. The fitting coefficients of each energy module were obtained by conducting experiments on a LMW-Smarturn CNC lathe machine tool and integrated to establish the energy consumption model. The validation experiments were carried out in the dry and wet environment to ensure the proposed model's prediction accuracy. The

validation results show that the developed model's accuracy was 97% in each test. Based on the elementary information of machine tools, sequence of operations and the part drawing, the developed model can be used by the process planners to identify the most energy-efficient based process plan before actual machining of a cylindrical part. Moreover, accurate and practical energy consumption models of machine tools can bring many advantages to the manufacturing industry, ranging from sustainable process planning to energy monitoring of machine tools.

The proposed model can be utilized for development of an empirical model to quantify carbon emissions for machining of cylindrical parts.

Chapter 6:

Modelling the Carbon Emissions of Machine tools

In this chapter, an empirical model is developed to quantify the carbon emissions (CEM) of machine tools for machining cylindrical parts. The CEM associated with a cylindrical part machining are decomposed into CEM from electrical energy consumption, material consumption, cutting tool wear, coolant consumption and from the disposal of machining waste materials. The corresponding CEM models are developed and are integrated to quantify the total CEM of the machine tool for machining cylindrical parts. Finally, the developed model is applied on a cylindrical part with three different process plans to validate the developed model for practical implementation in industry.

6.1. Introduction

Establishing an accurate carbon emissions (CEM*)* model of machine tool as a function of process parameters is the basis for implementing energy-efficient and low carbon emission process planning and scheduling (Lv et al., 2018; Wang et al., 2015).

A review of the currently available literature presented in **Chapter 2** demonstrates the substantial advancements in this area. One group of researchers attempts to solve this problem by modelling and evaluating the energy consumption of CNC machine tools, processes, and systems. As a result of growing environmental issues and stringent carbon emission regulations imposed throughout the globe, a growing number of another group of authors are focusing on assessing the CEM of machining processes. Although the existing carbon emission quantification approaches discussed in **Chapter 2** are significant but still lacks to accurately evaluate the CEM of a CNC-based machining process for industrial applications. As highlighted in **Chapter 5**, In industry, the length and diameter are reduced to obtain the final dimensions of a cylindrical part. Typically, external turning operation is

used to reduce the diameter of the part i.e. Constant-Power Consumption (CPC) machining process and end facing operation is conducted to reduce the length of the part i.e. Variable-Power Consumption (VPC) machining process. The existing CEM models only consider CPC machining processes, whereas cylindrical part machining includes both CPC and VPC machining processes to manufacture the final product, which result in inaccurate quantification of the CEM. Furthermore, majority of studies considered the energy consumed for a particular period of a machining process. However, machining of a cylindrical part includes spindle acceleration periods, standby periods, idle periods, air-cut periods, tool changing periods, and cutting periods (CPC and VPC machining process), due to which existing models are incapable to assess CEM accurately in industries for machining of cylindrical parts.

To overcome the above-mentioned research gaps, the objective of this Chapter is to develop an empirical model that accurately quantifies the CEM of a cylindrical part before it is machined. A detailed description of the entire machining process breakdown to quantify the source of CEM is presented in the next section. The CEM associated with a cylindrical part machining are decomposed into CEM from electrical energy consumption, material consumption, cutting tool wear, coolant consumption and from the disposal of machining waste materials. The corresponding CEM models are developed and are integrated to quantify the total CEM of the machine tool for machining cylindrical parts. Finally, the developed model is applied on a cylindrical part with three different process plans, in which the influence of process parameters on CEM is analyzed.

6.2. Carbon Emission Modelling

This chapter aims to accurately estimate carbon emissions for machining a cylindrical part on a CNC machine tool. Carbon dioxide (CO_2) is the most significant contributor to

greenhouse gases. The amount of CO_2 produced during the machining process is referred to as carbon emissions (Panagiotopoulou et al., 2022). It is expressed in kilogrammes of CO_2 equivalent. During the CNC machine tool-based machining process, numerous factors (direct and indirect) contribute to CEM. For example, CEM is not directly produced by the use of electrical energy on a machine tool, rather, it is produced due to generation of electricity in power plants utilizing fossil fuels (Li et al., 2015). Therefore, in the present study, the extended system boundaries of a machining process recommended in the literature (Dahmus and Gutowski, 2004; Yi et al., 2015) are adopted to account for the indirect causes of CEM. Accordingly, the CEM of a machining process as shown in Figure 6.1 include (a) CEM due to the generation of electricity consumed in a machining process, (b) CEM due to the production of raw materials, tooling and coolants consumed in a machining process and (c) CEM due to the disposal of wastes (chips, scrap cutting tools and scrap coolant) produced in a machining process, Thus, the total carbon emission (CEM_{total}) for a machining process can be expressed as (Li et al., 2015; Zhang et al., 2017):

$$CEM_{total} = CEM_{elec} + CEM_{cool} + CEM_{tool} + CEM_{m} + CEM_{chip} \quad (1)$$

Where CEM_{elec} is the carbon emissions due to electrical energy consumption of the machine tool, CEM_{cool} is the carbon emissions due to the coolant consumption, CEM_{tool} is the carbon emissions due to the tool wear, CEM_{m} is the carbon emissions due to the material consumption which include the emissions due to the raw material production and transportation; and CEM_{chip} is the carbon emissions due to post-processing of chips for material recovery.

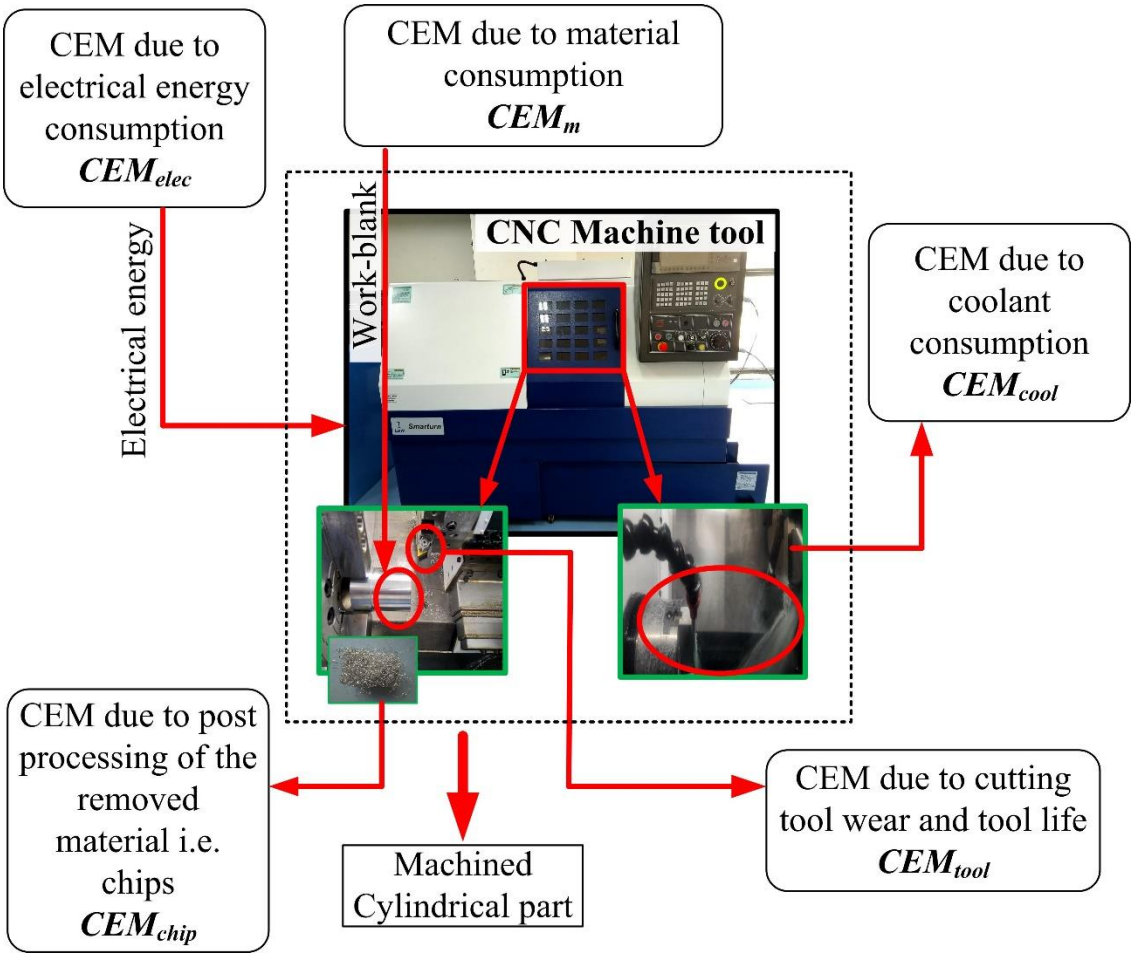

Figure 6.1 CEM from a CNC based machining process.

6.2.1. Quantification of CEM_{elec}

The CEM due to the electrical energy consumption can be quantified using the following equation:

$$CEM_{elec}(kgCO_2) = CEF_{elec} \times E_{total} \quad (2)$$

Where CEF_{elec} is the CEM factor for the machine tool's electrical energy consumption which depends on how the electricity is generated and it differs from nation to nation. E_{total} is the total electrical energy of the machine tool during the machining process.

The detailed procedure for modelling the total electrical energy consumption for machining a cylindrical part considering various energy modules: start-up, standby, spindle acceleration, idle, rapid positioning, air-cutting, and cutting (CPC machining process and VPC machining process) is presented in Chapter 5. Energy consumption models are developed for each module in Chapter 5 and are integrated to establish the total energy consumption model of the machine tool as shown in Eq. (3).

$$E_{total} = \left\{ \begin{array}{l} \sum_{j=1}^{Q_{stp}} E_{startup} + \sum_{j=1}^{Q_{std}} \left(P_{standby} \times t_{std} \right) + \\ \sum_{j=1}^{Q_{acc}} \left(x_1 \times n^2 + x_2 \times n + x_3 \right) + \sum_{j=1}^{Q_{idle}} \left(P_{idle} \times t_{idle} \right) + \sum_{j=1}^{Q_{tc}} \left(P_{tc} \times t_{tc} \right) + \sum_{j=1}^{Q_{air}} \left(P_{air} \times t_{air} \right) + \\ \sum_{J=1}^{Q_{cool}} (P_{cool} \times t_{cool}) + \sum_{j=1}^{Q_{CPC}} (P_{idle} \times t_{CPC} + P_{fz} \times t_{CPC} + C_{CM} \times v_c^{\alpha_c} \times f_r^{\beta_c} \times d_c^{\gamma_c} \times r^{\delta_c} \times t_{CPC}) \\ + \sum_{j=1}^{Q_{VPC}} \left(\begin{array}{l} P_{idle} \times t_{VPC} + P_{fx} \times t_{VPC} + \\ \int_0^{t_{VPC}} \left(C_{VP} \times \left(v_{max} - \left(\frac{2 \times f_r \times \pi \times n^2}{60000} \right) \times t \right)^{\alpha_v} \times f_r^{\beta_v} \times d_c^{\gamma_v} \times r^{\delta_v} \right) dt \end{array} \right) \end{array} \right\} \quad (3)$$

Where $P_{startup}(t)$, $P_{standby}$, $P_{acc}(t)$, $P_{rapid}(t)$, P_{idle}, P_{tc}, P_{air} and P_{cool} are the startup power at an instant t, standby power, spindle acceleration power at an instant t, rapid power at an instant *t*, idle power, tool change power, air-cut power and coolant pump power respectively. P_{cut_CPC} is the power consumption in the CPC machining process and $P_{cut\_VPC}(t)$ is the power consumption at an instant *t* in the VPC machining process. t_{stp}, t_{std}, t_{acc}, t_{rpd}, t_{idle}, t_{tc}, t_{air}, t_{cool} and t_{cut} ($t_{cut} = t_{CPC} + t_{VPC}$) are the periods of different modules: startup, standby, spindle acceleration, rapid positioning, idle, tool change, air-cut, coolant, and cutting respectively. t_{CPC} and t_{VPC} are the time of the CPC machining and VPC machining process respectively. x_1, x_2 and x_3 are fitting coefficients, *n* is spindle angular velocity in *rev*/*min*. y_1, y_2 and y_3 are fitting coefficients. P_{fz} and P_{fx} are the z-axis and x-axis feed power

respectively. C_{CP} is a constant and α_c, β_c, and γ_c are exponents (i.e. coefficients) of cutting velocity, feed rate and cutting depth respectively in P_{m_CPC} model. C_{VP} is a constant and α_c, β_c, γ_c and δ_v are exponents of cutting velocity, feed rate, cutting depth and tool nose radius respectively in P_{m_VPC} model. Q_{stp}, Q_{std}, Q_{acc}, Q_{idle}, Q_{tc}, Q_{air}, Q_{cool}, Q_{CPC} and Q_{VPC} represents the quantity of: standby, spindle acceleration, idle, tool change, air-cut, coolant ON, CPC cutting, and VPC cutting modules respectively.

By substituting the Eq. (3) in Eq. (2), the CEM_{elec} due to the electrical energy consumption can be expressed as:

$$CEM_{elec}(kgCO_2) = CEF_{elec} \times \left\{ \begin{array}{l} \sum_{j=1}^{Q_{stp}} E_{startup} + \sum_{j=1}^{Q_{std}} \left(P_{standby} \times t_{std} \right) + \\ \sum_{j=1}^{Q_{acc}} \left(x_1 \times n^2 + x_2 \times n + x_3 \right) + \sum_{j=1}^{Q_{idle}} \left(P_{idle} \times t_{idle} \right) + \sum_{j=1}^{Q_{tc}} \left(P_{tc} \times t_{tc} \right) + \sum_{j=1}^{Q_{air}} \left(P_{air} \times t_{air} \right) + \\ \sum_{J=1}^{Q_{cool}} (P_{cool} \times t_{cool}) + \\ \sum_{j=1}^{Q_{CPC}} (P_{idle} \times t_{CPC} + P_{fz} \times t_{CPC} + C_{CM} \times v_c^{\alpha_c} \times f_r^{\beta_c} \times d_c^{\gamma_c} \times r^{\delta_c} \times t_{CPC}) + \\ \sum_{j=1}^{Q_{VPC}} \left(\begin{array}{l} P_{idle} \times t_{VPC} + P_{fx} \times t_{VPC} + \\ \int_0^{t_{VPC}} \left(C_{VP} \times \left(v_{max} - \left(\frac{2 \times f_r \times \pi \times n^2}{60000} \right) \times t \right)^{\alpha_v} \times f_r^{\beta_v} \times d_c^{\gamma_v} \times r^{\delta_v} \right) dt \end{array} \right) \end{array} \right\} \quad (4)$$

6.2.2. Quantification of CEM_{cool}

The carbon emissions due to the coolant consumption comprises the CEM from the manufacture of pure mineral oil (CEM_{oil}) and CEM from the disposal of cutting fluid waste (CEM_{wc}). The carbon emissions due to the coolant consumption can be calculated using the following equation (Sihag and Sangwan, 2019):

$$CEM_{cool}(kgCO_2) = \frac{t_{proc}}{t_{cool}} \times \left(CEM_{oil} + CEM_{wc}\right) \quad (5)$$

Where $CEM_{oil} = CEF_{oil} \times (V_{in} + V_{ad})$ and $CEM_{wc} = CEF_{wc} \times \frac{V_{in} + V_{ad}}{\delta}$. Thus Eq. (51) can be re-written as:

$$CEM_{cool}(kgCO_2) = \frac{t_{proc}}{t_{cool}} \times \left(CEF_{oil} \times \left(V_{in} + V_{ad}\right) + CEF_{wc} \times \left(\frac{V_{in} + V_{ad}}{\delta} \right) \right) \quad (6)$$

Where CEF_{oil} is the CEM factor to account for the manufacturing of coolant, CEF_{wc} is the CEM factor for the disposal of the used coolant. V_{in} is the initial volume of the coolant, V_{ad} is the additional volume of the coolant, δ is the coolant's predetermined concentration, t_{cool} is the average time of coolant replacement and t_{proc} is the time for which coolant is used.

6.2.3. Quantification of CEM_{tool}

The CEM due to the cutting tool wear can be calculated using the following Eq. (7):

$$CEM_{tool}(kgCO_2) = \frac{t_c}{60 \times T_{life}} \times CEF_{tool} \times w_{tool} \quad (7)$$

Where CEF_{tool} is the CEM factor for cutting tool wear, w_{tool} is the weight of the cutting tool, and T_{life} is the tool life in minutes. In this study, The tool life is estimated based on Taylor's extended tool life equation, where the tool life is expressed as a function of cutting speed (v_c), feed rate (f_r) and cutting depth (d_c) (Bonilla Hernández et al., 2016).

$$S \times T_{life}^{m} \times d_c^{p} \times f_r^{q} = K \quad (8)$$

Eq. (8) can be rewritten as:

$$T_{life} = \left(\frac{K}{v_c \times d_c^{\,p} \times f_r^{\,q}} \right)^{\frac{1}{m}} \tag{9}$$

Based on Eq. (7) and Eq. (9), CEM_{tool} can be calculated as:

$$CEM_{tool}(kgCO_2) = \frac{t_c}{60} \times \left(\frac{v_c \times d_c^{\,p} \times f_r^{\,q}}{K} \right)^{\frac{1}{m}} \times CEF_{tool} \times w_{tool} \tag{10}$$

Where K, n, p and q are tool life constants that depend upon cutting conditions and tool-part combinations.

6.2.4. Quantification of CEM_m and CEM_{chip}

The carbon emissions due to the material consumption and the post-processing of chips can be calculated using the following equations:

$$CEM_m(kgCO_2) = CEF_m \times Q_m \tag{11}$$

$$CEM_{chip}(kgCO_2) = CEF_{chip} \times Q_m \tag{12}$$

Where CEF_m and CEF_{chip} are the CEM factor for material consumption and chips post-processing (i.e. recycling of chips), and Q_m is the mass of material (i.e. chips) removed during the cutting time t_c. Q_m can be determined as:

$$Q_m(kg) = MRR \times t_c \times \frac{\rho}{10^6} \tag{13}$$

Where MRR is the material removal rate in mm^3/sec and ρ is the material's density in gm/cm^3. The material removal rate (MRR) in the CPC machining (turning) process can be calculated using the following expression:

$$MRR_{CPC}\left(\frac{mm^3}{\sec}\right)=\frac{v_c\times f_r\times d_c\times 1000}{60} \tag{14}$$

Due to variable cutting speed, the *MRR* is changing continuously during the VPC machining (end facing) process, and therefore the average-*MRR* is calculated as (Jia et al., 2016):

$$MRR_{VPC}\left(\mathrm{mm}^3/\sec\right)=\frac{\pi\times D^2\times d_c}{4\times t_{VPC}} \tag{15}$$

Where D is the diameter of the part in mm, and t_{VPC} is the end facing time in seconds. By substituting the expressions of corresponding *MRR* in Eqs. (13), the mass of the removed material for the CPC machining and VPC machining can be expressed as:

$$Q_{m_{CPC}}(kg)=\frac{v_c\times f_r\times d_c\times 1000}{60}\times t_{CPC}\times\frac{\rho}{10^6}==\frac{v_c\times f_r\times d_c}{60}\times t_{CPC}\times\frac{\rho}{1000} \tag{16}$$

$$Q_{m_{VPC}}(kg)=\frac{\pi\times D^2\times d_c}{4\times t_{VPC}}\times t_{VPC}\times\frac{\rho}{10^6} \tag{17}$$

The Q_m can be calculated as follows:

$$Q_m=\sum_{j=1}^{Q_{CPC}}Q_{m_{CPC}}+\sum_{j=1}^{Q_{VPC}}Q_{m_{VPC}}$$

$$Q_m=\sum_{j=1}^{Q_{CPC}}\left(\frac{v_c\times f_r\times d_c}{60}\times t_{CPC}\times\frac{\rho}{1000}\right)+\sum_{j=1}^{Q_{VPC}}\left(\frac{\pi\times D^2\times d_c}{4\times t_c}\times t_{VPC}\times\frac{\rho}{10^6}\right) \tag{18}$$

By substituting the Eq. (18) of Q_m in Eqs. (11) and (12), the carbon emissions due to the material consumption and post-processing of chips respectively can be expressed as:

$$CEM_m\left(kgCO_2\right) = CEF_m \times \left(\begin{array}{l} \sum_{j=1}^{Q_{CPC}} \left(\frac{v_c \times f_r \times d_c}{60} \times t_{CPC} \times \frac{\rho}{1000} \right) + \\ \sum_{j=1}^{Q_{VPC}} \left(\frac{\pi \times D^2 \times d_c}{4 \times t_{VPC}} \times t_{VPC} \times \frac{\rho}{10^6} \right) \end{array} \right) \tag{19}$$

$$CEM_{chip}\left(kgCO_2\right) = CEF_{chip} \times \left(\begin{array}{l} \sum_{j=1}^{Q_{CPC}} \left(\frac{v_c \times f_r \times d_c}{60} \times t_{CPC} \times \frac{\rho}{1000} \right) + \\ \sum_{j=1}^{Q_{VPC}} \left(\frac{\pi \times D^2 \times d_c}{4 \times t_{VPC}} \times t_{VPC} \times \frac{\rho}{10^6} \right) \end{array} \right) \tag{20}$$

As stated in Eq. (1) and based on Eqs. (4), (6), (10), (19) and (20), the total CEM during the machining of a cylindrical workpiece can be expressed as:

$$\left[\begin{array}{l} CEM_{total} = \\ \underbrace{CEF_{elec} \times \left\{ \begin{array}{l} \sum_{j=1}^{Q_{stp}} E_{startup} + \sum_{j=1}^{Q_{std}} \left(P_{standby} \times t_{std} \right) + \sum_{j=1}^{Q_{acc}} \left(x_1 \times n^2 + x_2 \times n + x_3 \right) + \\ \sum_{j=1}^{Q_{idle}} \left(P_{idle} \times t_{idle} \right) + \sum_{j=1}^{Q_{tc}} \left(P_{tc} \times t_{tc} \right) + \sum_{j=1}^{Q_{air}} \left(P_{air} \times t_{air} \right) + \sum_{J=1}^{Q_{cool}} \left(P_{cool} \times t_{cool} \right) + \\ \sum_{j=1}^{Q_{CPC}} \left[P_{idle} \times t_{CPC} + P_{fz} \times t_{CPC} + C_{CP} \times v_c^{\alpha_c} \times f_r^{\beta_c} \times d_c^{\gamma_c} \times r^{\delta_c} \times t_{CPC} \right] + \\ \sum_{j=1}^{Q_{VPC}} \left(\begin{array}{l} P_{idle} \times t_{VPC} + P_{fx} \times t_{VPC} + \\ \int_0^{t_{VPC}} \left(\begin{array}{l} C_{VP} \times \left(v_{max} - \left(\frac{2 \times f_r \times \pi \times n^2}{60000} \right) \times t \right)^{\alpha_v} \\ \times f_r^{\beta_v} \times d_c^{\gamma_v} \times r^{\delta_v} \end{array} \right) dt \end{array} \right) \end{array} \right\}}_{CEM_{elec}} + \\ \underbrace{\sum_{j=1}^{Q_{cool}} \left(\frac{t_{proc}}{t_{cool}} \times \left(CEF_{oil} \times \left(V_{in} + V_{ad} \right) + CEF_{wc} \times \left(\frac{V_{in} + V_{ad}}{\delta} \right) \right) \right)}_{CEM_{cool}} + \\ \underbrace{\sum_{j=1}^{Q_{tool}} \left(\frac{t_c}{60} \times \left(\frac{v_c \times d_c^p \times f_r^q}{K} \right)^{\frac{1}{m}} \times CEF_{tool} \times w_{tool} \right)}_{CEM_{tool}} + \\ \underbrace{\left(\sum_{j=1}^{Q_{CPC}} \left(\frac{v_c \times f_r \times d_c}{60} \times t_{CPC} \times \frac{\rho}{1000} \right) + \sum_{j=1}^{Q_{VPC}} \left(\frac{\pi \times D^2 \times d_c}{4 \times t_{VPC}} \times t_{VPC} \times \frac{\rho}{10^6} \right) \right) \times CEF_m}_{CEM_m} + \\ \underbrace{\left(\sum_{j=1}^{Q_{CPC}} \left(\frac{v_c \times f_r \times d_c}{60} \times t_{CPC} \times \frac{\rho}{1000} \right) + \sum_{j=1}^{Q_{VPC}} \left(\frac{\pi \times D^2 \times d_c}{4 \times t_{VPC}} \times t_{VPC} \times \frac{\rho}{10^6} \right) \right) \times CEF_{chip}}_{CEM_{chip}} \end{array} \right] \tag{21}$$

6.3. Experimental Planning and Determining the Fitting Coefficients of the Models

Figure 6.2 depicts the experimental setup and overview of the adopted methodology in the present Chapter.

The detailed information on the experimental setup, machine tool, power consumption measurement equipment, experiment design, and related peripheral conditions are shown in **Chapter 5, Section 5.3**. The fitting coefficients of the energy consumption model for machining a cylindrical part shown in Eq. (26) were determined in a previous **Chapter 5, Section 5.4** for the same workpiece and cutting tool combination (i.e. aluminium Al 6061 and carbide inserts). As shown in Eq. (40) of **Chapter 5**, the total energy consumption prediction model of a machine tool for the machining of a cylindrical part can be expressed as shown in Eq. (22).

After determining the coefficients of various models, the various CEM factors and other essential parameters such as the weight of the cutting tool and tool life constant need to be defined first. Because the various CEM factors and basic data are closely related to machining conditions e.g. CEM_{elec} depends on how the electricity is generated and varying from nation to nation. This study is conducted in India, therefore, the CEM factor for electrical energy consumption (CEF_{elec}) for the Indian electricity mix is taken to be 1.41 kg CO_2/kWh from the literature (Sihag and Sangwan, 2019). Generally, water-soluble mineral oil with a 5% concentration (5 per cent mineral oil and remaining water) was used as the cutting fluid for the wet cutting environment, and the value of the CEF_{oil} ($kgCO_2/m^3$) and CEF_{wc} ($kgCO_2/m^3$) are considered as 500 and 200 respectively (Yi et al., 2015). The value CEM_{tool} is taken to be 29.6 $kgCO_2$/kg from the literature (Li et al., 2015; Zhang et al., 2017) for the carbide inserts, and the weight of the Sandvik cutting inserts (w_{tool}) used in the present study is 9.1g.

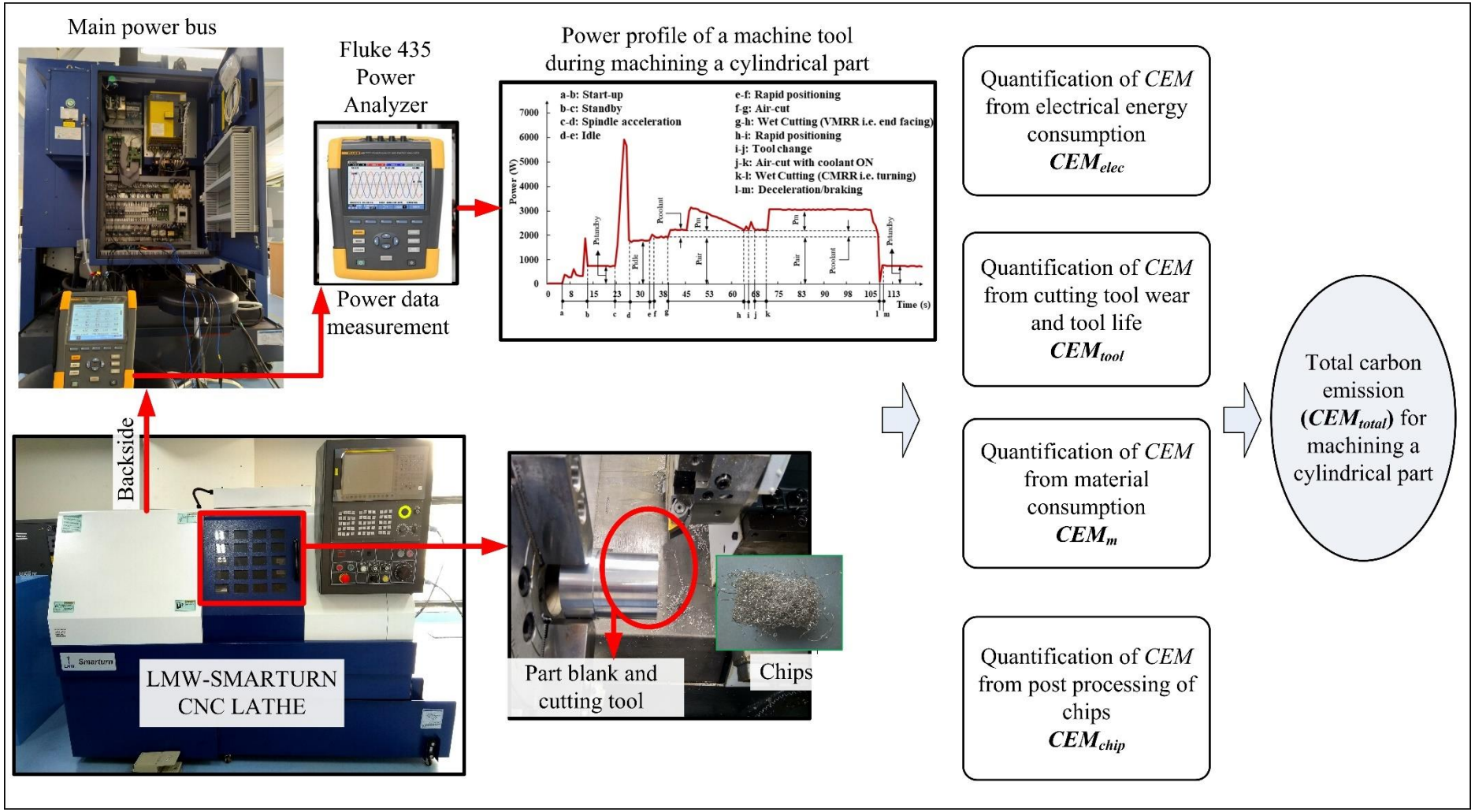

Figure 6.2. Experimental setup and adopted methodology.

$$
\begin{aligned}
E_{total}(kJ) = \Bigg[& \underbrace{\sum_{j=1}^{Q_{stp}} 21.125}_{E_{star-up}} + \underbrace{\sum_{j=1}^{Q_{std}} \left(0.75 \times t_{std}\right)}_{E_{standby}} + \sum_{j=1}^{Q_{acc}} \left(\frac{\left(\left(0.0017 \times n^2\right) + \left(0.6112 \times n\right) + 589.93\right)}{1000} \right) + \\
& \sum_{j=1}^{Q_{idle}} \left(\left(\frac{\left(\left(-3.3 \times 10^{-5} \times n^2\right) + \left(0.6035 \times n\right) + 786.95\right)}{1000} \right) \times t_{idle} \right) + \sum_{J=1}^{Q_{tc}} (P_{tc} \times t_{tc}) + \\
& \sum_{j=1}^{Q_{air}} \left\{ \left(\left(\frac{\left(\left(\left(-3.3 \times 10^{-5} \times n^2\right) + \left(0.6035 \times n\right) + 786.95\right) + P_f\right)}{1000} \right) \times t_{air} \right) + \right\} + \\
& \left. \sum_{J=1}^{Q_{cool}} (P_{cool} \times t_{cool}) \right) \\
& \sum_{j=1}^{Q_{CPC}} \left(\begin{array}{l} \left(\frac{\left(-3.3 \times 10^{-5} \times n^2 + 0.6035 \times n + 786.95\right)}{1000} \right) \times t_{CPC} + \\ \left(\frac{\left(0.0149 \times f_r + 20.00\right)}{1000} \right) \times t_{CPC} \\ + \left(0.3071 \times v_c^{\alpha_C} \times f_r^{\beta_C} \times d_c^{\gamma_C} \times r^{\delta_C}\right) \times t_{CPC} \end{array} \right) + \\
& \sum_{j=1}^{Q_{VPC}} \left(\begin{array}{l} \left(\frac{\left(-3.3 \times 10^{-5} \times n^2 + 0.6035 \times n + 786.95\right)}{1000} \right) \times t_{VPC} + \left(\frac{\left(0.0087 \times f_r + 8.00\right)}{1000} \right) \times t_{VPC} + \\ \int_0^{t_{VPC}} \left(99.51 \times 10^{-3} \left(v_{max} - \frac{2 \times f_r \times \pi \times n^2}{60000} \times t \right)^{\alpha_V} \times f_r^{\beta_V} \times d_c^{\gamma_V} \times r^{\delta_V} \right) dt \end{array} \right) \Bigg]
\end{aligned}
\tag{22}
$$

The values of the constants of the tool life can be determined experimentally or adopted from the data handbook. In the present study, the values are taken to be $K = 250$, $m = 0.35$, $p = 0.15$, and $q = 0.60$ from the literature and data handbook (Drozda and Wick, 1983;

Ghosh, 1991). The material of the cylindrical part is aluminium and the values of CEM factors CEF_m and CEF_{chip} for aluminium material is taken 16.13 $kgCO_2/kg$ and 0.256 $kgCO_2/kg$ respectively from the literature (Li et al., 2015). Finally, the CEM_{total} for machining a cylindrical part can be expressed as:

$$CEM_{total} = \underbrace{\left[\begin{array}{l} \underbrace{\sum_{j=1}^{Q_{stp}} 21.125}_{E_{star-up}} + \underbrace{\sum_{j=1}^{Q_{std}} \left(0.75 \times t_{std}\right)}_{E_{standby}} + \sum_{j=1}^{Q_{acc}} \left(\frac{\left(\left(0.0017 \times n^2\right) + \left(0.6112 \times n\right) + 589.93\right)}{1000} \right) + \\ \sum_{j=1}^{Q_{idle}} \left(\left(\frac{\left(\left(-3.3 \times 10^{-5} \times n^2\right) + \left(0.6035 \times n\right) + 786.95\right)}{1000} \right) \times t_{idle} \right) + \sum_{J=1}^{Q_{tc}} (P_{tc} \times t_{tc}) + \\ \sum_{j=1}^{Q_{air}} \left(\left(\frac{\left(\left(\left(-3.3 \times 10^{-5} \times n^2\right) + \left(0.6035 \times n\right) + 786.95\right) + P_f\right)}{1000} \right) \times t_{air} \right) + \sum_{J=1}^{Q_{cool}} (P_{cool} \times t_{cool}) + \\ \sum_{j=1}^{Q_{CPC}} \left(\begin{array}{l} \left(\frac{\left(-3.3 \times 10^{-5} \times n^2 + 0.6035 \times n + 786.95\right)}{1000} \right) \times t_{CPC} + \left(\frac{\left(0.0149 \times f_r + 20.00\right)}{1000} \right) \times t_{CPC} \\ + \left(0.3071 \times v_c^{\alpha_C} \times f_r^{\beta_C} \times d_c^{\gamma_C} \times r^{\delta_C}\right) \times t_{CPC} \end{array} \right) + \\ \sum_{j=1}^{Q_{VPC}} \left(\begin{array}{l} \left(\frac{\left(-3.3 \times 10^{-5} \times n^2 + 0.6035 \times n + 786.95\right)}{1000} \right) \times t_{VPC} + \left(\frac{\left(0.0087 \times f_r + 8.00\right)}{1000} \right) \times t_{VPC} + \\ \int_0^{t_{VPC}} \left(99.51 \times 10^{-3} \left(v_{max} - \frac{2 \times f_r \times \pi \times n^2}{60000} \times t \right)^{\alpha_V} \times f_r^{\beta_V} \times d_c^{\gamma_V} \times r^{\delta_V} \right) dt \end{array} \right) \end{array} \right]}_{CEM_{elec}} \times 1.41 + \\ \underbrace{\sum_{j=1}^{Q_{cool}} \left(\frac{t_{proc}}{t_{cool}} \times \left(500 \times \left(V_{in} + V_{ad}\right) + 200 \times \left(\frac{V_{in} + V_{ad}}{\delta} \right) \right) \right)}_{CEM_{cool}} + \underbrace{\sum_{j=1}^{Q_{tool}} \left(\frac{t_c}{60} \times \left(\frac{v_c \times d_c^{0.15} \times f_r^{0.60}}{K} \right)^{\frac{1}{0.35}} \times \frac{1}{29.6 \times 9.1} \right)}_{CEM_{tool}} + \\ \underbrace{\left(\sum_{j=1}^{Q_{CPC}} \left(\frac{v_c \times f_r \times d_c}{60} \times t_{CPC} \times \frac{2.7}{1000} \right) + \sum_{j=1}^{Q_{VPC}} \left(\frac{\pi \times D^2 \times d_c}{4 \times t_{VPC}} \times t_{VPC} \times \frac{2.7}{10^6} \right) \right) \times 16.13}_{CEM_m} + \\ \underbrace{\left(\sum_{j=1}^{Q_{CPC}} \left(\frac{v_c \times f_r \times d_c}{60} \times t_{CPC} \times \frac{2.7}{1000} \right) + \sum_{j=1}^{Q_{VPC}} \left(\frac{\pi \times D^2 \times d_c}{4 \times t_{VPC}} \times t_{VPC} \times \frac{2.7}{10^6} \right) \right) \times 0.256}_{CEM_{chip}} \end{array} \right]$$

(23)

The values of the fitting coefficients for the cutting power models corresponding to the cutting environment can be seen in Table 5.6 of Chapter 5. The various CEM factors and calculation parameters are summarized in Table 6.1.

Table 6.1 Carbon emission factors and parameters used in the present study

V_{in} (m^3)	V_{ad} (m^3)	δ (%)	t_{cool} (*month*)	CEF_{oil} ($kgCO_2/m^3$)	CEF_{wc} ($kgCO_2/m^3$)
12.5×10^{-3}	5.5×10^{-3}	5%	3	500	200

CEF_{elec} ($kgCO_2/kWh$)	CEF_{tool} ($kgCO_2/kg$)	CEF_m ($kgCO_2/kg$)	CEF_{chip} ($kgCO_2/kg$)
1.41	29.6	16.13	0.256

6.4. Case Study

To validate the developed model and for practical implementation in industry, the developed model is applied on a cylindrical part with three different process plans. The range of process parameters for each process plan is shown in Table 6.2, and the same workpiece as shown in Figure 5.5 of Chapter 5 is adopted for the case study.

Table 6.2 Process parameters.

Process Plan No.	D (mm)	n (rev/min)	v_c (m/min)	f_r (mm/rev)	d_c (mm)	r (mm)	Length (mm)
I	50	800	125.60	0.05	0.6	0.8	50
II	50	1200	188.40	0.10	0.8	0.8	50
III	50	1600	251.20	0.15	1.2	0.8	50

The use of coolant definitely enhances the tool life but potentially causes major environmental concerns such as coolant waste and work-related illnesses. According to

literature (Li et al., 2015), wet cutting produces 30% higher CEM than dry machining at the same process parameters. Therefore, the cutting experiments were performed in a dry environment, and the CEM from coolant consumption (CEM_{cool}) is not calculated for estimating the total CEM.

According to the developed carbon emission model shown in Eq. (23), the quantification of CEM_{total} for process plan-I (PP-I) is discussed as follows:

6.4.1. Calculation of CEM_{elec}

The electrical energy consumption according to the PP-I can be evaluated using Eq. (22). The detailed calculation can be seen in Section 5.5 of Chapter 5. The corresponding CEM due to electrical energy consumption can be calculated using Eq. (23). The values of the CEF_{elec} is adopted 1.41 $kgCO_2/kWh$ (Sihag and Sangwan, 2019) as shown in Table 6.1.

$$CEM_{elec} = \frac{195.6842}{60 \times 60} \times 1.41 = 0.0766 \ kgCO_2 \tag{24}$$

6.4.2. Calculations of CEM_{tool}

The CEM due to the cutting tool wear can be calculated using Eq. (10). The value of CEF_{tool} is 29.6 kgCO2/kg (Li et al., 2015; Zhang et al., 2017) and w_{tool} for the Sandvik CNMG 12 04 08 inserts is 9.1 g. The values of exponents of tool life Eq. (55), K, m, p and q are 250, 0.35, 0.15 and 0.60 respectively (Drozda and Wick, 1983; Ghosh, 1991). The CEM_{tool} for the PP-I can be calculated as:

$$CEM_{tool} = \frac{112.5}{60} \times \left(\frac{125.60 \times 0.6^{0.15} \times 0.05^{0.60}}{250} \right)^{\frac{1}{0.35}} \times 29.6 \times 9.1$$

$$CEM_{tool} = 0.3340 \, kgCO_2 \tag{25}$$

6.4.3. Calculation of CEM_m and CEM_{chip}

CEM_m and CEM_{chip} is calculated by first determining the mass of the removed material with Eq (64), Where the density of the aluminium ρ is 2.7 gm/cm^3. Q_m for PP-I can be calculated as:

$$Q_m = \left(\frac{125.60 \times 0.05 \times 0.6}{60} \times 75 \times \frac{2.7}{1000}\right) + \left(\frac{3.14 \times 50^2 \times 0.6}{4 \times t_c} \times 37.5 \times \frac{\rho}{10^6}\right)$$

$$Q_m = 0.0286 \ kg$$

In the present study, the values of CEM factors CEF_m and CEF_{chip} for an aluminium part are 16.13 kgCO_2/kg and 0.256 kgCO_2/kg respectively (Li et al., 2015). By substituting the Q_m in Eqs. (19) and (20), the carbon emissions CEM_m and CEM_{chip} respectively can be calculated:

$$CEM_m = 16.13 \times 0.0286 = 0.4615 \ kgCO_2 \quad (26)$$

$$CEM_{chip} = 0.256 \times 0.0286 = 0.0073 \ kgCO_2 \quad (27)$$

6.4.4. Calculation of total carbon emission

Finally, the total carbon emission for machining of a cylindrical part according to the PP-I can be determined by aggregating the various CEM i.e. Eqs. (24), (25), (26) and (27) as shown in Eq. (1):

$$CEM_{total} = CEM_{elec} + CEM_{tool} + CEM_m + CEM_{chip}$$

$$CEM_{total} = 0.8712 \ kg$$

Following the same procedure, the CEM_{total} for machining a cylindrical part based on the other process plans can be determined and summarised in Table 6.3.

Table 6.3 The CEM_{total} related to different process plans

Carbon emission ($kgCO_2$)	Process plan number		
	I	II	III
CEM_{elec}	0.0766	0.0409	0.0328
CEM_{tool}	0.3340	1.3076	3.5698
CEM_{m}	0.4615	0.6113	0.9231
CEM_{chip}	0.0073	0.0097	0.0146
CEM_{total}	0.8795	1.9694	4.5403

6.5. Discussion

As shown in Table 6.3, the CEM of the machining process varied significantly with the different process plans, indicating that process parameters have a significant impact on the CEM of the machining process. Thus, the proper selection of the process parameters is critical in view of the low CEM. The various carbon emissions (CEM_{elec}, CEM_{tool}, CEM_{m} and CEM_{chip}) related to each process plan are shown in Figure 6.3. With changes in the process parameters, the different *CEMs* also show substantial variation, as shown in Figure 6.3 (a), (b), (c) and (d). It can be seen in Figure 6.3 (a) that CEM due to electrical energy consumption decreases at the high values of the process parameters, such as an increase in spindle speed and feed rate. It is evident that the faster the feed rate and spindle speed, the shorter the processing time resulting in low E_{total} and CEM_{elec}. These results are consistent with a similar CEM trend reported in the literature (Li et al., 2015). On the other hand, as shown in Figure 6.3 (b), *CEM* due to the cutting tool shows significant growth with higher process parameter values. Given that higher cutting speeds shorten tool life and cutting experiments were performed in dry environments, higher cutting speeds and feed rates caused high temperature at the work-tool interface and increased abrasion resulting in

increased tool wear and CEM_{tool}. As shown in Figure 6.3 (c) and Figure 6.3 (d), carbon emissions from material consumption and chip post-processing increased as cutting depth is increased. These carbon emissions are determined by the quantity of material removed during the machining process. The greater the cutting depth, the more mass is taken from the part, resulting in higher mass and related *CEMs*: CEM_m and CEM_{chip}.

As shown in Table 6.3, it is significant to highlight that CEM due to material consumption and chip disposal is solely dependent on the depth of the cut, where CEM_m is a substantial contributor to total CEM. Therefore, the process plan from the case study was replicated in a similar manner while keeping the same cutting depth of 1.2 mm to investigate the impact of process parameters on CEM due to energy consumption and cutting tool, and the results are summarised in Table 6.4.

Table 6.4 The CEM_{total} associated with the different process plans for 1.2 mm depth of cut.

Carbon emission	Process plan number		
($kgCO_2$)	I	II	III
CEM_{elec}	0.0822	0.0433	0.0328
CEM_{tool}	0.4496	1.5662	3.5698
CEM_m	0.9231	0.9231	0.9231
CEM_{chip}	0.0146	0.0146	0.0146
CEM_{total}	1.4695	2.5472	4.5403

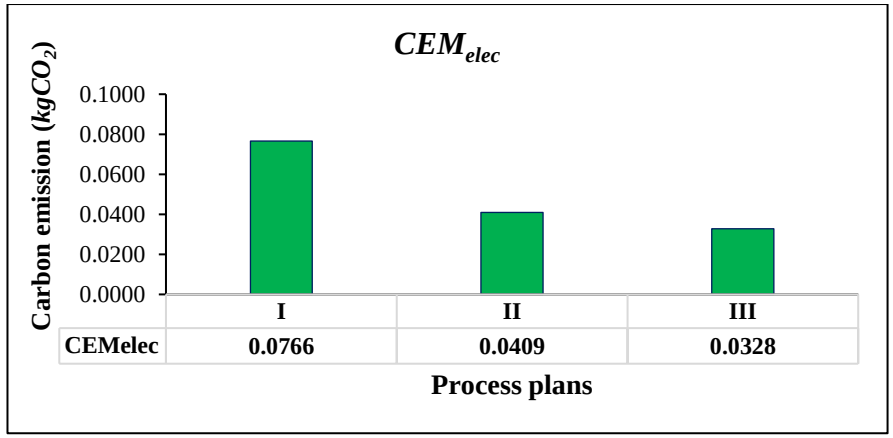

(a) CEM_{elec} related to different process plans.

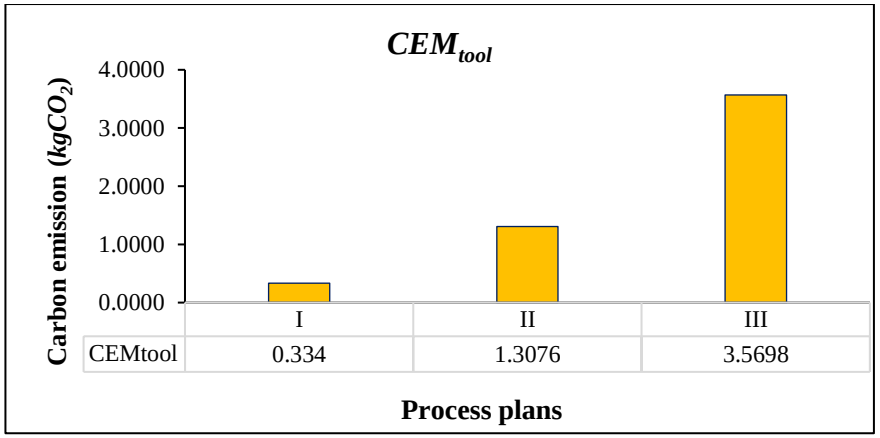

(b) CEM_{tool} related to different process plans.

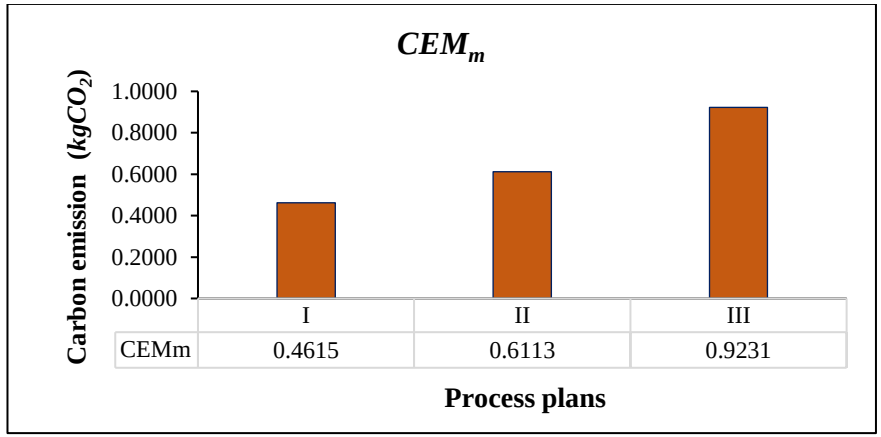

(c) CEM_m related to different process plans.

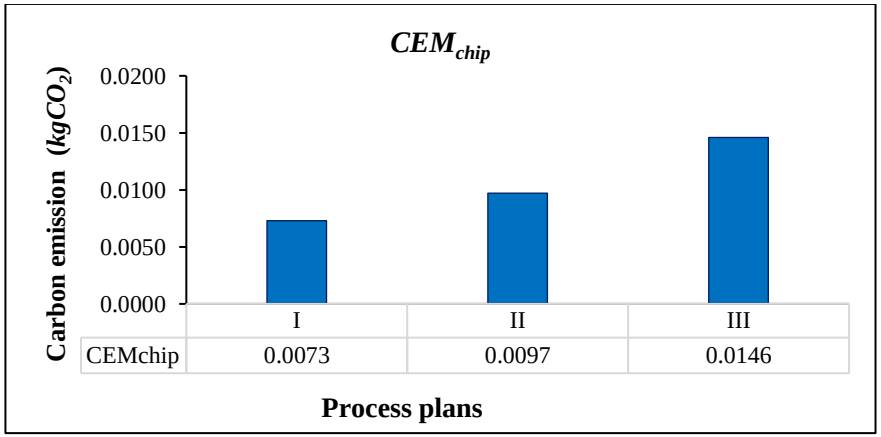

(d) CEM_{chip} related to different process plans.

Figure 6.3. Carbon emissions related to different process plans (a) due to electrical energy (CEM_{elec}) (b) due to tool (CEM_{tool}) (c) due to material (CEM_m) and (d) due to chip (CEM_{chip}).

Since the cutting depth is constant in all process plans, the amount of material removed remains constant regardless of cutting speed or feed rate; thus, the corresponding CEM due to material consumption and chip disposal remains unchanged across all process plans. Meanwhile, changes in cutting speed and feed rate have a significant impact on the CEM associated with electrical energy consumption and the cutting tool. The CEM_{elec} and CEM_{tool} related to repeated set of process plan are shown in Figure 6.4.

So, even if the volume of material removal and associated CEM, i.e. CEM_m and CEM_{chip}, are the same, a change in the other process parameters have a significant impact on the total CEM. The case study with different process plans is depicted to show the correlation of carbon emissions and process parameters.

The developed model fully accounts the effect of process parameters on CEM, and improves the transparency of the CEM of the machining process and facilitates the exploration of low energy efficiency and high CEM machining process. The proposed model is not only useful for identifying low-CEM process parameters, but can also be applied in multi-objective optimization to trade-off with other important machining process indicators such as productivity and product quality.

The proposed model can accurately quantify carbon emissions for machining of a cylindrical part based on process parameters and CEM factors. The current model is capable to quantify carbon emissions for industrial applications because it can include the multiple energy consumption modules, CPC-machining process and VPC-machining process that commonly occurred throughout the machining of the cylindrical work part in an industry.

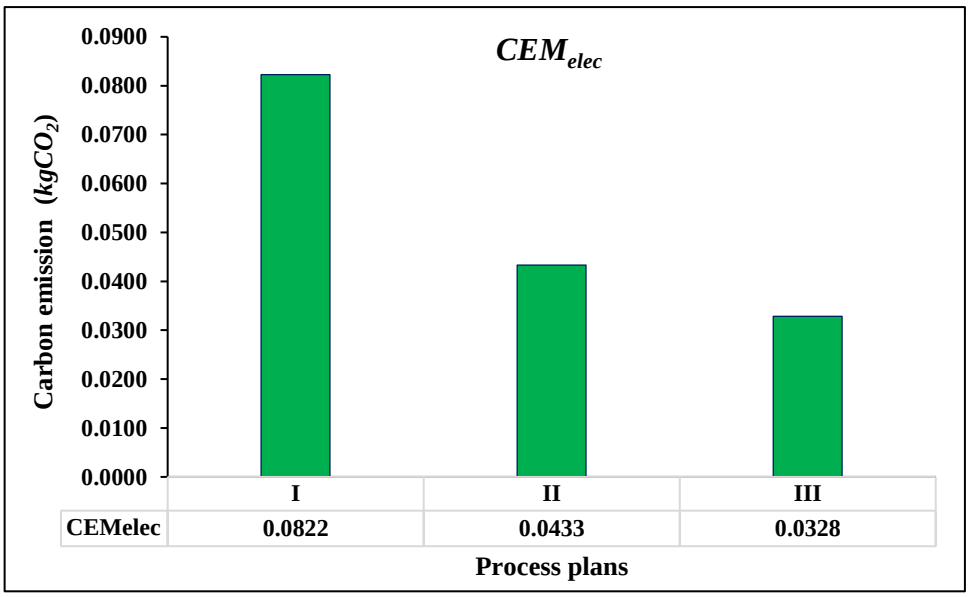

(a) CEM_{elec} related to repeated process plans.

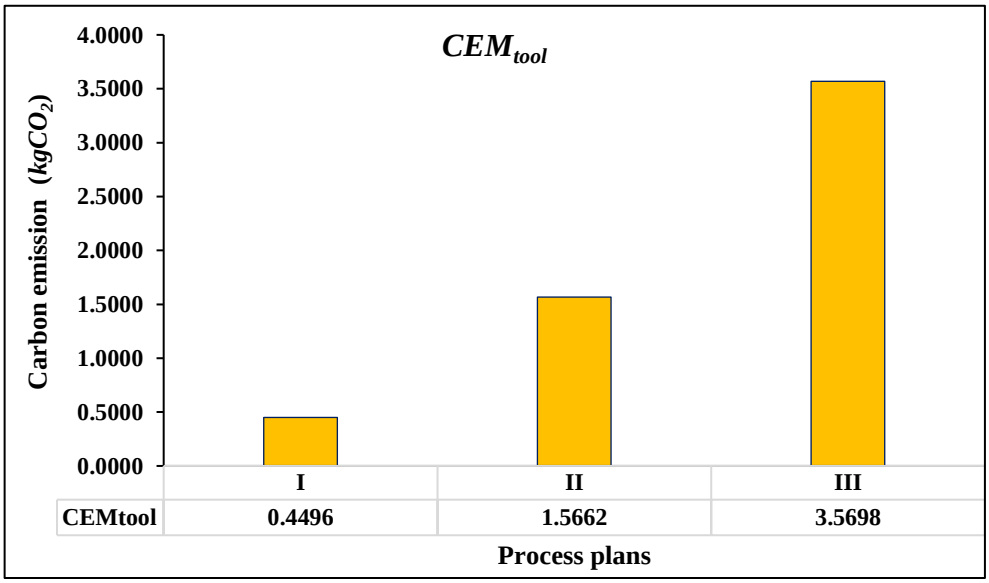

(b) CEM_{tool} related to repeated process plans.

Figure 6.4. Carbon emissions related to repeated process plans for 1.2 mm depth of cut (a) CEM_{elec} and (b) CEM_{tool}.

6.6. Summary

The focus of this chapter is to develop an empirical model to quantify CEM for machining of a cylindrical part. The CEM associated with a cylindrical part machining are decomposed into CEM from electrical energy consumption, material consumption, cutting tool wear,

coolant consumption and from the disposal of machining waste materials. Electrical energy consumption of a machine tool is further decomposed into different energy modules: startup, standby, spindle acceleration, idle, rapid positioning, air-cutting, and cutting for accurate quantification of CEM. The cutting energy consumption module of machine tool is further decomposed into the CPC and VPC machining processes. The developed model is applied on a cylindrical part with three different process plans, in which the influence of process parameters on CEM is analyzed. To validate the developed model and for practical implementation in industry, the developed model is applied on a cylindrical part with three different process plans. It is shown that the CEM of the machining process varied significantly with the different process plans, indicating that process parameters have a significant impact on the CEM of the machining process. The proposed model can accurately quantify carbon emissions for machining of a cylindrical part based on process parameters and CEM factors. The current model is capable to quantify carbon emissions accurately for industrial applications because it can include the multiple energy consumption modules that commonly occurs during the machining of the cylindrical work parts in an industry. The proposed model can be utilized in the manufacturing industry to quantify carbon emissions based on different process parameters before machining a cylindrical part to achieve low carbon manufacturing process planning and scheduling.

Chapter 7:

Prediction of Energy Efficiency, Power Factor and associated Carbon Emissions Using Soft Computing Techniques

In the present chapter, three soft computing techniques, multi-gene genetic programming (MGGP), least square-support vector machine (LS-SVM) and fuzzy logic, are applied to model a machine tool's energy efficiency (*EE*), power factor (*PF*) and associated carbon emission (CEM). The performance of the models was evaluated on six statistical indicators and hypothesis testing were conducted to validate the goodness of fit of the developed models. The developed models can be used to eliminate the need for advanced costly laboratory set-up and time-consuming measurement procedures required for performing experiments.

7.1. Introduction

Low-carbon emission of machine tools, which aims to reduce carbon intensity and improve process efficiency, has evolved as an emerging issue that has encouraged a lot of research into accurate prediction of energy-related performance characteristics such as energy efficiency (*EE*), power factor (*PF*) and associated carbon emission (CEM) of machine tools. Establishing an accurate CEM model for machine tools as a function of process parameters is the basis for implementing energy-efficient and low-carbon emission process planning and scheduling (Lv et al., 2018). The lack of accurate and realistic energy consumption models has hindered the implementation of energy-efficient approaches (Lv et al., 2018; Wang et al., 2015).

In practice, *EE* and *PF* are the two significant indicators of a machine tool's effective electrical energy utilization. The modelling of *EE* of machine tools is useful for implementing low carbon emission measures. According to literature review on energy-

saving strategies and technologies toward greener machine tools, *EE* should be accurately modelled for the future market (Arriaza et al., 2017; Bilga et al., 2016; Kumar et al., 2017). The *PF* is an important indicator of efficient electrical energy utilization of the machine tool's electrical system (Behrendt et al., 2012). The *PF* is the ratio of active power to apparent power (O'Driscoll and O'Donnell, 2013). The main machine tool components, such as electric motors, feed drives, coolant pumps, etc., are powered by inductive loads that accumulate to a low *PF*. Low *PF* reduces the distribution capacity of the electrical power grid by increasing current flow and lowering the voltage. If *PF* value falls below a certain level, electrical boards impose penalties (Behrendt et al., 2012). The accumulation of inductive load of machine tool components is one of the leading causes of power losses and low *PF*. Machine tools have variable drive systems and can be operated at variable loads, resulting in inductive load and corresponding *PF* changes. This implicate that the change in process parameters have significant influence on the PF (Bilga et al., 2016). Process parameters are known to have a considerable impact on the energy consumption of a machining process (Newman et al., 2012), and hence influence the CEM, *EE* and *PF* implicitly or explicitly. Therefore, reliable and accurate estimations of CEM, *EE* and *PF* based on process parameters can significantly enhance efforts to achieve sustainable manufacturing at the early design stage of product development. Accurate predicting models of these performance characteristics can be useful for process planners to select the appropriate process parameters in the early process planning phase without conducting the actual experiments. To select the process parameters for the machine tools, the formulation of a mathematical model representing the relationship between the outputs (*EE*, *PF* and CEM) and inputs is essential.

Conventional modelling tools, such as response surface methodology (RSM) and physics-based models, have limitations when it comes to capturing the non-linear

behaviour between performance characteristics and process parameters (Garg et al., 2016; Kant and Sangwan, 2015). RSM requires the form of polynomial functions to be defined first, which can affect the accuracy of the approximation model (Garg et al., 2016). The physics-based models were built on overly simplistic assumptions, rendering them incapable of predicting accurate results (Dirikolu and Childs, 2000). Further, the complex and stochastic nature of the machining process make it challenging to estimate the coefficient of a physics-based model (Kant and Sangwan, 2015). Therefore, soft computing techniques have been increasingly popular in recent years for modelling in a variety of engineering applications due to their reliable predictability, ability to work with the inherent complexity and to capture non-linear behaviour between input and output parameters. As previously stated in the literature review **Chapter 2** that an increasing number of authors employed soft computing for modelling in different engineering applications (Abd and Abd, 2017; Garg et al., 2016, 2014; Naseri et al., 2017; Rajabi et al., 2022; Shafiullah et al., 2019; Tseng et al., 2016; Zhang and Zhang, 2016).

The literature indicates that soft computing techniques such as GP (Garg et al., 2016, 2015), SVM (Su et al., 2021) , and fuzzy logic (Iqbal and Dar, 2011; Liman et al., 2021; Vukman et al., 2020) are widely used for modelling in a variety of engineering applications and manufacturing processes, showing their ability to manage complex input-output behaviour. However, there appears to be an abundance of literature on the modelling of various process responses such as energy consumption, productivity and surface quality (Bhinge et al., 2017; Garg et al., 2016, 2015; Gupta, 2010; Pan et al., 2021), but to the best of the author's knowledge, none of the literature reported modelling of *EE*, *PF* and CEM using soft computing techniques for machine tools. In this chapter, three soft computing techniques MGGP, LS-SVM, and fuzzy logic were applied to model the *EE*, *PF* and associated total carbon emission (CEM_t) of a machine tool. The experiments were

performed on a CNC lathe machine tool to capture the data required for development of models. Coefficients of determination and five error indices were used to evaluate and compare the accuracy of the developed models. Further, hypothesis testing i.e. mean paired t-test and variance of F-test were used to calculate the goodness of fit of the models.

7.2. An Overview of the Soft Computing Techniques

A brief description of three soft computing methods viz. MGGP, LS-SVM, and Fuzzy logic are presented as follows.

7.2.1. Multi gene genetic programming (MGGP)

The approximate optimal solution in a high-dimensional search space can be found using evolutionary algorithms e.g. genetic programming, which are frequently used in modelling processes of complex nature (Garg et al., 2014). Genetic programming is governed by the Darwinian theories of natural selection, evolvement, and the survival of the best (Orove et al., 2015). Genetic programming has been improved with multi-gene genetic programming (MGGP) (Gandomi and Atefi, 2020). Unlike GP, MGGP initiates with a population of multi-tree alternatives derived by a random vector of trees. Following that, using a potential Pareto tournament, a predetermined proportion of the population is opted to be a parent based on the statistical fitness parameters i.e. coefficient of determination of each alternative (Gandomi and Atefi, 2020). After which, the next generation is formed based on the mutation and cross-over of the selected solutions. This evolution is recurrent until a user-defined termination criterion is achieved. If any population member fails to meet the threshold evaluation criteria, individuals are subjected to genetic operations in order to create a new population. These actions are widely recognized as crossover, mutation, and replication. The iterative process doesn't come to an end until the predefined termination criteria are satisfied. Most members of a population are formed by crossover and mutation.

A crossover is the swap of arbitrary branches of two individual expressions. In a mutation, randomly a branch is selected and changed by another randomly generated branch. The flowchart of the proposed MGGP method is shown in Figure 7.1 and parametrical multi-gene model expression is shown in Eq. (1):

$$y = C_0 + C_1 * tree1 + C_2 * tree2 \ldots.. + C_z * tree_z \quad (1)$$

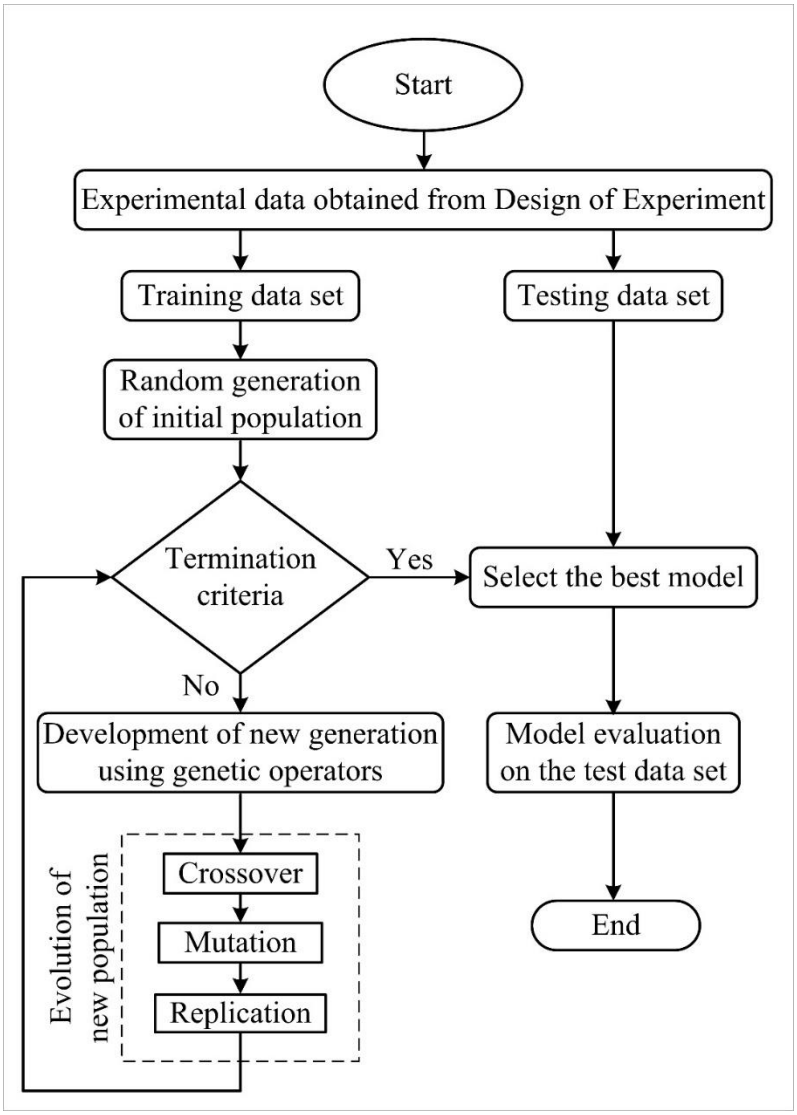

Figure 7.1. The flowchart of the proposed MGGP method.

Where C_0 represent the bias or offset term, z represents the quantity of genes and $C_1 \sim C_z$ represents the relative importance (weights) associated to each gene. The elements of the terminal and functional sets combine to form trees. The number, composition, and structure

of these trees change randomly during a run using the training data, depending on user-defined constraints. The MGGP model is linear in terms of bias and weights but not in terms of tree elements. The maximum depth of trees should be defined to keep the overall model's complexity under control and to develop relatively compact models (Hoang et al., 2017). In genetic programming, a population member is a hierarchically arranged tree that consists of members of a functional set.

7.2.2. Least square-support vector machines (LS-SVM)

Support Vector Machine is a supervised machine learning technique for creating a function from training data. The training data is a set of pairs that includes input objects and selected outputs. The output can be a continuous value or a classification of the input objects (Kant and Sangwan, 2015). After observing a finite number of training data samples, the SVM creates a 'decision maker' system to predict the value of the function for any valid input point (Gupta, 2010). When SVM is used to solve regression problems, it is referred to as support vector regression (SVR). The structure of the SVM is shown in Figure 7.2, which comprises input variables, support vectors, kernels, and output variables (Garg et al., 2018).

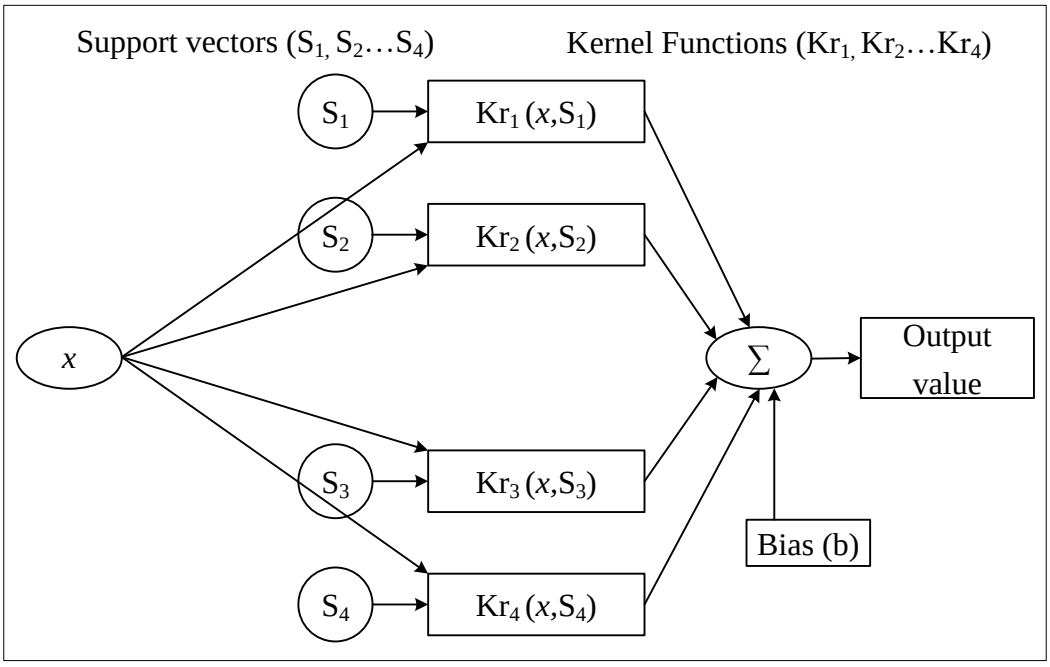

Figure 7.2. Line Diagram for LS-SVM (Garg et al., 2018).

The SVR does not use statistical assumptions, model structure and error dependence and so does not require any model structural assumptions. The SVM model is built on the principle of structural risk minimization. The SVM initially transforms the original input space into a higher-dimensional feature space. For such transformations, a non-linear hyperspace function is used. In order to learn non-linear relationships with linear machine learning, a collection of non-linear features must be selected, and the data must be expressed in a new representation. In a feature space, non-linear regression problems can be transformed into linear regression problems.

The SVM model is provided with a set of training data (r) to learn the input-output relationship function $f(x)$. The training data is provided in pairs $\{(x_i, y_i)\}_{i=1}^{r}$, $x_i \in R^r$ where x_i and y_i are the input and output variables respectively. The SVM function can be established as shown in Eq. (2) (Gupta, 2010; Kant and Sangwan, 2015).

$$f\left(x,w\right)=\sum_{i=1}^{r}w_i\varphi_i\left(x\right)=w^Tx+b \tag{2}$$

Where $\varphi_i(x)$ is features, w is the weight and b is the bias. Thus, a linear regression hyperplane $f(x,w)=w^Tx+b$ can be estimated by minimizing the function as follows:

$$R=\frac{1}{2}w^2+C\left(\sum_{i=1}^{r}\left|y_i-f\left(x_i,w\right)\right|_\varepsilon\right) \tag{3}$$

Where C is the cost function, ε is the insensitive loss function and satisfies the following relation:

$$\left|y_i-f\left(x_i,w\right)\right|_\varepsilon=\begin{cases}0, & if\ \left|y_i-f\left(x_i,w\right)\right|\le\varepsilon\\ \left|y_i-f\left(x_i,w\right)\right|-\varepsilon, & \text{otherwise}\end{cases} \tag{4}$$

The trade-off between the weight vector (w) and approximation error is controlled by the cost function.

7.2.3. Fuzzy logic

Fuzzy logic was introduced by Zadeh (1975) and applied in decision-making processes to translate linguistic variables to quantitative variables. Fuzzy logic works with parameter ranges rather than individual data points, therefore it can accurately predict results for all data points within the parameter ranges (Garud et al., 2021). Fuzzy sets, membership functions, linguistic variables, and fuzzy rules are the four elements of fuzzy logic (Tseng et al., 2016). Figure 7.3 shows the basic structure of a fuzzy logic model for four inputs and single output parameters.

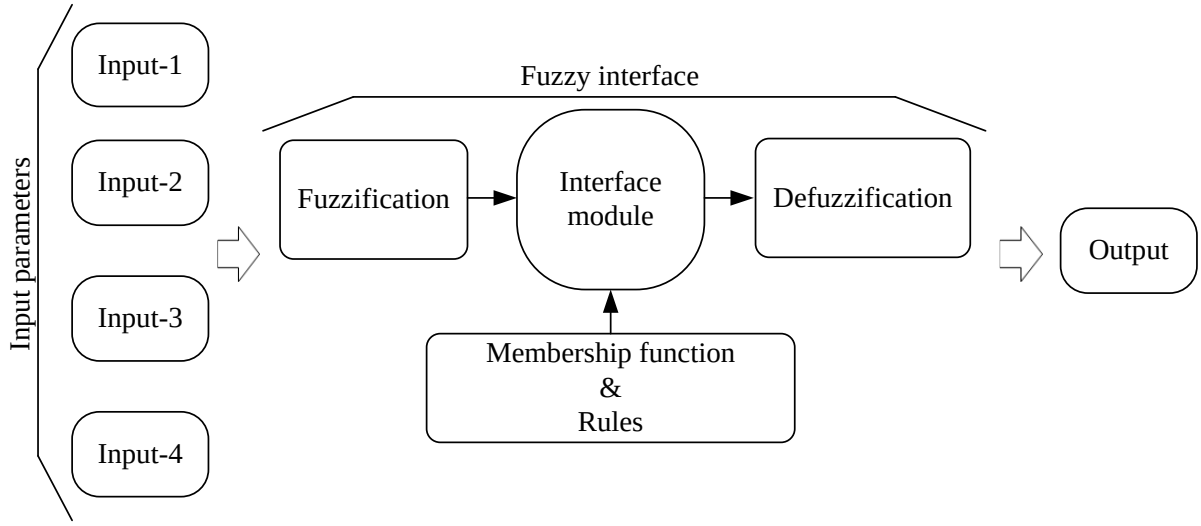

Figure 7.3. A typical outline for a fuzzy logic model with four inputs and one output.

A fuzzy set is a collection of objects without clear-cut or predefined boundaries between things that are or are not group members (Shemshadi et al., 2011) boundaries do not exist in fuzzy sets. The degree to which an object belongs to the fuzzy set ranges from 0 to 1, with 0 representing 0% membership and 1 representing 100% participation (Tseng et al., 2016). This value is known as the membership value of that particular parameter. Each input/output parameter's whole range is divided into several smaller ranges. The variation of each small range is represented by the appropriate elementary curve which is called the membership function. The membership function is a curve that specifies each point's

membership value. It refers to the degree of trueness and are generally represented graphically. There are many different types of membership functions available including triangular, Gaussian, trapezoidal, and sinusoidal. The number of membership functions and the limits of each membership function is determined by the behaviour of the imported input-output data. Linguistic variables can be defined qualitatively or quantitatively using the membership function. This is how human factors are taken into account by fuzzy logic. The linguistic variables' values are usually "slow", "fast," and "hard". The fuzzy model's governing rulesets are known as fuzzy rules. The "IF-Then" statement and "AND," "OR," or "NOR" Booleans are used in rules to correlate input and output parameters. It correlates the circumstances that must be applied to a linguistic variable in order to achieve the intended result. The rules primarily establish a connection between the input and output parameters.

7.3. Experimental Planning and Calculations

The turning experiments were conducted on a LMW-Smarturn CNC lathe machine tool under a dry environment in the interest of environment conscious production using carbide inserts of ISO designations CNMG 12 04 04, CNMG 12 04 08, and CNMG 12 04 12. The cutting inserts were mounted on the tool holder of ISO designation PCLNR 2020 K 12. The workpiece material was aluminium Al 6061 alloy. The main process parameters that can be easily managed on the shop floor are used as input process parameters: cutting speed (v_c), feed rate (f_r), depth of cut (d_c) and cutting tool nose radius (r). The Taguchi L_{27} orthogonal array was used to design the experimental run. The level of process parameters and combinations according to the L_{27} orthogonal array are summarized in Table 7.1. The Fluke 435 series II Power Analyzer was used to measure the power drawn by the CNC machine tool from the main power bus, as shown in Figure 7.4.

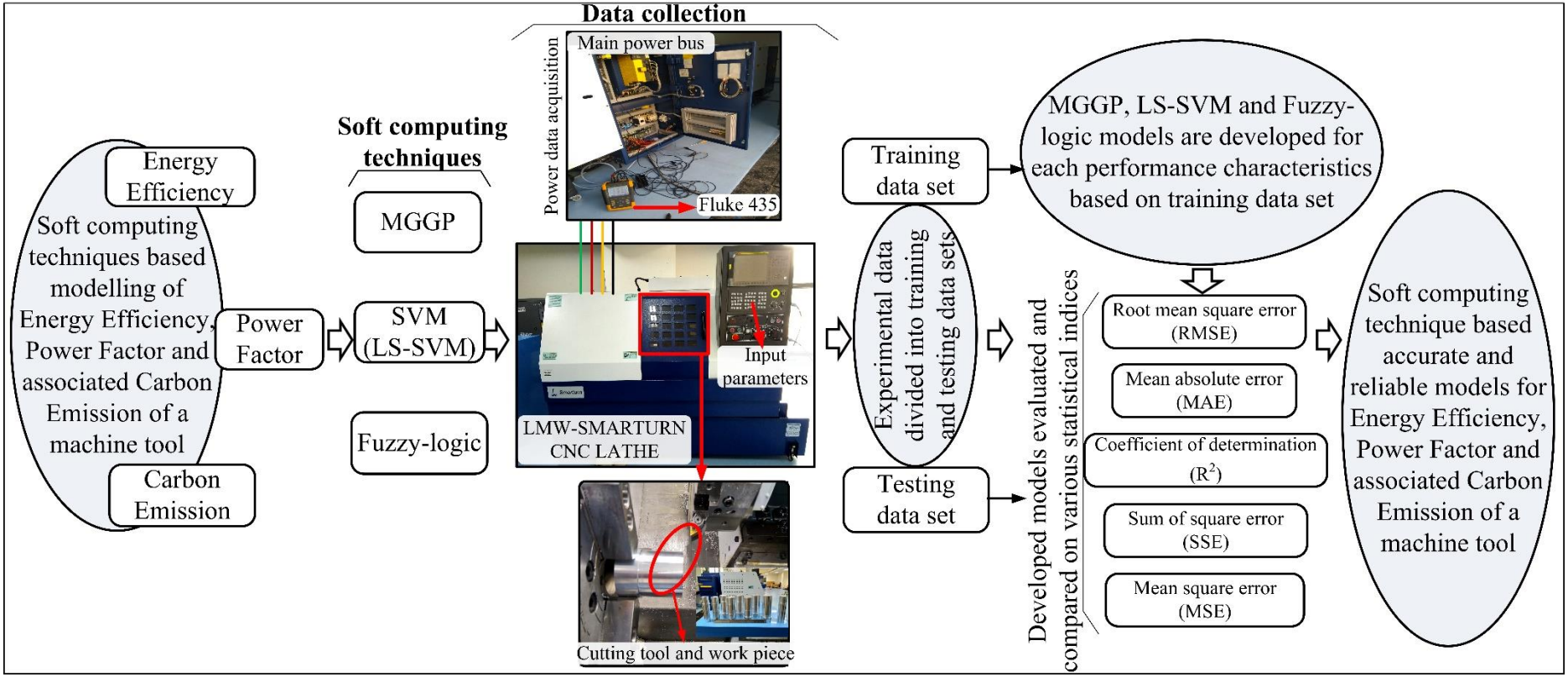

Figure 7.4. Experimental setup and outline of the study.

Table 7.1 Process parameters and their considered levels.

Process parameters		v_c (*m/min*)	f_r (*mm/rev*)	d_c (*mm*)	r (*mm*)
Levels	I	144	0.10	0.50	0.4
	II	184	0.15	1.00	0.8
	III	224	0.20	1.50	1.2
Experiment run	1*	144	0.10	0.50	0.4
	2	144	0.10	1.00	0.8
	3	144	0.10	1.50	1.2
	4	144	0.15	0.50	0.8
	5	144	0.15	1.00	1.2
	6*	144	0.15	1.50	0.4
	7	144	0.20	0.50	1.2
	8	144	0.20	1.00	0.4
	9	144	0.20	1.50	0.8
	10	184	0.10	0.50	0.4
	11*	184	0.10	1.00	0.8
	12	184	0.10	1.50	1.2
	13	184	0.15	0.50	0.8
	14	184	0.15	1.00	1.2
	15	184	0.15	1.50	0.4
	16*	184	0.20	0.50	1.2
	17	184	0.20	1.00	0.4
	18	184	0.20	1.50	0.8
	19	224	0.10	0.50	0.4
	20	224	0.10	1.00	0.8
	21*	224	0.10	1.50	1.2
	22	224	0.15	0.50	0.8
	23	224	0.15	1.00	1.2
	24	224	0.15	1.50	0.4
	25	224	0.20	0.50	1.2
	26*	224	0.20	1.00	0.4
	27	224	0.20	1.50	0.8

* Represents the test's experimental run

Three current probes and three voltage probes embedded with alligator clips were used to connect the power analyser to the 3-phase main power bus supply. The power analyser was pre-set to capture the readings every 0.25 seconds for each experiment and the average of all reading were adopted for calculations.

The total power consumption (P_{total}) was measured with actual cutting operations, and the cutting power was calculated by subtracting the air-cutting power (P_{air}). The P_{air} is the amount of power used without machining while all other process parameters remain constant. The total energy consumption (E_{total}) and cutting energy consumption (E_{cut}) was calculated by multiplying the machining time and corresponding power consumption P_{total} and P_{air} respectively. Subsequently, the *EE* of a machining process was calculated using Eq. (5).

$$EE(\%) = \frac{E_{cut}}{E_{total}} \times 100 \tag{5}$$

The calculated values of the EE corresponding to the experimental runs are summarized in Figure 7.5.

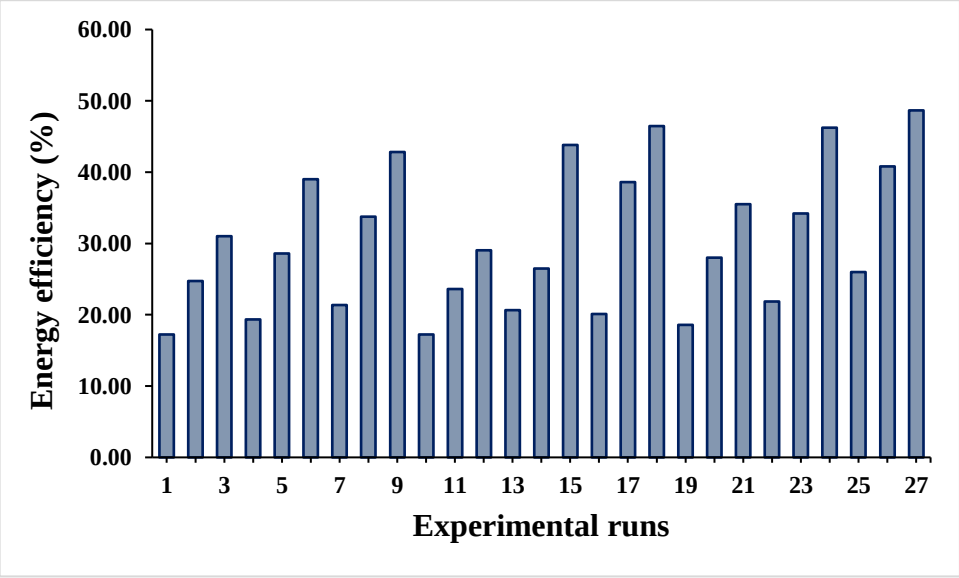

Figure 7.5. The summary of the experimental results for *EE*.

The *PF* for each experimental run was directly acquired from the power analyser and is summarized in Figure 7.6.

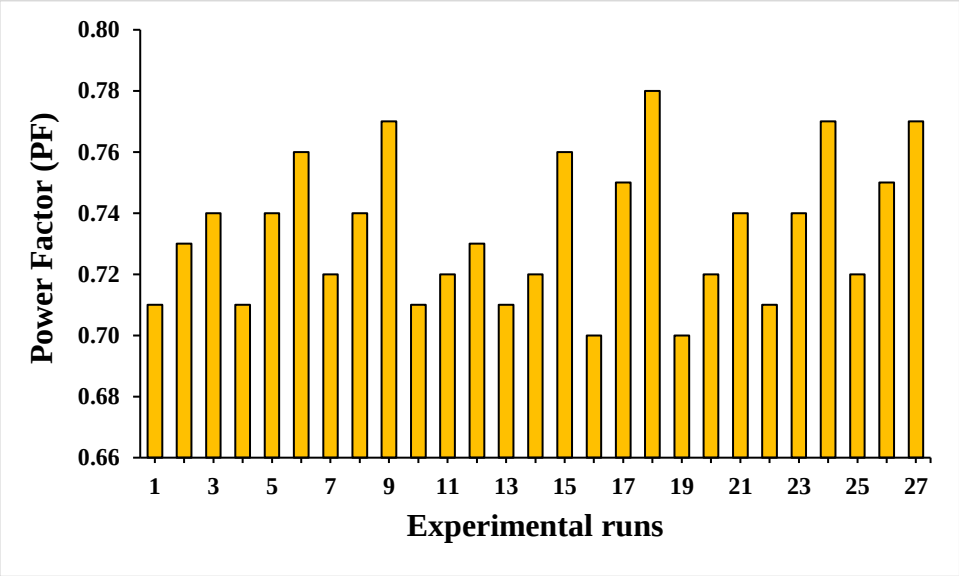

Figure 7.6. The summary of the experimental results for *PF*.

As previously mentioned in **Chapter 6**, in a dry machining process, the carbon emissions are caused due to various factors such as the carbon emissions due to electrical energy consumption of machine tool (CEM_{elec}), the carbon emission due to cutting tool wear (CEM_{tool}), the carbon emission due to material consumption (CEM_m) (which include the emissions due to the raw material production and transportation), and the emissions due to post-processing of chips (CEM_{chip}) for material recovery (Zhang et al., 2017). The total carbon emission (CEM_t) can be expressed as (Li et al., 2015; Zhang et al., 2017):

$$CEM_t = CEM_{elec} + CEM_{tool} + CEM_m + CEM_{chip} \quad (6)$$

The detailed description and calculation procedure for each CEM: CEM_{elec}, CEM_{tool}, CEM_m and CEM_{chip} are provided in **Chapter 6, Section 6.2**. The various *CEFs* and other related factors presented in **Chapter 6** were used for the calculation of CEM in the current work because the experiments were performed for the same workpiece and cutting tool

combination i.e. aluminium Al 6061 and carbide inserts. The calculated values of the CEM_t corresponding to the experimental runs are summarized in Figure 7.7.

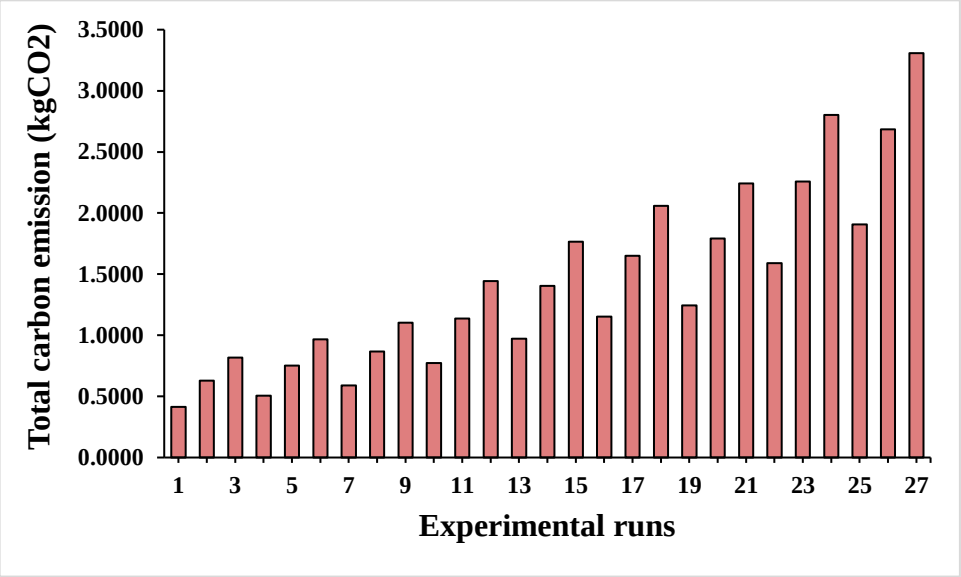

Figure 7.7. The summary of the experimental results for CEM_t.

7.4. Parameter Settings for Implementing Soft Computing Techniques

Experimental data is commonly divided into two groups prior to the application of soft computing techniques. The model is trained using the training data set, and its performance is evaluated using the testing data set. Zhang et al. (1998) recommended that the ratio of training and testing samples could be given as percent, such as 90%:10%, 85%:15% and 80%:20% with a total of 100% for the combined ratio. In the present study, an 80:20 ratio was chosen as the preferred ratio. The ratio of the training and testing data set was kept same for all methods: MGGP, LS-SVM, and fuzzy logic so that the models were trained and tested on identical experimental runs and their performance could be evaluated on a common scale. The similar approaches were reported in the literature (Bhattacharya et al., 2021; Garg et al., 2016; Garg and Lam, 2016; Rajabi et al., 2022; Sukonna et al., 2022). Accordingly, the 21 experimental runs were used to train the models, and the model performance was tested on the remaining six. As shown in Table 7.1, experimental runs with mixed levels of process parameters from the lower, middle, and higher ranges were

used in training and testing to incorporate the overall effect of the process parameters while training and evaluating the models. The following section discusses the parameter settings for the considered soft computing techniques implementation.

7.4.1. Parameter settings for implementing MGGP

The parameter settings include population size, generations, the terminal set of input design variables, and the functional set. There are no set rules for determining the initial settings for MGGP implementation. The initial settings are usually made using information from the literature, the nature/complexity of the data to be analysed, and a trial-and-error technique (Garg et al., 2014).

The number of models produced in a generation is referred as the population size. The number of generations refers to how many iterations an algorithm goes through before the termination requirement is met. In this study, the population size and number of generations are set at 100 and 150, respectively. The terminal set consists of the four input processing parameters (S, f_r, d_c and N_r). The probability of crossover, mutation, and mutation rate was adopted at standard levels of 85%, 10%, and 5%, respectively (Garg et al., 2016, 2014). The functional set includes non-linear functions such as *tanh, sin, cos, exp, and log*, as well as arithmetic operators like addition, subtraction, and multiplication. The summary of parameter settings used for the MGGP model is tabulated in Table 7.2. The experimental data shown in Figures 7.5, 7.6 and 7.7 are used as input to develop the MGGP models.

An open-source platform GPTIPS 2.0 (https://sites.google.com/site/gptips4matlab/) written in MATLAB based on multi-gene GP was applied to develop the model.

Table 7.2 Parameter settings of MGGP

Parameters	Allocation
Population size	100
Maximum Generations	150
Number of input variables	4
Size of tournament	6
Maximum number of genes to be combined	8
Maximum depth of a gene	4
Functional set elements	$tanh$, sin, cos, exp, $plog$ and arithmetic operators: addition, subtraction and multiplication
Terminal set elements	x_1, x_2, x_3 and x_4
Cross-over Probability	0.85
Mutation Probability	0.1

Based on parameter settings shown in Table 7.2, the best selected MGGP models of EE, PF and CEM_t are written in Eqs. (7), (8), and (9) respectively.

$$\boldsymbol{EE} = \begin{pmatrix} 0.104\times v_c + 79.9\times f_r - 2.47\times cos\left(v_c\times r^2\right) - 24.3\times cos\left(d_c + cos\left(f_r\right)\right) - \\ 3.9\times tanh\left(cos\left(v_c\times r\right)\right) - 1.1\times cos\left(log\left(abs\left(v_c\right)\right)\times log\left(abs\left(f_r\right)\right)\right) + \\ 20.4\times \tanh\left(r^2\times sin\left(f_r\right)\right) - 8.54\times cos\left(log\left(abs\left(v_c\right)\right)\right) - \\ 8.54\times log\left(abs\left(tanh\left(r\right)\right)\right) - 16.86 \end{pmatrix} \quad (7)$$

$$\boldsymbol{PF} = \begin{pmatrix} (0.0301\times d_c) - 1.63\left(f_r - r\right) - 0.00682\times \log\left(abs\left(d_c + r\right)\right) + \\ 0.0247\times \log\left(abs\left(d_c\right)\right) + 1.39\times \exp\left(\sin\left(\exp\left(f_r\right)\right)\right) + \\ 13.2\times \sin\left(r\right) - 13.0\times \tanh\left(r\right) + (0.352\times f_r\times r) - 2.08 \end{pmatrix} \quad (8)$$

$$\boldsymbol{CEM_t} = \begin{pmatrix} 0.0251\times v_c - 11.7\times f_r + 0.0568\times r - 0.277\times log\left(abs\left(d_c\right)\right) + \\ 11.2\times sin\left(1.51\times f_r\right) + 3.88\times tanh\left(exp\left(cos\left(d_c\right)\right)\right) - \\ 0.0523\times sin\left(S\right) - 0.013\times v_c\times cos\left(d_c\right) + 0.013\times f_r\times \cos\left(d_c\right) - 6.37 \end{pmatrix} \quad (9)$$

7.4.2. Parameter settings for implementing LS-SVM

The kernel function is an important parameter in the development of the LS-SVM model since it has a significant impact on the model's generalization ability. The Radial Basis Function (RBF) kernel shown in Eq. (10) was utilised in this work, which is one of the most widely used and capable of faster computing (Garg et al., 2016).

$$K\left(x, y\right) = e^{\left\{-\frac{x_i - y_i^2}{2\sigma^2}\right\}} \quad (10)$$

The Least Squares Support Vector Machines (LS-SVM) toolbox developed in MATLAB is used for the LS-SVM modelling of the *PF*, *CEM* and *EE*. The values of the cost function (C) and sigma parameters (σ^2) were calculated using a hybrid method of simulated annealing and a grid search technique. The grid search technique uses cross-validation to fine-tune the model parameters. The optimal C and σ^2 values for the LS-SVM model of *EE* are found to be 9.2149E5 and 690.97 respectively. The LS-SVM model of *PF* is found to have optimal values of C and σ^2 of 8.7329E5 and 4241.67 respectively, and for the CEM_t LS-SVM model, 9.5091E6 and 551.55 respectively are the optimal values for C and σ^2.

7.4.3. Parameter settings for implementing fuzzy logic

The primary idea behind fuzzy logic is to reliably classify input-output variables into fuzzy sets in order to account for flaws and vagueness in data structures and human knowledge without the need for complex mathematical models (Tseng et al., 2016). The fuzzy logic approach utilizes rule-based algorithms to predict the outcome, and the rules are defined by the relationship of the input-output parameters. In the present study, there are four input

parameters (s, f_r, d_c and N_r) and three output parameters (*EE*, *PF* and CEM_t). A non-linear functional relationship is established by fuzzy predictor (f: *EE*, *PF* and CEM_t) as expressed in Eq. (11), Eq. (12) and Eq. (13) respectively.

$$f : v_c, f_r, d_c, r, \qquad D \rightarrow EE_{set} \tag{11}$$

$$f : v_c, f_r, d_c, r, \qquad D \rightarrow PF_{set} \tag{12}$$

$$f : v_c, f_r, d_c, r, \qquad D \rightarrow CEM_{t\_set} \tag{13}$$

Where EE_{set}, PF_{set} and CEM_{t_set} are the fuzzy outputs and subset of *EE*, *PF* and CEM_t respectively. The graphical representation of one of the fuzzy predictors for *PF* is shown in Figure 7.8.

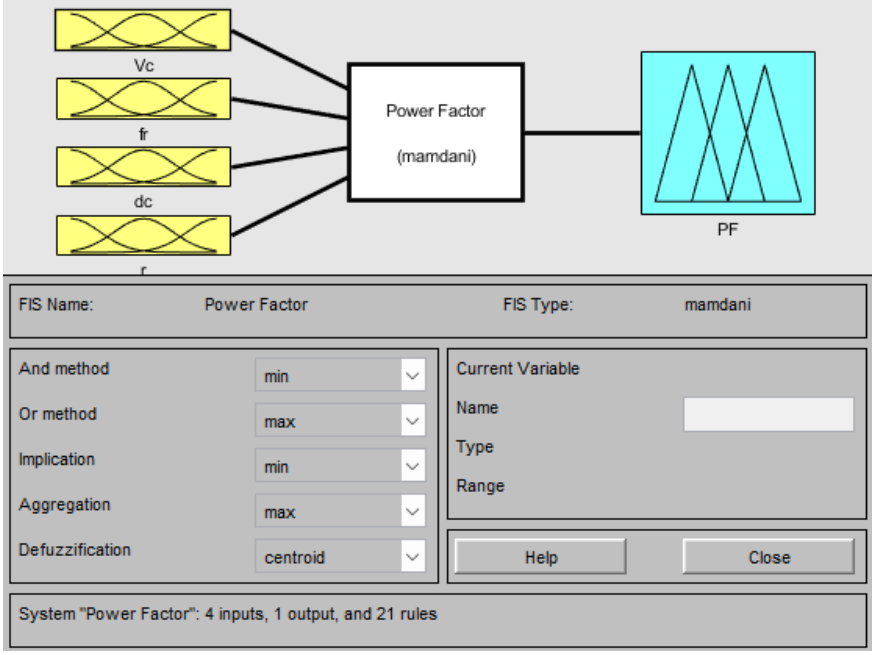

Figure 7.8. Fuzzy predictors for *PF*.

Following that, the membership functions of these input variables are discussed. The selection of the shape of the membership function is significant for the model's accuracy, and according to Iqbal and Dar (2011), a triangle shape is one of the better choices for the

membership function and was chosen in this study. The fuzzy sets for the input variables and output variables are shown in Figure 7.9 and Figure 7.10 respectively.

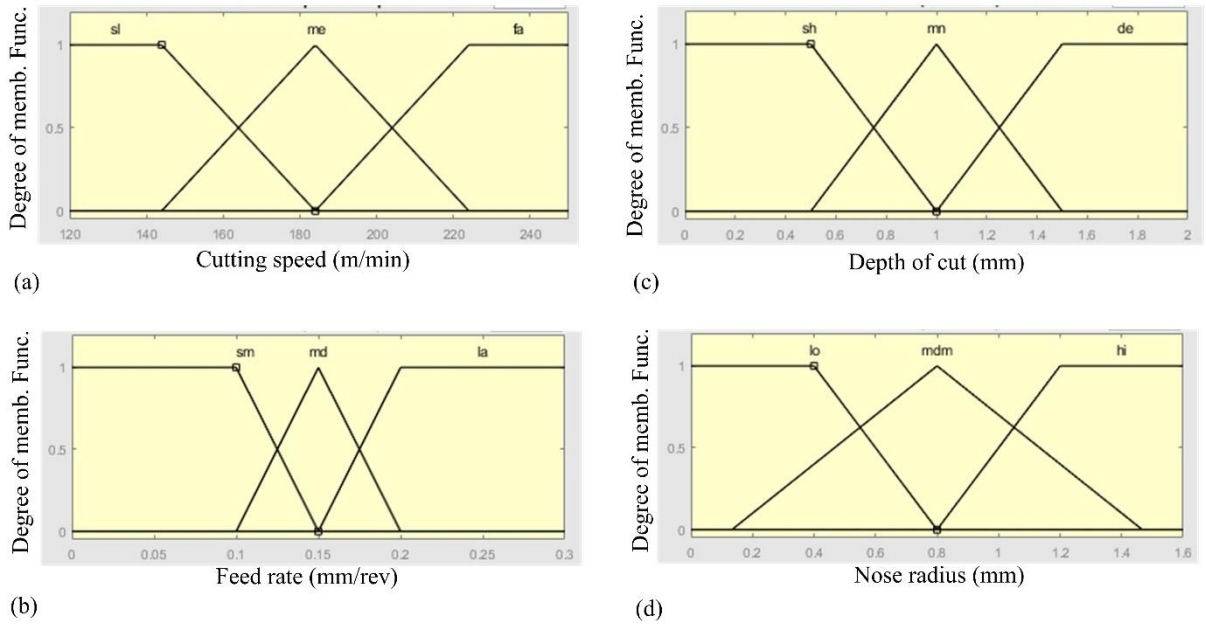

Figure 7.9. The fuzzy set for input variables: (a) cutting speed, (b) feed rate, (c) depth of cut, and (d) nose radius.

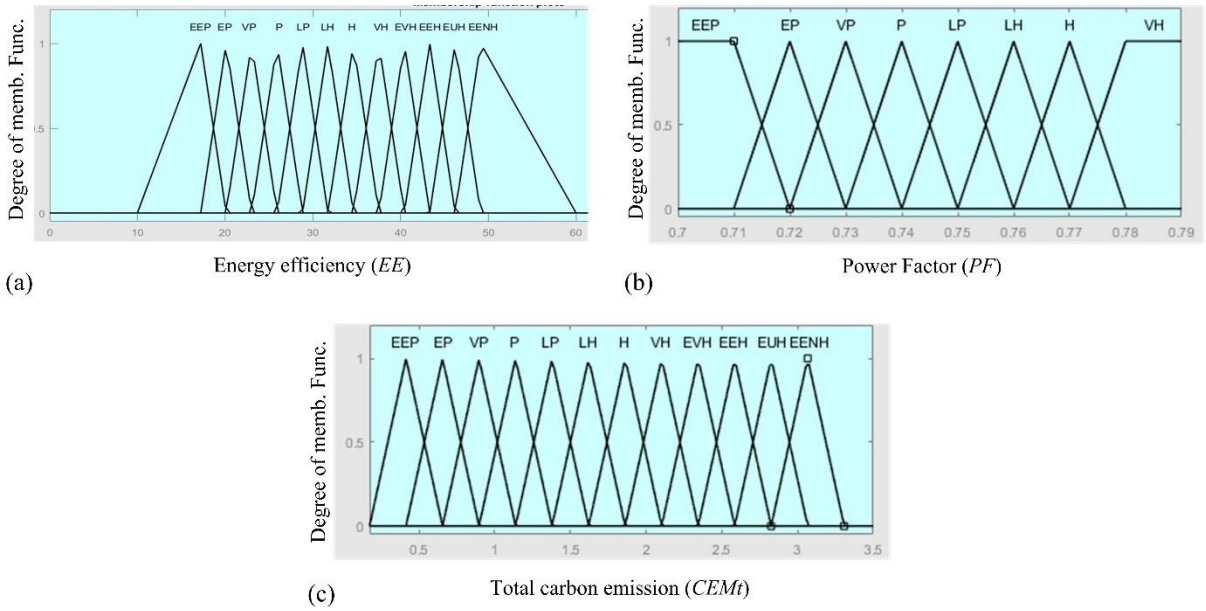

Figure 7.10. Fuzzy set for output variables: (a) *EE* (b) *PF* and (c) CEM_t.

The abbreviations of the derivations of the membership functions used in Figure 7.9 and Figure 7.10 are provided in Table 7.3.

Table 7.3 Descriptions of the derivations used in Figure 7.9 and Figure 7.10.

Process parameters (input variable)		Performance characteristics (output variable)	
Abbreviation	Description	Abbreviation	Description
sl	Slow	EEP	Exceptionally Extreme poor
me	Medium	EP	Extreme poor
fa	Fast	VP	Very poor
sm	Small	P	poor
md	Medium	LP	Lightly poor
la	Large	LH	Lightly high
sh	Shallow	H	High
mn	Medium	VH	Very higher
de	Deep	EVH	Extreme very higher
lo	Low	EEH	Extreme extreme high
mm	Medium	EUH	Extreme ultimate high
hi	High	EENH	extreme enormously high

Next, the fuzzy rules were decided. The interdependency of the input and output variables is dictated by fuzzy rules, allowing for proper selection using fuzzy logic. The number of rules depends upon the partition of the fuzzy input parameters i.e. process parameters. In the present case four process parameters with three levels, theoretically, there should be 3^4 i.e. 81 rules.

Table 7.4 The 21 fuzzy rules used in the prediction module.

Rule No.	v_c	f_r	d_c	r	*EE*	*PF*	CEM_t
1	sl	sm	mn	mdm	VP	VP	EP
2	sl	sm	de	hi	LH	P	VP
3	sl	md	sh	mdm	EEP	EEP	EEP
4	sl	md	mn	hi	LP	P	EP
5	sl	la	sh	hi	EP	EP	EP
6	sl	la	mn	lo	LH	P	VP
7	sl	la	de	mdm	EVH	H	P
8	me	sm	sh	lo	EEP	EEP	VP
9	me	sm	de	hi	LP	VP	LP
10	me	md	sh	mdm	EP	EEP	VP
11	me	md	mn	hi	P	EP	LP
12	me	md	de	lo	EEH	LH	H
13	me	la	mn	lo	VH	LP	LH
14	me	la	de	mdm	EUH	VH	VH
15	fa	sm	sh	lo	EEP	EEP	P
16	fa	sm	mn	mdm	LP	EP	H
17	fa	md	sh	mdm	EP	EEP	LH
18	fa	md	mn	hi	H	P	EVH
19	fa	md	de	lo	EUH	H	EUH
20	fa	la	sh	hi	P	EP	H
21	fa	la	de	mdm	EENH	H	EENH

However, 27 experiments were carried out according to the design of the experiments, and they were separated into training i.e. 21 and testing i.e. 6 data sets. Hence 21

experimental runs adopted for fuzzy rules and are listed in Table 7.4. Further, the centroid approach was used for defuzzification.

7.5. Results and Discussion

Figures 7.11, 7.12, and 7.13 show the results obtained using the three models (MGGP, LS-SVM, and fuzzy logic) for *EE*, *PF* and CEM_t respectively with corresponding experimental values, for the training and test data sets.

(a) Training

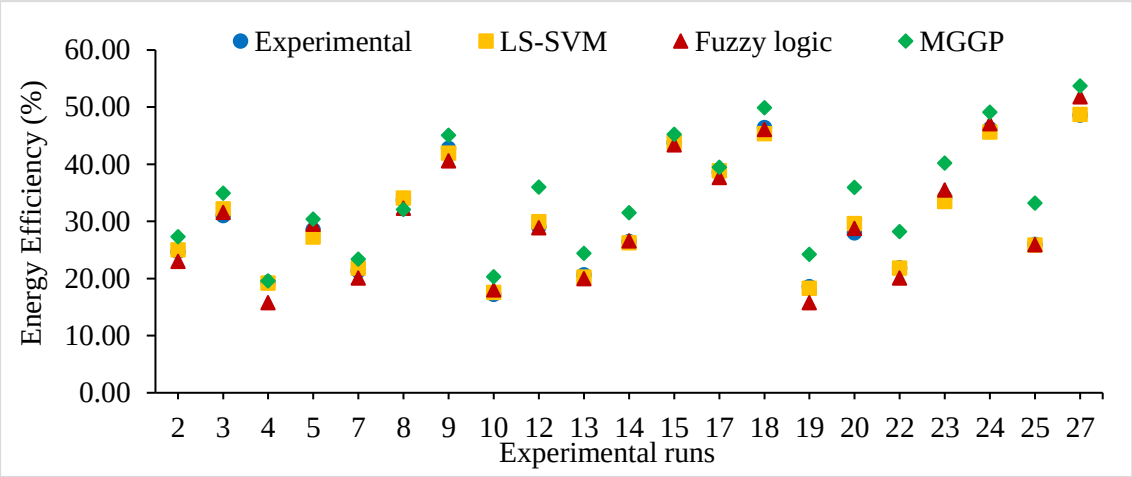

(b) Testing

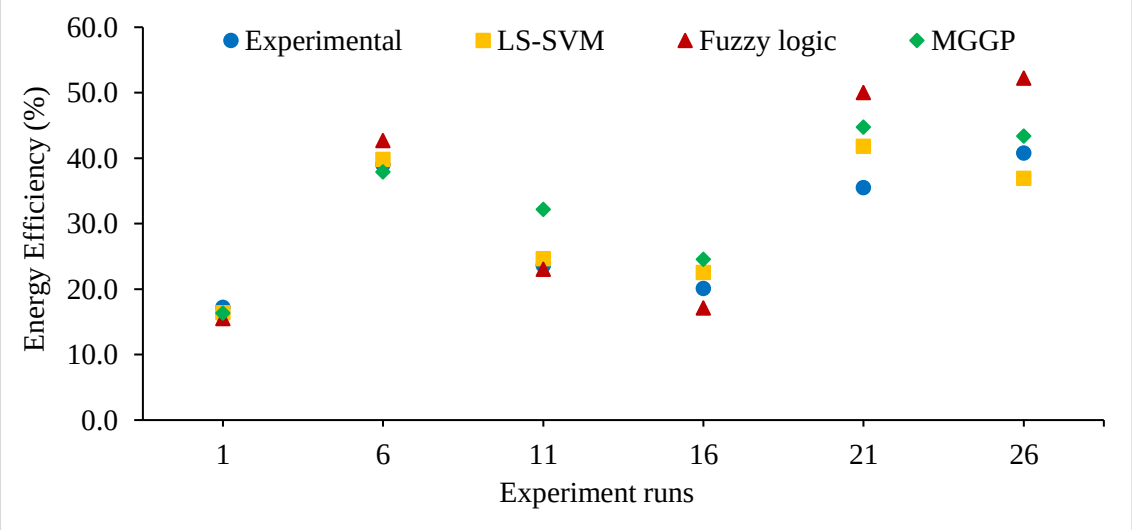

Figure 7.11. Models' predicted vs experimental values for *EE* (a) Training (b) Testing.

(a) Training

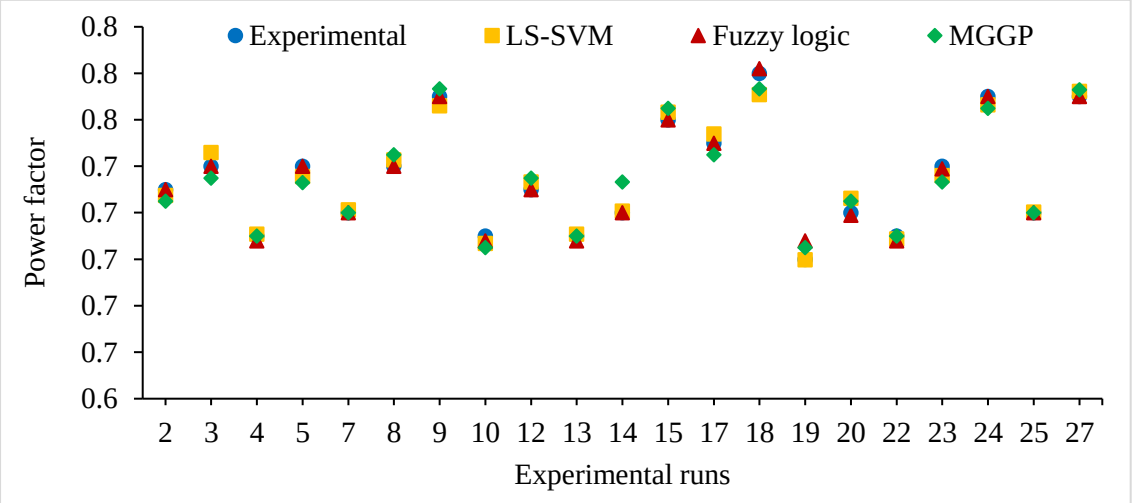

(b) Testing

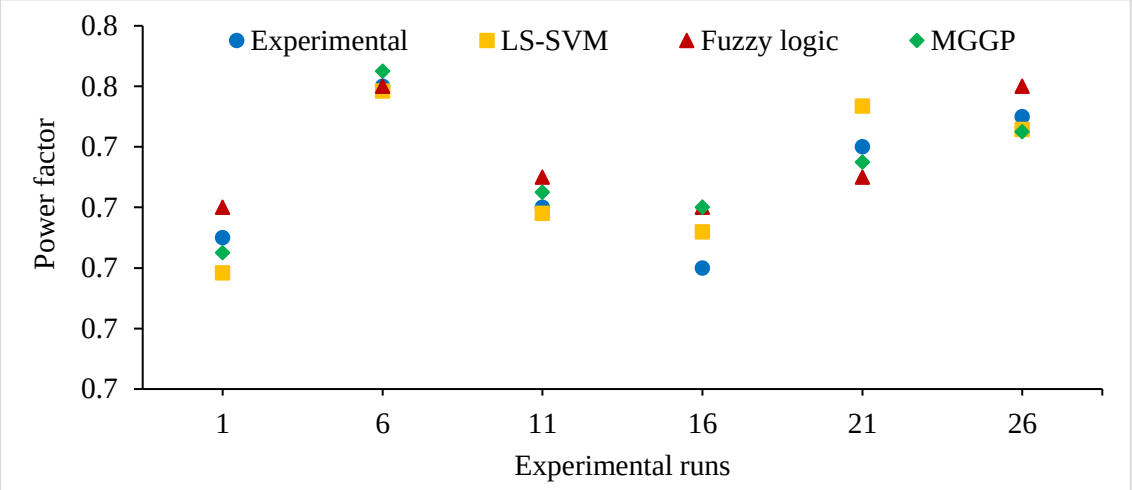

Figure 7.12. Models' predicted vs experimental values for *PF* (a) Training (b) Testing.

(a) Training

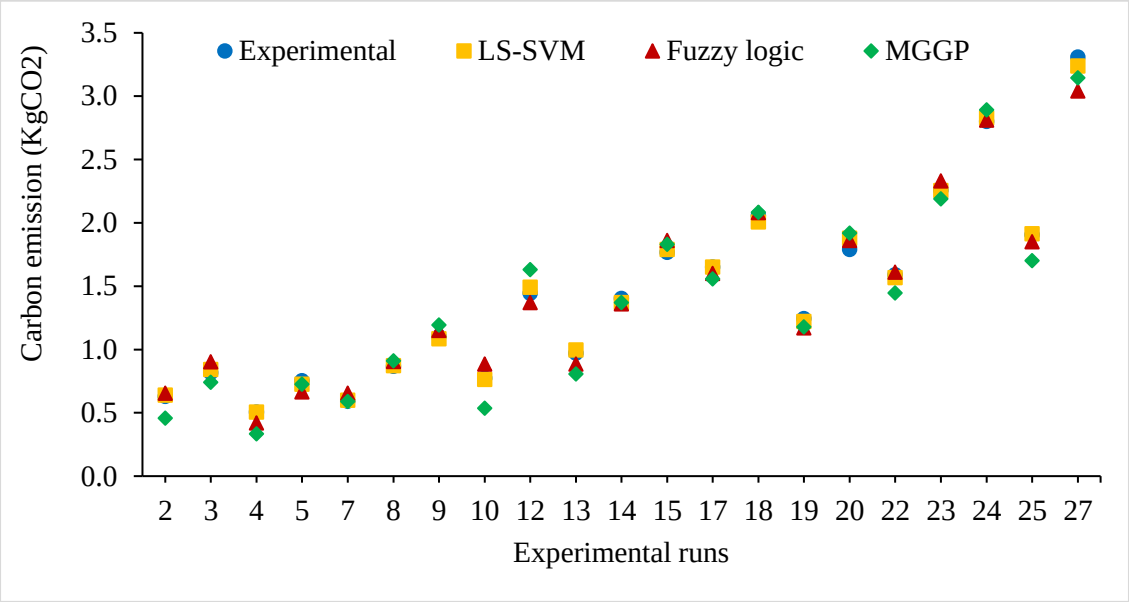

(b) Testing

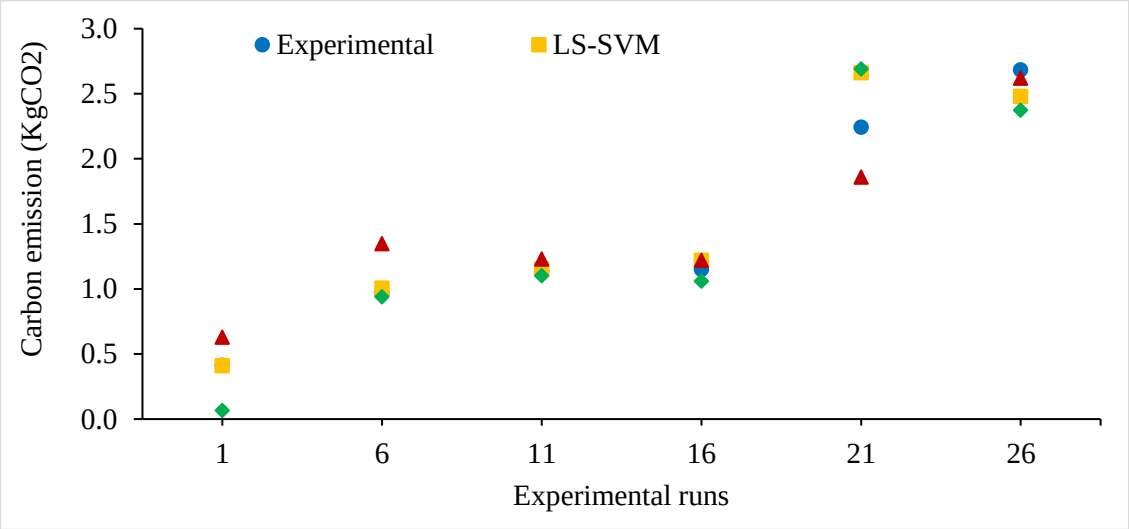

Figure 7.13. Models' predicted vs experimental values for CEM_t (a) Training (b) Testing.

The predicted *EE* and corresponding experimental values by each model for the training and test data set are shown in Figure 7.11 (a) and Figure 7.11 (b) respectively. It can be seen in Figure 7.11 (a) and Figure 7.11 (b) that each model's predicted values of the *EE* on training as well as testing data set are in proximity with the corresponding experimental values. Figures 7.12 (a) and 7.12 (b) depict the models' predicted vs experimental values of

the *PF* on training and testing data set respectively. It can be revealed from Figure 7.12 (a) and Figure 7.12 (b) that the predicted *PF* values on each model's training and testing data set are close to the corresponding experimental values. Figures 7.13 (a) and 7.13 (b) shows the predicted CEM_t and experimental values for the training and testing data sets, respectively and indicates that the developed models efficiently predicted the CEM_t values for both the training and test data sets.

The aforementioned results indicate that all three models perform well in both the training and test data sets for each performance characteristics (*EE*, *PF* and CEM_t). The performance of the three models is evaluated using various statistical indicators in the next section.

7.5.1. Performance evaluation of the models

The performance of the three methods (MGGP, LS-SVM, and fuzzy logic) on training and test data is evaluated using the following six statistical indicators. These indices are mathematically expressed below.

$$\text{Coefficient of determination } (R^2) = \left(\frac{\sum_{i=1}^{n} (A_i - \overline{A_i})(M_i - \overline{M_i})}{\sqrt{\sum_{i=1}^{n} (A_i - \overline{A_i}) \sum_{i=1}^{n} (M_i - \overline{M_i})}} \right)^2 \quad (14)$$

$$\text{Root mean square error } (RMSE) = \sqrt{\frac{\sum_{i=1}^{n} (M_i - A_i)^2}{n}} \quad (15)$$

$$\text{Mean absolute error } (MAE) = \frac{\sum_{i=1}^{n} |M_i - A_i|}{n} \quad (16)$$

$$\text{Sum of squared error } (SSE) = \sum_{i=1}^{n} (M_i - A_i)^2 \quad (17)$$

$$\text{Mean square error } (MSE) = \frac{\sum_{i=1}^{n} (M_i - A_i)^2}{n} \quad (18)$$

Relative percentage error $RPE\ (\%) = \left|\frac{M_i - A_i}{A_I}\right| \times 100$ (19)

Where M_i is the model predicted value, and A_i is the experimental values and n is the sample size.

The scatter plots on training and testing data sets of the three models (MGGP, LS-SVM, and fuzzy logic) related to performance characteristics *EE*, *PF* and CEM_t are shown in Figures 7.14, 7.15 and 7.16 respectively. It can be revealed from Figures 7.14, 7.15 and 7.16 that the three models were efficiently learned from the training data samples, resulting in all models with a high coefficient of determinations and small error values for the three responses. The similar trend for the scatter plots were reported in the literature by Garg and Lam (2015) and Sukonna et al. (2022). As shown in Figures 7.14, 7.15 and 7.16, the coefficients of determination of the MGGP, LS-SVM and fuzzy logic models of three performance characteristics (*EE*, *PF* and CEM_t) were found to be in the range of 94% to 99% in training and 84-94% in testing. In all cases, R^2 values are greater than 84%, signifying a strong relationship between the experimental and predicted values. The similar range of R^2 values were reported by Garg and Lam (2015) and Garg et al. (2014). The value of the coefficient of determination on the test data set for LS-SVM model are found to be 89.69%, 84.61% and 94.80% for *EE*, *PF* and CEM_t respectively indicates that for each performance characteristic, the LS-SVM model performed better than the other two models (MGGP and fuzzy logic).

The calculated values of R^2, *RSME*, *MAE*, *SSE* and *MSE* based on Eqs. (14), (15), (16), (17), and (18) respectively are summarized in Table 7.5. As shown in Table 7.5, one of the important error indicators *RSME* is low and acceptable for three models of each performance characteristic. The values of the statistical metrics shown in Table 7.5 are in line with the results reported in the literature by Garg et al. (2015) and Sukonna et al.

(2022). When the *RSME* values of the models are compared, the LS-SVM outperforms the MGGP and fuzzy logic with the values of 3.2417, 0.0090 and 0.1934, and for the *EE*, *PF* and CEM_t respectively. Furthermore, as shown in Table 7.5, three models (MGGP, LS-SVM, and fuzzy logic) of each performance characteristic have satisfactory and low values for various error indices such as *MAE*, *SSE*, *MSE* and *MAPE*. The *MAE*, *SSE*, *MSE* and *MAPE* values obtained in this study are within the range reported by Garg and Lam (2016) and Bhattacharya et al. (2021). Based on the comparison of these error indices, the LS-SVM model of each performance characteristic performs better than the corresponding MGGP and fuzzy logic model. As shown in Table 7.5, the LS-SVM model related to three performance characteristics have the lowest values of the various error indicators *MAE*, *SSE*, *MSE* and *MAPE*.

Table 7.5. Summary of different statistical indicators of the models on testing data set.

	Model	Parameters					
		R^2	*RSME*	*MAE*	*SSE*	*MSE*	*MAPE*
EE	LS-SVM	0.8969	3.2417*	2.5423*	6.31E+01*	1.05E+01*	8.4353*
	Fuzzy logic	0.9362*	7.8155	5.8185	3.66E+02	6.11E+01	17.6188
	MGGP	0.8375	5.5815	4.4715	1.87E+02	3.12E+01	16.4563
PF	LS-SVM	0.8461*	0.0090*	0.0074*	4.83E-04*	8.044E-05*	1.0344*
	Fuzzy logic	0.8242	0.0115	0.0100	8.00E-04	1.33E-04	1.3899
	MGGP	0.8265	0.0094	0.0075	5.25E-04	8.75E-05	1.0427
CEM_t	LS-SVM	0.9480*	0.1934*	0.1259*	2.24E-01*	3.74E-02*	6.4983*
	Fuzzy logic	0.9354	0.2442	0.2014	3.58E-01	5.96E-02	20.8617
	MGGP	0.9234	0.2673	0.2098	4.29E-01	7.14E-02	21.5267

***** Represent the best performing value

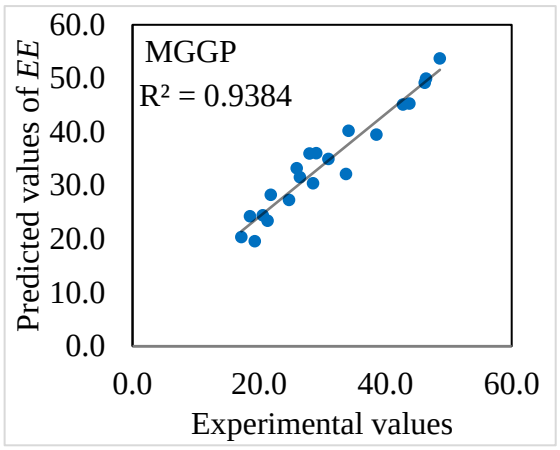

(a) (i) Training phase

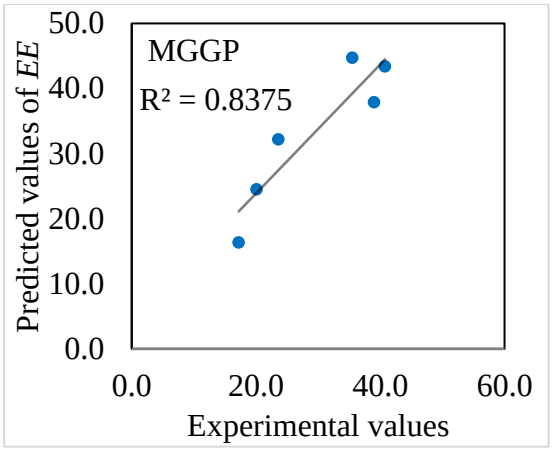

(ii) Testing phase

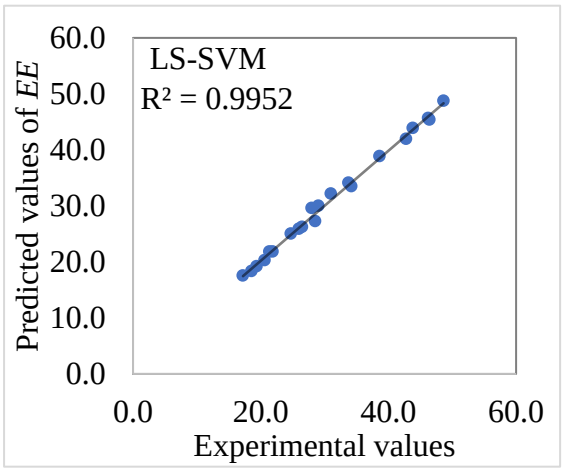

(b) (i) Training phase

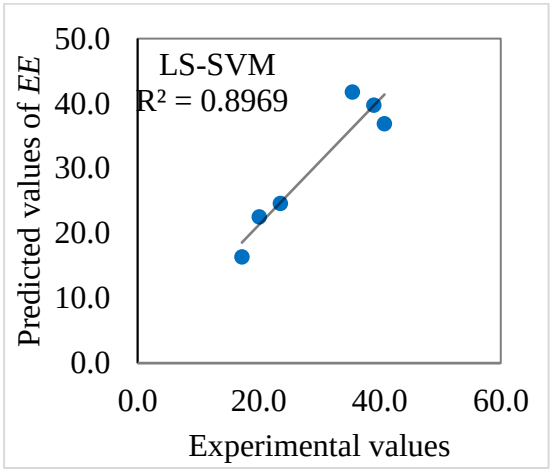

(ii) Testing phase

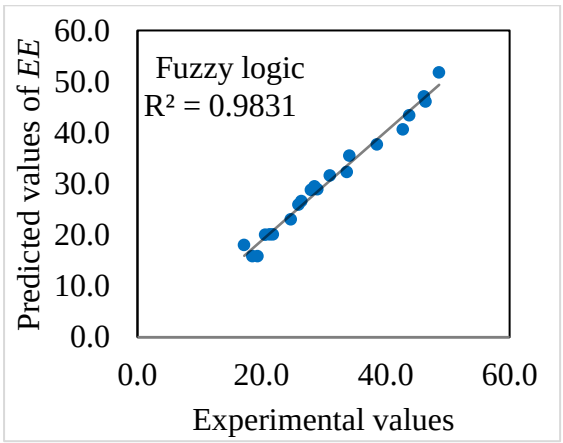

(c) (i) Training phase

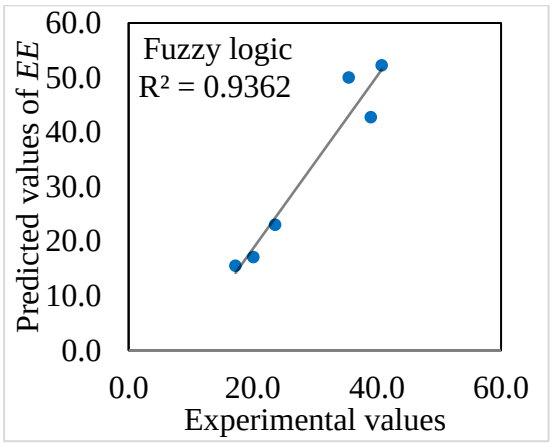

(ii) Testing phase

Figure 7.14. The statistical fit of the models in the testing phase for *EE* (a) MGGP (b) LS-SVM and (c) Fuzzy logic.

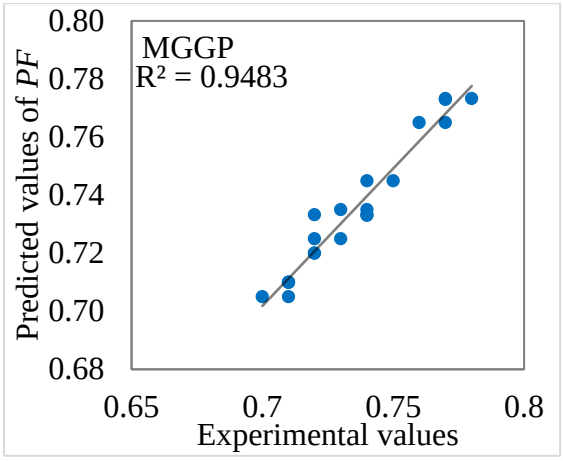

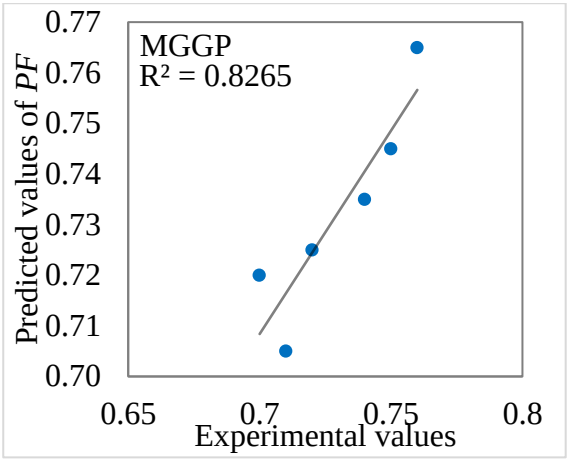

(a) (i) Training phase (ii) Testing phase

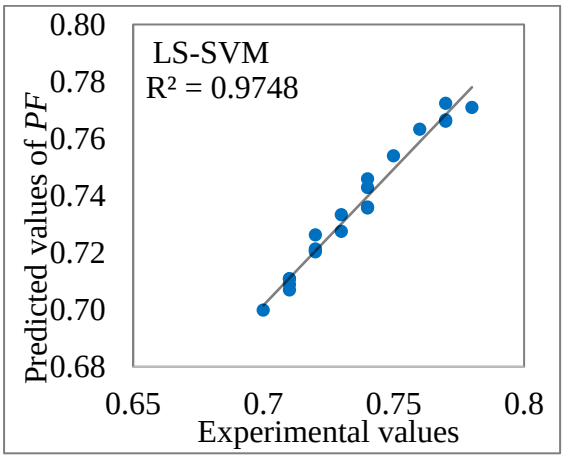

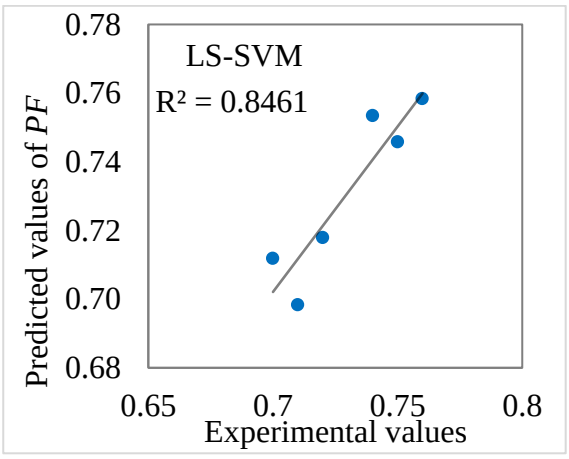

(b) (i) Training phase (ii) Testing phase

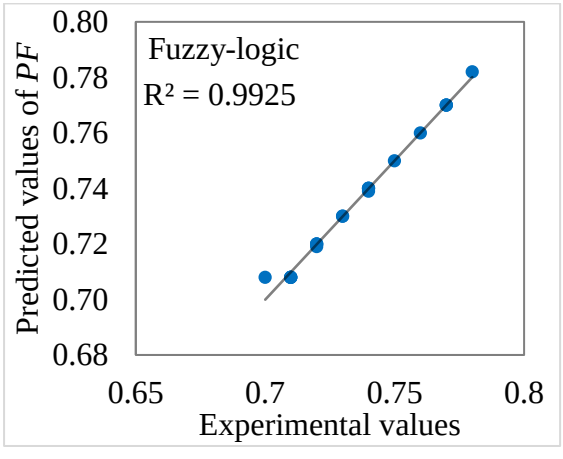

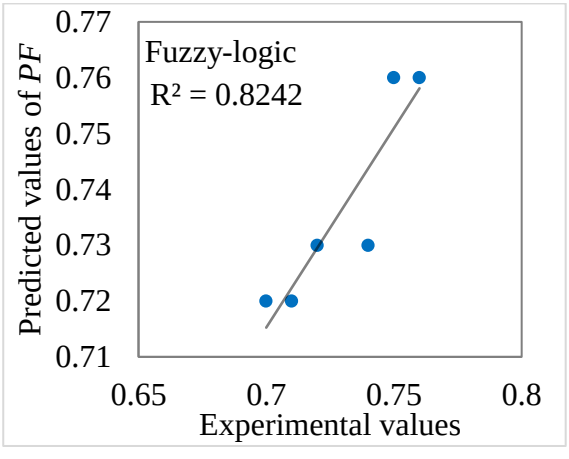

(c) (i) Training phase (ii) Testing phase

Figure 7.15. The statistical fit of the models in the testing phase for *PF* (a) MGGP (b) LS-SVM and (c) Fuzzy logic.

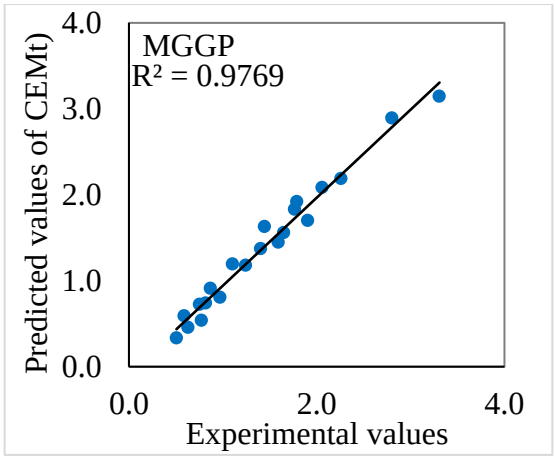

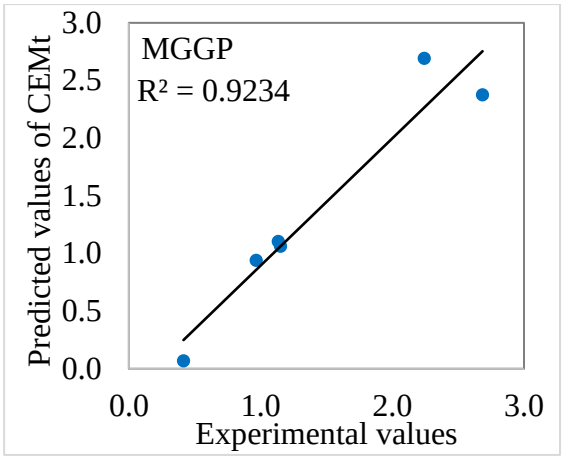

(a) (i) Training phase (ii) Testing phase

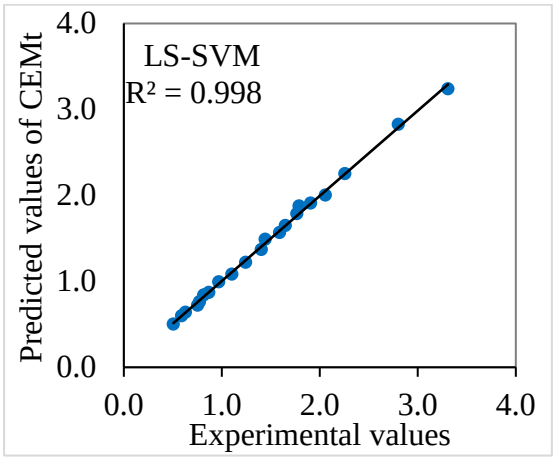

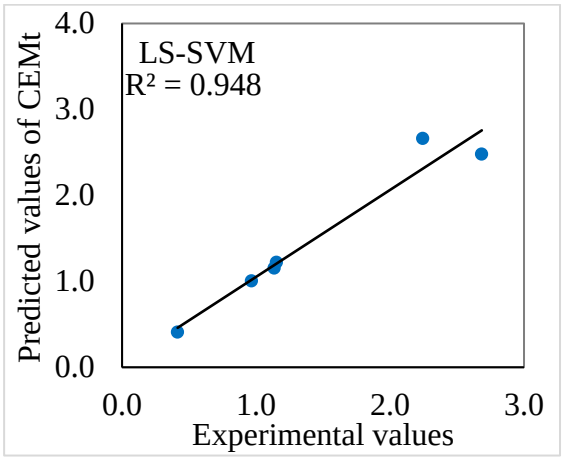

(b) (i) Training phase (ii) Testing phase

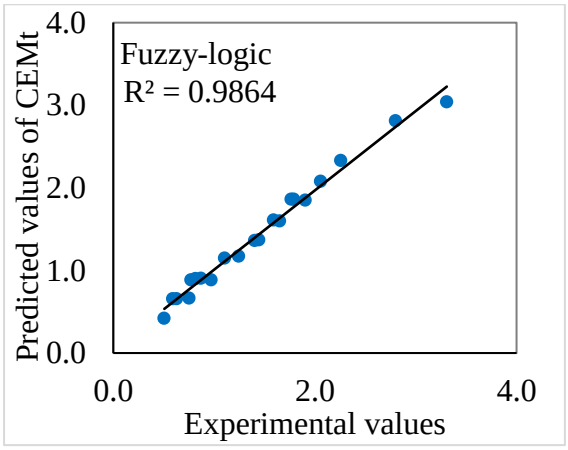

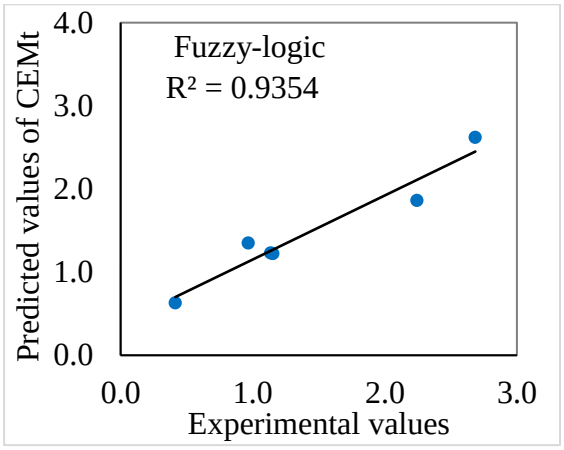

(c) (i) Training phase (ii) Testing phase

Figure 7.16. The statistical fit of the models in the testing phase for CEM_t (a) MGGP (b) LS-SVM and (c) Fuzzy logic.

The relative percentage error (*RPE*) of the developed three models (MGGP, LS-SVM, and fuzzy logic) of each performance characteristic was calculated using Eq. (19) for the training and testing data sets, and are shown in Figures 7.17, 7.18 and 7.19 for *EE*, *PF* and CEM_t respectively. The *RPE* values are in agreement to the results reported by Garg et al. (2016) and Garg and Lam (2015), indicating that the three models made reliable predictions with acceptable errors.

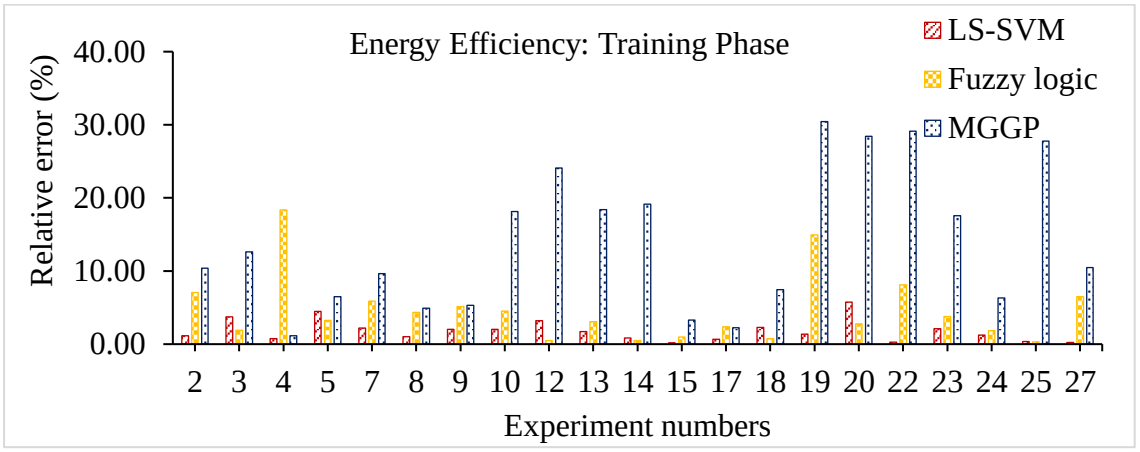

(a) Training

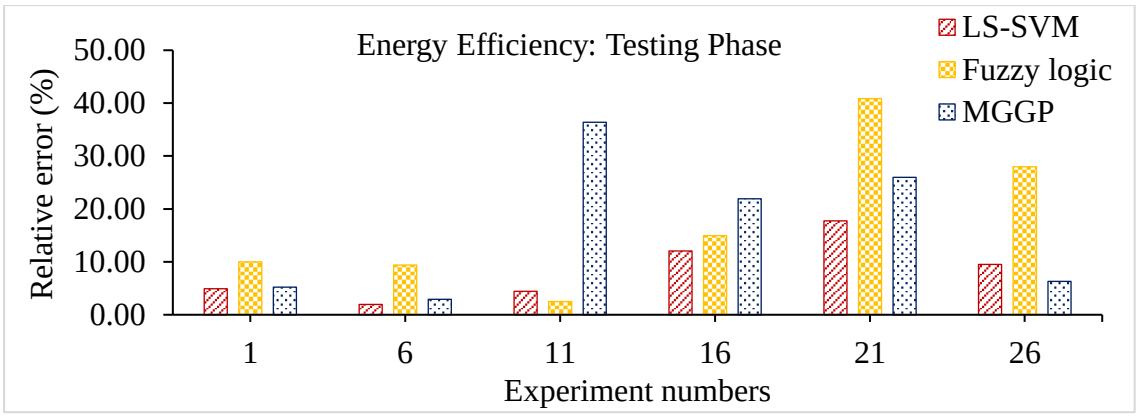

(b) Testing

Figure 7.17. The relative error between experimental and predicted *EE* values for three models (a) Training (b) Testing.

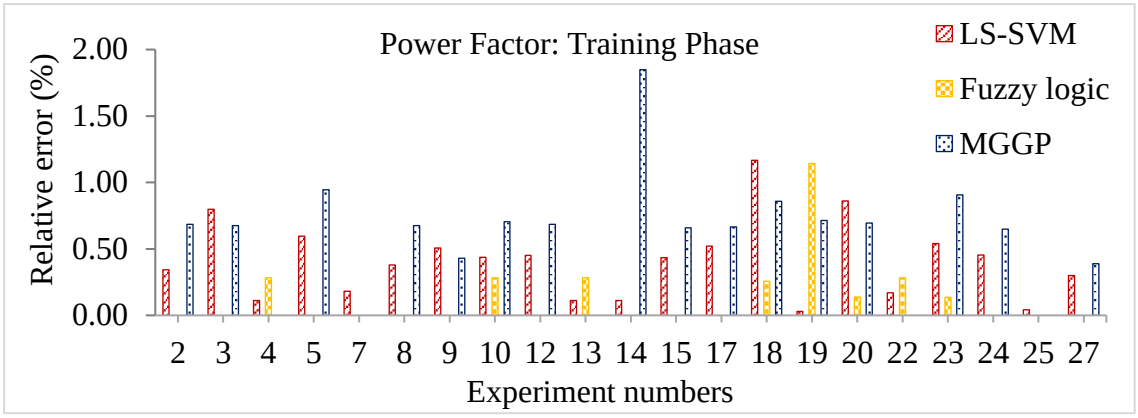

(a) Training

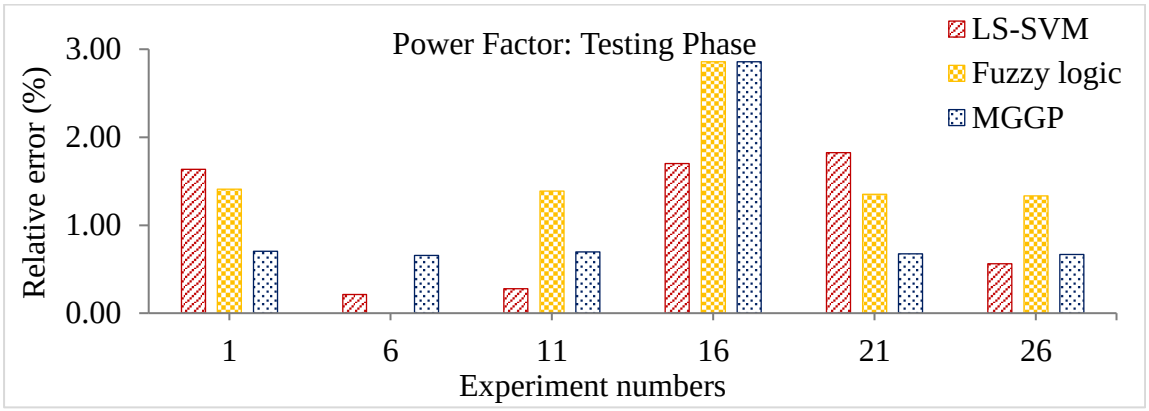

(b) Testing

Figure 7.18. The relative error between experimental and predicted *PF* values for three models (a) Training (b) Testing.

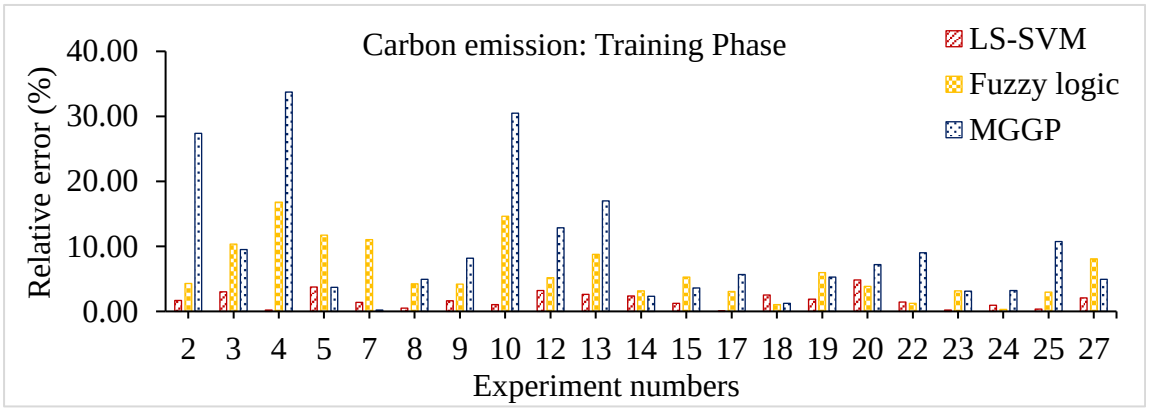

(a) Training

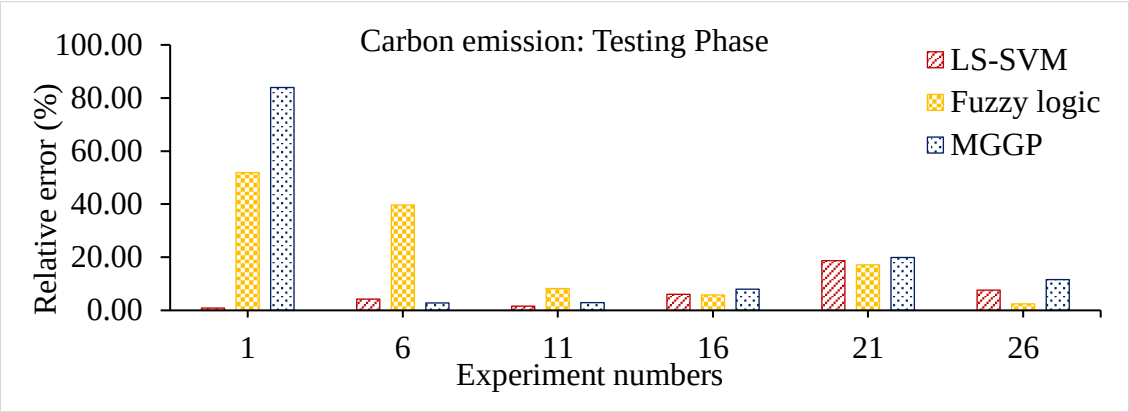

(b) Testing

Figure 7.19. The relative error between experimental and predicted CEM_t values for three models (a) Training (b) Testing**.**

The descriptive statistical analysis of the relative error of three models (MGGP, LS-SVM, and fuzzy logic) for the three performance characteristics (*EE*, *PF* and CEM_t) on testing data set are reported in Table 7.6. The descriptive data includes the various statistical parameters namely mean, standard error (Std Error), median, standard deviation (Std dev), range, minimum error (Min), maximum error (Max), and sum of error (Sum) for the three models on the testing data set.

The descriptive statistics results shown in Table 7.6 on the test data samples are comparable to the descriptive statistics reported in the literature by Garg et al. (2016), Garg et al. (2015) and Garg and Lam (2015), showing that all models accurately predicted the performance characteristics. The descriptive statistics results shown in Table 7.6 also endorse that the LS-SVM models perform better than the other two MGGP and fuzzy logic with the best values of various descriptive statistical parameters: mean, Std error, median, Std dev, range, minimum error, maximum error and sum of error. In total, the comparison of coefficient of determination, different error values, and descriptive statistics of RPE of the three models for three performance characteristics, shows that the LS-SVM model outperformed the other two models (MGGP and fuzzy logic).

Table 7.6. Descriptive statistics of the relative error for three models on the testing data set.

	Model	Mean	Std error	Median	Std dev	Range	Min.	Max.	Sum
EE	LS-SVM	0.084*	0.024*	0.072*	0.059*	0.158*	0.019*	0.178*	0.506*
	Fuzzy logic	0.176	0.058	0.125	0.142	0.384	0.025	0.409	1.057
	MGGP	0.165	0.056	0.141	0.136	0.334	0.029	0.364	0.987
PF	LS-SVM	0.010*	0.003*	0.011	0.008*	0.016*	0.002	0.018*	0.062*
	Fuzzy logic	0.014	0.004	0.014	0.009	0.029	0.000*	0.029	0.083
	MGGP	0.010	0.004	0.007*	0.009	0.022	0.007	0.029	0.063
CEM_t	LS-SVM	0.065*	0.027*	0.051*	0.065*	0.178*	0.009*	0.187*	0.390*
	Fuzzy logic	0.209	0.083	0.127	0.203	0.495	0.024	0.519	1.252
	MGGP	0.215	0.128	0.098	0.312	0.812	0.028	0.840	1.292

***** Represent the best performing value

7.5.2. Validation of the model

The statistical fitness of the three models (MGGP, LS-SVM, and fuzzy logic) for the three performance characteristics *EE*, *PF* and CEM_t) was validated using two hypothesis tests viz. mean paired t-test and variance F-test using the Eq. (32) and Eq. (33) respectively.

$$t = \frac{(\bar{M}+\bar{A})}{\sqrt{((s_1^2/n_1)+(s_2^2/n_2))}} \tag{32}$$

$$F = \frac{s_1^2}{s_2^2} \tag{33}$$

Where $\bar{M}$ and $\bar{A}$ represent the sample mean of predicted and experimental data set. respectively. s_1 and s_2 represent the standard deviation of predicted and experimental data set respectively. n_1 and n_2 represent the sample size of predicted and experimental data set

i.e. n, experimental runs in the present case. The calculated hypothesis tests results are shown in Table 7.7.

Table 7.7 Hypothesis test results of three models for each performance characteristic

Model	LS-SVM	Fuzzy logic	MGGP
Energy efficiency (*EE*)			
Mean paired *t* test	0.9367	0.8499	0.1790
Variance *F* test	0.4818	0.1634	0.4806
Power factor (*PF*)			
Mean paired *t* test	0.9730	0.8136	0.9330
Variance *F* test	0.4648	0.4227	0.4032
Carbon emission (CEM_t)			
Mean paired *t* test	0.9517	0.9791	0.8132
Variance *F* test	0.4913	0.3538	0.3759

The *p* values of the three models for the *t*-test and *F*-test were found to be more than 0.05, indicate that there is not enough evidence to conclude that the actual and predicted values from these models differ. In conclusion, from a modelling standpoint, all three models exhibit statistically acceptable goodness of fit for each performance characteristic.

In Industry, process planners select appropriate process parameters in design stage itself to manufacture the final product. Evaluating each option to ascertain *EE*, *PF* and *CEM* is not realistic, because it requires a large number of lengthy experiments, which increases time and costs. The developed models can be utilized by the process planners to identify the most energy efficient and low *CEM* based process plan before actual machining of a part on a machine tool.

7.6. Summary

In this chapter, three soft computing techniques (MGGP, LS-SVM, and fuzzy logic) were used to predict *EE*, *PF* and associated *CEM* of a machine tool because these techniques are known for their ability to incorporate the nonlinear complicated relationship between input parameters and machining performances. Each model's predicted values on the training and test data sets were found to be close to their respective experimental values, showing that the models were trained efficiently from the training data samples and predicted satisfactorily. A set of statistical indicators was used to evaluate and compare the performance of the developed models (MGGP, LS-SVM, and fuzzy logic) for each performance characteristic, including coefficient of determination, root mean square error, mean absolute error, sum of square error, mean square error and relative percentage error. The results of statistical indicators revealed that all models (MGGP, LS-SVM, and fuzzy logic) of each performance characteristic have appropriate coefficients of determination with satisfactory and low values of various errors. The comparative results indicated that LS-SVM outperformed the other two models (MGGP and fuzzy logic). The superiority of LS-SVM models for each performance characteristic over the other two models (MGGP and fuzzy logic) was also validated by descriptive statistics findings for the relative error on the testing data set. Further, the goodness of fit of the three models was validated by the hypothesis testing (mean paired t-test and variance of F-test).

The proposed models are important because the measurements of energy-efficiency-related performance characteristics necessitate an advanced laboratory set-up (specialized equipment), which is costly, and measurement procedures are time-consuming and cannot be used on a regular basis for any machining process. Accurate and reliable predictions from soft computing-based models can be used directly as an input parameter for energy-efficient process planning in practice.

Chapter 8:

Multi-Objective Optimization of Power Factor, Carbon Emissions, Productivity and Product Quality

The present chapter aims to optimize the sustainability responses: power factor, carbon emissions, material removal rate (i.e. productivity) and surface roughness (i.e. product quality) considering the impact of weight assignment methods on optimization results. In addition to equal weight method, four methods were used to assign the weight of the responses: Principal Component Analysis (PCA), entropy weights, Weighted Grey Relational Analysis (WGRA), and Analytical Hierarchy Process (AHP). The Grey Relational Analysis (GRA) coupled with Taguchi technique is used for the multi-objective optimization. The multiple responses were converted into a multi-objective combined index (*MOCI)* related to different weight assigning methods using the GRA technique and their corresponding optimal cutting parameters were determined using the Taguchi technique. The *MOCIs* at the optimum cutting parameters improved as compared to the *MOCIs* at the optimum cutting parameters with equal weight method, indicating that weight assignment methods are better for optimising responses than equal weight method.

8.1. Introduction

The Intergovernmental Panel on Climate Change (IPCC) report periodically warns to reduce greenhouse gas (GHG) emissions to limit average global temperature rise to below 2°C (IPCC, 2014, 2007, 2001; Pye et al., 2021), where carbon dioxide (CO_2) is one of the most prominent GHGs (Li et al., 2015). As the world's third largest carbon emission country, India has established a national goal for a 45% reduction in the carbon intensity of gross domestic product by 2030 and a Net Zero target by 2070 (Pradhan and Ghosh, 2022). The industrial sector is the most energy-intensive and accounts for about 56% of total energy consumption in India (Bal et al., 2022; National Statistics Office, 2020), where more

than 60% of industrial energy consumption is contributed by the manufacturing industries (Soni et al., 2017).

As previously stated that the potential strategies for reducing energy consumption and carbon emissions in the manufacturing sector include can be achieved either by development of energy-efficient machine tools or by optimizing existing machine tools and machining processes (Jiang et al., 2022; Warsi et al., 2018). Given the large amount of existing machine tools in use, the first strategies require solid economic provisions for technological development and can only be implemented by replacing existing production lines. The second approach can be implemented with relative ease and lesser resources. Parameter optimization of existing machining processes and machine tools can be applied to existing production lines with relative ease and with minimal resources (Bagaber and Yusoff, 2019; Hu et al., 2020). Since changes in cutting parameters have a significant impact on the energy consumption of a machining process (Newman et al., 2012), unreasonable cutting parameters can result in an increase in energy consumption and associated carbon emissions. Previous research has shown that appropriate selection of the cutting parameters can result in carbon emission reduction up to 40% (Zhao et al., 2021). An increasing number of researchers focus on reducing energy consumption and carbon emissions. Moreover, focusing solely on environmental performance may impede other critical performance indicators such as productivity and product quality of machining processes. Therefore, with the increasing global adoption of carbon neutralization policies (carbon tax and carbon labelling) and increased manufacturer competitiveness, the machining process must achieve low carbon emissions with efficient energy utilization without compromising productivity and product quality.

Multi-objective optimization is a practical approach for setting optimal cutting parameters where multiple responses need to be optimized simultaneously (Bagaber and Yusoff, 2017). As presented in the Chapter 2 Literature review, extensive research has been published on the trade-off/multi-objective optimization of machining process performances such as energy consumption, cutting force, productivity, and product quality (Nguyen et al., 2020). In practice, the power factor (*PF*) is an important measure of an electric system's efficient electrical energy utilization (Behrendt et al., 2012). The power factor is the ratio of active power to apparent power (O'Driscoll and O'Donnell, 2013). The main machine tool components, such as electric motors, feed drives, coolant pumps, etc., are powered by inductive loads that accumulate to a low *PF*. Low *PF* reduces the distribution capacity of the electrical power grid by increasing current flow and lowering the voltage. If it falls below a certain level, electrical boards impose penalties. This chapter proposes an optimization method for low carbon emission and high efficiency from the perspectives of carbon emission, power factor, surface quality and productivity of the machining process.

The literature review presented in Chapter 2 revealed that several authors have recently focused on optimizing cutting parameters in machining processes while considering energy consumption, productivity, and product quality. With growing environmental issues and stringent carbon emission regulations, low carbon emission has become one of the essential requirements of manufacturing industries. Due to this increasing number of authors are considering *CEM* as machining performance in multi-objective optimization.

The existing literature survey (**Chapter 2, Table 2.1**) shows that limited authors optimized the cutting parameters for low carbon emission, and only two studies (Kumar et al., 2017; Nguyen et al., 2020) considered *PF* as a machining response in multi-objective optimization. As explained previously, *PF* is an important indicator of the energy efficiency

of an electrical system, such as a machine tool. *PF* values range from 0 to 1, and higher values are desirable to avoid penalties imposed by electrical boards for their low values (Behrendt et al., 2012). As a result, capacitor banks are now used to maintain a certain level of *PF* in order to avoid such penalties (O'Driscoll and O'Donnell, 2013). Several studies (El-Moniem et al., 2014; Mather and Maksimović, 2011; Mitwalli et al., 1996) on *PF* correction equipment (i.e. rectifiers) have been published in the literature. However, the expense of buying and installing this equipment adds to the financial strain on the manufacturing sector. The accumulation of inductive load of machine tool components is one of the leading causes of power losses and low *PF*. Machine tools have variable drive systems and can be operated at variable loads, resulting in inductive load and corresponding *PF* changes. However, there appears to be an abundance of literature on the optimization of machining responses such as energy consumption, productivity and surface quality but only handful of studies on *PF* optimization. Behrendt et al. (2012) study only emphasized the significance of *PF*. He underlined the significance of *PF* as an indicator of energy efficiency of machine tool, and reported that five of the six machine tools studied had less than 70% *PF*. To the best of the author's knowledge, only Nguyen et al. (2020) and Kumar et al. (2017) considered *PF* as a machining process response in multi-objective optimization but ignored the productivity and carbon emission respectively.

In addition, Table 2.1 of **Chapter 2** shows that in most multi-objective optimization, equal importance (weight) are assigned to the responses. The selection of the weight of responses can provide a better solution to determine the optimal cutting parameter for a machining process (Nguyen et al., 2020). The relative weight of the responses should be decided based on the machining process requirement. The weights of the performance characteristics can be decided based on qualitative techniques and quantitative techniques

e.g. qualitative technique: AHP (Gurumurthy and Kodali, 2012); quantitative techniques: PCA (Kant and Sangwan, 2014), WGRA (Yan and Li, 2013) and entropy method (Bhuyan and Routara, 2015; Sivasankar and Jeyapaul, 2012). Kumar et al. (2017) is the only significant study reported so far that used two different weight assigning methods in addition to equal weigh methods for multi-objective optimization of the machining process.

For fulfilling the existing above-mentioned research gaps to achieve low carbon emissions without compromising the productivity and product quality of a machining process, this chapter proposes a multi-objective optimization for low carbon emission in terms of carbon emission and power factor, surface roughness, and material removal rate. Here *PF* is the indicator of the energy efficiency of machine tool, carbon emissions (*CEMt*) is one of the foremost GHGs, material removal rate (*MRR*) represents the productivity of the machining process, and surface roughness (R_a) signifies the surface quality of the machined product.

Furthermore, in this chapter, the optimization results of the equal weight method compared with four different methods for allocating response weights, including quantitative methods i.e. PCA, entropy weights, WGRA and qualitative method i.e. AHP. The multiple responses were transformed into a multi-objective combined index (*MOCI*) related to different weight assigning methods using the GRA method. The corresponding optimal cutting parameters were determined using the Taguchi technique.

8.2. Experimental Planning

Figure 8.1 shows the outline and adopted the methodology of the proposed multi-objective optimization. The turning experiments were performed on a LMW-Smarturn CNC lathe machine on an aluminium workpiece Al6061 under a dry cutting environment.

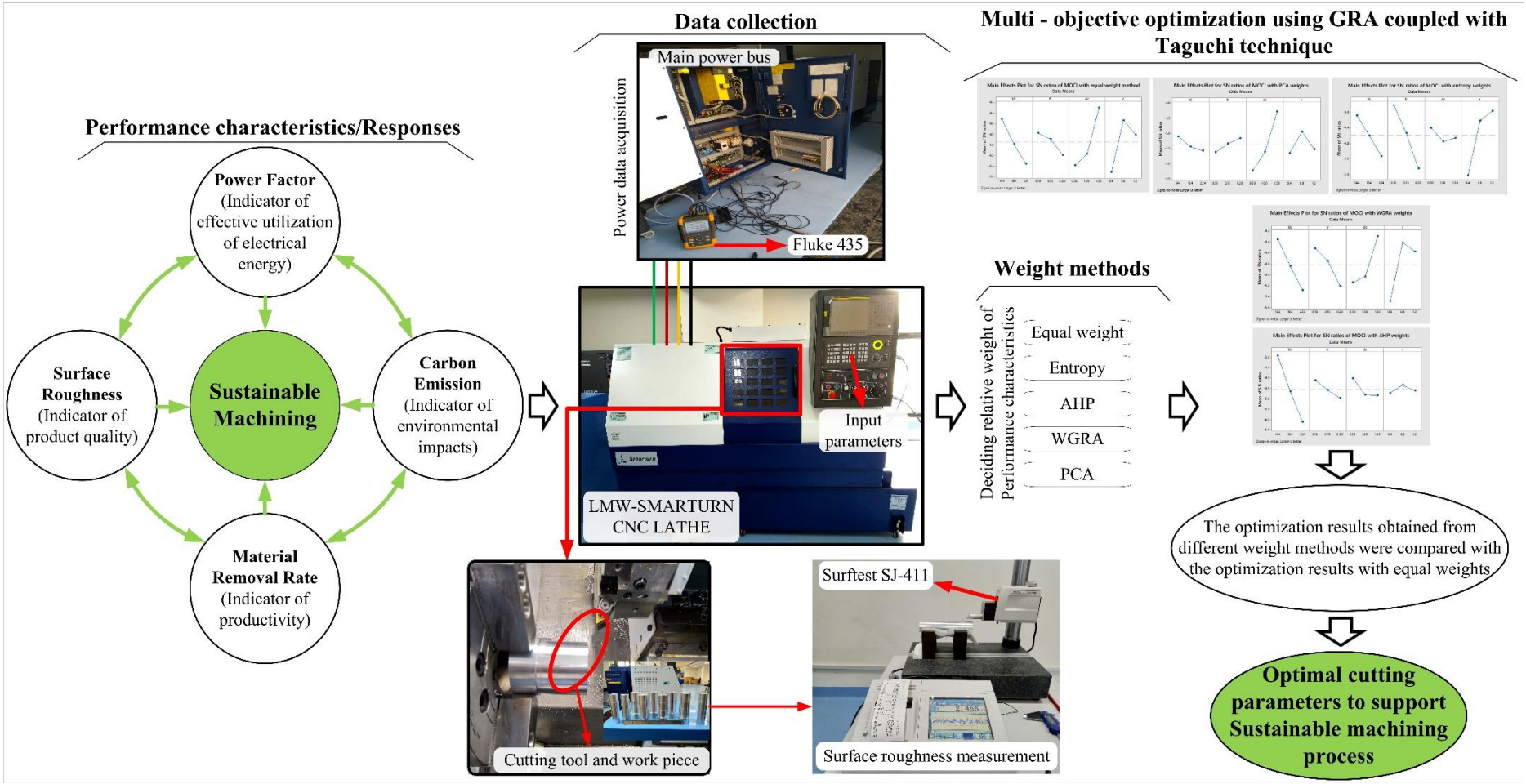

Figure 8.1. Outline of the proposed work and adopted methodology.

The technical specifications of the machine tool can be seen in **Table 5.1 of Chapter 5**. Sandvik carbide inserts of different nose radii of designation: CNMG 120404, 08, 12 were selected as cutting tools with tool holder of ISO designation PCLNR 2020 K12. The cutting parameters for the turning process were cutting speed (v_c), cutting depth (d_c), feed rate (f_r), and cutting tool nose radius (r). The levels of the cutting parameters were chosen based on machine tool relevant factors, cutting tool supplier recommendations, and relevant information found in the literature (Bharathi Raja and Baskar, 2011; Camposeco-Negrete, 2015; Lv et al., 2018). The level of the cutting parameters and their combinations according to the Taguchi L_{27} (3^4) orthogonal array are provided in Table 8.1.

The *PF* and total power drawn by the CNC machine tool were measured directly with the help of the Fluke 435 series II Power Analyzer and provided in Table 8.1. As shown in Figure 8.1, the power analyzer was connected to the CNC machine tool's 3-phase main power bus supply via three current probes and three voltage probes embedded with alligator clips. The power consumption readings were taken every 0.25 seconds.

The surface roughness (R_a) was measured with the help of Mitutoyo's Surftest SJ-411 as a surface quality indicator of the machined workpieces. The Ra was measured at three equal angles on the workpiece's periphery, and the average values were used in the calculations. The material removal rate (*MRR*) in the turning process can be calculated using the following expression:

$$MRR\left(\frac{mm^3}{sec}\right) = \frac{v_c \times f_r \times d_c \times 1000}{60} \tag{1}$$

In a dry machining process, the carbon emissions are caused due to various factors: carbon emissions due to electrical energy consumption of machine tool (CEM_{elec}), the carbon emission due to cutting tool wear (CEM_{tool}), the carbon emission due to material

consumption (CEM_m), include the emissions due to the raw material production and transportation, and the emissions due to post-processing of chips (CEM_{chip}) for material recovery (Zhang et al., 2017). The total carbon emission (CEM_t) can be expressed as (Li et al., 2015; Zhang et al., 2017):

$$CEM_t = CEM_{elec} + CEM_{tool} + CEM_m + CEM_{chip} \quad (2)$$

The detailed description and calculation procedure for each CEM: CEM_{elec}, CEM_{tool}, CEM_m and CEM_{chip} are provided in **Chapter 6, Section 6.2**. The various *CEFs* and other related factors presented in **Chapter 6** were used for the calculation of CEM in the current work because the experiments were performed for the same workpiece and cutting tool combination i.e. aluminium Al 6061 and carbide inserts. The calculated values of the CEM_t corresponding to the experimental runs are summarized in Figure 8.1.

Table 8.1. *PF*, *MRR*, R_a and CEM_t under the different combinations of cutting parameters based on Taguchi L_{27} orthogonal array.

Exp. No.	v_c (m/min)	f_r (mm/rev)	d_c (mm)	r (mm)	*PF*	*MRR* (mm^3/sec)	R_a (μm)	CEM_t ($kgCO_2$)
1	144	0.10	0.50	0.4	0.71	120.00	1.353	0.4148
2	144	0.10	1.00	0.8	0.73	240.00	0.777	0.6290
3	144	0.10	1.50	1.2	0.74	360.00	0.524	0.8174
4	144	0.15	0.50	0.8	0.71	180.00	0.992	0.5060
5	144	0.15	1.00	1.2	0.74	360.00	0.927	0.7533
6	144	0.15	1.50	0.4	0.76	540.00	2.210	0.9667
7	144	0.20	0.50	1.2	0.72	240.00	1.070	0.5908
8	144	0.20	1.00	0.4	0.74	480.00	3.229	0.8683

9	144	0.20	1.50	0.8	0.77	720.00	2.203	1.1035
10	184	0.10	0.50	0.4	0.71	153.33	1.176	0.7729
11	184	0.10	1.00	0.8	0.72	306.67	0.681	1.1361
12	184	0.10	1.50	1.2	0.73	460.00	0.505	1.4446
13	184	0.15	0.50	0.8	0.71	230.00	0.798	0.9712
14	184	0.15	1.00	1.2	0.72	460.00	0.551	1.4041
15	184	0.15	1.50	0.4	0.76	690.00	1.970	1.7668
16	184	0.20	0.50	1.2	0.70	306.67	1.087	1.1525
17	184	0.20	1.00	0.4	0.75	613.33	3.395	1.6508
18	184	0.20	1.50	0.8	0.78	920.00	1.864	2.0584
19	224	0.10	0.50	0.4	0.70	186.67	1.314	1.2441
20	224	0.10	1.00	0.8	0.72	373.33	0.523	1.7910
21	224	0.10	1.50	1.2	0.74	560.00	0.376	2.2434
22	224	0.15	0.50	0.8	0.71	280.00	0.898	1.5904
23	224	0.15	1.00	1.2	0.74	560.00	0.616	2.2586
24	224	0.15	1.50	0.4	0.77	840.00	2.288	2.8015
25	224	0.20	0.50	1.2	0.72	373.33	1.387	1.9065
26	224	0.20	1.00	0.4	0.75	746.67	3.588	2.6851
27	224	0.20	1.50	0.8	0.77	1120.00	2.396	3.3080

8.3. Multi-Objective Optimization using Different Weight Assigning Methods

The GRA method was used to combine the various responses into a single multi-objective combined index (*MOCI*) related to different weight assigning methods i.e. equal weight method, AHP, PCA, entropy weights, and WGRA. The obtained *MOCI* were then analysed further using a Taguchi signal to noise (*SN*) ratio-based approach to determine the optimum cutting parameters. Taguchi evaluates the *MOCI* on cutting parameters using the *SN* ratio.

In the Taguchi method, three types of principles (larger is better, smaller is better, and nominal is better) are available to calculate the *SN* ratios and can be used depending on the nature of the objective or aim of the study (Mia, 2018). In the present study, the maximization of *MOCI* was desirable; therefore, Eq. (3) for 'Larger is the better' principle can be used to calculate the *SN* ratios.

$$SN \text{ ratio } = -\log\frac{1}{q}\left(\sum\left(\frac{1}{y^2}\right)\right) \tag{3}$$

Where y is the experimental outcomes of the dependent variable and q is the total number of experimental runs. The general procedure/stages used for multi-objective optimization using GRA coupled with Taguchi are discussed below.(Hanafi et al., 2012; Kant and Sangwan, 2014).

Stage-I: Selection of the machining process responses

Machining processes can be evaluated based on several performance characteristics/responses and thus, depending on the study's aim, responses are selected and optimized simultaneously.

Stage II: Pre-processing of data

The performance of the machining process can be evaluated based on several responses that can be measured in different units e.g. power consumption in watts and product quality in microns. The experimental sequence is thus transformed into comparable sequences ranging from 0 to 1 by normalization. The following three equations are used in the GRA for normalization depending on the characteristics of the response.

'Smaller the better': $$x_p^*(q) = \frac{Max\ x_p(q) - x_p(q)}{Max\ x_p(q) - Min\ x_p(q)} \tag{4}$$

'Larger the better': $$x_p^*(q) = \frac{x_p(q) - Min\ x_p(q)}{Max\ x_p(q) - Min\ x_p(q)} \quad (5)$$

'Specific desired value': $$x_p^*(q) = \frac{\left| x_p(q) - D_v \right|}{Max.\left\{ Max\ x_p(q) - D_v,\quad D_v - Min\ x_p(q) \right\}} \quad (6)$$

Where $x_p^*(q)$ is the normalized sequence, $x_p(q)$ is the actual (experimental) sequence, D_v is the targeted value of the performance, $Max\ x_p(q)$ is the maximum value in the sequence, $Min\ x_p(q)$ is the minimum value in the sequence, p is the number of responses (1,2,3… number of responses), and q is the number of experimental runs (1, 2, . . ., number of experimental runs).

After normalising the responses sequence, the corresponding Grey Relational Coefficients (GRC) are calculated using the following equation;

$$GRC(q) = \frac{\Delta_{min} + \zeta\Delta_{max}}{\Delta_{op}(q) + \zeta\Delta_{max}} \quad (7)$$

Where $\Delta_{op}(q) = \left| x_p^{\circ}(q) - x_p^*(q) \right|$, $\Delta_{mini} = \frac{mini}{p}\frac{mini}{q}\Delta_{op}(q)$, $\Delta_{maxi} = \frac{maxi}{p}\frac{maxi}{q}\Delta_{op}(q)$.

$\Delta_{op}(q)$ is the absolute difference between the ideal $x_p^{\circ}(q)$ and the current $x_p^*(q)$ sequence and called a deviational sequence. ζ is the distinguish coefficient and can attain a value in the range of 0 to 1, and in the present study, it is considered 0.5.

Stage-III: Weight calculations of responses

In multi-objective optimization, the relative importance (i.e. weight) of the responses is determined in such a way that such that $\sum_{j=1}^{p} w_j = 1$, p is the number of responses and w_j is the allocated weight of the j^{th} response. The detailed calculation for each weight assigning method is discussed below.

(a) Equal weight

In the equal weight method, each response is given the same weight. The weight of each response can be calculated using Eq. (8).

$$w_j = 1/p,\ j = 1,2,3.....p \tag{8}$$

(b) Principal Component Analysis (PCA)

PCA is a well-known method for analysing multivariate data. PCA converts higher-dimensional space information into lower-dimensional space information (Monfreda, 2012). Furthermore, the weights obtained through the PCA method are independent of the decision-makers choices/preferences. The general methodology adopted for the PCA analysis is discussed below.

Firstly, an original multiple quality characteristics matrix $[G]_{q\times p}$ is developed as expressed in Eq. (9). The elements of this matrix $g_i(j)$ represent the GRC corresponding to each response, where $i = 1,2,3,$ ....number of experiments (q)) and $j = 1,2,3,$ ... number of responses p.

$$G = \begin{bmatrix} g_1(1) & g_1(2) & .. & .. & g_1(p) \\ g_2(1) & g_2(2) & .. & .. & g_2(p) \\ .. & .. & .. & .. & .. \\ .. & .. & .. & .. & .. \\ g_q(1) & g_q(2) & .. & .. & g_q(p) \end{bmatrix} \tag{9}$$

The correlation coefficient matrix (R_{ij}) is then computed using Eq (10).

$$R_{jl} = \left(\frac{Cov(g_i(j), g_i(l))}{\sigma g_i(j) \times \sigma g_i(l)} \right),\ j = 1,2,3,....p, \text{ and } l = 1,2,3,....p \tag{10}$$

Where $Cov\,(g_i(j), g_i(l))$ is the covariance of sequence $g_i(j)$ and $g_i(l)$, $\sigma g_i(j)$ is the standard deviation of sequence $g_i(j)$ and $\sigma g_i(j)$ is the standard deviation of the sequence $g_i(l)$. Following that, as shown in Eq. (11), eigenvalues and eigenvectors are calculated using correlation coefficient arrays.

$$\left(R - \lambda_k I_q\right) V_{lk} = 0 \tag{11}$$

Where λ_k is the eigenvalues and $\sum_{k=1}^{p} \lambda_k = p, k = 1,2,3, \ldots, p,$ $V_{lk} = \left[a_{kl}\ a_{k2} \ldots\ldots\ldots a_{kq}\right]^T$ are the eigenvectors corresponding to the eigenvalues λ_k. Thirdly, the Principal Components are computed using Eq. (12).

$$Z_{pk} = \sum_{i=1}^{p} g_q\left(i\right).\, V_{ik} \tag{12}$$

Where Zp1 represents the first Principal Component, Zp2 the second, and so on. The contribution of the response to the Principal Component can calculate as the square of their eigenvector. Accordingly, in the present study, the square of the eigen vector of the first Principal Component was adopted as the weight of the related response and can be calculated using Eq. (13)

$$w_j = \left(Z_{p1}^2\right)_i \,/\, \sum_{i=1}^{p} \left(Z_{p1}^2\right)_i \tag{13}$$

(c) Entropy weight

Entropy analysis explains the interaction between factors and responses and accordingly suggests the relative importance (weight) of the responses (Shemshadi et al., 2011). Entropy analysis uses probability theory to measure information uncertainty. The entropy weight method does not incorporate the decision-maker's choices/priorities to evaluate the relative weight of the responses. The following section discusses the generalised

methodology used to determine the weight of the responses using the entropy method (Kumar et al., 2017).

The experimental results are used as elements of the Decision Matrix $[DC]_{q\times p}$, where q represents the number of experimental runs and p represents the number of responses. The elements d_{ij} represent the values of the responses for each experimental run, where $i = 1,2,3, \ldots q$ and $j = 1,2,3, \ldots . p$. As shown in Eq. (14), in the decision matrix, rows equal the number of experimental runs and columns equal the number of responses.

$$DC = \begin{bmatrix} d_{11} & d_{12} & d_{1j} & .. & .. & d_{1p} \\ d_{21} & d_{22} & d_{2j} & .. & .. & d_{2p} \\ d_{i1} & d_{i2} & d_{ij} & .. & .. & d_{ip} \\ .. & .. & .. & .. & .. & .. \\ .. & .. & .. & .. & .. & .. \\ d_{q1} & d_{q2} & d_{qj} & .. & .. & d_{qp} \end{bmatrix} \quad (14)$$

It is not necessary to measure every response on the same scale. Eq. (14) is used to convert the responses to a comparable scale of dimensionless values ranging from 0 to 1. The normalization is based on the characteristics of the response such as whether maximisation or minimization is preferable. In Eq. (15), the maximum criterion refers to the responses which need to be maximized. The minimum criterion is related to the responses which are preferred with lower values.

$$NM_{ij} = \begin{cases} \dfrac{d_{ij}}{Max\left(d_{ij}\right)_j} & \text{for maximum criteria} \\ \dfrac{Mini\left(d_{ij}\right)_j}{d_{ij}} & \text{:for minimum criteria} \end{cases} \quad (15)$$

The probability of occurrence (PO_{ij}) of the criterion is calculated by using equation (16).

$$PO_{ij} = \frac{NM_{ij}}{\sum_{i=1}^{q} NM_{ij}} \tag{16}$$

The entropy index (EI_j) of the j^{th} criterion is calculated using equation (17).

$$EI_j = -P\sum_{i=1}^{q} PO_{ij} log\left(PO_{ij}\right) \tag{17}$$

Where $P = \frac{1}{log_e(q)}$ is a constant having value in the range of $0 \leq EI_j \leq 1$ and p are the total number of experimental runs. The degree of divergence (DIV_j) of the average information confined by each response is calculated using Eq. (18).

$$DIV_j = \left|1 - EI_j\right| \tag{18}$$

Finally, the entropy weights (EW_j) of the j^{th} response can be calculated using Eq. (19).

$$Ew_j = \frac{DIV_j}{\sum_{j=1}^{p} DIV_j} \tag{19}$$

(d) Weighted Grey Relational Analysis (WGRA)

Yan and Li (2013) proposed the WGRA method wherein, the degree to which controllable parameters (i.e., input parameters) affect the responses determines their relative importance (weight). The general methodology to calculate the WGRA weights is discussed below.

Firstly, the average values of the GRC (average GRC) of the performance characteristics are calculated at each level of the cutting parameters e.g. the average GRC of the performance characteristics for level 1 of the cutting speed can be calculated using the GRC values of the experimental runs 1-9. Similarly, the average GRC of all performance characteristics for each level of the cutting parameters can be calculated. The degree of influence of each response is quantitatively calculated by the sum-average of the

GRC ranges (maximum-minimum) as shown in Eq. (20). The ratio of quantitative value (i.e. GRC ranges) for each response is the basis for their relative importance i.e. weight. The WGRA weights can be calculated using Eq. (21).

$$R_{ij} = \text{maximum}\left\{K_{i,j,1},\ K_{i,j,2},\ldots K_{i,j,k}\right\} - \text{minimum}\left\{K_{i,j,1},\ K_{i,j,2},\ldots K_{i,j,k}\right\} \quad (20)$$

$$w_i = \frac{\sum_{j=1}^{s} R_{i,j}}{\sum_{i=1}^{p}\sum_{j=1}^{s} R_{i,j}} \quad (21)$$

Where $i = 1,2,3,\ldots..p,\ j = 1,2,3,\ldots.s,\ k = 1,2,3,\ldots.q$. p is the number of responses, s is the number of input parameters (cutting parameters), q is the number of experiments, K is the mean GRC for each input parameter at each level of each response, and w_i is the weight of each response.

(e) Analytic Hierarchy Process (AHP)

AHP categorises the decision maker's preferences to determine the responses' relative importance (i.e. weight). The decision-maker specifies the relative importance of the responses in a pairwise matrix that define relative priorities among the responses. The relative importance is determined using Saaty's nine-point preference scale (Saaty, 2008), as shown in Table 8.2. The relative importance of the performance characteristics is determined using this pairwise matrix. The AHP weight method's standard procedure is discussed below (Saaty, 2008).

Table 8.2 Nine-point scale of the relative importance, Saaty (2008).

Intensity of importance	Meaning	Description
1	Equally important	Indifferent

2	Slightly important	
3	Moderately important	A little better
4	Moderately plus important	
5	Strongly important	Better
6	Strongly plus important	
7	Very strongly important	Much better
8	Very very strongly important	
9	Extremely important	Absolutely much better

Assume there are *p* responses (R_p), which are used as elements (r_{ij}, i & $j = 1,2,3 \ldots . p$) of a pairwise matrix $[R_p]_{p\times p}$, as shown in Eq (22). The pairwise matrix is structured to compare the performance characteristics R_i to R_j mutually. The matrix elements are determined by comparing the responses in each row ($R_1, R_2, \ldots . R_p$) to the responses in the column ($R_1, R_2, \ldots . R_p$) using Saaty's (Saaty, 2008) nine-point scale shown in Table 8.2. Where for $i = j$, $r_{ij} = 1$, because a response is equally important for itself. The other half elements in the matrix for $i \neq j$ are determined by comparing the responses. The other half of the elements are essentially the reciprocal of their corresponding element such that $r_{ij} = 1/r_{ji}$. After constructing the pairwise matrix, Eq. (23) calculates the geometric mean of each row.

Response (j) (i)	R_1	R_2	R_3	R_j		R_p
R_1	1	r_{12}	r_{1j}	---	---	r_{1p}
R_2	r_{21}	1	r_{23}	---	---	r_{2p}

$$R_{\mathrm{p\times p}} = \begin{array}{c|cccccc} R_3 & r_{i1} & r_{i2} & 1 & --- & --- & r_{3\mathrm{p}} \\ --- & --- & --- & --- & --- & --- & --- \\ R_i & --- & --- & --- & --- & --- & --- \\ R_p & r_{\mathrm{p}1} & r_{\mathrm{p}2} & r_{\mathrm{p}3} & --- & --- & 1 \end{array} \quad (22)$$

$$GM_i = \left[\prod_{j=1}^{p} r_{ij}\right]^{\frac{1}{p}} \quad (23)$$

The responses' relative importance (i.e. weight) is determined by dividing the geometric mean of the corresponding row of the comparison matrix by the sum of the geometric mean of all the rows as shown in Eq. (24).

$$w_j = GM_i \,/\, \sum_{i=1}^{p} GM_i \quad (24)$$

The consistency of the decision-makers should be tested before finalising the relative weights using AHP. The estimated weights of the responses are used to calculate the consistency index (CI) using Eq. (25).

$$CI = \frac{\lambda_{max} - p}{p - 1} \quad (25)$$

Where λ_{max} represent the maximum Eigen value of the matrix and p is the number of responses. Eq. (26) was used to calculate the consistency ratio (CR).

$$CR = \frac{CI}{RI} \quad (26)$$

RI is the random index value shown in Table 8.3. A value of $CR \leq 0.10$ indicates the consistency of the decision-maker in assigning the relative importance of the responses in the pairwise matrix i.e. Eq. (22).

Table 8.3. Random Index (RI) values (Saaty, 2008)**.**

Number of responses	1	2	3	4	5	6	7	8	9	10
Random Index	0.00	0.00	0.58	0.90	1.12	1.24	1.32	1.41	1.45	1.49

Stage-IV: Calculation of the *MOCIs*

The MOCI is the weighted sum of the GRCs of responses for each experimental run. The MOCI can be calculated using Eq. (27).

$$MOCI = \sum_{j=0}^{p} \left[w_j * GRC_i \right] \tag{27}$$

Stage-V: The responses are simultaneously optimised and perform better when the *MOCI* value is high (Mia, 2018).

8.4. Results and Discussion

8.4.1. Calculation of *MOCI* related to different weight methods

Four responses are chosen for simultaneous optimization in stage I: *PF*, *MRR*, R_a and CEM_t. *PF* and *MRR* are beneficial with 'larger the better' characteristics; therefore, their normalized sequences were obtained using Eq. (5).

Table 8.4 Normalized values, Deviational sequence and GRC of the responses

Normalized sequences				Deviational sequences				Grey Relational Coefficients			
PF	MRR	R_a	CEM_t	*PF*	MRR	R_a	CEM_t	*PF*	MRR	R_a	CEM_t
0.1250	0.0000	0.6958	1.0000	0.8750	1.0000	0.3042	0.0000	0.3636	0.3333	0.6218	1.0000
0.3750	0.1200	0.8752	0.9259	0.6250	0.8800	0.1248	0.0741	0.4444	0.3623	0.8002	0.8710
0.5000	0.2400	0.9539	0.8608	0.5000	0.7600	0.0461	0.1392	0.5000	0.3968	0.9156	0.7823
0.1250	0.0600	0.8082	0.9685	0.8750	0.9400	0.1918	0.0315	0.3636	0.3472	0.7228	0.9407
0.5000	0.2400	0.8285	0.8830	0.5000	0.7600	0.1715	0.1170	0.5000	0.3968	0.7446	0.8104
0.7500	0.4200	0.4290	0.8092	0.2500	0.5800	0.5710	0.1908	0.6667	0.4630	0.4669	0.7238
0.2500	0.1200	0.7839	0.9392	0.7500	0.8800	0.2161	0.0608	0.4000	0.3623	0.6983	0.8915
0.5000	0.3600	0.1118	0.8432	0.5000	0.6400	0.8882	0.1568	0.5000	0.4386	0.3602	0.7613
0.8750	0.6000	0.4312	0.7620	0.1250	0.4000	0.5688	0.2380	0.8000	0.5556	0.4678	0.6775
0.1250	0.0333	0.7509	0.8762	0.8750	0.9667	0.2491	0.1238	0.3636	0.3409	0.6675	0.8015
0.2500	0.1867	0.9050	0.7507	0.7500	0.8133	0.0950	0.2493	0.4000	0.3807	0.8404	0.6673
0.3750	0.3400	0.9598	0.6441	0.6250	0.6600	0.0402	0.3559	0.4444	0.4310	0.9256	0.5842

0.1250	0.1100	0.8686	0.8077	0.8750	0.8900	0.1314	0.1923	0.3636	0.3597	0.7919	0.7222
0.2500	0.3400	0.9455	0.6581	0.7500	0.6600	0.0545	0.3419	0.4000	0.4310	0.9017	0.5939
0.7500	0.5700	0.5037	0.5327	0.2500	0.4300	0.4963	0.4673	0.6667	0.5376	0.5019	0.5169
0.0000	0.1867	0.7786	0.7450	1.0000	0.8133	0.2214	0.2550	0.3333	0.3807	0.6931	0.6623
0.6250	0.4933	0.0601	0.5728	0.3750	0.5067	0.9399	0.4272	0.5714	0.4967	0.3472	0.5393
1.0000	0.8000	0.5367	0.4319	0.0000	0.2000	0.4633	0.5681	1.0000	0.7143	0.5191	0.4681
0.0000	0.0667	0.7080	0.7133	1.0000	0.9333	0.2920	0.2867	0.3333	0.3488	0.6313	0.6356
0.2500	0.2533	0.9542	0.5243	0.7500	0.7467	0.0458	0.4757	0.4000	0.4011	0.9161	0.5125
0.5000	0.4400	1.0000	0.3680	0.5000	0.5600	0.0000	0.6320	0.5000	0.4717	1.0000	0.4417
0.1250	0.1600	0.8375	0.5937	0.8750	0.8400	0.1625	0.4063	0.3636	0.3731	0.7547	0.5517
0.5000	0.4400	0.9253	0.3627	0.5000	0.5600	0.0747	0.6373	0.5000	0.4717	0.8700	0.4396
0.8750	0.7200	0.4047	0.1751	0.1250	0.2800	0.5953	0.8249	0.8000	0.6410	0.4565	0.3774
0.2500	0.2533	0.6852	0.4844	0.7500	0.7467	0.3148	0.5156	0.4000	0.4011	0.6137	0.4923
0.6250	0.6267	0.0000	0.2153	0.3750	0.3733	1.0000	0.7847	0.5714	0.5725	0.3333	0.3892
0.8750	1.0000	0.3711	0.0000	0.1250	0.0000	0.6289	1.0000	0.8000	1.0000	0.4429	0.3333

R_a and CEM_t are advantageous with 'Smaller the better' characteristics; therefore, their normalized sequences were calculated using Eq. (4). The calculated normalized values of the responses are provided in Table 8.4. The GRC for each experimental run and response was calculated using Eq. (7) according to stage II, and the results are tabulated in Table 8.4. The following are the calculation of the weights of the responses using the various methods presented in stage III.

According to the equal weight approach, equal importance (weight) is assigned to each response which can be calculated using Eq. (8). The GRCs in Table 8.4 were chosen as elements, i.e. $g_i(j)$ of the matrix $[G]_{q\times p}$, to calculate the weight of the response using the PCA method, as stated in Eq (10). Eq. (11) was then used to compute the correlational coefficient matrix (R_{ij}). Following that, Eqs. (12) and (13) were used to compute the eigenvalues and Principal Components and are tabulated in Table 8.5 and Table 8.6 respectively. The Eigen analysis of the correlation coefficient matrix R_{ij} is shown in Table 8.5. The Principal Components' contributions can be calculated as the square of their respective eigenvectors. Therefore, the square of the first Principal Component's eigenvector in Table 8.6 was adopted as the weight of the corresponding response.

The matrix DC was created for entropy weights according to Eq. (14) where $q = 27$ (number of experimental runs) and $p = 4$ (number of responses). The DC matrix elements are the responses' experimental outcomes shown in Table 8.1. The maximization of *PF* and *MRR* is beneficial. Therefore, their normalized sequences were calculated using the 'maximum criterion' of Eq. (15). Minimization of R_a and CEM_t is advantageous. Therefore, their normalized sequences were calculated using the 'minimum criterion' of Eq. (15).

Table 8.5 Eigen analysis of the correlation coefficient matrix R_{ij}

Eigenvalue	2.6422	0.845	0.3786	0.1342
Proportion (%)	0.6610	0.2110	0.0950	0.0340
Cumulative	0.6610	0.8720	0.9660	1.0000

Table 8.6 Eigen vectors for principal components and corresponding weights

Responses	Z_{p1}	Z_{p2}	Z_{p3}	Z_{p4}	PCA weights
PF	-0.5550	0.1130	-0.5840	0.5820	0.3080
MRR	-0.5790	-0.1250	-0.2400	-0.7690	0.3352
R_a	0.4020	-0.7390	-0.5400	-0.0140	0.1616
CEM_t	0.4410	0.6520	-0.5570	-0.2640	0.1945

The obtained normalized matrix (NM_{ij}) is shown in Table 8.7. Following that, Eqs. (16), (17) and (18) were used to calculate the EI_j, DIV_j and Ew_j respectively and are tabulated in Table 8.7.

Table 8.7. NM_{ij}, $POij$, EI_j, DIV_j and corresponding entropy weights (Ew_j)

NM_{ij}				PO_{ij}			
PF	*MRR*	R_a	CEM_t	*PF*	*MRR*	R_a	CEM_t
0.9103	0.1071	0.2779	1.0000	0.0358	0.0097	0.0267	0.0969
0.9359	0.2143	0.4839	0.6594	0.0368	0.0193	0.0464	0.0639
0.9487	0.3214	0.7176	0.5074	0.0373	0.0290	0.0688	0.0492
0.9103	0.1607	0.3790	0.8196	0.0358	0.0145	0.0364	0.0794
0.9487	0.3214	0.4056	0.5506	0.0373	0.0290	0.0389	0.0534
0.9744	0.4821	0.1701	0.4290	0.0383	0.0435	0.0163	0.0416
0.9231	0.2143	0.3514	0.7021	0.0363	0.0193	0.0337	0.0680

0.9487	0.4286	0.1164	0.4777	0.0373	0.0386	0.0112	0.0463
0.9872	0.6429	0.1707	0.3759	0.0388	0.0580	0.0164	0.0364
0.9103	0.1369	0.3197	0.5366	0.0358	0.0123	0.0307	0.0520
0.9231	0.2738	0.5521	0.3651	0.0363	0.0247	0.0530	0.0354
0.9359	0.4107	0.7446	0.2871	0.0368	0.0370	0.0714	0.0278
0.9103	0.2054	0.4712	0.4271	0.0358	0.0185	0.0452	0.0414
0.9231	0.4107	0.6824	0.2954	0.0363	0.0370	0.0655	0.0286
0.9744	0.6161	0.1909	0.2348	0.0383	0.0556	0.0183	0.0227
0.8974	0.2738	0.3459	0.3599	0.0353	0.0247	0.0332	0.0349
0.9615	0.5476	0.1108	0.2513	0.0378	0.0494	0.0106	0.0243
1.0000	0.8214	0.2017	0.2015	0.0394	0.0741	0.0194	0.0195
0.8974	0.1667	0.2861	0.3334	0.0353	0.0150	0.0275	0.0323
0.9231	0.3333	0.7189	0.2316	0.0363	0.0301	0.0690	0.0224
0.9487	0.5000	1.0000	0.1849	0.0373	0.0451	0.0959	0.0179
0.9103	0.2500	0.4187	0.2608	0.0358	0.0225	0.0402	0.0253
0.9487	0.5000	0.6104	0.1836	0.0373	0.0451	0.0586	0.0178
0.9872	0.7500	0.1643	0.1480	0.0388	0.0676	0.0158	0.0143
0.9231	0.3333	0.2711	0.2175	0.0363	0.0301	0.0260	0.0211
0.9615	0.6667	0.1048	0.1545	0.0378	0.0601	0.0101	0.0150
0.9872	1.0000	0.1569	0.1254	0.0388	0.0902	0.0151	0.0121
			EI_j	0.9999	0.9573	0.9475	0.9565
			DIV_j	0.0001	0.0427	0.0525	0.0435
			Ew_j	0.0011	0.3077	0.3782	0.3130

For WGRA, the average GRC of each response for each cutting parameter is calculated and summarized in Table 8.8.

Table 8.8 The average value of $\boldsymbol{GRC}$ of each parameter at their every level and corresponding WGRA weights

Cutting parameter	*PF*				*MRR*				R_a				CEM_t			
Level	v_c	f_r	d_c	r	v_c	f_r	d_c	r	v_c	f_r	d_c	r	v_c	f_r	d_c	r
1	0.5043	0.4166	0.3650	0.5374	0.4062	0.3852	0.3608	0.4636	0.6442	0.8132	0.6883	0.4874	0.8287	0.6996	0.7442	0.6383
2	0.5048	0.5138	0.4764	0.5484	0.4525	0.4468	0.4391	0.4993	0.6876	0.6901	0.6793	0.6951	0.6173	0.6307	0.6205	0.6382
3	0.5187	0.5974	0.6864	0.4420	0.5201	0.5469	0.5790	0.4159	0.6687	0.4973	0.6329	0.8181	0.4637	0.5794	0.5450	0.6331
Range	0.0144	0.1807	0.3214	0.1064	0.1139	0.1617	0.2182	0.0834	0.0434	0.3159	0.0554	0.3307	0.3650	0.1201	0.1992	0.0052
Sum of ranges	0.6230				0.5772				0.7454				0.6895			
WGRA weights	0.2364				0.2190				0.2829				0.2617			

In the present study, the values of *p*, *s* and *q* are 4 (number of responses), 3 (number of cutting parameters) and 27 (number of experimental runs) respectively. Eqs. (20) and (21) were used to calculate the ranges and WGRA weights respectively, and the results are tabulated in Table 8.8.

The pairwise matrix is now prepared as stated in Eq. (22) and is shown in Table 8.9 to calculate the weights using AHP. The AHP weights can be calculated using Eq. (24) and are tabulated in Table 8.10.

Table 8.9 Pairwise matrix of responses

Responses	*PF*	*MRR*	R_a	CEM_t
PF	1	1	2	1/3
MRR	1	1	1	1/7
R_a	1/2	1	1	1/9
CEM_t	3	7	9	1

Table 8.10 AHP weights

Responses	Geometric mean	Eigen vector (AHP weights)
PF	0.9036	0.1582
MRR	0.6148	0.1076
R_a	0.4855	0.0850
CEM_t	3.7078	0.6492

The consistency with which the decision-makers assigned the relative weights to the responses in the pairwise matrix is then verified. The value of λ_{max} and CI (Eq. 25) were found to be 4.0899 and 0.02996 respectively. The value of CR was calculated using Eq. 26

and found to be 0.0333 (< 0.10). The CR value for the present pairwise matrix is less than 0.10, which confirms the decision-makers consistency in assigning the relative importance of the responses in the pairwise matrix. The calculated weights of the responses related to different weight methods are summarized in Table 8.11.

Table 8.11 Calculated weights with different weight methods

Response	*PF*	*MRR*	R_a	CEM_t
Weight method	Weight			
Equal	0.2500	0.2500	0.2500	0.2500
PCA	0.3080	0.3352	0.1616	0.1945
Entropy	0.0011	0.3077	0.3782	0.3130
WGRA	0.2364	0.2190	0.2829	0.2617
AHP	0.1582	0.1076	0.0850	0.6492

Following that, Eq. (27) and Eq. (3) were used to calculate the *MOCI* and their corresponding *SN* ratios related to different weight methods respectively, and the results are tabulated in Table 8.12.

8.4.2. Analysis of variance (ANOVA)

ANOVA analysis is used to analyze the effects and significance of the cutting parameters on the means of *MOCI*. The ANOVA determines "how much" variation and "which" factor has caused it, using F-statistics, P value (for significance level 5 %), source, degrees of freedom, sum of squares, mean squares, and percentage contribution. F-values, p-values, and percentage contribution (PC) were calculated for linear terms, square terms, and their two-way interactions.

Table 8.12 *MOCI* with different weights and their *SN* ratios.

Exp.	Equal weight		PCA weight		Entropy weight		WGRA weight		AHP weight	
run	*MOCI*	*SN* Ratio	*MOCI*	*SN* Ratio	*MOCI*	*SN* Ratio	*MOCI*	*SN* Ratio	*MOCI*	*SN* Ratio
1	0.5797	-4.7362	0.5187	-5.7014	0.6511	-3.7264	0.5965	-4.4873	0.7954	-1.9881
2	0.6195	-4.1593	0.5571	-5.0818	0.6873	-3.2576	0.6387	-3.8940	0.7427	-2.5832
3	0.6487	-3.7594	0.5871	-4.6251	0.7138	-2.9283	0.6688	-3.4938	0.7075	-3.0060
4	0.5936	-4.5306	0.5282	-5.5448	0.6750	-3.4133	0.6126	-4.2562	0.7670	-2.3044
5	0.6129	-4.2518	0.5650	-4.9596	0.6579	-3.6368	0.6278	-4.0438	0.7111	-2.9608
6	0.5801	-4.7303	0.5768	-4.7800	0.5463	-5.2512	0.5805	-4.7242	0.6649	-3.5455
7	0.5880	-4.6120	0.5309	-5.4997	0.6551	-3.6740	0.6047	-4.3687	0.7404	-2.6109
8	0.5150	-5.7636	0.5073	-5.8945	0.5100	-5.8483	0.5154	-5.7575	0.6511	-3.7266
9	0.6252	-4.0795	0.6400	-3.8761	0.5608	-5.0240	0.6204	-4.1461	0.6659	-3.5317
10	0.5434	-5.2977	0.4900	-6.1952	0.6087	-4.3126	0.5592	-5.0487	0.6713	-3.4618
11	0.5721	-4.8506	0.5164	-5.7399	0.6443	-3.8182	0.5903	-4.5788	0.6089	-4.3096
12	0.5963	-4.4904	0.5446	-5.2785	0.6661	-3.5298	0.6142	-4.2341	0.5746	-4.8127
13	0.5594	-5.0460	0.5010	-6.0027	0.6367	-3.9218	0.5778	-4.7652	0.6324	-3.9802
14	0.5817	-4.7066	0.5289	-5.5320	0.6600	-3.6090	0.5994	-4.4450	0.5718	-4.8545
15	0.5558	-5.1021	0.5672	-4.9250	0.5178	-5.7175	0.5526	-5.1518	0.5415	-5.3273
16	0.5174	-5.7242	0.4711	-6.5375	0.5870	-4.6278	0.5316	-5.4891	0.5825	-4.6935

17	0.4887	-6.2200	0.5035	-5.9597	0.4536	-6.8671	0.4832	-6.3170	0.5234	-5.6226
18	0.6754	-3.4092	0.7224	-2.8244	0.5637	-4.9791	0.6622	-3.5802	0.5831	-4.6853
19	0.4873	-6.2447	0.4452	-7.0279	0.5454	-5.2654	0.5001	-6.0188	0.5565	-5.0900
20	0.5574	-5.0764	0.5054	-5.9276	0.6308	-4.0028	0.5757	-4.7967	0.5170	-5.7303
21	0.6033	-4.3887	0.5596	-5.0417	0.6621	-3.5809	0.6200	-4.1526	0.5016	-5.9929
22	0.5108	-5.8352	0.4664	-6.6257	0.5733	-4.8319	0.5255	-5.5879	0.5200	-5.6804
23	0.5703	-4.8775	0.5382	-5.3805	0.6123	-4.2602	0.5827	-4.6917	0.4892	-6.2100
24	0.5687	-4.9019	0.6085	-4.3150	0.4889	-6.2160	0.5574	-5.0762	0.4793	-6.3871
25	0.4768	-6.4339	0.4526	-6.8860	0.5100	-5.8478	0.4848	-6.2882	0.4782	-6.4076
26	0.4666	-6.6207	0.4975	-6.0640	0.4247	-7.4390	0.4566	-6.8086	0.4330	-7.2700
27	0.6441	-3.8215	0.7181	-2.8767	0.5804	-4.7256	0.6207	-4.1425	0.4882	-6.2275

The regression mean square to the mean square error ratio is defined as the F-value. A cutting parameter with an F-value greater than 4 significantly affects the response (Kant and Sangwan, 2014). The p-value shows the statistical significance of the cutting parameters for the results at a given confidence level (Kant and Sangwan, 2014). The significance (confidence) level in this analysis is set to 0.05. Thus, the p-value should be less than 0.05; otherwise, the contribution of the corresponding cutting parameter to the response is statistically insignificant. The results of ANOVA for means of *MOCI* related to different weight methods are provided in Table 8.13.

Table 8.13 ANOVA for the means of *MOCI* related to the different weight methods

Weight method	Source	DF	Adj SS	Adj MS	F-Value	P-Value	PC (%)
	v_c	1	0.013	0.013	51.210	0.000*	21.131
	f_r	1	0.002	0.002	9.970	0.008*	4.113
	d_c	1	0.013	0.013	54.230	0.000*	22.378
	r	1	0.013	0.013	54.180	0.000*	22.358
	$v_c * v_c$	1	0.000	0.000	0.350	0.566	0.144
	$f_r * f_r$	1	0.000	0.000	0.280	0.602	0.117
Equal	$d_c * d_c$	1	0.002	0.002	6.190	0.027*	2.556
	$r * r$	1	0.003	0.003	11.370	0.005*	4.694
	$v_c * f_r$	1	0.000	0.000	1.170	0.298	0.484
	$v_c * d_c$	1	0.005	0.005	20.840	0.001*	8.600
	$v_c * r$	1	0.000	0.000	0.750	0.404	0.307
	$f_r * d_c$	1	0.004	0.004	18.150	0.001*	7.488
	$f_r * r$	1	0.000	0.000	0.640	0.438	0.264

	Error	13	0.003	0.000			5.365
	Total	26	0.076				100.000
		$R^2 = 95.79\%$			Adj. $R^2 = 91.58\%$		
PCA	v_c	1	0.003	0.003	8.790	0.011*	3.280
	f_r	1	0.006	0.006	18.570	0.001*	6.931
	d_c	1	0.041	0.041	133.640	0.000*	49.892
	r	1	0.005	0.005	17.970	0.001*	6.708
	$v_c * v_c$	1	0.000	0.000	0.760	0.399	0.284
	$f_r * f_r$	1	0.000	0.000	0.000	0.955	0.001
	$d_c * d_c$	1	0.002	0.002	7.260	0.018*	2.711
	$r * r$	1	0.003	0.003	8.670	0.011*	3.236
	$v_c * f_r$	1	0.002	0.002	5.560	0.035*	2.075
	$v_c * d_c$	1	0.007	0.007	23.930	0.000*	8.935
	$v_c * r$	1	0.001	0.001	1.790	0.203	0.670
	$f_r * d_c$	1	0.008	0.008	26.420	0.000*	9.862
	$f_r * r$	1	0.000	0.000	1.500	0.243	0.560
	Error	13	0.004	0.000			4.853
	Total	26	0.123				100.000
		$R^2 = 96.77\%$			Adj. $R^2 = 93.54\%$		
Entropy	v_c	1	0.022	0.022	68.450	0.000*	17.328
	f_r	1	0.052	0.052	160.680	0.000*	40.674
	d_c	1	0.001	0.001	3.130	0.100	0.794
	r	1	0.037	0.037	114.440	0.000*	28.971
	$v_c * v_c$	1	0.000	0.000	0.010	0.941	0.002

	$f_r * f_r$	1	0.000	0.000	0.380	0.546	0.098
	$d_c * d_c$	1	0.001	0.001	2.260	0.157	0.571
	$r * r$	1	0.003	0.003	9.170	0.010*	2.321
	$v_c * f_r$	1	0.000	0.000	0.000	0.961	0.001
	$v_c * d_c$	1	0.006	0.006	17.930	0.001*	4.537
	$v_c * r$	1	0.000	0.000	0.010	0.921	0.002
	$f_r * d_c$	1	0.002	0.002	5.170	0.041*	1.309
	$f_r * r$	1	0.000	0.000	0.400	0.539	0.101
	Error	13	0.004	0.000			3.291
	Total	26	0.148				100.000
		$R^2 = 97.17\%$			Adj. $R^2 = 94.34\%$		
	v_c	1	0.016	0.016	66.140	0.000*	24.776
	f_r	1	0.008	0.008	33.160	0.000*	12.423
	d_c	1	0.008	0.008	33.580	0.000*	12.580
	r	1	0.017	0.017	69.410	0.000*	26.002
	$v_c * v_c$	1	0.000	0.000	0.170	0.684	0.065
	$f_r * f_r$	1	0.000	0.000	0.600	0.452	0.225
WGRA	$d_c * d_c$	1	0.001	0.001	5.340	0.038*	2.000
	$r * r$	1	0.003	0.003	11.880	0.001*	4.450
	$v_c * f_r$	1	0.000	0.000	0.300	0.591	0.114
	$v_c * d_c$	1	0.004	0.004	18.140	0.001*	6.796
	$v_c * r$	1	0.000	0.000	0.430	0.524	0.161
	$f_r * d_c$	1	0.004	0.004	14.390	0.002*	5.389
	$f_r * r$	1	0.000	0.000	0.400	0.538	0.150

	Error	13	0.003	0.000			4.869
	Total	26	0.080				100.000
		$R^2 = 95.98\%$			Adj. $R^2 = 91.95\%$		
AHP	v_c	1	0.218	0.218	2746.670	0.000*	86.410
	f_r	1	0.016	0.016	195.900	0.000*	6.163
	d_c	1	0.007	0.007	84.620	0.000*	2.662
	r	1	0.001	0.001	16.540	0.001*	0.520
	$v_c * v_c$	1	0.002	0.002	25.350	0.000*	0.797
	$f_r * f_r$	1	0.000	0.000	1.040	0.326	0.033
	$d_c * d_c$	1	0.002	0.002	29.170	0.000*	0.917
	$r * r$	1	0.001	0.001	6.960	0.021*	0.219
	$v_c * f_r$	1	0.000	0.000	0.160	0.692	0.005
	$v_c * d_c$	1	0.003	0.003	33.580	0.000*	1.056
	$v_c * r$	1	0.000	0.000	2.360	0.148	0.074
	$f_r * d_c$	1	0.002	0.002	21.940	0.000*	0.690
	$f_r * r$	1	0.000	0.000	1.410	0.257	0.044
	Error	13	0.001	0.000			0.409
	Total	26	0.266				100.000
		$R^2 = 99.61\%$			Adj. $R^2 = 99.21\%$		

*Significant parameters

P-value < 0.05 and F-value > 4 for linear terms in Table 8.13 related to different weight methods, shows that the selected cutting parameters have significant impacts on the *MOCI* and better statistical fitness of the experimental results. Further, in each case, the coefficient of determination (i.e. R^2) is more than 95% which confirms the statistical significance of the experimental data for *MOCI* related to different weight methods. The percentage

contribution (PC) of each parameter for *MOCI* related to different weight methods are summarized in Table 8.14.

Table 8.14 Summary of the percentage contribution of cutting parameter for *MOCI* related to the different weight methods

Method	Cutting parameters percentage contribution			
	v_c	f_r	d_c	r
Equal weight	21.13	4.11	22.38	22.36
PCA weight	3.28	6.93	49.89	6.71
Entropy weight	17.33	40.67	0.79	28.97
WGRA weight	24.78	12.58	12.42	26.00
AHP weight	86.41	6.16	2.66	0.52

8.4.3. Taguchi analysis

The *SN* ratios of *MOCI* related to different weight methods are summarized in Table 8.12. Genichi Taguchi developed the Taguchi method. It used the signal-to-noise ratio principle that minimises variation and improves the mean for the given set of data (Öztürk et al., 2019). The SN ratio is the ratio of expected signal values with unexpected noise values (Meral et al., 2019). Therefore, the cutting parameter level corresponding to the highest *SN* ratio is considered as the optimal level for the corresponding response (Sivaiah and Chakradhar, 2019).

Accordingly, the optimum cutting parameters with different weight methods (equal, PCA, entropy, WGRA and AHP) and their corresponding *SN* ratios and *MOCIs* are provided in Table 8.15. The optimal levels of cutting parameters are different for *MOCIs*

belonging to different weight methods, and only they are the same for equal and WGRA weight methods.

Table 8.15 Optimal cutting parameters with different weight methods

Cutting parameter	Weight method				
	Equal	PCA	Entropy	WGRA	AHP
	Optimal level of cutting parameter				
v_c	144	144	144	144	144
f_r	0.10	0.20	0.10	0.10	0.10
d_c	1.5	1.50	0.50	1.50	0.50
r	0.8	0.8	1.2	0.8	0.8
MOCI	0.6253	0.6400	0.7464	0.6419	0.8047
SN ratio	-4.0777	-3.8761	-2.5405	-3.8501	-1.8879

Further, the main effect plot of *SN* ratios are used to analyze the influence of the cutting parameters on the responses and are shown in Figure 8.2, Figure 8.3, Figure 8.4, Figure 8.5 and Figure 8.6 for the *MOCI* related to equal, PCA, entropy, WGRA and AHP methods respectively.

The *MOCI* related to equal (Figure 8.2), PCA (Figure 8.3), entropy (Figure 8.4), WGRA (Figure 8.5) and AHP (Figure 8.6) are deteriorating with an increase in cutting speed. Figures 8.2, 8.4, 8.5 and 8.6 shows that the *MOCI* related to equal, entropy, WGRA and AHP decreases as the feed rate increases, whereas *MOCI* related to PCA shows the reverse trend as shown in Figure 8.3. The *MOCI* related to equal weight method as shown in (Figure 8.2), PCA (Figure 8.3) and WGRA (Figure 8.5) shows improvement with an increase in the depth of cut. The *MOCI* related to AHP (Figure 8.6) shows deterioration with an increase in the depth of cut, while *MOCI* related to entropy (Figure 8.4) shows decrement

with the decrease in depth of cut with level-1 to level-2 and improves with a further increase from level-2 to level-3. The *MOCI* corresponding to equal weight (Figure 8.2), PCA (Figure 8.3), WGRA (Figure 8.5) and AHP (Figure 8.6) increases with a change in nose radius from level-1 to level-2, and when nose radius advances from level-2 to level-3, it shows a decrement. Whereas the *MOCI* related to entropy (Figure 8.4) weight improves with an increase in nose radius.

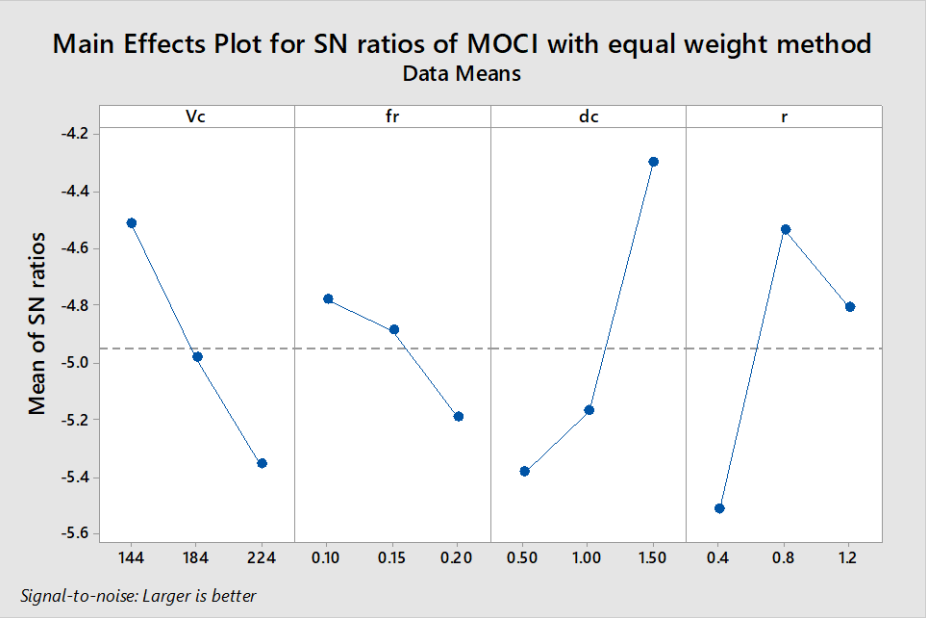

Figure 8.2. Main effect plot for *SN* ratios of *MOCI* with equal weight method.

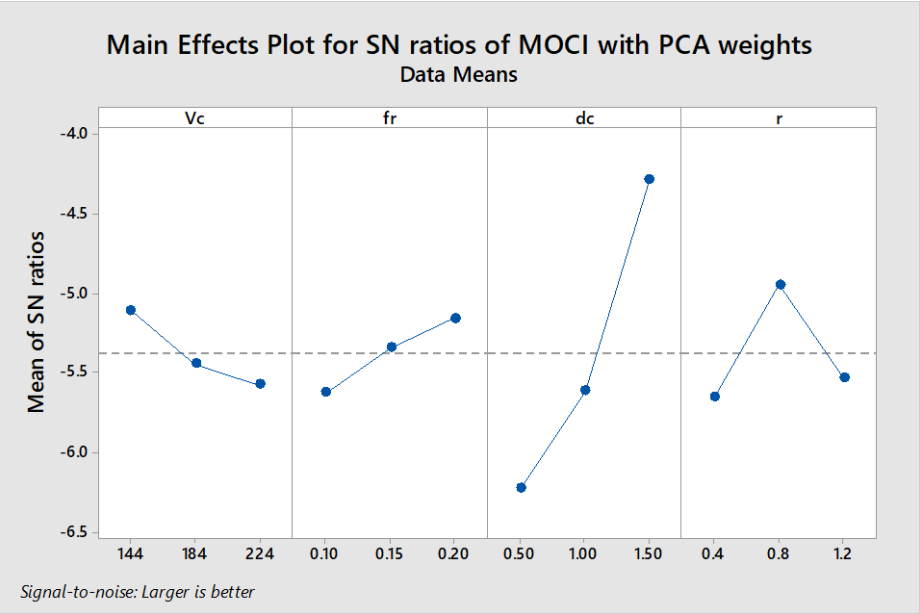

Figure 8.3. Main effect plot for *SN* ratios of *MOCI* with PCA.

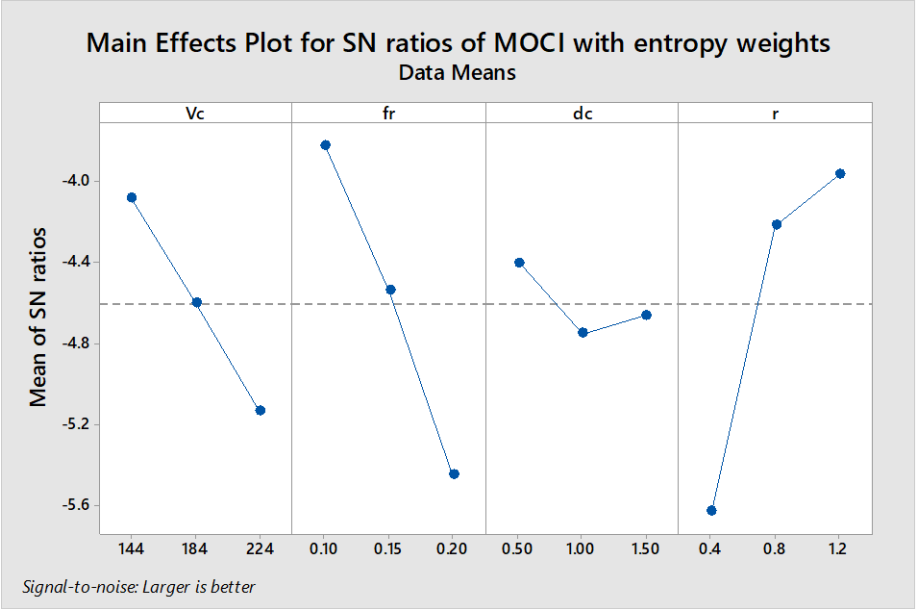

Figure 8.4. Main effect plot for *SN* ratios of *MOCI* with entropy weight method.

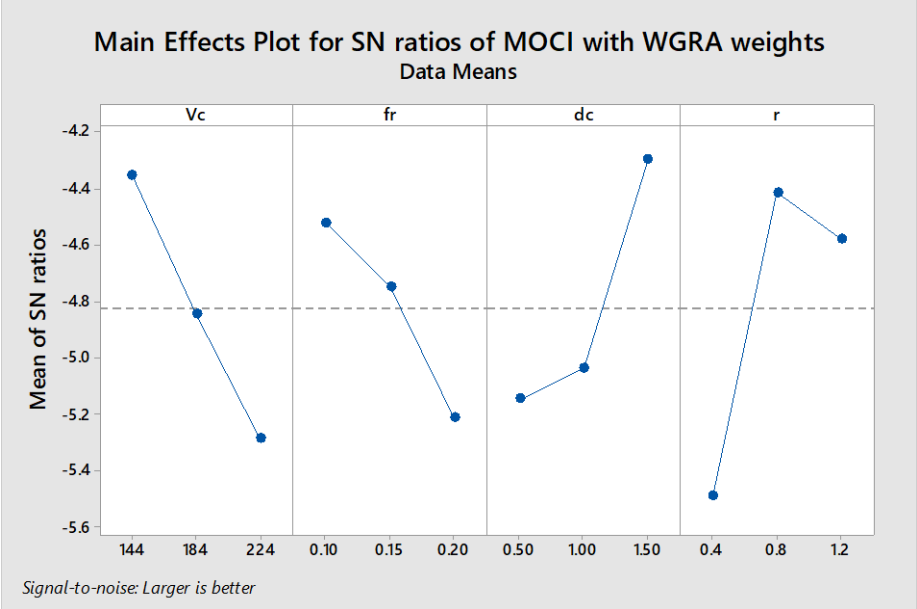

Figure 8.5. Main effect plot for *SN* ratios of *MOCI* with WGRA.

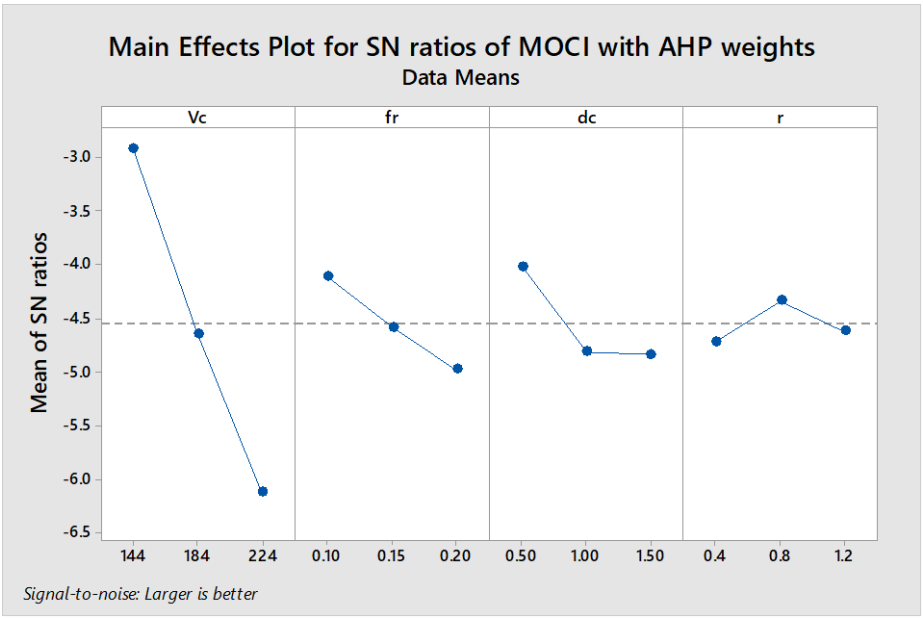

Figure 8.6. Main effect plot for *SN* ratios of *MOCI* with AHP.

8.4.4. Validation of optimization results and comparative analysis

The combination of optimal levels of cutting parameters for MOCI related to equal weight method, WGRA weights, entropy weights, and AHP weights differ from the L_{27} orthogonal

array as shown in Table 8.1. Therefore, Experiments were performed at optimal cutting parameters of *MOCI* related to different weight methods to obtain the corresponding values of the responses. The experiments were repeated three times, and the average was adopted. The results are tabulated in Table 8.16. Eq. (28) can be used to predict the values of the *MOCI* related to different weight methods on optimal cutting parameters (Sivaiah and Chakradhar, 2019).

$$\gamma_{predicted} = \gamma_m + \sum_{i=1}^{s} \gamma_o - \gamma_m \tag{28}$$

γ_m is the average of *MOCIs* or *SN* ratios value, γ_o is the mean of *MOCI* or *SN* ratio at optimal levels, and *s* is the total number of the cutting parameters. The experimental values of *MOCI* and *SN* ratios on optimal cutting parameters related to different weight methods and their predicted values are compared in Table 8.16.

Table 8.16 Predicted and measured values of the *SN* ratios and *MOCI* on optimum cutting parameters related to different weight methods.

Weight method	Measured		Predicted		Difference in %	
	MOCI	*SN* Ratio	*MOCI*	*SN* Ratio	*MOCI*	*SN* Ratio
Equal	0.6253	-4.0777	0.6764	-3.2719	-8.16	19.76
PCA	0.6400	-3.8761	0.6762	-3.3690	-5.65	13.08
Entropy	0.7464	-2.5405	0.7345	-2.4650	1.59	2.97
WGRA	0.6419	-3.8501	0.6878	-3.1090	-7.14	19.25
AHP	0.8047	-1.8879	0.7991	-1.7201	0.69	8.89

The comparative analysis in Table 8.16 shows that the experimental and predicted values of the *SN* ratios and *MOCI* are very close, with no significant difference. In addition, the

MOCIs for PCA, entropy weights, WGRA, and AHP are compared to the *MOCI* for equal weight method in Table 8.17.

Table 8.17 Improvement in *MOCI* related to different weight methods compared to equal weight method.

Method	Equal	PCA	Entropy	WGRA	AHP
MOCI at optimum cutting parameters	0.6253	0.6400	0.7464	0.6419	0.8047
Percentage improvement in *MOCI* compared to the equal weight	-	2.35	19.36	2.66	28.67

Compared to the *MOCI* using equal weight method, the *MOCIs* related to PCA, entropy weights, WGRA, and AHP show an improvement of 2.35 %, 19.36 %, 2.66 %, and 28.67 % on corresponding optimal cutting parameters. The larger the *MOCI*, the better the corresponding responses (Kant and Sangwan, 2014; Meral et al., 2019). A higher value of *MOCI* shows a better performance of the responses simultaneously (Meral et al., 2019). Therefore, the improvement in the *MOCIs* suggests that using different weight methods rather than equal weight method would result in better optimisation results.

Table 8.18 summarizes the values of the responses (*PF*, *MRR*, R_a and CEM_t) on the optimal cutting parameters related to the different weight methods and their deviations from the values at the optimal cutting parameters using equal weight method.

The weights of the responses using the WGRA method were nearly the same as those using the equal weight method (Table 8.11), and thus their optimal cutting parameters are found to be the same (Table 8.15). Therefore, with equal and WGRA weights, the responses have the same values.

Table 8.18. Summary of optimized values of responses with equal weight method versus other weight assigning methods.

Performance characteristics		*PF*	*MRR* (mm^3/sec)	R_a (μm)	CEM_t ($kgCO_2$)
Values of responses on optimal cutting parameters with equal weight method		0.74	360.00	0.778	0.7658
PCA	At optimal cutting parameters	0.77	720.00	2.203	1.1035
	Deviation compared to optimal cutting parameters with equal weight method (%)	4.05	100.00	183.16	44.10
Entropy	At optimal cutting parameters	0.72	120.00	0.534	0.4823
	Deviation compared to optimal cutting parameters with equal weight method (%)	-2.70	-66.67	-31.35	-37.02
WGRA	At optimal cutting parameters	0.74	360.00	0.778	0.7658
	Deviation compared to optimal cutting parameters with equal weight method (%)	0.00	0.00	0.00	0.00
AHP	At optimal cutting parameters	0.72	120	0.641	0.4528
	Deviation compared to optimal cutting parameters with equal weight method (%)	-2.70	-66.67	-17.57	-40.87

$+$ change shows improvement in PF and MRR; $-$ change shows improvement in R_a and CEM_t

As shown in Table 8.11, *PF* and *MRR* were assigned higher weights in PCA than equal weight method and the highest weights among all weight methods. This is also reflected in their percentage improvement of 4.05% and 100% respectively as shown in Table 8.18 on the optimal cutting parameters using PCA when compared to the optimal cutting parameters with equal weight method.

The entropy method assigned a higher weight to R_a than equal weight method, as shown in Table 8.11, which is the highest weight for R_a among all weight assigning methods. As a result, the percentage improvement in R_a of 31.35 (Table 8.18) on the optimal cutting parameters using entropy weights was observed to be the highest when compared to the optimal cutting parameters using equal weight method.

A similar phenomenon was observed for the response CEM_t to which a higher weight was given in AHP than the equal weight (Table 8.11) and is the highest weight for CEM_t among all weight assigning methods. When the value of CEM on optimal cutting parameters with AHP was compared to the value on optimal cutting parameters with equal weight method, the highest reduction in CEM_t was found to be 40.87 %, as shown in Table 7.18.

In the preceding discussion and as shown in Table 8.18, based on the weight assigning method, given weights to the responses change the optimal cutting parameters, and the responses exhibit improvement or degradation in accordance with those changes when compared to the optimal cutting parameters using equal weight method.

As shown in Table 8.18, *PF* and *MRR* show an improvement of 4.05% and 100% respectively on optimal cutting parameters using PCA as compared to the equal weight method, whereas the responses R_a and CEM_t deteriorate by 183.16% and 44.10%

respectively. The decline in R_a and CEM_t is due to their lower given weightage of 16.16% and 19.45% respectively, as shown in Table 8.11.

As shown in Table 8.18, on the optimal cutting parameters with entropy weights, the responses *PF* and *MRR* show a decrement of 2.70% and 66.67% respectively when compared to the optimal cutting parameters using equal weight method, while R_a and CEM_t improved by 31.35% and 37.02% respectively. The improvement in R_a and CEM_t is found because of their larger weights of 37.82% and 31.30% respectively with the entropy weight method, as shown in Table 8.11.

Table 8.18 shows that the *PF* and *MRR* at the optimal cutting parameters with AHP decreased by 2.70% and 66.67%, respectively when compared with the optimum cutting parameters using equal weight, while the R_a and CEM_t showed an improvement of 17.57% and 40.87% respectively. The changes in the optimized values of the response related to different weight methods as compared to their optimized values with equal weight method are summarized in Table 8.19.

Table 8.19. Summary of the changes in the optimized values of the response related to different weight methods as compared to their optimized values with equal weight method.

Weight method	Responses			
	PF	*MRR*	R_a	CEM_t
PCA	Improved[IV]	Improved[II]	Deteriorate[I]	Deteriorate[III]
Entropy	Deteriorate[IV]	Deteriorate[I]	Improved[III]	Improved[II]
WGRA	No change	No change	No change	No change
AHP	Deteriorate[IV]	Deteriorate[I]	Improved[III]	Improved[II]

[I, II, II and IV] shows the ranking of the response based on their percentage change

As shown in Table 8.18, when entropy and AHP are used instead of equal weight method, the values of R_a and CEM_t improve significantly, and this improvement is more significant than using WGRA and PCA weights. In addition, when comparing the optimization results produced by AHP weights and entropy weights, AHP bring better CEM_t reduction while entropy weights give better R_a.

An improvement in the performance of one response during the optimization of multiple responses can even lead to a deterioration in another response (Camposeco-Negrete, 2015; Yan and Li, 2013), which is primarily driven by the weight assigned to the response (Kumar et al., 2017). Therefore, the weights assigned to the responses are critical and should be adopted based on qualitative or quantitative techniques, not be fixed arbitrarily like equal weight method.

Further, the improvement in the *MOCIs* related to different weight methods compared to the *MOCI* using equal weight shows that the system is better optimized with different wight methods than the equal weight method in which the AHP method shows the greatest improvement. Further, in the present case, the comparative analysis shows that the AHP method can be a suitable alternative for determining the weights of the responses. This method also provides flexibility if a particular response needs to be focused.

8.5. Summary

This chapter includes key machining process responses: power factor (*PF*), productivity (*MRR*), product quality (R_a) and carbon emission (CEM_t) for multi-objective optimization to achieve sustainable and cleaner machining, where *PF* is one of the indicators of the effective use of electricity and has rarely optimized with CEM_t in the literature. In this chapter, the optimization results with different weight methods (i.e. PCA, entropy, WGRA

and AHP) were compared with the optimization results with equal weight method. The optimal level of cutting parameters was found to be different for *MOCIs* related to different weight methods. The optimization results were validated by the Taguchi method in which the experimental and predicted values of *SN* ratio and *MOCI* are found to be close to each other. The *MOCIs* on optimal cutting parameters related to the PCA weights, entropy weights, WGRA weights and AHP weights are compared with the *MOCI* related to equal weight and found to be improved by 2.35%, 19.36%, 2.66% and 28.67% respectively. The improvement in *MOCI* reflects the improved performance of the response on the optimal cutting parameters obtained through different weight methods compared to the equal weight method indicating that these methods have a significant impact on multi-objective optimization.

Further, in the present case, the AHP weight method can be a suitable alternative for determining the weights of the responses. Since the *MOCI* shows highest improvement of 28.67% with AHP compared to the equal weight. In comparison to the equal weight method, with AHP weights, the surface quality of the machined components can be improved by 17.61% with low carbon emission around 40.87%. However, *PF* shows a nominal deterioration of 4.05% and MRR decreased by 66.67%.

Chapter 9:

Conclusions

Machine tools plays a significant role in manufacturing industries and are unfortunately responsible for huge energy consumption and associated greenhouse gas emissions. Machine tools have a complex and dynamic structure due to the diverse and complex interaction of various materials, process parameters, and cutting tools, which directly impact their behaviour analysis. Developing an accurate industry-applicable energy consumption model of machine tools is still challenging. This study provides modelling of energy consumption and associated carbon emission (CEM) of machine tools for machining cylindrical parts. This study demonstrates the application of soft computing techniques to model the performance indicators of machine tools. Further, process parameters are optimised for low carbon emissions and efficient energy utilisation without compromising productivity and product quality.

In Chapter 2, more than 100 research articles including modelling approaches of the energy consumption of machine tools and optimization of process parameters are reviewed. The literature reveals several advances in this area. One group of researchers attempts to address this issue by modelling and assessing the energy consumption and CEM of CNC machine tools, processes, and systems, and a large number of authors are focusing on optimization of machining processes.

The early studies on machining process energy consumption focused on modelling the tooltip-work interface energy consumption i.e. material removal energy consumption. Literature shows that the energy required for material removal was significant, but the total energy demand of a machine tool is predominant. In numerous studies the energy consumption of machine tools segregated at their component level such as energy

consumed by spindle, feed axis, coolant pump, tool change system. Some authors modelled the energy consumption of machine tool by dividing into energy consumed in different states such as standby, idle, air-cut and cutting. Some researchers investigated machine tools' transient states: spindle and feed acceleration, and incorporated them to evaluate the total energy consumption of machine tools to improve the accuracy of energy consumption models. The review revealed that in recent years artificial intelligence-based algorithms are widely employed to assess the energy consumption of machine tools, and a growing number of other authors are focusing on assessing the CEM of machining processes. Finally, the literature review is summarised, highlighting the strengths and limitations of existing modelling approaches. It shows that the existing energy consumption evaluation models only consider constant power consumption (CPC) machining processes, whereas cylindrical part machining includes both CPC and variable power consumption (VPC) machining processes to manufacture the final product, which result in inaccurate quantification of the energy consumption and associated CEM for machining a cylindrical part.

Further, literature survey on optimization of machining processes in terms of process performance and weight assigning methods is presented. The literature review revealed that the limited authors optimized the cutting parameters for low carbon emission, and rarely for the power factors and VPC machining process in multi-objective optimization. The majority of authors assigned equal weights to responses in multi-objective optimization. Therefore, the process parameters should be optimized for CEM, *PF* and for the VPC machining processes. The impact of weighting methods on multi-objective optimization results should be investigated.

In Chapter 3, an empirical model for evaluating the cutting energy consumption of the VPC machining process i.e., end facing is presented. The statistical analysis shows that the

considered process parameters (cutting speed, feed rate, cutting depth and cutting tool nose radius) are statistically significant. The developed model adequately predicts cutting power under various process parameters, with a coefficient of determination values greater than 91% in both dry and wet environments. The validation experiments confirm the prediction accuracy of the developed model is more than 96%. Further, the predicted power profiles of the end facing found to be in good agreement with the measured power profiles, indicating that the developed model satisfactorily encompasses the influences of the process parameters on the cutting power consumption.

The proposed model can be employed to optimize cutting parameters for a VPC machining process and to develop a total energy consumption model for a machining process. Predicting the total energy consumption of a machine tool in workpiece machining remains challenging because the previous energy prediction models are typically developed with CPC machining processes.

In Chapter 4, an integrated modelling and optimization approach is presented to optimize process parameters for a VPC-machining process to trade-off between productivity and cutting energy consumption. The empirical model developed in Chapter 3 is employed to determine the values of cutting energy consumption without conducting actual experiments and is integrated to the optimization model. The presented integrated approach reduced the cost required for the time-consuming measurement procedures and advanced laboratory setup. The multi-objective optimization model is developed using Grey Relational Analysis coupled with Taguchi to select the common optimal level of process parameters on which cutting energy consumption and average-material removal rate are optimized simultaneously, resulting in better-compromised decisions. The validation experiments are performed on the optimization results, and the error in each case found to be 4% only. The analysis of variance (ANOVA) revealed that all process

parameters have statistical significance where the cutting depth was found to be the most influencing process parameter with a value of percentage contribution of 45.39% followed by the spindle speed, feed rate, and nose radius with the values of percentage contribution of 20.24%, 15.12%, and 10.82% respectively. The results obtained by ANOVA analysis validated the effect of process parameters found with the integrated modelling and optimization approach.

In Chapter 5, a novel approach to model the energy consumption of a machine tool for the machining of cylindrical parts in dry and wet environment is presented. The developed model overcomes the limitations of existing energy consumption models to evaluate the total energy consumption of a machine tool during the machining of a cylindrical part for industrial applications. The energy evaluation models reported in the literature for machine tools were developed based on CPC machining processes only, while the machining of a cylindrical part includes the CPC and VPC both processes to manufacture the final product. The validation results confirm that the developed model's accuracy is more than 97%. Hence the model can be effectively employed to predict the total energy consumption of a machine tool beforehand. which is an important information for a process planner in a manufacturing industry. Based on this data, the process planner can evaluate several processes plans and identify the most energy-efficient ones.

In Chapter 6, an empirical model to quantify CEM for machining of a cylindrical part is presented. The model is developed with extended system boundaries to incorporate the direct and indirect associated CEM for machining a cylindrical part on a CNC machine tool. The developed model capable to encompasses the CEM from electrical energy consumption, material consumption, cutting tool wear, coolant consumption and from the disposal of machining waste materials for a CNC based machining of a cylindrical part. The case study with different process plans is depicted the correlation of carbon emissions

and process parameters. The case studies shows that the presented model is capable to quantify carbon emissions for industrial applications as it can able to incorporated the multiple energy consumption modules, CPC-machining process and VPC-machining process. The developed model fully accounts the effect of process parameters on *CEM*, and improves the transparency of the CEM of the machining process and facilitates the exploration of low energy efficiency and high CEM machining process. The proposed model is not only useful for identifying low-CEM process parameters, but can also be applied in multi-objective optimization to trade-off with other important machining process indicators such as productivity and product quality.

In Chapter 7, soft computing-based modelling of machine tools' effective electrical energy utilisation and associated CEM performance indicators are presented. Three soft computing techniques, multi-gene genetic programming (MGGP), least square-support vector machine (LS-SVM) and fuzzy logic, are used to develop the model a machine tool's *EE*, *PF* and associated CEM. The performance of the models was evaluated on different statistical error indices and coefficient of determination. The performance evaluation results show that the LS-SVM model consistently outperforms the corresponding MGGP and fuzzy logic models for each performance: *PF*, *EE*, and CEM. The hypothesis testing (mean paired t-test and F-test variance) validated the three models' goodness of fit.

The soft computing-based models are capable of incorporating non-linear complicated relationships between cutting parameters and machining performance, and providing reliable and realistic prediction models to achieve energy-efficient manufacturing and reduced carbon footprints. The developed models can be used to eliminate the need for advanced costly laboratory set-up and time-consuming measurement procedures required for performing experiments.

In chapter 8, a multi-objective optimization model is developed to select optimal parameters to optimize power factor (*PF*), productivity (*MRR*), product quality (R_a) and carbon emission (CEM_t). The optimization model is developed using GRA coupled with the Taguchi technique and determined optimal cutting parameters for better performance of the considered responses. This study optimizes power factor, carbon emissions, material removal rate and surface roughness as indicators of efficient electrical energy use, leading GHG, productivity and product quality, respectively. This study compares the influence of response weight assigning methods i.e. Principal Component Analysis (PCA), entropy weights, Weighted Grey Relational Analysis (WGRA) and Analytical Hierarchy Process (AHP). on optimization results (i.e. optimal parameters) to equal weights of responses. The results revealed that the optimal parameters significantly changed with change in their weight in multi-objective optimization. The responses are better optimized with the weight assigning methods than the equal weights, indicating that these methods are significant for the multi-objective optimization. The optimization results were validated by the Taguchi method in which the experimental and predicted values are found to be close to each other. In the present study, the AHP weight method is found to be suitable alternative for determining the weights of the responses. Since the MOCI shows highest improvement of 28.67% with AHP compared to the equal weight.

Major Contributions of the Thesis

- Development of an empirical model for variable power consumption machining processes
- Development of an integrated modelling and optimization approach for the selection of process parameters for variable power consumption machining processes.

- Development of empirical model to quantify energy consumption and associated carbon emission of machine tools for machining cylindrical parts
- Development of MGGP, LS-SVM, and fuzzy logic-based model for energy efficiency, power factor and associated CEM of a machine tool.
- Development of multi-objective optimization model to optimize sustainability performance indicators of machine tools using GRA coupled with Taguchi considering the impact of weight assignment methods

Limitations and future scope of the research

The developed model's performance is found to be better while predicting the total energy consumption of machine tool for machine a cylindrical part. However, there are some limitations that must be pointed out for further improvement.

The present study assumes that the spindle speed is constant during the end facing. However, in CNC machine tools, the spindle speed can be adjusted to maintain a given cutting speed irrespective to the change in the diameter of the part. Modelling of VPC machining process specifically for CNC lathe with variable spindle speed can be further explored as an independent research topic. In this study, the impact of part weight on the spindle acceleration and idle energy consumption was ignored because the weight and volume of the part to be machined on the turning centre is low as compared to the work holding device. If the part weight is significant, further investigation is required. The spindle acceleration energy consumption model is established in this work when the spindle accelerates from zero to a higher speed. The modelling aspect of spindle acceleration energy from non-zero speed to desired speed is not considered in this study and can be explored for the servo motor-based spindle system in the future.

Further, in future, the proposed energy consumption and associated carbon emission model for machining a cylindrical part can be integrated with multi-objective optimization model to trade-off with other important process indicators such as productivity and product quality. This work modelled and optimized the energy consumption and associated carbon emission of a CNC machine tool for machining aluminium part and can be extended to include the advanced materials such as super alloys and composites.

References

Abd, A.M., Abd, S.M., 2017. Modelling the strength of lightweight foamed concrete using support vector machine (SVM). Case Stud. Constr. Mater. 6, 8–15. https://doi.org/10.1016/j.cscm.2016.11.002

Aggarwal, A., Singh, H., Kumar, P., Singh, M., 2008. Optimizing power consumption for CNC turned parts using response surface methodology and Taguchi's technique-A comparative analysis. J. Mater. Process. Technol. 200, 373–384. https://doi.org/10.1016/j.jmatprotec.2007.09.041

Alswat, H.M., Mativenga, P.T., 2022. Modelling the direct and embodied energy requirements of machining. J. Clean. Prod. 366, 132767. https://doi.org/10.1016/j.jclepro.2022.132767

Alswat, H.M., Mativenga, P.T., 2020. Extended model for selection of optimum turning conditions based on minimum energy considerations. Proc. Inst. Mech. Eng. Part B J. Eng. Manuf. https://doi.org/10.1177/0954405420937558

Aramcharoen, A., Mativenga, P.T., 2014. Critical factors in energy demand modelling for CNC milling and impact of toolpath strategy. J. Clean. Prod. 78, 63–74. https://doi.org/10.1016/j.jclepro.2014.04.065

Arriaza, O.V., Kim, D.W., Lee, D.Y., Suhaimi, M.A., 2017. Trade-off analysis between machining time and energy consumption in impeller NC machining. Robot. Comput. Integr. Manuf. 43, 164–170. https://doi.org/10.1016/j.rcim.2015.09.014

Avram, O.I., Xirouchakis, P., 2011. Evaluating the use phase energy requirements of a machine tool system. J. Clean. Prod. 19, 699–711. https://doi.org/10.1016/j.jclepro.2010.10.010

Bagaber, S.A., Yusoff, A.R., 2019. Energy and cost integration for multi-objective optimisation in a sustainable turning process. Measurement 136, 795–810. https://doi.org/10.1016/j.measurement.2018.12.096

Bagaber, S.A., Yusoff, A.R., 2018. Multi-responses optimization in dry turning of a stainless steel as a key factor in minimum energy. Int. J. Adv. Manuf. Technol. 96,

1109–1122. https://doi.org/10.1007/s00170-018-1668-8

Bagaber, S.A., Yusoff, A.R., 2017. Multi-objective optimization of cutting parameters to minimize power consumption in dry turning of stainless steel 316. J. Clean. Prod. 157, 30–46. https://doi.org/10.1016/j.jclepro.2017.03.231

Bal, D.P., Patra, S.K., Mohanty, S., 2022. Impact of sectoral decompositions of electricity consumption on economic growth in India: evidence from SVAR framework. Environ. Sci. Pollut. Res. 51554–51566. https://doi.org/10.1007/s11356-022-19352-2

Balogun, V.A., Gu, H., Mativenga, P.T., 2015. Improving the integrity of specific cutting energy coefficients for energy demand modelling. Proc. Inst. Mech. Eng. Part B J. Eng. Manuf. 229, 2109–2117. https://doi.org/10.1177/0954405414546145

Balogun, V.A., Mativenga, P.T., 2013. Modelling of direct energy requirements in mechanical machining processes. J. Clean. Prod. 41, 179–186. https://doi.org/10.1016/j.jclepro.2012.10.015

Bayoumi, A.E., Yücesan, G., Hutton, D. V, 1994. On the closed form mechanistic modeling of milling: Specific cutting energy, torque, and power. J. Mater. Eng. Perform. 3, 151–158. https://doi.org/10.1007/BF02654511

Behrendt, T., Zein, A., Min, S., 2012. Development of an energy consumption monitoring procedure for machine tools. CIRP Ann. - Manuf. Technol. 61, 43–46. https://doi.org/10.1016/j.cirp.2012.03.103

Bharathi Raja, S., Baskar, N., 2011. Particle swarm optimization technique for determining optimal machining parameters of different work piece materials in turning operation. Int. J. Adv. Manuf. Technol. 54, 445–463. https://doi.org/10.1007/s00170-010-2958-y

Bhattacharya, S., Protim Das, P., Chatterjee, P., Chakraborty, S., 2021. Prediction of Reponses in a Sustainable Dry Turning Operation: A Comparative Analysis. Math. Probl. Eng. 2021. https://doi.org/10.1155/2021/9967970

Bhinge, R., Park, J., Law, K.H., Dornfeld, D.A., Helu, M., Rachuri, S., 2017. Toward a Generalized Energy Prediction Model for Machine Tools. J. Manuf. Sci. Eng. Trans.

ASME 139, 1–12. https://doi.org/10.1115/1.4034933

Bhushan, R.K., 2013. Optimization of cutting parameters for minimizing power consumption and maximizing tool life during machining of Al alloy SiC particle composites. J. Clean. Prod. 39, 242–254. https://doi.org/10.1016/j.jclepro.2012.08.008

Bhuyan, R.K., Routara, B.C., 2015. Optimization the machining parameters by using VIKOR and Entropy Weight method during EDM process of Al–18% SiCp Metal matrix composite. Decis. Sci. Lett. 269–282. https://doi.org/10.5267/j.dsl.2015.11.001

Bilga, P.S., Singh, S., Kumar, R., 2016. Optimization of energy consumption response parameters for turning operation using Taguchi method. J. Clean. Prod. 137, 1406–1417. https://doi.org/10.1016/j.jclepro.2016.07.220

Bonilla Hernández, A.E., Beno, T., Repo, J., Wretland, A., 2016. Integrated optimization model for cutting data selection based on maximal MRR and tool utilization in continuous machining operations. CIRP J. Manuf. Sci. Technol. 13, 46–50. https://doi.org/10.1016/j.cirpj.2016.02.002

Brillinger, M., Wuwer, M., Abdul Hadi, M., Haas, F., 2021. Energy prediction for CNC machining with machine learning. CIRP J. Manuf. Sci. Technol. 35, 715–723. https://doi.org/10.1016/j.cirpj.2021.07.014

Campatelli, G., Lorenzini, L., Scippa, A., 2014. Optimization of process parameters using a Response Surface Method for minimizing power consumption in the milling of carbon steel. J. Clean. Prod. 66, 309–316. https://doi.org/10.1016/j.jclepro.2013.10.025

Campatelli, G., Scippa, A., Lorenzini, L., Sato, R., 2015. Optimal workpiece orientation to reduce the energy consumption of a milling process. Int. J. Precis. Eng. Manuf. - Green Technol. 2, 5–13. https://doi.org/10.1007/s40684-015-0001-3

Camposeco-Negrete, C., 2015. Optimization of cutting parameters using Response Surface Method for minimizing energy consumption and maximizing cutting quality in turning of AISI 6061 T6 aluminum. J. Clean. Prod. 91, 109–117.

https://doi.org/10.1016/j.jclepro.2014.12.017

Camposeco-Negrete, C., 2013. Optimization of cutting parameters for minimizing energy consumption in turning of AISI 6061 T6 using Taguchi methodology and ANOVA. J. Clean. Prod. 53, 195–203. https://doi.org/10.1016/j.jclepro.2013.03.049

Camposeco-Negrete, C., de Dios Calderón-Nájera, J., 2019. Optimization of energy consumption and surface roughness in slot milling of AISI 6061 T6 using the response surface method. Int. J. Adv. Manuf. Technol. 103, 4063–4069. https://doi.org/10.1007/s00170-019-03848-2

Chen, X., Li, C., Tang, Y., Li, L., Li, H., 2021. Energy efficient cutting parameter optimization. Front. Mech. Eng. https://doi.org/10.1007/s11465-020-0627-x

Chetan, Ghosh, S., Rao, P. V., 2018. Specific cutting energy modeling for turning nickel-based Nimonic 90 alloy under MQL condition. Int. J. Mech. Sci. 146–147, 25–38. https://doi.org/10.1016/j.ijmecsci.2018.07.033

Da Costa, D.D., Gussoli, M., Valle, P.D., Rebeyka, C.J., 2022. A methodology to assess energy efficiency of conventional lathes. Energy Effic. 15. https://doi.org/10.1007/s12053-021-10006-9

Dahmus, J.B., Gutowski, T.G., 2004. An environmental analysis of machining, in: American Society of Mechanical Engineers, Manufacturing Engineering Division, MED. pp. 643–652. https://doi.org/10.1115/IMECE2004-62600

Dautzenberg, J.H., Veenstra, P.C., van der Wolf, A.C.H., 1981. The Minimum Energy Principle for the Cutting Process in Theory and Experiment. CIRP Ann. - Manuf. Technol. 30, 1–4. https://doi.org/10.1016/S0007-8506(07)60884-1

Deng, Z., Lv, L., Huang, W., Wan, L., Li, S., 2020. Modelling of carbon utilisation efficiency and its application in milling parameters optimisation. Int. J. Prod. Res. 58, 2406–2420. https://doi.org/10.1080/00207543.2019.1633026

Deng, Z., Zhang, H., Fu, Y., Wan, L., Liu, W., 2017. Optimization of process parameters for minimum energy consumption based on cutting specific energy consumption. J. Clean. Prod. 166, 1407–1414. https://doi.org/10.1016/j.jclepro.2017.08.022

Diaz-Elsayed, N., Dornfeld, D., Horvath, A., 2015. A comparative analysis of the environmental impacts of machine tool manufacturing facilities. J. Clean. Prod. 95, 223–231. https://doi.org/10.1016/j.jclepro.2015.02.047

Diaz, N., Choi, S., Helu, M., Chen, Y., Jayanathan, S., Yasui, Y., Kong, D., Pavanaskar, S., Dornfeld, D., 2010. Machine Tool Design and Operation Strategies for Green Manufacturing, in: Proceedings of 4th CIRP Internatinal Conference on High Performance Cutting. pp. 1–6.

Dirikolu, M.H., Childs, T.H.C., 2000. Modelling requirements for computer simulation of metal machining. Turkish J. Eng. Environ. Sci. 24, 81–93.

Drozda, T.J., Wick, C., 1983. Tool and Manufacturing Engineers Handbook: Volume 1 - Machining. Society of Manufacturing Engineers (SME).

Duflou, J.R., Sutherland, J.W., Dornfeld, D., Herrmann, C., Jeswiet, J., Kara, S., Hauschild, M., Kellens, K., 2012. Towards energy and resource efficient manufacturing: A processes and systems approach. CIRP Ann. - Manuf. Technol. 61, 587–609. https://doi.org/10.1016/j.cirp.2012.05.002

Edem, I.F., Balogun, V.A., 2018. Sustainability analyses of cutting edge radius on specific cutting energy and surface finish in side milling processes. Int. J. Adv. Manuf. Technol. 95, 3381–3391. https://doi.org/10.1007/s00170-017-1452-1

Edem, I.F., Balogun, V.A., Mativenga, P.T., 2017. An investigation on the impact of toolpath strategies and machine tool axes configurations on electrical energy demand in mechanical machining. Int. J. Adv. Manuf. Technol. 92, 2503–2509. https://doi.org/10.1007/s00170-017-0342-x

Edem, I.F., Mativenga, P.T., 2017. Modelling of energy demand from computer numerical control (CNC) toolpaths. J. Clean. Prod. 157, 310–321. https://doi.org/10.1016/j.jclepro.2017.04.096

Edem, I.F., Mativenga, P.T., 2016. Impact of feed axis on electrical energy demand in mechanical machining processes. J. Clean. Prod. 137, 230–240. https://doi.org/10.1016/j.jclepro.2016.07.095

El-Moniem, M.S.A., Azazi, H.Z., Mahmoud, S.A., 2014. A current sensorless power factor correction control for LED lamp driver. Alexandria Eng. J. 53, 69–79. https://doi.org/10.1016/j.aej.2014.01.001

Feng, C., Guo, H., Zhang, J., Huang, Y., Huang, S., 2022. A systematic method of optimization of machining parameters considering energy consumption, machining time, and surface roughness with experimental analysis. Int. J. Adv. Manuf. Technol. 119, 7383–7401. https://doi.org/10.1007/s00170-022-08772-6

Filippi, A., Ippolito, R., 1981. NC Machine Tools as Electric Energy Users. CIRP Ann. - Manuf. Technol. 30, 323–326. https://doi.org/10.1016/S0007-8506(07)60950-0

Gandomi, A.H., Atefi, E., 2020. Software review: the GPTIPS platform. Genet. Program. Evolvable Mach. 21, 273–280. https://doi.org/10.1007/s10710-019-09366-0

Garg, A., Lam, J.S.L., 2016. Modeling multiple-response environmental and manufacturing characteristics of EDM process. J. Clean. Prod. 137, 1588–1601. https://doi.org/10.1016/j.jclepro.2016.04.070

Garg, A., Lam, J.S.L., 2015. Improving environmental sustainability by formulation of generalized power consumption models using an ensemble based multi-gene genetic programming approach. J. Clean. Prod. 102, 246–263. https://doi.org/10.1016/j.jclepro.2015.04.068

Garg, A., Lam, J.S.L., Gao, L., 2016. Power consumption and tool life models for the production process. J. Clean. Prod. 131, 754–764. https://doi.org/10.1016/j.jclepro.2016.04.099

Garg, A., Lam, J.S.L., Gao, L., 2015. Energy conservation in manufacturing operations: Modelling the milling process by a new complexity-based evolutionary approach. J. Clean. Prod. 108, 34–45. https://doi.org/10.1016/j.jclepro.2015.06.043

Garg, A., Shankhwar, K., Jiang, D., Vijayaraghavan, V., Panda, B.N., Panda, S.S., 2018. An evolutionary framework in modelling of multi-output characteristics of the bone drilling process. Neural Comput. Appl. 29, 1233–1241. https://doi.org/10.1007/s00521-016-2632-x

Garg, Akhil, Garg, Ankit, Tai, K., 2014. A multi-gene genetic programming model for estimating stress-dependent soil water retention curves. Comput. Geosci. 18, 45–56. https://doi.org/10.1007/s10596-013-9381-z

Garud, K.S., Jayaraj, S., Lee, M.Y., 2021. A review on modeling of solar photovoltaic systems using artificial neural networks, fuzzy logic, genetic algorithm and hybrid models. Int. J. Energy Res. 45, 6–35. https://doi.org/10.1002/er.5608

Ghosh, S.K., 1991. Manufacturing engineering and technology. J. Mater. Process. Technol. 25, 112–113. https://doi.org/10.1016/0924-0136(91)90107-p

Gok, A., 2015. A new approach to minimization of the surface roughness and cutting force via fuzzy TOPSIS, multi-objective grey design and RSA. Measurement 70, 100–109. https://doi.org/10.1016/j.measurement.2015.03.037

Guo, Y., Loenders, J., Duflou, J., Lauwers, B., 2012. Optimization of energy consumption and surface quality in finish turning. Procedia CIRP 1, 512–517. https://doi.org/10.1016/j.procir.2012.04.091

Gupta, A.K., 2010. Predictive modelling of turning operations using response surface methodology, artificial neural networks and support vector regression. Int. J. Prod. Res. 48, 763–778. https://doi.org/10.1080/00207540802452132

Gurumurthy, A., Kodali, R., 2012. An application of analytic hierarchy process for the selection of a methodology to improve the product development process. J. Model. Manag. 7, 97–121. https://doi.org/10.1108/17465661211208820

Gutowski, T., Dahmus, J., Thiriez, A., 2006. Electrical Energy Requirements for Manufacturing Processes, in: 13th CIRP International Conference on Life Cycle Engineering, Leuven. pp. 623–628.

HA, K., S, K., M, B., 2004. An Energy Based Analytical Force Model for Orthogonal Cutting of Metal. CIRP Ann Manuf Technol 53, 91–94.

Hanafi, I., Khamlichi, A., Cabrera, F.M., Almansa, E., Jabbouri, A., 2012. Optimization of cutting conditions for sustainable machining of PEEK-CF30 using TiN tools. J. Clean. Prod. 33, 1–9. https://doi.org/10.1016/j.jclepro.2012.05.005

He, K., Tang, R., Zhang, Z., Sun, W., 2016. Energy Consumption Prediction System of Mechanical Processes Based on Empirical Models and Computer-Aided Manufacturing. J. Comput. Inf. Sci. Eng. 16, 041008. https://doi.org/10.1115/1.4033921

He, Yan, Liu, B., Zhang, X., Gao, H., Liu, X., 2012. A modeling method of task-oriented energy consumption for machining manufacturing system. J. Clean. Prod. 23, 167–174. https://doi.org/10.1016/j.jclepro.2011.10.033

He, Y, Liu, F., Wu, T., Zhong, F.P., Peng, B., 2012. Analysis and estimation of energy consumption for numerical control machining. Proc. Inst. Mech. Eng. Part B J. Eng. Manuf. 226, 255–266. https://doi.org/10.1177/0954405411417673

Hoang, N.D., Chen, C.T., Liao, K.W., 2017. Prediction of chloride diffusion in cement mortar using Multi-Gene Genetic Programming and Multivariate Adaptive Regression Splines. Meas. J. Int. Meas. Confed. 112, 141–149. https://doi.org/10.1016/j.measurement.2017.08.031

Hu, L., Cai, W., Shu, L., Xu, K., Zheng, H., Jia, S., 2020. Energy Optimisation For End Face Turning With Variable Material Removal Rate Considering the Spindle Speed Changes. Int. J. Precis. Eng. Manuf. - Green Technol. https://doi.org/10.1007/s40684-020-00210-w

Hu, L., Peng, C., Evans, S., Peng, T., Liu, Y., Tang, R., Tiwari, A., 2017. Minimising the machining energy consumption of a machine tool by sequencing the features of a part. Energy 121, 292–305. https://doi.org/10.1016/j.energy.2017.01.039

Huang, J., Liu, F., Xie, J., 2016. A method for determining the energy consumption of machine tools in the spindle start-up process before machining. Proc. Inst. Mech. Eng. Part B J. Eng. Manuf. 230, 1639–1649. https://doi.org/10.1177/0954405415600679

Iç, Y.T., Akkoç, F.S., Gümüşboğa, N., Ballı, Z., 2022. A New Multi-response Taguchi-Based Goal Programming Model for Sustainable Turning Process. Arab. J. Sci. Eng. 47, 3915–3928. https://doi.org/10.1007/s13369-021-06312-0

IEA, 2021. India Energy Outlook 2021. India Energy Outlook 2021. https://doi.org/10.1787/ec2fd78d-en

Imani Asrai, R., Newman, S.T., Nassehi, A., 2018. A mechanistic model of energy consumption in milling. Int. J. Prod. Res. 56, 642–659. https://doi.org/10.1080/00207543.2017.1404160

IMTMA, 2022. The Indian Machine Tool Manufacturers' Association-Annual Report 2020-21.pdf.

IPCC, 2014. Climate Change 2014: Synthesis Report. Contribution of Working Groups I, II and III to the Fifth Assessment Report of the Intergovernmental Panel on Climate Change [Core Writing Team, R.K. Pachauri and L.A. Meyer (eds.)]., IPCC, Geneva, Switzerland,.

IPCC, 2007. Climate Change 2007: Synthesis Report. Contribution of Working Groups I, II and III to the Fourth Assess_ment Report of the Intergovernmental Panel on Climate Change [Core Writing Team, Pachauri, R.K and Reisinger, A. (eds.)]., IPCC, Geneva, Switzerland.

IPCC, 2001. Climate Change 2001: Synthesis Report. A Contribution of Working Groups I, II, and III to the Third Assessment Report of the Integovernmental Panel on Climate Change [Watson, R.T. and the Core Writing Team (eds.)]., Cambridge University Press, Cambridge, United Kingdom, and New York, NY, USA,.

Iqbal, A., Dar, N.U., 2011. Optimal formation of fuzzy rule-base for predicting process's performance measures. Expert Syst. Appl. 38, 4802–4808. https://doi.org/10.1016/j.eswa.2010.09.166

Ji, Q., Li, C., Zhu, D., Jin, Y., Lv, Y., He, J., 2020. Structural design optimization of moving component in CNC machine tool for energy saving. J. Clean. Prod. 246, 118976. https://doi.org/10.1016/j.jclepro.2019.118976

Jia, S., Tang, R., Lv, J., Yuan, Q., Peng, T., 2017a. Energy consumption modeling of machining transient states based on finite state machine. Int. J. Adv. Manuf. Technol. 88, 2305–2320. https://doi.org/10.1007/s00170-016-8952-2

Jia, S., Tang, R., Lv, J., Zhang, Z., Yuan, Q., 2016. Energy modeling for variable material removal rate machining process: an end face turning case. Int. J. Adv. Manuf. Technol. 85, 2805–2818. https://doi.org/10.1007/s00170-015-8133-8

Jia, S., Yuan, Q., Ren, D., Lv, J., 2017b. Energy demand modeling methodology of key state transitions of turning processes. Energies 10, 1–19. https://doi.org/10.3390/en10040462

Jiang, Z., Gao, D., Lu, Y., Shang, Z., Kong, L., 2022. Optimisation of cutting parameters for minimising carbon emissions and cost in the turning process. Proc. Inst. Mech. Eng. Part C J. Mech. Eng. Sci. 236, 1973–1985. https://doi.org/10.1177/0954406220922872

Kant, G., Sangwan, K.S., 2015. Predictive modeling for power consumption in machining using artificial intelligence techniques. Procedia CIRP 26, 403–407. https://doi.org/10.1016/j.procir.2014.07.072

Kant, G., Sangwan, K.S., 2014. Prediction and optimization of machining parameters for minimizing power consumption and surface roughness in machining. J. Clean. Prod. 83, 151–164. https://doi.org/10.1016/j.jclepro.2014.07.073

Kara, S., Li, W., 2011. Unit process energy consumption models for material removal processes. CIRP Ann. - Manuf. Technol. 60, 37–40. https://doi.org/10.1016/j.cirp.2011.03.018

Khan, A.M., Liang, L., Mia, M., Gupta, M.K., Wei, Z., Jamil, M., Ning, H., 2021. Development of process performance simulator (PPS) and parametric optimization for sustainable machining considering carbon emission, cost and energy aspects. Renew. Sustain. Energy Rev. 139, 110738. https://doi.org/10.1016/j.rser.2021.110738

Kim, S.-Y., Shin, Y.-J., Kim, M.-S., Lee, J.-Y., Kim, E.-S., Ahn, S.-H., Yoon, H.-S., Yoon, Y.-C., Min, S., 2015. A Simplified Machine-Tool Power-Consumption Measurement Procedure and Methodology for Estimating Total Energy Consumption. J. Manuf. Sci. Eng. 138, 051004. https://doi.org/10.1115/1.4031713

Kumar, R., Bilga, P.S., Singh, S., 2017. Multi objective optimization using different methods of assigning weights to energy consumption responses, surface roughness and material removal rate during rough turning operation. J. Clean. Prod. 164, 45–57. https://doi.org/10.1016/j.jclepro.2017.06.077

Kuram, E., 2017. Nose radius and cutting speed effects during milling of AISI 304 material.

Mater. Manuf. Process. 32, 185–192. https://doi.org/10.1080/10426914.2016.1198019

Kuram, E., Ozcelik, B., Bayramoglu, M., Demirbas, E., Simsek, B.T., 2013. Optimization of cutting fluids and cutting parameters during end milling by using D-optimal design of experiments. J. Clean. Prod. 42, 159–166. https://doi.org/10.1016/j.jclepro.2012.11.003

Lee, J.Y., Shin, Y.J., Kim, M.S., Kim, E.S., Yoon, H.S., Kim, S.Y., Yoon, Y.C., Ahn, S.H., 2016. A Simplified Machine-Tool Power-Consumption Measurement Procedure and Methodology for Estimating Total Energy Consumption. J. Manuf. Sci. Eng. Trans. ASME 138, 1–9. https://doi.org/10.1115/1.4031713

Li, B., Tian, X., Zhang, M., 2022. Modeling and Multi-objective Optimization Method of Machine Tool Energy Consumption Considering Tool Wear. Int. J. Precis. Eng. Manuf. - Green Technol. 9, 127–141. https://doi.org/10.1007/s40684-021-00320-z

Li, C., Tang, Y., Cui, L., Li, P., 2015. A quantitative approach to analyze carbon emissions of CNC-based machining systems. J. Intell. Manuf. 26, 911–922. https://doi.org/10.1007/s10845-013-0812-4

Li, L., Deng, X., Zhao, J., Zhao, F., Sutherland, J.W., 2018. Multi-objective optimization of tool path considering efficiency, energy-saving and carbon-emission for free-form surface milling. J. Clean. Prod. 172, 3311–3322. https://doi.org/10.1016/j.jclepro.2017.07.219

Li, L., Yan, J., Xing, Z., 2013. Energy requirements evaluation of milling machines based on thermal equilibrium and empirical modelling. J. Clean. Prod. 52, 113–121. https://doi.org/10.1016/j.jclepro.2013.02.039

Li, W., Kara, S., 2011. An empirical model for predicting energy consumption of manufacturing processes: A case of turning process. Proc. Inst. Mech. Eng. Part B J. Eng. Manuf. 225, 1636–1646. https://doi.org/10.1177/2041297511398541

Li, W., Zein, A., Kara, S., Herrmann, C., 2011. An Investigation into Fixed Energy Consumption of Machine Tools, in: Glocalized Solutions for Sustainability in Manufacturing: Proceedings of the 18th CIRP International Conference on Life Cycle

Engineering. Springer Berlin Heidelberg, Berlin, Heidelberg, pp. 268–275. https://doi.org/10.1007/978-3-642-19692-8

Liman, M.M., Abou-El-Hossein, K., Abdulkadir, L.N., 2021. Fuzzy logic-based modeling and analysis of surface roughness, electrostatic charge, and material removal rate in ultrahigh precision diamond turning of rigid contact lens polymer. J. Thermoplast. Compos. Mater. 34, 952–976. https://doi.org/10.1177/0892705719850602

Liu, F., Xie, J., Liu, S., 2015. A method for predicting the energy consumption of the main driving system of a machine tool in a machining process. J. Clean. Prod. 105, 171–177. https://doi.org/10.1016/j.jclepro.2014.09.058

Liu, P., Liu, F., Qiu, H., 2017. A novel approach for acquiring the real-time energy efficiency of machine tools. Energy 121, 524–532. https://doi.org/10.1016/j.energy.2017.01.047

Liu, W., Li, Li, Cai, W., Li, C., Li, Lingling, Chen, X., Sutherland, J.W., 2020. Dynamic characteristics and energy consumption modelling of machine tools based on bond graph theory. Energy 212. https://doi.org/10.1016/j.energy.2020.118767

Lu, H.S., Chang, C.K., Hwang, N.C., Chung, C.T., 2009. Grey relational analysis coupled with principal component analysis for optimization design of the cutting parameters in high-speed end milling. J. Mater. Process. Technol. 209, 3808–3817. https://doi.org/10.1016/j.jmatprotec.2008.08.030

Luan, X., Zhang, S., Chen, J., Li, G., 2019. Energy modelling and energy saving strategy analysis of a machine tool during non-cutting status. Int. J. Prod. Res. 57, 4451–4467. https://doi.org/10.1080/00207543.2018.1436787

Lv, J., Peng, T., Tang, R., 2019. Energy modeling and a method for reducing energy loss due to cutting load during machining operations. Proc. Inst. Mech. Eng. Part B J. Eng. Manuf. 233, 699–710. https://doi.org/10.1177/0954405418769922

Lv, J., Tang, R., Jia, S., 2014. Therblig-based energy supply modeling of computer numerical control machine tools. J. Clean. Prod. 65, 168–177. https://doi.org/10.1016/j.jclepro.2013.09.055

Lv, J., Tang, R., Jia, S., Liu, Y., 2016. Experimental study on energy consumption of computer numerical control machine tools. J. Clean. Prod. 112, 3864–3874. https://doi.org/10.1016/j.jclepro.2015.07.040

Lv, J., Tang, R., Tang, W., Jia, S., Liu, Y., Cao, Y., 2018. An investigation into methods for predicting material removal energy consumption in turning. J. Clean. Prod. 193, 128–139. https://doi.org/10.1016/j.jclepro.2018.05.035

Lv, J., Tang, R., Tang, W., Liu, Y., Zhang, Y., Jia, S., 2017. An investigation into reducing the spindle acceleration energy consumption of machine tools. J. Clean. Prod. 143, 794–803. https://doi.org/10.1016/j.jclepro.2016.12.045

Ma, J., Ge, X., Chang, S.I., Lei, S., 2014. Assessment of cutting energy consumption and energy efficiency in machining of 4140 steel. Int. J. Adv. Manuf. Technol. 74, 1701–1708. https://doi.org/10.1007/s00170-014-6101-3

Mather, B.A., Maksimović, D., 2011. A simple digital power-factor correction rectifier controller. IEEE Trans. Power Electron. 26, 9–19. https://doi.org/10.1109/TPEL.2010.2051458

Meral, G., Sarıkaya, M., Mia, M., Dilipak, H., Şeker, U., Gupta, M.K., 2019. Multi-objective optimization of surface roughness, thrust force, and torque produced by novel drill geometries using Taguchi-based GRA. Int. J. Adv. Manuf. Technol. 101, 1595–1610. https://doi.org/10.1007/s00170-018-3061-z

Mia, M., 2018. Mathematical modeling and optimization of MQL assisted end milling characteristics based on RSM and Taguchi method. Meas. J. Int. Meas. Confed. 121, 249–260. https://doi.org/10.1016/j.measurement.2018.02.017

Mia, M., Dhar, N.R., 2017. Optimization of surface roughness and cutting temperature in high-pressure coolant-assisted hard turning using Taguchi method. Int. J. Adv. Manuf. Technol. 88, 739–753. https://doi.org/10.1007/s00170-016-8810-2

Mia, M., Gupta, M.K., Lozano, J.A., Carou, D., Pimenov, D.Y., Królczyk, G., Khan, A.M., Dhar, N.R., 2019. Multi-objective optimization and life cycle assessment of eco-friendly cryogenic N2 assisted turning of Ti-6Al-4V. J. Clean. Prod. 210, 121–133. https://doi.org/10.1016/j.jclepro.2018.10.334

Mitwalli, A.H., Leeb, S.B., Verghese, G.C., Thottuvelil, V.J., 1996. An adaptive digital controller for a unity power factor converter. IEEE Trans. Power Electron. 11, 374–382. https://doi.org/10.1109/63.486188

Monfreda, M., 2012. Principal Component Analysis: A Powerful Interpretative Tool at the Service of Analytical Methodology, in: Principal Component Analysis. InTech, pp. 49–66. https://doi.org/10.5772/36929

Mori, M., Fujishima, M., Inamasu, Y., Oda, Y., 2011. A study on energy efficiency improvement for machine tools. CIRP Ann. - Manuf. Technol. 60, 145–148. https://doi.org/10.1016/j.cirp.2011.03.099

Munoz, A.A., Sheng, P., 1995. An analytical approach for determining the environmental impact of machining processes. J. Mater. Process. Tech. 53, 736–758. https://doi.org/10.1016/0924-0136(94)01764-R

Naseri, F., Jafari, F., Mohseni, E., Tang, W., Feizbakhsh, A., Khatibinia, M., 2017. Experimental observations and SVM-based prediction of properties of polypropylene fibres reinforced self-compacting composites incorporating nano-CuO. Constr. Build. Mater. 143, 589–598. https://doi.org/10.1016/j.conbuildmat.2017.03.124

National Statistics Office, I., 2022. Energy Statistics 2022.

National Statistics Office, I., 2020. Energy Statistics 2020.

Newman, S.T., Nassehi, A., Imani-Asrai, R., Dhokia, V., 2012. Energy efficient process planning for CNC machining. CIRP J. Manuf. Sci. Technol. 5, 127–136. https://doi.org/10.1016/j.cirpj.2012.03.007

Nguyen, T.T., Mia, M., Dang, X.P., Le, C.H., Packianather, M.S., 2020. Green machining for the dry milling process of stainless steel 304. Proc. Inst. Mech. Eng. Part B J. Eng. Manuf. 234, 881–899. https://doi.org/10.1177/0954405419888126

O'Driscoll, E., O'Donnell, G.E., 2013. Industrial power and energy metering - a state-of-the-art review. J. Clean. Prod. 41, 53–64. https://doi.org/10.1016/j.jclepro.2012.09.046

Orove, J.O., Osegi, N.E., Eke, B.O., 2015. A Multi-Gene Genetic Programming

Application for Predicting Students Failure at School. African J. Comput. ICT 7, 1–12.

Öztürk, B., Uğur, L., Yildiz, A., 2019. Investigation of effect on energy consumption of surface roughness in X-axis and spindle servo motors in slot milling operation. Measurement 139, 92–102. https://doi.org/10.1016/j.measurement.2019.02.009

Pan, J., Li, C., Tang, Y., Li, W., Li, X., 2021. Energy Consumption Prediction of a CNC Machining Process with Incomplete Data. IEEE/CAA J. Autom. Sin. 8, 987–1000. https://doi.org/10.1109/JAS.2021.1003970

Panagiotopoulou, V.C., Stavropoulos, P., Chryssolouris, G., 2022. A critical review on the environmental impact of manufacturing: a holistic perspective. Int. J. Adv. Manuf. Technol. 118, 603–625. https://doi.org/10.1007/s00170-021-07980-w

Parida, A.K., Maity, K., 2017. Effect of nose radius on forces, and process parameters in hot machining of Inconel 718 using finite element analysis. Eng. Sci. Technol. an Int. J. 20, 687–693. https://doi.org/10.1016/j.jestch.2016.10.006

Park, H.S., Nguyen, T.T., Dang, X.P., 2016. Multi-objective optimization of turning process of hardened material for energy efficiency. Int. J. Precis. Eng. Manuf. 17, 1623–1631. https://doi.org/10.1007/s12541-016-0188-4

Pawade, R.S., Sonawane, H.A., Joshi, S.S., 2009. An analytical model to predict specific shear energy in high-speed turning of Inconel 718. Int. J. Mach. Tools Manuf. 49, 979–990. https://doi.org/10.1016/j.ijmachtools.2009.06.007

Pradhan, B.K., Ghosh, J., 2022. A computable general equilibrium (CGE) assessment of technological progress and carbon pricing in India's green energy transition via furthering its renewable capacity. Energy Econ. 106, 105788. https://doi.org/10.1016/j.eneco.2021.105788

Pusavec, F., Deshpande, A., Yang, S., M'Saoubi, R., Kopac, J., Dillon, O.W., Jawahir, I.S., 2015. Sustainable machining of high temperature Nickel alloy - Inconel 718: Part 2 - Chip breakability and optimization. J. Clean. Prod. 87, 941–952. https://doi.org/10.1016/j.jclepro.2014.10.085

Pye, S., Broad, O., Bataille, C., Brockway, P., Daly, H.E., Freeman, R., Gambhir, A., Geden, O., Rogan, F., Sanghvi, S., Tomei, J., Vorushylo, I., Watson, J., 2021. Modelling net-zero emissions energy systems requires a change in approach. Clim. Policy 21, 222–231. https://doi.org/10.1080/14693062.2020.1824891

Rajabi, Z., Eftekhari, M., Ghorbani, M., Ehteshamzadeh, M., Beirami, H., 2022. Prediction of the degree of steel corrosion damage in reinforced concrete using field-based data by multi-gene genetic programming approach. Soft Comput. 26, 9481–9496. https://doi.org/10.1007/s00500-021-06704-2

Rief, M., Karpuschewski, B., Kalhöfer, E., 2017. Evaluation and modeling of the energy demand during machining. CIRP J. Manuf. Sci. Technol. 19, 62–71. https://doi.org/10.1016/j.cirpj.2017.05.003

Saaty, T.L., 2008. Decision making with the analytic hierarchy process. Int. J. Serv. Sci. 1, 83. https://doi.org/10.1504/IJSSCI.2008.017590

Sadat-Shojai, M., Khorasani, M.T., Jamshidi, A., 2012. Hydrothermal processing of hydroxyapatite nanoparticles - A Taguchi experimental design approach. J. Cryst. Growth 361, 73–84. https://doi.org/10.1016/j.jcrysgro.2012.09.010

Sato, R., Shirase, K., Hayashi, A., 2018. Energy Consumption of Feed Drive Systems Based on Workpiece Setting Position in Five-Axis Machining Center. J. Manuf. Sci. Eng. Trans. ASME 140, 1–7. https://doi.org/10.1115/1.4037427

Schudeleit, T., Züst, S., Weiss, L., Wegener, K., 2016. The Total Energy Efficiency Index for machine tools. Energy 102, 682–693. https://doi.org/10.1016/j.energy.2016.02.126

Sealy, M.P., Liu, Z.Y., Zhang, D., Guo, Y.B., Liu, Z.Q., 2016. Energy consumption and modeling in precision hard milling. J. Clean. Prod. 135, 1591–1601. https://doi.org/10.1016/j.jclepro.2015.10.094

Shafiullah, M., Rana, M.J., Shahriar, M.S., Zahir, M.H., 2019. Low-frequency oscillation damping in the electric network through the optimal design of UPFC coordinated PSS employing MGGP. Meas. J. Int. Meas. Confed. 138, 118–131. https://doi.org/10.1016/j.measurement.2019.02.026

Shameem P, M., Villanthenkodath, M.A., Chittedi, K.R., 2022. Economic growth and sectoral level electricity consumption nexus in India: new evidence from combined cointegration and frequency domain causality approaches. Int. J. Sustain. Energy 1–18. https://doi.org/10.1080/14786451.2022.2095386

Shao, H., Wang, H.L., Zhao, X.M., 2004. A cutting power model for tool wear monitoring in milling. Int. J. Mach. Tools Manuf. 44, 1503–1509. https://doi.org/10.1016/j.ijmachtools.2004.05.003

Shemshadi, A., Shirazi, H., Toreihi, M., Tarokh, M.J., 2011. A fuzzy VIKOR method for supplier selection based on entropy measure for objective weighting. Expert Syst. Appl. 38, 12160–12167. https://doi.org/10.1016/j.eswa.2011.03.027

Sihag, N., Sangwan, K.S., 2020. A systematic literature review on machine tool energy consumption. J. Clean. Prod. 275, 123125. https://doi.org/10.1016/j.jclepro.2020.123125

Sihag, N., Sangwan, K.S., 2019. An improved micro analysis-based energy consumption and carbon emissions modeling approach for a milling center. Int. J. Adv. Manuf. Technol. 104, 705–721. https://doi.org/10.1007/s00170-019-03807-x

Singh, H., Kumar, P., 2006. Optimizing multi-machining characteristics through Taguchi's approach and utility concept. J. Manuf. Technol. Manag. 17, 255–274. https://doi.org/10.1108/17410380610642304

Sivaiah, P., Chakradhar, D., 2019. Performance improvement of cryogenic turning process during machining of 17-4 PH stainless steel using multi objective optimization techniques. Measurement 136, 326–336. https://doi.org/10.1016/j.measurement.2018.12.094

Sivasankar, S., Jeyapaul, R., 2012. Application of grey entropy and regression analysis for modelling and prediction on tool materials performance during EDM of hot pressed ZrB2at different duty cycles. Procedia Eng. 38, 3977–3991. https://doi.org/10.1016/j.proeng.2012.06.455

Soni, A., Mittal, A., Kapshe, M., 2017. Energy Intensity analysis of Indian manufacturing industries. Resour. Technol. 3, 353–357. https://doi.org/10.1016/j.reffit.2017.04.009

Su, Y., Li, Congbo, Zhao, Guoyong, Li, Chunxiao, Zhao, Guangxi, 2021. Prediction models for specific energy consumption of machine tools and surface roughness based on cutting parameters and tool wear. Proc. Inst. Mech. Eng. Part B J. Eng. Manuf. 235, 1225–1234. https://doi.org/10.1177/0954405420971064

Sukonna, R.T., Zaman, P.B., Dhar, N.R., 2022. Estimation of machining responses in hard turning under dry and HPC conditions using different AI based and statistical techniques. Int. J. Interact. Des. Manuf. https://doi.org/10.1007/s12008-022-00964-4

Triebe, M.J., Zhao, F., Sutherland, J.W., 2021. Genetic optimization for the design of a machine tool slide table for reduced energy consumption. J. Manuf. Sci. Eng. Trans. ASME 143, 1–10. https://doi.org/10.1115/1.4050551

Tseng, T.L. (Bill), Konada, U., Kwon, Y. (James), 2016. A novel approach to predict surface roughness in machining operations using fuzzy set theory. J. Comput. Des. Eng. 3, 1–13. https://doi.org/10.1016/j.jcde.2015.04.002

Tuo, J., Liu, F., Liu, P., Zhang, H., Cai, W., 2018. Energy efficiency evaluation for machining systems through virtual part. Energy 159, 172–183. https://doi.org/10.1016/j.energy.2018.06.096

U.S. EIA, 2021. International Energy Outlook with projections to 2050, U.S. Energy Information Administration.

U.S. EIA, 2019. International Energy Outlook 2019, U.S. Energy Information Administration. https://doi.org/https://www.eia.gov/outlooks/ieo/pdf/ieo2019.pdf

U.S. EIA, 2017. International Energy Outlook 2017, U.S. Energy Information Administration.

U.S. EIA, 2016. International Energy Outlook 2016, U.S. Energy Information Administration.

U.S. Energy Information Adm, 2022. CO2 emissions, EIA. https://www.eia.gov. Accessed 22 Apr 2022

Vukman, J., Lukic, D., Borojevic, S., Rodic, D., Milosevic, M., 2020. Application of Fuzzy Logic in the Analysis of Surface Roughness of Thin-Walled Aluminum Parts. Int. J.

Precis. Eng. Manuf. 21, 91–102. https://doi.org/10.1007/s12541-019-00229-3

Wang, B., Liu, Z., Song, Q., Wan, Y., Shi, Z., 2016. Proper selection of cutting parameters and cutting tool angle to lower the specific cutting energy during high speed machining of 7050-T7451 aluminum alloy. J. Clean. Prod. 129, 292–304. https://doi.org/10.1016/j.jclepro.2016.04.071

Wang, J., Tian, Y., Hu, X., Li, Y., Zhang, K., Liu, Y., 2021. Predictive modelling and Pareto optimization for energy efficient grinding based on aANN-embedded NSGA II algorithm. J. Clean. Prod. 327, 129479. https://doi.org/10.1016/j.jclepro.2021.129479

Wang, Q., Liu, F., Wang, X., 2014. Multi-objective optimization of machining parameters considering energy consumption. Int. J. Adv. Manuf. Technol. 71, 1133–1142. https://doi.org/10.1007/s00170-013-5547-z

Wang, Y., He, Y., Li, Y., Yan, P., Feng, L., 2015. An analysis framework for characterization of electrical power data in machining. Int. J. Precis. Eng. Manuf. 16, 2717–2723. https://doi.org/10.1007/s12541-015-0347-z

Warsi, S.S., Jaffery, S.H.I., Ahmad, R., Khan, M., Ali, L., Agha, M.H., Akram, S., 2018. Development of energy consumption map for orthogonal machining of Al 6061-T6 alloy. Proc. Inst. Mech. Eng. Part B J. Eng. Manuf. 232, 2510–2522. https://doi.org/10.1177/0954405417703424

Xiao, Q., Li, C., Tang, Y., Li, Lingling, Li, Li, 2019. A knowledge-driven method of adaptively optimizing process parameters for energy efficient turning. Energy 166, 142–156. https://doi.org/10.1016/j.energy.2018.09.191

Xie, J., Cai, W., Du, Y., Tang, Y., Tuo, J., 2021. Modelling approach for energy efficiency of machining system based on torque model and angular velocity. J. Clean. Prod. 293, 126249. https://doi.org/10.1016/j.jclepro.2021.126249

Xie, J., Liu, F., Huang, J., Qiu, H., 2016. Mapping acquisition of loading loss coefficient of main driving system of machine tools. Proc. Inst. Mech. Eng. Part B J. Eng. Manuf. 230, 1264–1271. https://doi.org/10.1177/0954405415623488

Yan, J., Li, L., 2013. Multi-objective optimization of milling parameters-the trade-offs

between energy, production rate and cutting quality. J. Clean. Prod. 52, 462–471. https://doi.org/10.1016/j.jclepro.2013.02.030

Yi, Q., Li, C., Tang, Y., Chen, X., 2015. Multi-objective parameter optimization of CNC machining for low carbon manufacturing. J. Clean. Prod. 95, 256–264. https://doi.org/10.1016/j.jclepro.2015.02.076

Yoon, H.S., Lee, J.Y., Kim, M.S., Ahn, S.H., 2014. Empirical power-consumption model for material removal in three-axis milling. J. Clean. Prod. 78, 54–62. https://doi.org/10.1016/j.jclepro.2014.03.061

Zadeh, L.A., 1975. The concept of a linguistic variable and its application to approximate reasoning-I. Inf. Sci. (Ny). 8, 199–249. https://doi.org/10.1016/0020-0255(75)90036-5

Zerti, A., Yallese, M.A., Meddour, I., Belhadi, S., Haddad, A., Mabrouki, T., 2019. Modeling and multi-objective optimization for minimizing surface roughness, cutting force, and power, and maximizing productivity for tempered stainless steel AISI 420 in turning operations. Int. J. Adv. Manuf. Technol. 102, 135–157. https://doi.org/10.1007/s00170-018-2984-8

Zhang, C., Li, W., Jiang, P., Gu, P., 2017. Experimental investigation and multi-objective optimization approach for low-carbon milling operation of aluminum. Proc. Inst. Mech. Eng. Part C J. Mech. Eng. Sci. 231, 2753–2772. https://doi.org/10.1177/0954406216640574

Zhang, C., Zhang, H., 2016. Modelling and prediction of tool wear using LS-SVM in milling operation. Int. J. Comput. Integr. Manuf. 29, 76–91. https://doi.org/10.1080/0951192X.2014.1003408

Zhang, G., Eddy Patuwo, B., Y. Hu, M., 1998. Forecasting with artificial neural networks: The state of the art. Int. J. Forecast. 14, 35–62. https://doi.org/10.1016/S0169-2070(97)00044-7

Zhang, H., Deng, Z., Fu, Y., Lv, L., Yan, C., 2017. A process parameters optimization method of multi-pass dry milling for high efficiency, low energy and low carbon emissions. J. Clean. Prod. 148, 174–184.

https://doi.org/10.1016/j.jclepro.2017.01.077

Zhang, Y., Li, Li, Liu, W., Li, Lingling, Gao, Y., Cai, W., Sutherland, J.W., 2022. Dynamics analysis and energy consumption modelling based on bond graph: Taking the spindle system as an example. J. Manuf. Syst. 62, 539–549. https://doi.org/10.1016/j.jmsy.2022.01.009

Zhao, G.Y., Liu, Z.Y., He, Y., Cao, H.J., Guo, Y.B., 2017. Energy consumption in machining: Classification, prediction, and reduction strategy. Energy 133, 142–157. https://doi.org/10.1016/j.energy.2017.05.110

Zhao, L., Fang, Y., Lou, P., Yan, J., Xiao, A., 2021. Cutting Parameter Optimization for Reducing Carbon Emissions Using Digital Twin. Int. J. Precis. Eng. Manuf. 22, 933–949. https://doi.org/10.1007/s12541-021-00486-1

Zhong, Q., Tang, R., Lv, J., Jia, S., Jin, M., 2016. Evaluation on models of calculating energy consumption in metal cutting processes: a case of external turning process. Int. J. Adv. Manuf. Technol. 82, 2087–2099. https://doi.org/10.1007/s00170-015-7477-4

Zhou, G., Lu, Q., Xiao, Z., Zhou, C., Tian, C., 2019. Cutting parameter optimization for machining operations considering carbon emissions. J. Clean. Prod. 208, 937–950. https://doi.org/10.1016/j.jclepro.2018.10.191

Zhou, G., Yuan, S., Lu, Q., Xiao, X., 2018a. A carbon emission quantitation model and experimental evaluation for machining process considering tool wear condition. Int. J. Adv. Manuf. Technol. 98, 565–577. https://doi.org/10.1007/s00170-018-2281-6

Zhou, G., Zhou, C., Lu, Q., Tian, C., Xiao, Z., 2018b. Feature-based carbon emission quantitation strategy for the part machining process. Int. J. Comput. Integr. Manuf. 31, 406–425. https://doi.org/10.1080/0951192X.2017.1328561

Zhou, L., Li, F., Wang, Y., Wang, L., Wang, G., 2022. A new empirical standby power and auxiliary power model of CNC machine tools. Int. J. Adv. Manuf. Technol. https://doi.org/10.1007/s00170-021-08274-x

Zhou, L., Li, J., Li, F., Xu, X., Wang, L., Wang, G., Kong, L., 2017. An improved cutting power model of machine tools in milling process. Int. J. Adv. Manuf. Technol. 91, 2383–2400. https://doi.org/10.1007/s00170-016-9929-x

Appendix-A: Variable Power Consumption Experimental data

Variable Power Consumption experimental data under dry environment

Exp. No.	n (rev/min)	Tc (s)	v_c (m/min)	f_r (mm/rev)	d_c (mm)	r (mm)	P_t (W)	P_{air} (W)	P_c (W)
	1600	1.00	285.03	0.08	1.0	0.4	2280	1740	540
	1600	1.25	279.67	0.08	1.0	0.4	2280	1740	540
	1600	1.50	274.31	0.08	1.0	0.4	2280	1740	540
	1600	1.75	268.95	0.08	1.0	0.4	2250	1740	510
	1600	2.00	263.59	0.08	1.0	0.4	2220	1740	480
	1600	2.25	258.23	0.08	1.0	0.4	2250	1740	510
	1600	2.50	252.87	0.08	1.0	0.4	2250	1740	510
	1600	2.75	247.52	0.08	1.0	0.4	2250	1740	510
	1600	3.00	242.16	0.08	1.0	0.4	2220	1740	480
	1600	3.25	236.80	0.08	1.0	0.4	2190	1740	450
	1600	3.50	231.44	0.08	1.0	0.4	2190	1740	450
	1600	3.75	226.08	0.08	1.0	0.4	2190	1740	450
	1600	4.00	220.72	0.08	1.0	0.4	2190	1740	450
	1600	4.25	215.36	0.08	1.0	0.4	2190	1740	450
1	1600	4.50	210.00	0.08	1.0	0.4	2160	1740	420
	1600	4.75	204.64	0.08	1.0	0.4	2160	1740	420
	1600	5.00	199.29	0.08	1.0	0.4	2130	1740	390
	1600	5.25	193.93	0.08	1.0	0.4	2160	1740	420
	1600	5.50	188.57	0.08	1.0	0.4	2130	1740	390
	1600	5.75	183.21	0.08	1.0	0.4	2130	1740	390
	1600	6.00	177.85	0.08	1.0	0.4	2100	1740	360
	1600	6.25	172.49	0.08	1.0	0.4	2130	1740	390
	1600	6.50	167.13	0.08	1.0	0.4	2100	1740	360
	1600	6.75	161.77	0.08	1.0	0.4	2100	1740	360
	1600	7.00	156.41	0.08	1.0	0.4	2100	1740	360
	1600	7.25	151.05	0.08	1.0	0.4	2070	1740	330
	1600	7.50	145.70	0.08	1.0	0.4	2070	1740	330
	1600	7.75	140.34	0.08	1.0	0.4	2070	1740	330
	1600	8.00	134.98	0.08	1.0	0.4	2040	1740	300

	1600	8.25	129.62	0.08	1.0	0.4	2040	1740	300
	1600	8.50	124.26	0.08	1.0	0.4	2040	1740	300
	1600	8.75	118.90	0.08	1.0	0.4	2040	1740	300
	1600	9.00	113.54	0.08	1.0	0.4	2040	1740	300
	1600	9.25	108.18	0.08	1.0	0.4	2040	1740	300
	1600	9.50	102.82	0.08	1.0	0.4	2040	1740	300
	1600	9.75	97.47	0.08	1.0	0.4	2040	1740	300
	1600	10.00	92.11	0.08	1.0	0.4	2010	1740	270
	1600	10.25	86.75	0.08	1.0	0.4	2010	1740	270
	1600	10.50	81.39	0.08	1.0	0.4	2010	1740	270
	1600	10.75	76.03	0.08	1.0	0.4	2010	1740	270
	1600	11.00	70.67	0.08	1.0	0.4	1950	1740	210
	1600	11.25	65.31	0.08	1.0	0.4	1920	1740	180
	1600	11.50	59.95	0.08	1.0	0.4	1920	1740	180
	1600	11.75	54.59	0.08	1.0	0.4	1890	1740	150
	1600	12.00	49.24	0.08	1.0	0.4	1860	1740	120
	1600	12.25	43.88	0.08	1.0	0.4	1860	1740	120
	1600	12.50	38.52	0.08	1.0	0.4	1860	1740	120
	1600	12.75	33.16	0.08	1.0	0.4	1830	1740	90
	1600	13.00	27.80	0.08	1.0	0.4	1830	1740	90
	1600	13.25	22.44	0.08	1.0	0.4	1800	1740	60
	1600	13.50	17.08	0.08	1.0	0.4	1770	1740	30
	1600	0.50	290.39	0.12	1.4	1.2	2670	1800	870
	1600	0.75	282.35	0.12	1.4	1.2	2670	1800	870
	1600	1.00	274.31	0.12	1.4	1.2	2670	1800	870
	1600	1.25	266.27	0.12	1.4	1.2	2640	1800	840
	1600	1.50	258.23	0.12	1.4	1.2	2610	1800	810
2	1600	1.75	250.20	0.12	1.4	1.2	2610	1800	810
	1600	2.00	242.16	0.12	1.4	1.2	2580	1800	780
	1600	2.25	234.12	0.12	1.4	1.2	2550	1800	750
	1600	2.50	226.08	0.12	1.4	1.2	2550	1800	750
	1600	2.75	218.04	0.12	1.4	1.2	2520	1800	720
	1600	3.00	210.00	0.12	1.4	1.2	2490	1800	690

	1600	3.25	201.96	0.12	1.4	1.2	2490	1800	690
	1600	3.50	193.93	0.12	1.4	1.2	2460	1800	660
	1600	3.75	185.89	0.12	1.4	1.2	2430	1800	630
	1600	4.00	177.85	0.12	1.4	1.2	2430	1800	630
	1600	4.25	169.81	0.12	1.4	1.2	2400	1800	600
	1600	4.50	161.77	0.12	1.4	1.2	2400	1800	600
	1600	4.75	153.73	0.12	1.4	1.2	2370	1800	570
	1600	5.00	145.70	0.12	1.4	1.2	2370	1800	570
	1600	5.25	137.66	0.12	1.4	1.2	2340	1800	540
	1600	5.50	129.62	0.12	1.4	1.2	2340	1800	540
	1600	5.75	121.58	0.12	1.4	1.2	2310	1800	510
	1600	6.00	113.54	0.12	1.4	1.2	2310	1800	510
	1600	6.25	105.50	0.12	1.4	1.2	2280	1800	480
	1600	6.50	97.47	0.12	1.4	1.2	2250	1800	450
	1600	6.75	89.43	0.12	1.4	1.2	2220	1800	420
	1600	7.00	81.39	0.12	1.4	1.2	2190	1800	390
	1600	7.25	73.35	0.12	1.4	1.2	2160	1800	360
	1600	7.50	65.31	0.12	1.4	1.2	2130	1800	330
	1600	7.75	57.27	0.12	1.4	1.2	2100	1800	300
	1600	8.00	49.24	0.12	1.4	1.2	2040	1800	240
	1600	8.25	41.20	0.12	1.4	1.2	2010	1800	210
	1600	8.50	33.16	0.12	1.4	1.2	1980	1800	180
	1600	8.75	25.12	0.12	1.4	1.2	1920	1800	120
	1600	9.00	17.08	0.12	1.4	1.2	1890	1800	90
	1600	9.25	9.04	0.12	1.4	1.2	1830	1800	30
3	1600	1.00	263.59	0.16	1.8	0.8	3360	1740	1620
	1600	1.25	252.87	0.16	1.8	0.8	3360	1740	1620
	1600	1.50	242.16	0.16	1.8	0.8	3210	1740	1470
	1600	1.75	231.44	0.16	1.8	0.8	3210	1740	1470
	1600	2.00	220.72	0.16	1.8	0.8	3150	1740	1410
	1600	2.25	210.00	0.16	1.8	0.8	3120	1740	1380
	1600	2.50	199.29	0.16	1.8	0.8	3030	1740	1290
	1600	2.75	188.57	0.16	1.8	0.8	3000	1740	1260

	1600	3.00	177.85	0.16	1.8	0.8	3000	1740	1260
	1600	3.25	167.13	0.16	1.8	0.8	2910	1740	1170
	1600	3.50	156.41	0.16	1.8	0.8	2850	1740	1110
	1600	3.75	145.70	0.16	1.8	0.8	2820	1740	1080
	1600	4.00	134.98	0.16	1.8	0.8	2760	1740	1020
	1600	4.25	124.26	0.16	1.8	0.8	2670	1740	930
	1600	4.50	113.54	0.16	1.8	0.8	2610	1740	870
	1600	4.75	102.82	0.16	1.8	0.8	2610	1740	870
	1600	5.00	92.11	0.16	1.8	0.8	2490	1740	750
	1600	5.25	81.39	0.16	1.8	0.8	2430	1740	690
	1600	5.50	70.67	0.16	1.8	0.8	2370	1740	630
	1600	5.75	59.95	0.16	1.8	0.8	2330	1740	590
	1600	6.00	49.24	0.16	1.8	0.8	2300	1740	560
	1600	6.25	38.52	0.16	1.8	0.8	2200	1740	460
	1600	6.50	27.80	0.16	1.8	0.8	2180	1740	440
	1600	6.75	17.08	0.16	1.8	0.8	2120	1740	380
	1600	7.00	6.36	0.16	1.8	0.8	2050	1740	310
4	2000	0.75	357.96	0.08	1.4	0.8	2640	1860	780
	2000	1.00	349.59	0.08	1.4	0.8	2610	1860	750
	2000	1.25	341.21	0.08	1.4	0.8	2610	1860	750
	2000	1.50	332.84	0.08	1.4	0.8	2610	1860	750
	2000	1.75	324.47	0.08	1.4	0.8	2580	1860	720
	2000	2.00	316.09	0.08	1.4	0.8	2550	1860	690
	2000	2.25	307.72	0.08	1.4	0.8	2550	1860	690
	2000	2.50	299.35	0.08	1.4	0.8	2520	1860	660
	2000	2.75	290.97	0.08	1.4	0.8	2520	1860	660
	2000	3.00	282.60	0.08	1.4	0.8	2490	1860	630
	2000	3.25	274.23	0.08	1.4	0.8	2490	1860	630
	2000	3.50	265.85	0.08	1.4	0.8	2460	1860	600
	2000	3.75	257.48	0.08	1.4	0.8	2460	1860	600
	2000	4.00	249.11	0.08	1.4	0.8	2430	1860	570
	2000	4.25	240.73	0.08	1.4	0.8	2400	1860	540
	2000	4.50	232.36	0.08	1.4	0.8	2400	1860	540

	2000	4.75	223.99	0.08	1.4	0.8	2370	1860	510
	2000	5.00	215.61	0.08	1.4	0.8	2370	1860	510
	2000	5.25	207.24	0.08	1.4	0.8	2340	1860	480
	2000	5.50	198.87	0.08	1.4	0.8	2310	1860	450
	2000	5.75	190.49	0.08	1.4	0.8	2310	1860	450
	2000	6.00	182.12	0.08	1.4	0.8	2280	1860	420
	2000	6.25	173.75	0.08	1.4	0.8	2250	1860	390
	2000	6.50	165.37	0.08	1.4	0.8	2250	1860	390
	2000	6.75	157.00	0.08	1.4	0.8	2220	1860	360
	2000	7.00	148.63	0.08	1.4	0.8	2220	1860	360
	2000	7.25	140.25	0.08	1.4	0.8	2190	1860	330
	2000	7.50	131.88	0.08	1.4	0.8	2190	1860	330
	2000	7.75	123.51	0.08	1.4	0.8	2160	1860	300
	2000	8.00	115.13	0.08	1.4	0.8	2130	1860	270
	2000	8.25	106.76	0.08	1.4	0.8	2130	1860	270
	2000	8.50	98.39	0.08	1.4	0.8	2100	1860	240
	2000	8.75	90.01	0.08	1.4	0.8	2070	1860	210
	2000	9.00	81.64	0.08	1.4	0.8	2070	1860	210
	2000	9.25	73.27	0.08	1.4	0.8	2040	1860	180
	2000	9.50	64.89	0.08	1.4	0.8	2040	1860	180
	2000	9.75	56.52	0.08	1.4	0.8	2040	1860	180
	2000	10.00	48.15	0.08	1.4	0.8	1980	1860	120
	2000	10.25	39.77	0.08	1.4	0.8	1950	1860	90
	2000	10.50	31.40	0.08	1.4	0.8	1920	1860	60
	2000	10.75	23.03	0.08	1.4	0.8	1890	1860	30
	2000	11.00	14.65	0.08	1.4	0.8	1880	1860	20
	2000	11.25	6.28	0.08	1.4	0.8	1870	1860	10
5	2000	0.75	345.40	0.12	1.8	0.4	3690	1860	1830
	2000	1.00	332.84	0.12	1.8	0.4	3690	1860	1830
	2000	1.25	320.28	0.12	1.8	0.4	3600	1860	1740
	2000	1.50	307.72	0.12	1.8	0.4	3540	1860	1680
	2000	1.75	295.16	0.12	1.8	0.4	3480	1860	1620
	2000	2.00	282.60	0.12	1.8	0.4	3510	1860	1650

	2000	2.25	270.04	0.12	1.8	0.4	3390	1860	1530
	2000	2.50	257.48	0.12	1.8	0.4	3450	1860	1590
	2000	2.75	244.92	0.12	1.8	0.4	3450	1860	1590
	2000	3.00	232.36	0.12	1.8	0.4	3300	1860	1440
	2000	3.25	219.80	0.12	1.8	0.4	3270	1860	1410
	2000	3.50	207.24	0.12	1.8	0.4	3120	1860	1260
	2000	3.75	194.68	0.12	1.8	0.4	3030	1860	1170
	2000	4.00	182.12	0.12	1.8	0.4	3010	1860	1150
	2000	4.25	169.56	0.12	1.8	0.4	3000	1860	1140
	2000	4.50	157.00	0.12	1.8	0.4	2850	1860	990
	2000	4.75	144.44	0.12	1.8	0.4	2760	1860	900
	2000	5.00	131.88	0.12	1.8	0.4	2700	1860	840
	2000	5.25	119.32	0.12	1.8	0.4	2670	1860	810
	2000	5.50	106.76	0.12	1.8	0.4	2580	1860	720
	2000	5.75	94.20	0.12	1.8	0.4	2520	1860	660
	2000	6.00	81.64	0.12	1.8	0.4	2430	1860	570
	2000	6.25	69.08	0.12	1.8	0.4	2400	1860	540
	2000	6.50	56.52	0.12	1.8	0.4	2310	1860	450
	2000	6.75	43.96	0.12	1.8	0.4	2220	1860	360
	2000	7.00	31.40	0.12	1.8	0.4	2130	1860	270
	2000	7.25	18.84	0.12	1.8	0.4	2050	1860	190
	2000	7.50	6.28	0.12	1.8	0.4	1900	1860	40
	2000	0.50	349.59	0.16	1.0	1.2	2820	1890	930
	2000	0.75	332.84	0.16	1.0	1.2	2790	1890	900
	2000	1.00	316.09	0.16	1.0	1.2	2760	1890	870
	2000	1.25	299.35	0.16	1.0	1.2	2730	1890	840
	2000	1.50	282.60	0.16	1.0	1.2	2700	1890	810
6	2000	1.75	265.85	0.16	1.0	1.2	2670	1890	780
	2000	2.00	249.11	0.16	1.0	1.2	2610	1890	720
	2000	2.25	232.36	0.16	1.0	1.2	2580	1890	690
	2000	2.50	215.61	0.16	1.0	1.2	2520	1890	630
	2000	2.75	198.87	0.16	1.0	1.2	2490	1890	600
	2000	3.00	182.12	0.16	1.0	1.2	2490	1890	600

	2000	3.25	165.37	0.16	1.0	1.2	2430	1890	540
	2000	3.50	148.63	0.16	1.0	1.2	2370	1890	480
	2000	3.75	131.88	0.16	1.0	1.2	2370	1890	480
	2000	4.00	115.13	0.16	1.0	1.2	2340	1890	450
	2000	4.25	98.39	0.16	1.0	1.2	2280	1890	390
	2000	4.50	81.64	0.16	1.0	1.2	2250	1890	360
	2000	4.75	64.89	0.16	1.0	1.2	2190	1890	300
	2000	5.00	48.15	0.16	1.0	1.2	2160	1890	270
	2000	5.25	31.40	0.16	1.0	1.2	2070	1890	180
	2000	5.50	14.65	0.16	1.0	1.2	1980	1890	90
	2400	0.75	423.52	0.08	1.8	1.2	3300	2070	1230
	2400	1.00	411.47	0.08	1.8	1.2	3300	2070	1230
	2400	1.25	399.41	0.08	1.8	1.2	3270	2070	1200
	2400	1.50	387.35	0.08	1.8	1.2	3240	2070	1170
	2400	1.75	375.29	0.08	1.8	1.2	3210	2070	1140
	2400	2.00	363.24	0.08	1.8	1.2	3180	2070	1110
	2400	2.25	351.18	0.08	1.8	1.2	3150	2070	1080
	2400	2.50	339.12	0.08	1.8	1.2	3120	2070	1050
	2400	2.75	327.06	0.08	1.8	1.2	3090	2070	1020
	2400	3.00	315.00	0.08	1.8	1.2	3060	2070	990
	2400	3.25	302.95	0.08	1.8	1.2	3000	2070	930
7	2400	3.50	290.89	0.08	1.8	1.2	2970	2070	900
	2400	3.75	278.83	0.08	1.8	1.2	2940	2070	870
	2400	4.00	266.77	0.08	1.8	1.2	2940	2070	870
	2400	4.25	254.72	0.08	1.8	1.2	2910	2070	840
	2400	4.50	242.66	0.08	1.8	1.2	2850	2070	780
	2400	4.75	230.60	0.08	1.8	1.2	2820	2070	750
	2400	5.00	218.54	0.08	1.8	1.2	2790	2070	720
	2400	5.25	206.49	0.08	1.8	1.2	2760	2070	690
	2400	5.50	194.43	0.08	1.8	1.2	2730	2070	660
	2400	5.75	182.37	0.08	1.8	1.2	2670	2070	600
	2400	6.00	170.31	0.08	1.8	1.2	2650	2070	580
	2400	6.25	158.26	0.08	1.8	1.2	2630	2070	560

	2400	6.50	146.20	0.08	1.8	1.2	2600	2070	530
	2400	6.75	134.14	0.08	1.8	1.2	2580	2070	510
	2400	7.00	122.08	0.08	1.8	1.2	2570	2070	500
	2400	7.25	110.03	0.08	1.8	1.2	2540	2070	470
	2400	7.50	97.97	0.08	1.8	1.2	2510	2070	440
	2400	7.75	85.91	0.08	1.8	1.2	2490	2070	420
	2400	8.00	73.85	0.08	1.8	1.2	2450	2070	380
	2400	8.25	61.80	0.08	1.8	1.2	2310	2070	240
	2400	8.50	49.74	0.08	1.8	1.2	2280	2070	210
	2400	8.75	37.68	0.08	1.8	1.2	2220	2070	150
	2400	9.00	25.62	0.08	1.8	1.2	2190	2070	120
	2400	9.25	13.56	0.08	1.8	1.2	2160	2070	90
	2400	0.50	423.52	0.12	1.0	0.8	3030	1980	1050
	2400	0.75	405.44	0.12	1.0	0.8	2970	1980	990
	2400	1.00	387.35	0.12	1.0	0.8	2940	1980	960
	2400	1.25	369.26	0.12	1.0	0.8	2880	1980	900
	2400	1.50	351.18	0.12	1.0	0.8	2940	1980	960
	2400	1.75	333.09	0.12	1.0	0.8	2850	1980	870
	2400	2.00	315.00	0.12	1.0	0.8	2760	1980	780
	2400	2.25	296.92	0.12	1.0	0.8	2730	1980	750
	2400	2.50	278.83	0.12	1.0	0.8	2670	1980	690
	2400	2.75	260.75	0.12	1.0	0.8	2640	1980	660
8	2400	3.00	242.66	0.12	1.0	0.8	2610	1980	630
	2400	3.25	224.57	0.12	1.0	0.8	2550	1980	570
	2400	3.50	206.49	0.12	1.0	0.8	2490	1980	510
	2400	3.75	188.40	0.12	1.0	0.8	2460	1980	480
	2400	4.00	170.31	0.12	1.0	0.8	2410	1980	430
	2400	4.25	152.23	0.12	1.0	0.8	2400	1980	420
	2400	4.50	134.14	0.12	1.0	0.8	2390	1980	410
	2400	4.75	116.05	0.12	1.0	0.8	2370	1980	390
	2400	5.00	97.97	0.12	1.0	0.8	2340	1980	360
	2400	5.25	79.88	0.12	1.0	0.8	2310	1980	330
	2400	5.50	61.80	0.12	1.0	0.8	2220	1980	240

	2400	5.75	43.71	0.12	1.0	0.8	2160	1980	180
	2400	6.00	25.62	0.12	1.0	0.8	2130	1980	150
	2400	6.25	7.54	0.12	1.0	0.8	2100	1980	120
9	2400	0.50	411.47	0.16	1.4	0.4	3990	2040	1950
	2400	0.75	387.35	0.16	1.4	0.4	3990	2040	1950
	2400	1.00	363.24	0.16	1.4	0.4	3900	2040	1860
	2400	1.25	339.12	0.16	1.4	0.4	3780	2040	1740
	2400	1.50	315.00	0.16	1.4	0.4	3660	2040	1620
	2400	1.75	290.89	0.16	1.4	0.4	3510	2040	1470
	2400	2.00	266.77	0.16	1.4	0.4	3420	2040	1380
	2400	2.25	242.66	0.16	1.4	0.4	3330	2040	1290
	2400	2.50	218.54	0.16	1.4	0.4	3210	2040	1170
	2400	2.75	194.43	0.16	1.4	0.4	3090	2040	1050
	2400	3.00	170.31	0.16	1.4	0.4	2970	2040	930
	2400	3.25	146.20	0.16	1.4	0.4	2880	2040	840
	2400	3.50	122.08	0.16	1.4	0.4	2760	2040	720
	2400	3.75	97.97	0.16	1.4	0.4	2640	2040	600
	2400	4.00	73.85	0.16	1.4	0.4	2520	2040	480
	2400	4.25	49.74	0.16	1.4	0.4	2460	2040	420
	2400	4.50	25.62	0.16	1.4	0.4	2430	2040	390
	2400	4.75	1.51	0.16	1.4	0.4	2220	2040	180

Variable Power Consumption experimental data under wet environment

Exp. No.	n (rev/min)	Tc (s)	v_c (m/min)	f_r (mm/rev)	d_c (mm)	r (mm)	P_t (W)	P_{air} (W)	P_c (W)
1	1600	1.25	279.67	0.08	1.0	0.4	2640	2130	510
	1600	1.50	274.31	0.08	1.0	0.4	2670	2130	540
	1600	1.75	268.95	0.08	1.0	0.4	2670	2130	540
	1600	2.00	263.59	0.08	1.0	0.4	2670	2130	540
	1600	2.25	258.23	0.08	1.0	0.4	2670	2130	540
	1600	2.50	252.87	0.08	1.0	0.4	2670	2130	540
	1600	2.75	247.52	0.08	1.0	0.4	2640	2130	510
	1600	3.00	242.16	0.08	1.0	0.4	2640	2130	510
	1600	3.25	236.80	0.08	1.0	0.4	2640	2130	510
	1600	3.50	231.44	0.08	1.0	0.4	2640	2130	510
	1600	3.75	226.08	0.08	1.0	0.4	2610	2130	480
	1600	4.00	220.72	0.08	1.0	0.4	2610	2130	480
	1600	4.25	215.36	0.08	1.0	0.4	2580	2130	450
	1600	4.50	210.00	0.08	1.0	0.4	2580	2130	450
	1600	4.75	204.64	0.08	1.0	0.4	2580	2130	450
	1600	5.00	199.29	0.08	1.0	0.4	2580	2130	450
	1600	5.25	193.93	0.08	1.0	0.4	2580	2130	450
	1600	5.50	188.57	0.08	1.0	0.4	2550	2130	420
	1600	5.75	183.21	0.08	1.0	0.4	2550	2130	420
	1600	6.00	177.85	0.08	1.0	0.4	2520	2130	390
	1600	6.25	172.49	0.08	1.0	0.4	2520	2130	390
	1600	6.50	167.13	0.08	1.0	0.4	2520	2130	390
	1600	6.75	161.77	0.08	1.0	0.4	2490	2130	360
	1600	7.00	156.41	0.08	1.0	0.4	2490	2130	360
	1600	7.25	151.05	0.08	1.0	0.4	2490	2130	360
	1600	7.50	145.70	0.08	1.0	0.4	2460	2130	330
	1600	7.75	140.34	0.08	1.0	0.4	2460	2130	330
	1600	8.00	134.98	0.08	1.0	0.4	2460	2130	330
	1600	8.25	129.62	0.08	1.0	0.4	2460	2130	330
	1600	8.50	124.26	0.08	1.0	0.4	2430	2130	300

	1600	8.75	118.90	0.08	1.0	0.4	2430	2130	300
	1600	9.00	113.54	0.08	1.0	0.4	2430	2130	300
	1600	9.25	108.18	0.08	1.0	0.4	2400	2130	270
	1600	9.50	102.82	0.08	1.0	0.4	2370	2130	240
	1600	9.75	97.47	0.08	1.0	0.4	2400	2130	270
	1600	10.00	92.11	0.08	1.0	0.4	2400	2130	270
	1600	10.25	86.75	0.08	1.0	0.4	2370	2130	240
	1600	10.50	81.39	0.08	1.0	0.4	2340	2130	210
	1600	10.75	76.03	0.08	1.0	0.4	2340	2130	210
	1600	11.00	70.67	0.08	1.0	0.4	2310	2130	180
	1600	11.25	65.31	0.08	1.0	0.4	2310	2130	180
	1600	11.50	59.95	0.08	1.0	0.4	2280	2130	150
	1600	11.75	54.59	0.08	1.0	0.4	2280	2130	150
	1600	12.00	49.24	0.08	1.0	0.4	2280	2130	150
	1600	12.25	43.88	0.08	1.0	0.4	2250	2130	120
	1600	12.50	38.52	0.08	1.0	0.4	2220	2130	90
	1600	12.75	33.16	0.08	1.0	0.4	2190	2130	60
	1600	13.00	27.80	0.08	1.0	0.4	2190	2130	60
	1600	13.25	22.44	0.08	1.0	0.4	2160	2130	30
	1600	13.50	17.08	0.08	1.0	0.4	2150	2130	20
	1600	13.75	11.72	0.08	1.0	0.4	2140	2130	10
2	1600	0.25	298.43	0.12	1.4	1.2	2460	2100	360
	1600	0.50	290.39	0.12	1.4	1.2	2910	2100	810
	1600	0.75	282.35	0.12	1.4	1.2	2940	2100	840
	1600	1.00	274.31	0.12	1.4	1.2	2940	2100	840
	1600	1.25	266.27	0.12	1.4	1.2	2940	2100	840
	1600	1.50	258.23	0.12	1.4	1.2	2910	2100	810
	1600	1.75	250.20	0.12	1.4	1.2	2910	2100	810
	1600	2.00	242.16	0.12	1.4	1.2	2880	2100	780
	1600	2.25	234.12	0.12	1.4	1.2	2880	2100	780
	1600	2.50	226.08	0.12	1.4	1.2	2850	2100	750
	1600	2.75	218.04	0.12	1.4	1.2	2790	2100	690
	1600	3.00	210.00	0.12	1.4	1.2	2790	2100	690

	1600	3.25	201.96	0.12	1.4	1.2	2790	2100	690
	1600	3.50	193.93	0.12	1.4	1.2	2730	2100	630
	1600	3.75	185.89	0.12	1.4	1.2	2700	2100	600
	1600	4.00	177.85	0.12	1.4	1.2	2700	2100	600
	1600	4.25	169.81	0.12	1.4	1.2	2700	2100	600
	1600	4.50	161.77	0.12	1.4	1.2	2670	2100	570
	1600	4.75	153.73	0.12	1.4	1.2	2670	2100	570
	1600	5.00	145.70	0.12	1.4	1.2	2640	2100	540
	1600	5.25	137.66	0.12	1.4	1.2	2640	2100	540
	1600	5.50	129.62	0.12	1.4	1.2	2610	2100	510
	1600	5.75	121.58	0.12	1.4	1.2	2610	2100	510
	1600	6.00	113.54	0.12	1.4	1.2	2580	2100	480
	1600	6.25	105.50	0.12	1.4	1.2	2580	2100	480
	1600	6.50	97.47	0.12	1.4	1.2	2550	2100	450
	1600	6.75	89.43	0.12	1.4	1.2	2520	2100	420
	1600	7.00	81.39	0.12	1.4	1.2	2490	2100	390
	1600	7.25	73.35	0.12	1.4	1.2	2490	2100	390
	1600	7.50	65.31	0.12	1.4	1.2	2430	2100	330
	1600	7.75	57.27	0.12	1.4	1.2	2400	2100	300
	1600	8.00	49.24	0.12	1.4	1.2	2370	2100	270
	1600	8.25	41.20	0.12	1.4	1.2	2310	2100	210
	1600	8.50	33.16	0.12	1.4	1.2	2250	2100	150
	1600	8.75	25.12	0.12	1.4	1.2	2190	2100	90
	1600	9.00	17.08	0.12	1.4	1.2	2160	2100	60
	1600	9.25	9.04	0.12	1.4	1.2	2130	2100	30
3	1600	0.50	285.03	0.16	1.8	0.8	3570	2100	1470
	1600	0.75	274.31	0.16	1.8	0.8	3570	2100	1470
	1600	1.00	263.59	0.16	1.8	0.8	3570	2100	1470
	1600	1.25	252.87	0.16	1.8	0.8	3510	2100	1410
	1600	1.50	242.16	0.16	1.8	0.8	3450	2100	1350
	1600	1.75	231.44	0.16	1.8	0.8	3450	2100	1350
	1600	2.00	220.72	0.16	1.8	0.8	3360	2100	1260
	1600	2.25	210.00	0.16	1.8	0.8	3330	2100	1230

	1600	2.50	199.29	0.16	1.8	0.8	3300	2100	1200
	1600	2.75	188.57	0.16	1.8	0.8	3280	2100	1180
	1600	3.00	177.85	0.16	1.8	0.8	3250	2100	1150
	1600	3.25	167.13	0.16	1.8	0.8	3180	2100	1080
	1600	3.50	156.41	0.16	1.8	0.8	3150	2100	1050
	1600	3.75	145.70	0.16	1.8	0.8	3030	2100	930
	1600	4.00	134.98	0.16	1.8	0.8	3030	2100	930
	1600	4.25	124.26	0.16	1.8	0.8	2910	2100	810
	1600	4.50	113.54	0.16	1.8	0.8	2850	2100	750
	1600	4.75	102.82	0.16	1.8	0.8	2790	2100	690
	1600	5.00	92.11	0.16	1.8	0.8	2730	2100	630
	1600	5.25	81.39	0.16	1.8	0.8	2670	2100	570
	1600	5.50	70.67	0.16	1.8	0.8	2610	2100	510
	1600	5.75	59.95	0.16	1.8	0.8	2550	2100	450
	1600	6.00	49.24	0.16	1.8	0.8	2490	2100	390
	1600	6.25	38.52	0.16	1.8	0.8	2400	2100	300
	1600	6.50	27.80	0.16	1.8	0.8	2340	2100	240
	1600	6.75	17.08	0.16	1.8	0.8	2280	2100	180
	1600	7.00	6.36	0.16	1.8	0.8	2160	2100	60
4	2000	0.50	366.33	0.08	1.4	0.8	3060	2220	840
	2000	0.75	357.96	0.08	1.4	0.8	3030	2220	810
	2000	1.00	349.59	0.08	1.4	0.8	3030	2220	810
	2000	1.25	341.21	0.08	1.4	0.8	3030	2220	810
	2000	1.50	332.84	0.08	1.4	0.8	3000	2220	780
	2000	1.75	324.47	0.08	1.4	0.8	3000	2220	780
	2000	2.00	316.09	0.08	1.4	0.8	3000	2220	780
	2000	2.25	307.72	0.08	1.4	0.8	2970	2220	750
	2000	2.50	299.35	0.08	1.4	0.8	2970	2220	750
	2000	2.75	290.97	0.08	1.4	0.8	2940	2220	720
	2000	3.00	282.60	0.08	1.4	0.8	2910	2220	690
	2000	3.25	274.23	0.08	1.4	0.8	2910	2220	690
	2000	3.50	265.85	0.08	1.4	0.8	2880	2220	660
	2000	3.75	257.48	0.08	1.4	0.8	2850	2220	630

	2000	4.00	249.11	0.08	1.4	0.8	2850	2220	630
	2000	4.25	240.73	0.08	1.4	0.8	2820	2220	600
	2000	4.50	232.36	0.08	1.4	0.8	2790	2220	570
	2000	4.75	223.99	0.08	1.4	0.8	2790	2220	570
	2000	5.00	215.61	0.08	1.4	0.8	2790	2220	570
	2000	5.25	207.24	0.08	1.4	0.8	2760	2220	540
	2000	5.50	198.87	0.08	1.4	0.8	2730	2220	510
	2000	5.75	190.49	0.08	1.4	0.8	2700	2220	480
	2000	6.00	182.12	0.08	1.4	0.8	2700	2220	480
	2000	6.25	173.75	0.08	1.4	0.8	2670	2220	450
	2000	6.50	165.37	0.08	1.4	0.8	2670	2220	450
	2000	6.75	157.00	0.08	1.4	0.8	2640	2220	420
	2000	7.00	148.63	0.08	1.4	0.8	2610	2220	390
	2000	7.25	140.25	0.08	1.4	0.8	2610	2220	390
	2000	7.50	131.88	0.08	1.4	0.8	2580	2220	360
	2000	7.75	123.51	0.08	1.4	0.8	2580	2220	360
	2000	8.00	115.13	0.08	1.4	0.8	2550	2220	330
	2000	8.25	106.76	0.08	1.4	0.8	2550	2220	330
	2000	8.50	98.39	0.08	1.4	0.8	2520	2220	300
	2000	8.75	90.01	0.08	1.4	0.8	2520	2220	300
	2000	9.00	81.64	0.08	1.4	0.8	2520	2220	300
	2000	9.25	73.27	0.08	1.4	0.8	2460	2220	240
	2000	9.50	64.89	0.08	1.4	0.8	2430	2220	210
	2000	9.75	56.52	0.08	1.4	0.8	2400	2220	180
	2000	10.00	48.15	0.08	1.4	0.8	2370	2220	150
	2000	10.25	39.77	0.08	1.4	0.8	2340	2220	120
	2000	10.50	31.40	0.08	1.4	0.8	2310	2220	90
	2000	10.75	23.03	0.08	1.4	0.8	2280	2220	60
	2000	11.00	14.65	0.08	1.4	0.8	2250	2220	30
5	2000	1.00	332.84	0.12	1.8	0.4	4050	2220	1830
	2000	1.25	320.28	0.12	1.8	0.4	3990	2220	1770
	2000	1.50	307.72	0.12	1.8	0.4	4020	2220	1800
	2000	1.75	295.16	0.12	1.8	0.4	3900	2220	1680

	2000	2.00	282.60	0.12	1.8	0.4	3840	2220	1620
	2000	2.25	270.04	0.12	1.8	0.4	3810	2220	1590
	2000	2.50	257.48	0.12	1.8	0.4	3750	2220	1530
	2000	2.75	244.92	0.12	1.8	0.4	3660	2220	1440
	2000	3.00	232.36	0.12	1.8	0.4	3600	2220	1380
	2000	3.25	219.80	0.12	1.8	0.4	3540	2220	1320
	2000	3.50	207.24	0.12	1.8	0.4	3480	2220	1260
	2000	3.75	194.68	0.12	1.8	0.4	3450	2220	1230
	2000	4.00	182.12	0.12	1.8	0.4	3360	2220	1140
	2000	4.25	169.56	0.12	1.8	0.4	3330	2220	1110
	2000	4.50	157.00	0.12	1.8	0.4	3270	2220	1050
	2000	4.75	144.44	0.12	1.8	0.4	3210	2220	990
	2000	5.00	131.88	0.12	1.8	0.4	3180	2220	960
	2000	5.25	119.32	0.12	1.8	0.4	3090	2220	870
	2000	5.50	106.76	0.12	1.8	0.4	3060	2220	840
	2000	5.75	94.20	0.12	1.8	0.4	2970	2220	750
	2000	6.00	81.64	0.12	1.8	0.4	2910	2220	690
	2000	6.25	69.08	0.12	1.8	0.4	2850	2220	630
	2000	6.50	56.52	0.12	1.8	0.4	2760	2220	540
	2000	6.75	43.96	0.12	1.8	0.4	2670	2220	450
	2000	7.00	31.40	0.12	1.8	0.4	2580	2220	360
	2000	7.25	18.84	0.12	1.8	0.4	2490	2220	270
	2000	7.50	6.28	0.12	1.8	0.4	2370	2220	150
6	2000	0.50	349.59	0.16	1.0	1.2	3120	2220	900
	2000	0.75	332.84	0.16	1.0	1.2	3090	2220	870
	2000	1.00	316.09	0.16	1.0	1.2	3090	2220	870
	2000	1.25	299.35	0.16	1.0	1.2	3000	2220	780
	2000	1.50	282.60	0.16	1.0	1.2	2940	2220	720
	2000	1.75	265.85	0.16	1.0	1.2	2940	2220	720
	2000	2.00	249.11	0.16	1.0	1.2	2880	2220	660
	2000	2.25	232.36	0.16	1.0	1.2	2880	2220	660
	2000	2.50	215.61	0.16	1.0	1.2	2820	2220	600
	2000	2.75	198.87	0.16	1.0	1.2	2790	2220	570

	2000	3.00	182.12	0.16	1.0	1.2	2760	2220	540
	2000	3.25	165.37	0.16	1.0	1.2	2760	2220	540
	2000	3.50	148.63	0.16	1.0	1.2	2760	2220	540
	2000	3.75	131.88	0.16	1.0	1.2	2730	2220	510
	2000	4.00	115.13	0.16	1.0	1.2	2640	2220	420
	2000	4.25	98.39	0.16	1.0	1.2	2610	2220	390
	2000	4.50	81.64	0.16	1.0	1.2	2580	2220	360
	2000	4.75	64.89	0.16	1.0	1.2	2520	2220	300
	2000	5.00	48.15	0.16	1.0	1.2	2490	2220	270
	2000	5.25	31.40	0.16	1.0	1.2	2370	2220	150
	2000	5.50	14.65	0.16	1.0	1.2	2250	2220	30
7	2400	0.75	423.52	0.08	1.8	1.2	3630	2400	1230
	2400	1.00	411.47	0.08	1.8	1.2	3630	2400	1230
	2400	1.25	399.41	0.08	1.8	1.2	3600	2400	1200
	2400	1.50	387.35	0.08	1.8	1.2	3570	2400	1170
	2400	1.75	375.29	0.08	1.8	1.2	3540	2400	1140
	2400	2.00	363.24	0.08	1.8	1.2	3510	2400	1110
	2400	2.25	351.18	0.08	1.8	1.2	3480	2400	1080
	2400	2.50	339.12	0.08	1.8	1.2	3450	2400	1050
	2400	2.75	327.06	0.08	1.8	1.2	3420	2400	1020
	2400	3.00	315.00	0.08	1.8	1.2	3390	2400	990
	2400	3.25	302.95	0.08	1.8	1.2	3360	2400	960
	2400	3.50	290.89	0.08	1.8	1.2	3330	2400	930
	2400	3.75	278.83	0.08	1.8	1.2	3300	2400	900
	2400	4.00	266.77	0.08	1.8	1.2	3270	2400	870
	2400	4.25	254.72	0.08	1.8	1.2	3240	2400	840
	2400	4.50	242.66	0.08	1.8	1.2	3180	2400	780
	2400	4.75	230.60	0.08	1.8	1.2	3180	2400	780
	2400	5.00	218.54	0.08	1.8	1.2	3150	2400	750
	2400	5.25	206.49	0.08	1.8	1.2	3090	2400	690
	2400	5.50	194.43	0.08	1.8	1.2	3060	2400	660
	2400	5.75	182.37	0.08	1.8	1.2	3030	2400	630
	2400	6.00	170.31	0.08	1.8	1.2	3000	2400	600

	2400	6.25	158.26	0.08	1.8	1.2	2970	2400	570
	2400	6.50	146.20	0.08	1.8	1.2	2940	2400	540
	2400	6.75	134.14	0.08	1.8	1.2	2910	2400	510
	2400	7.00	122.08	0.08	1.8	1.2	2880	2400	480
	2400	7.25	110.03	0.08	1.8	1.2	2910	2400	510
	2400	7.50	97.97	0.08	1.8	1.2	2850	2400	450
	2400	7.75	85.91	0.08	1.8	1.2	2820	2400	420
	2400	8.00	73.85	0.08	1.8	1.2	2790	2400	390
	2400	8.25	61.80	0.08	1.8	1.2	2730	2400	330
	2400	8.50	49.74	0.08	1.8	1.2	2670	2400	270
	2400	8.75	37.68	0.08	1.8	1.2	2640	2400	240
	2400	9.00	25.62	0.08	1.8	1.2	2580	2400	180
	2400	9.25	13.56	0.08	1.8	1.2	2490	2400	90
	2400	9.50	1.51	0.08	1.8	1.2	2430	2400	30
	2400	0.50	423.52	0.12	1.0	0.8	3240	2400	840
	2400	0.75	405.44	0.12	1.0	0.8	3240	2400	840
	2400	1.00	387.35	0.12	1.0	0.8	3210	2400	810
	2400	1.25	369.26	0.12	1.0	0.8	3180	2400	780
	2400	1.50	351.18	0.12	1.0	0.8	3150	2400	750
	2400	1.75	333.09	0.12	1.0	0.8	3120	2400	720
	2400	2.00	315.00	0.12	1.0	0.8	3090	2400	690
	2400	2.25	296.92	0.12	1.0	0.8	3060	2400	660
	2400	2.50	278.83	0.12	1.0	0.8	3000	2400	600
8	2400	2.75	260.75	0.12	1.0	0.8	2970	2400	570
	2400	3.00	242.66	0.12	1.0	0.8	2940	2400	540
	2400	3.25	224.57	0.12	1.0	0.8	2910	2400	510
	2400	3.50	206.49	0.12	1.0	0.8	2850	2400	450
	2400	3.75	188.40	0.12	1.0	0.8	2850	2400	450
	2400	4.00	170.31	0.12	1.0	0.8	2820	2400	420
	2400	4.25	152.23	0.12	1.0	0.8	2790	2400	390
	2400	4.50	134.14	0.12	1.0	0.8	2760	2400	360
	2400	4.75	116.05	0.12	1.0	0.8	2730	2400	330
	2400	5.00	97.97	0.12	1.0	0.8	2700	2400	300

	2400	5.25	79.88	0.12	1.0	0.8	2670	2400	270
	2400	5.50	61.80	0.12	1.0	0.8	2610	2400	210
	2400	5.75	43.71	0.12	1.0	0.8	2550	2400	150
	2400	6.00	25.62	0.12	1.0	0.8	2520	2400	120
	2400	6.25	7.54	0.12	1.0	0.8	2430	2400	30
	2400	0.50	411.47	0.16	1.4	0.4	4350	2400	1950
	2400	0.75	387.35	0.16	1.4	0.4	4320	2400	1920
	2400	1.00	363.24	0.16	1.4	0.4	4230	2400	1830
	2400	1.25	339.12	0.16	1.4	0.4	4170	2400	1770
	2400	1.50	315.00	0.16	1.4	0.4	4080	2400	1680
	2400	1.75	290.89	0.16	1.4	0.4	3960	2400	1560
	2400	2.00	266.77	0.16	1.4	0.4	3870	2400	1470
	2400	2.25	242.66	0.16	1.4	0.4	3780	2400	1380
9	2400	2.50	218.54	0.16	1.4	0.4	3690	2400	1290
	2400	2.75	194.43	0.16	1.4	0.4	3540	2400	1140
	2400	3.00	170.31	0.16	1.4	0.4	3450	2400	1050
	2400	3.25	146.20	0.16	1.4	0.4	3360	2400	960
	2400	3.50	122.08	0.16	1.4	0.4	3210	2400	810
	2400	3.75	97.97	0.16	1.4	0.4	3060	2400	660
	2400	4.00	73.85	0.16	1.4	0.4	2970	2400	570
	2400	4.25	49.74	0.16	1.4	0.4	2880	2400	480
	2400	4.50	25.62	0.16	1.4	0.4	2700	2400	300

Appendix-B: List of Publications

Peer Reviewed International Journals Publications

1. **Shailendra Pawanr,** Girish Kant Garg and Srikanta Routroy **(2022)** "A novel approach to model the energy consumption of machine tools for machining cylindrical parts" **Journal of Manufacturing Processes**, **Elsevier.** https://doi.org/10.1016/j.jmapro.2022.09.040 **(SCI/Q1/ I.F.: 5.684)**
2. **Shailendra Pawanr,** Girish Kant Garg and Srikanta Routroy **(2022)** "Development of an Empirical Model to Quantify Carbon Emissions for Machining of Cylindrical Parts" **Environmental Science and Pollution Research, Springer Nature.** https://doi.org/10.1007/s11356-022-23349-2 **(SCI/Q1/ I.F: 5.190)**
3. **Shailendra Pawanr,** Girish Kant Garg and Srikanta Routroy **(2021)** "Development of an Empirical Model for Variable Power Consumption Machining Processes - A Case of End Facing," **Arab J Sci Eng. Springer Nature**. https://doi.org/10.1007/s13369-021-06198-y **(SCI/Q1/ I.F.: 2.807)**
4. **Shailendra Pawanr,** Girish Kant Garg and Srikanta Routroy "Prediction of energy efficiency, Power Factor and associated carbon emission of machine tools using soft computing techniques" **International Journal on Interactive Design and Manufacturing, Springer Nature.** https://doi.org/10.1007/s12008-022-01089-4 **(ESCI/Q2/SJR: 0.49)**
5. **Shailendra Pawanr,** Girish Kant Garg and Srikanta Routroy (2022) "Prediction of Energy Consumption of Machine Tools Using Multi-Gene Genetic Programming," **Mater. Today Proc., (xxxx), Elsevier**, pp. 1–5. https://doi.org/10.1016/j.matpr.2022.01.156 **(Scopus/SNIP: 0.575)**
6. **Shailendra Pawanr,** Girish Kant Garg and Srikanta Routroy **(2021)** "Development of a Transient Energy Prediction Model for Machine Tools," **Procedia CIRP, Elsevier**, 98, pp. 678–683. https://doi.org/https://doi.org/10.1016/j.procir.2021.01.174 **(Scopus/SNIP: 0.899)**
7. **Shailendra Pawanr,** Girish Kant Garg and Srikanta Routroy **(2021)** "Modelling of Variable Energy Consumption for CNC Machine Tools," **Procedia CIRP, Elsevier**, 98, pp. 247–251. https://doi.org/10.1016/j.procir.2021.01.038 **(Scopus/SNIP: 0.899)**
8. **Shailendra Pawanr,** Tanamay Tanishk, Anuj Gulati, Girish Kant Garg and Srikanta Routroy **(2021)** "Fuzzy-TOPSIS Based Multi-Objective Optimization of

Machining Parameters for Improving Energy Consumption and Productivity," **Procedia CIRP, Elsevier**, 102, pp. 192–197. https://doi.org/10.1016/j.procir.2021.09.033 **(Scopus/SNIP: 0.899)**

9. **Shailendra Pawanr,** Girish Kant Garg and Srikanta Routroy **(2019)** "Multi-Objective Optimization of Machining Parameters to Minimize Surface Roughness and Power Consumption Using TOPSIS," **Procedia CIRP, Elsevier**, 86, pp. 116–120. https://doi.org/10.1016/j.procir.2020.01.036 **(Scopus/SNIP: 0.899)**
10. **Shailendra Pawanr,** Girish Kant Garg **(2019)** "Selection of Optimum Cutting Parameters for Minimization of Specific Energy Consumption during Machining of Al 6061," J. Phys. Conf. Ser., **IOP publishing**, **1240** (1), p. 012064. https://doi.org/10.1088/1742-6596/1240/1/012064 (**Scopus/Q4/SJR: 0.21**)
11. **Shailendra Pawanr,** Girish Kant Garg and Srikanta Routroy " An integrated modelling and optimization approach for the selection of process parameters for variable-power consumption machining processes", **Journal of the Brazilian Society of Mechanical Sciences and Engineering, Spriger** (**SCI impact factor: 2.361) (Under review)**
12. **Shailendra Pawanr,** Girish Kant Garg and Srikanta Routroy "Multi-objective optimization of machining process sustainability performance indicators considering the impact of weight assignment methods". **Journal of Manufacturing Processes**. **Elsevier. (SCI/Q1/ I.F.: 5.684) (Under review)**

Book Chapter

13. Girish Kant Garg, **Shailendra Pawanr**, Kuldip S Sangwan **(2020)** "A Comparative Analysis of Surface Roughness Prediction Models Using Soft Computing Techniques," pp. 149–155.In: Sangwan, K., Herrmann, C. (eds) Enhancing Future Skills and Entrepreneurship. Sustainable Production, Life Cycle Engineering and Management. **Springer, Cham**. https://doi.org/10.1007/978-3-030-44248-4_15 (**Scopus Indexed-Book chapter**)

Appendix-C: Brief Biography of the Candidate and Supervisors

Mr. Shailendra Pawanr (Candidate), have been working as a research scholar in the department of Mechanical Engineering of Birla Institute of Technology and Science (BITS) Pilani, Pilani Campus. He has received B Tech in Industrial & Production engineering from Shri G. S. Institute of Technology & Science (SGSITS), Indore, Govt. Aided Autonomous Institute Estd. in 1952, and M Tech in Industrial Engineering and Management from Govt. Engineering College Ujjain, Autonomous Institute Estd. in 1966 by Govt. of M.P. Presently he is a research scholar in the Department of Mechanical Engineering at Birla Institute of Technology and Science (BITS), Pilani, Rajasthan. He has more than six years of teaching experience. His research interest includes sustainable machining, CNC-machining, energy-efficient machining and modelling and optimization of the machining processes.

Dr. Girish Kant Garg (Supervisor) is working as Assistant Professor in the Department of Mechanical Engineering at BITS, Pilani, Rajasthan. He did his PhD from BITS, Pilani. He has more than eighteen years of teaching experience. He has published more than 30 research papers in reputed journals and conferences at international level. He has been a reviewer of many Journals of International repute such as Journal of Cleaner Production, Journal of Engineering Processes, etc. His broad areas of research interest lie in modelling of conventional and non-conventional manufacturing processes.

Prof. Srikanta Routroy (Co-Supervisor) has received B Tech in Mechanical Engineering from CET, Bhubaneswar and Master of Technology in Industrial Engineering and Management from IIT, Kharagpur. He has completed his Ph.D. in the area of Supply Chain Management from BITS, Pilani. At present, he is working as Professor and Head of Mechanical Engineering Department at BITS Pilani, Pilani Campus. He has more than twenty-two years of teaching experience both in under graduate and post graduate level. He has authored and co-authored more than 175 research papers in refereed Journals and Conferences; 03 book chapters and 02 case studies in the area of supply chain management. He has also authored two case studies in the area of Supply Chain Management. He received sponsored projects from UGC, DBT, ICSSR, DST, Ministry of Steel (India), DST Rajasthan and Department of Food & Public Distribution, New Delhi. He has guided 07 Ph.D. and currently 08 Ph.D. students are working with him. He is currently working in the area of Supply Chain Analytics, Value Added Products, Life Cycle Assessment and Supplier Development. He has developed the Supply Chain Analytics Laboratory and minor program in supply chain analytics in BITS Pilani. The details about Srikanta Routroy are available in the weblink: https://www.bits-pilani.ac.in/pilani/srikanta/profile.